University of Reading

# Development of Spray Dried Solid Dispersion Formulations to Improve Oral and Pulmonary Delivery

Submitted for the Degree of Doctor of Philosophy

School of Pharmacy

Thomas Hibbard

February 2023

## Declaration of original authorship

I confirm that this is my own work and the use of all material from other sources has been properly and fully acknowledged.

Thomas Hibbard 2023

## Acknowledgements

Firstly, my sincere thanks go to Dr Hisham Al-Obaidi and Prof. Kenneth Shankland for their thorough supervision, wise advice, and continual support over the past 3 years. I have learned so much from your experience and your approach to academic work and I hope we will continue to work together in the future.

The School of Pharmacy at the University of Reading have been exceptional in their support of PhD research, and I am proud to say that this is where I have made progress in learning my trade. My thanks go other academics at Reading University whom I have had the pleasure of working with, especially: Dr Glyn Barret (for cell culture work), Oliver Hancox (for HPLC advice), Dr Elena Kabova (for milling and X-ray diffraction advice), Vicky Kleanthous (for clinical teaching opportunities), and Dr Sarah Needs (for 3D printing and cell culture work). I have enjoyed working with many lab colleagues throughout the last few years: Fhata, Marta, Phong, Sam, Shiva, and Tareq to name a few. Your friendship has been invaluable. The work presented in this thesis would not have been possible without the support and constant background work of the technical team - especially Dr Pedro Rivas, Amanpreet Kaur, Nick Spencer, Mitch, and Murray. I have really enjoyed getting to know you all over the last few years. I would also like to thank the Engineering and Physical Sciences Research Council and Quotient Sciences for their financial support. Special thanks go to Dr Bildad Nyambura and Dr Mihaela Totolici for their advice and assistance. Also, my thanks to the Joint Pharmaceutical Analysis Group (JPAG) for their funding which allowed me to attend and speak at several interesting conferences.

A mention must go to my parents and close family who support me in so many ways and to my church family at Carey who constantly remind me of what is important in life. At times, this doctorate has been a difficult process, leading to moments where the accusation which was levelled at the apostle Paul could possibly be directed at myself (Acts ch26 v24). However, I acknowledge that ultimately all good and perfect gifts are attributed to God, and I am thankful for the ability and opportunity that He has given me to pursue my interests in Pharmacy and Pharmaceutical Sciences. Finally, to Abigail who is sat by me as I write this, your patience, understanding, and encouragement are a true motivation to me, and I trust we will spend many happy days together in our marriage. I'm sure you'll even try to read at least some of this thesis. Hopefully the following will be an enjoyable and stimulating read!

Thomas Hibbard, February 2023

## Abstract

Chapter 1 presents an introduction for crystal engineering in formulation development with emphasis on salt, co-crystal, and solid dispersion formation. Preparation, characterisation, and applications for oral and inhaled delivery are outlined, with a focus on preparation using spray drying.

Chapter 2 reviews literature on solid dispersion formulations for carrier free, dry powder inhalation, outlining applications for antimicrobial and anticancer therapies.

Chapter 3 reports four new ciprofloxacin salts with dicarboxylic acids and their X-ray, thermal, and spectroscopic characterisation. All salts showed enhanced saturated solubility, especially the glutaric acid salt which was higher than ciprofloxacin hydrochloride monohydrate.

Chapter 4 describes the formulation of ciprofloxacin salt solid dispersions with HPMC, through contrasting three-fluid nozzle spray drying methods. The formulations showed modified ciprofloxacin release and enhanced powder aerosolisation properties. Solution and suspension spray drying methods generated solid dispersions with differing *in vitro* and *in vivo* drug release.

Chapter 5 presents the preparation of spray dried progesterone formulations for dry powder inhalation. Form II progesterone polymorph was present in the crystalline state, independent of feedstock solvent or excipients. Formulations with HPMCAS showed no temperature induced phase change to Form I as well as increased kinetic solubility and fine particle fraction.

Chapter 6 describes a new progesterone co-crystal following *in silico* and experimental screening, followed by provisional scale up method testing. The co-crystal showed enhanced dissolution compared to progesterone and then Utrogestran$^{TM}$ when formulated as a tablet.

Chapter 7 explores how spray drying process parameters influence the preparation of salicylic acid:caffeine co-crystal. All two-fluid and three-fluid nozzle methods generated co-crytsal although to differing crystallinities and with additional crystalline caffeine phase dependent on feedstock composition.

Chapter 8 summarises key findings with their critical evaluation and suggestions for future work. Spray drying can prepare salts, co-crystals, and solid dispersions for use in inhaled and oral formulation development.

## List of Publications

Al-Obaidi, H.; Granger, A.; **Hibbard, T**.; Opesanwo, S. Pulmonary Drug Delivery of Antimicrobials and Anticancer Drugs Using Solid Dispersions. Pharmaceutics 2021, 13, 1056.

**Hibbard T**, Nyambura B, Scholes P, Totolici M, Shankland K, Al-Obaidi H. Preparation and Physiochemical Analysis of Novel Ciprofloxacin / Dicarboxylic Acid Salts. *J Pharm Sci*. 2023;112(1):195-203.

## Papers not related to this work:

Al-Obaidi H, Petraityte I, **Hibbard T**, Majumder M, Kalgudi R, Zariwala MG. Antifungal nanosuspensions with surfactants and silver for the treatment of onychomycosis. *Eur J Pharm Biopharm*. 2022;179:194-205.

## List of Conferences and Awards

APSGB PharmSci 2022, Belfast, September 2022 – Invited Speaker

IOM3 Young Person Lecture Competition, March 2022 – Podium Presentation

APSGB PharmSci 2021, online, September 2021 – On Demand Presentation

Respiratory Drug Delivery (RDD) Conference, online, May 2021 – On Demand Presentation

Young Entrepreneurs Scheme (YES), February 2021 – Winner of Best Elevator Pitch

Drug Delivery to the Lungs Conference (DDL), online December 2020 – On Demand Presentation

Joint Pharmaceutical Analysis Group (JPAG) Research Symposium, online November 2020 – Podium Presentation: Winner of Geoffrey Phillips Award for best presentation

## Table of Contents

## Abbreviations

| | |
|---|---|
| AA | Adipic acid |
| ACE | Acetone |
| ACI | Andersen cascade impactor |
| ANOVA | Analysis of variance |
| API | Active pharmaceutical ingredient |
| AS | Antisolvent |
| ATR | Attenuated total reflectance |
| BCS | Biopharmaceutical classification system |
| CASD | Co-amorphous solid dispersion |
| CAF | Caffeine |
| CF | Cystic fibrosis |
| CFC | Chlorofluorocarbon |
| CFX | Ciprofloxacin |
| Co | Colistin |
| COPD | Chronic obstructive pulmonary disorder |
| CsA | Cyclosporin A |
| CSD | Cambridge structural database |
| DPI | Dry powder inhaler |
| DSC | Differential scanning calorimetry |
| ED | Emitted dose |
| EDX | Energy dispersive X-ray Analysis |
| EtOH | Ethanol |
| FDA | Food and drug administration (USA) |
| FPD | Fine particle dose |
| FPF | Fine particle fraction |
| FTIR | Fourier-transform infrared spectroscopy |
| FWHM | Full width half max |
| GA | Glutaric acid |

| | |
|---|---|
| GIT | Gastrointestinal tract |
| GRAS | Generally regarded as safe (FDA list) |
| GSD | Geometric standard deviation |
| HFA | Hydrofluoroalkane |
| HPLC | High performance liquid chromotography |
| HPMC | Hydroxypropyl methylcellulose |
| HPMCAS | Hydroxypropyl methylcellulose |
| HRT | Hormone replacement therapy |
| HSP | Hansen solubility parameter |
| iBCS | Inhaled biopharmaceutical classification system |
| IPA | Isopropyl alcohol (Propan-2-ol) |
| LAG | Liquid assisted grinding |
| LEU | L-leucine |
| MIC | Minimum inhibitory concentration |
| MMAD | Mass median aerodynamic diameter |
| pMDI | Pressurised metered dose inhaler |
| PA | Pimelic acid |
| PABA | Para-aminobenzoic acid |
| PBS | Phosphate buffered saline |
| PROG | Progesterone |
| PXRD | Powder X-ray diffraction |
| SA | Succinic acid |
| SAL | Salicylic Acid |
| SEM | Scanning electron microscopy |
| SC-XRD | Single crystal X-ray diffraction |
| SD | Spray Drying |
| SLF | Simulated lung fluid |
| SLS | Sodium lauryl sulphate |
| SOL | Formulation from solution |

| | |
|---|---|
| SUS | Formulation from suspension |
| $T_g$ | Glass transition temperature |
| TGA | Thermogravimetric analysis |
| UV-VIS | Ultraviolet-visible spectroscopy |
| VT-PXRD | Variable temperature powder X-ray diffraction |
| δt | Total solubility parameter |
| 2-FN | Two-fluid nozzle |
| 3-FN | Three-fluid nozzle |

Chapter 1

# General Introduction

## 1 Introduction to the Use of Crystal Engineering in Formulation Development

High proportions of existing active pharmaceutical ingredients (APIs) and drug candidates in development display poor physicochemical properties, especially aqueous solubility [1]. High-throughput screening alongside limited solubility testing early in the drug discovery process has led to many APIs being highly lipophilic molecules [2]. Furthermore, new APIs often target more complex sites of action which can require molecules with greater complexity and therefore higher molecular weight [3]. The oral route of administration is preferable for most APIs due to convenience, cost effectiveness of formulations and the compatibility with a wide range of APIs. However, according to Lipinski's rules for predicting oral absorption, molecules with high lipophilicity and high molecular weight are more likely to have limited oral bioavailability [2]. Since the oral route remains the most favourable for delivery, formulation strategies to enhance bioavailability have become essential for many APIs [4]. Crystal engineering is a key area of formulation development and seeks to direct API intermolecular interactions in order to influence physicochemical properties without altering pharmacodynamic activity.

Limitations with oral bioavailability can also be addressed by reformulating an API for delivery through an alternative administration route. The inhaled route is an established means for local delivery of APIs to the lung tissue as well showing good promise as a site for systemic absorption [5, 6]. The lungs are a highly vascular organ with a thin diffusion pathway, designed for the efficient exchange of molecules into and from the blood stream [7]. Compared to the gastrointestinal tract (GIT), delivery to the lungs is minimally influenced by pH, enzymatic activity or first pass metabolism, making it an attractive option for systemic delivery of some APIs [8]. However, limitations associated with poor physicochemical properties still exist when using the inhaled route and therefore crystal engineering strategies can also be applied to the development of effective inhaled formulations.

The research presented in this thesis aims to explore a crystal engineering approach for the generation of solid dispersion formulations with modified physicochemical properties. Ultimately, the aim is to generate drug particles with suitable water-solubility, physical stability, and enhanced activity for oral or repurposed pulmonary delivery. A general background is included which summarises key crystal engineering formulation approaches with comment on their design, scalable manufacture, and characterisation. Then the challenges associated with poor physicochemical properties

for delivery through the oral and inhaled routes are discussed and how crystal engineering approaches can be used can address these issues.

## 2 Solid State Properties of Active Pharmaceutical Ingredients (APIs)

At standard temperature and pressure, most APIs exist in the solid state with molecules held closely together via intermolecular interactions. The physical properties of a solid are directed by the strength and nature of these interactions so for an API these interactions will largely determine the suitability for administration into the body.

### 2.1 Crystalline vs Amorphous

Viewed simply, the molecules of a solid can either exist in a crystalline or amorphous form. In a crystalline form, molecules are packed in such a way to form a crystal lattice that exhibits long-range order in three dimensions. This long-range order equates to a low energy state – all other things being equal, the lower the energy of the crystal, the more stable it is, and this stability can be correlated to physicochemical properties such as melting point and solubility. These properties are dependent on the type and extent of intermolecular bonding within the crystal structure and are therefore distinct for specific crystalline forms. For example, a crystal lattice held together through relatively weak van de Waals interactions will generally display a higher solubility and lower melting point than a crystal lattice held together through extensive hydrogen bonding.

Solids in an amorphous state do not display any long-range order but rather exhibit short-range order via intermolecular interactions. Since there is a higher level of disorder compared to crystalline materials, the amorphous form exists in a higher energy state and thus exhibit increased solubility and dissolution rates compared to crystalline forms. However, amorphous forms of molecules are metastable and likely to transform to lower energy crystalline states over time. To be used effectively within a formulation, the amorphous form needs to be stabilised.

### 2.2 Polymorphism

It is possible for the same API molecule to exist in multiple crystalline solid forms with different packing arrangement of molecules in 3D space [9]. When multiple forms of an API exist like this, they are known as polymorphs and their different crystal packing can produce marked differences in physical properties. If a polymorph exists at a higher energy state relative to the most stable polymorph, it is described as being metastable and these polymorphs will possess properties such as a lower melting point or slightly higher solubility [10]. However, similar to amorphous forms, a metastable polymorph of an API will eventually revert to the most stable crystalline form. Often this can be a

solvent mediated process during dissolution where, as the system reaches equilibrium, the API will recrystallise as the more stable form with lower solubility. It is possible that any API will display polymorphism so there must be a thorough screening process to identify different polymorphs and the preparation conditions which favour their generation.

## 3 Crystal Engineering Strategies

Many strategies can be used to direct intermolecular interactions within a solid with the aim of enhancing physicochemical properties. Using these techniques as an API formulation strategy has come to be described as a crystal engineering approach. This thesis mainly focusses on API salt forms, co-crystal and coamorphous forms, and the formation of polymeric solid dispersions with these. Many detailed reviews of crystal engineering and its use as a formulation strategy in pharmaceutical development have been published [10-13].

### 3.1 Salt Formation

Salt formation is a well-established means of increasing the water-solubility of a weakly acidic or weakly basic API through formation of an ionic crystalline complex [9]. Salt formation occurs as the product of an acid-base reaction between an API and a suitable counterion atom or molecule followed by the formation of an ionic compound (equation 1, where A = acid, B = base).

$$HA + B \leftrightarrow A^- + BH^+ \leftrightarrow A^-BH^+_{(solid)}$$

(Equation 1)

The potential for a salt to form depends on the affinity of API and counterion for each other and the ability of the functional groups involved to ionise. Most APIs are either weak acids or weak bases and so the ability to ionise is described by the acid dissociation constant (p$K_a$). This constant is calculated from the concentrations of ionised and non-ionised species at a specific pH (equation 2).

$$\mathrm{pH} = \mathrm{p}K_a + log\frac{[A^-]}{[HA]}$$

(Equation 2)

Whether proton transfer will occur between acid and base is directed by the difference in p$K_a$ values between acidic and basic functional groups in the molecules. In general, if the difference in p$K_a$ ($\Delta$p$K_a$) between the acidic and basic functional groups (i.e. p$K_a$

(protonated base) – p$K_a$ (acid)) is greater than 3, proton transfer will occur and an ionic bond will form on crystallisation [14]. Therefore, predictions can be made as to whether an API will be suitable for salt formation based on analysis of the chemical structure.

Many organic and inorganic counter ions have been used to produce successful API salt forms which are currently used in the clinic. Since different salt forms will have different crystal structures from those of the API, physical properties of the salt form are largely dependent on the counter ion. Some common examples of counterions and examples of their use in pharmaceutical salt formation are shown in **Table 1**.

Salt forms are known to dramatically increase the water-solubility of an API. The presence of a stabilised ionic charge instigates this higher water-solubility by increasing the hydrophilicity of the solid form leading to increased wettability. Following this, dissolving of the highly water-soluble counterion causes local pH changes which favour API dissolution. These effects greatly increase the gain in hydration enthalpy and if this increase gives an enthalpy larger or equal to the enthalpy required to break apart the crystal lattice, dissolving will occur much more favourably.

Careful screening and selection are necessary when developing new salt forms of existing APIs to assess the change to physicochemical properties. By generating new salt forms, product lifespan can be extended by overcoming issues with existing salt forms, for example with respect to hygroscopicity and stability [15].

**Table 1:** Pharmaceutical salt counterions and examples (adapted from [16])

**Basic APIs**

| **Anion** | **p$K_a$** | **Example** | **Counterion Structure** |
|---|---|---|---|
| Chloride | - 6.10 | Suxamethonium Chloride | $Cl^-$ |
| Sulphate | -3.00, 1.96 | Hydroxychloroquine Sulphate | 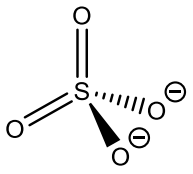 |
| Mesylate | -1.20 | Amlodipine Mesylate | 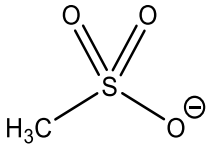 |
| Maleate | 1.92, 6.23 | Timolol Maleate | 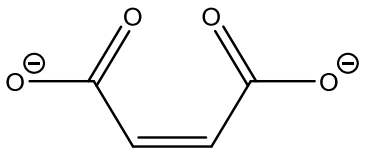 |

| | | | |
|---|---|---|---|
| Acetate | 4.76 | Fludrocortisone Acetate | 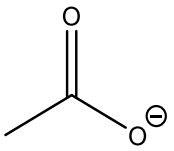 |

**Acidic APIs**

| Cation | p$K_a$ | Example | Structure |
|---|---|---|---|
| Potassium | 16.00 | Lorsartan Potassium |  |
| Sodium | 14.77 | Diclofenac Sodium |  |
| Calcium | 12.90 | Acamprosate Calcium |  |

## 3.2 Co-crystals

For APIs without easily ionisable functional groups, co-crystallisation can be a suitable alternative to salt formation and its use and development has been extensively documented in literature [17-21]. **Table 2** summarises all current marketed co-crystal formulations. Like salts, co-crystals are stable crystalline materials composed of an API and small molecule coformer(s) in a single phase, distinct from their constituent parts. However, co-crystals are distinct from salts due to their lack of ionisation and are primarily be held together through intermolecular hydrogen bonding, π-π stacking and van de Waals interactions. In theory there is no limit to the number of components which make up a co-crystal; however, the API and coformer(s) must exist in a distinct stoichiometric ratio.

Selection of the co-crystal coformer molecule is based on a combination of molecular compatibility between API and coformer and the presence of a desired physical characteristic. For example, the selection of a hydrophilic coformer with multiple sterically unhindered hydrogen bonding regions is likely to produce a co-crystal with improved API aqueous solubility and dissolution. As with polymorphs, changes to the strength of intermolecular interactions influence the dissolution process; however, like salts, the presence of a highly water-soluble coformer increases the hydration enthalpy. Wettability of the solid is also increased and the presence of coformer locally in solution acts to stabilise a super saturated state of the API [22]. This phenomenon has been coined the “spring and parachute” effect [23]. **Table 3** documents reported co-crystals between 2014 and 2020 which specifically include aqueous solubility data. The majority of these co-crystals exhibit a higher solubility than the original API; however,

there are a few exceptions where reported solubility has been reduced. Co-crystalisation has also been used as a means to generate a higher stability API containing compound which is less sensitive to degradation at high temperature and humidity [24]. Since a new solid form is being produced it is expected that the co-crystal will show properties distinct from the API and distinct from a physical mixture between API and coformer.

**Table 2:** Approved co-crystal formulations

| Brand Name | API | Coformer | Approved | Manufacturer |
|---|---|---|---|---|
| Seglentis® | Tramadol HCl | Celecoxib | 2022 | Kowa Pharma. America |
| Stlglatro ® | Ertugliflozin | L-pyroglutamic acid | 2017 | MSD |
| Entresto ® | Valsartan Trisodium | Sacubitril hemi-pentahydrate | 2015 | Novartis |
| Suglat ® | Ipragliflozin | L-proline | 2014 | Astellas Pharma |
| Lexapro ® | Escitalopram Oxalate | Oxalic Acid | 2009 | AbbVie |
| Depakote ® | Valproate Sodium | Valproic Acid | 2002 | Sanofi |

Co-crystals of APIs and coformers with weakly ionisable hydrogen bonding functional groups can differ from salts simply by the positioning of a hydrogen atom within the intermolecular bond. In these instances, comparing the p$K_a$ of the bonding functional groups is useful to predict ionisation and therefore whether the product will be a co-crystal or salt. As per salt formation, if $\Delta pK_a$ between API and coformer is greater than 3 then an ionic bond is likely to form but if less than 0, a hydrogen bond will form [14]. This leaves an ambiguous region if the $\Delta pK_a$ is between 0 and 3 where in theory it is possible for either salt or co-crystal to form; this is known as the salt co-crystal continuum [25, 26]. Co-crystal and salt forms of the same starting materials have been documented with salt or co-crystal formation dependent on the crystallisation conditions [27, 28].

**Table 3:** Summary of reported co-crystals in literature from Jan 2014 to Dec 2020. All solubilities are aqueous if pH is specified, then a buffer was used.

| API | Coformer (Molar Ratio) | API Solubility mg·mL$^{-1}$ | Coformer Solubility mg·mL$^{-1}$ | Co-crystal Solubility mg·mL$^{-1}$ | pH of media | Ref |
|---|---|---|---|---|---|---|
| 4-Aminosalicylic acid | Caffeine (1:1) | 8.422 | 21.7 | 20.673 | 7.4 | 29 |
| | Isoniazid (1:1) | | 140 | 15.314 | | |
| | Isonicotinamide (2:1) | | 191.7 | 16.845 | | |
| | Theophylline (1:2) | | 7.3 | 23.89 | | |
| | Nicotinamide.$H_2O$ (1:1:1) | | 500 | 14.548 | | |
| | Pyrazinamide.$H_2O$ (1:1:1) | | 15 | 13.476 | | |
| Caffeic Acid Phenethyl Ester | Caffeine (1:1) | 0.021 | 21.7 | 0.115 | - | 30 |
| | Isonicotinamide (1:1) | | 191.7 | 0.158 | | |
| | Nicotinamide (1:1) | | 500 | 0.371 | | |
| Carbamazepine | 4-Aminosalicylic acid (1:1) | 0.0113 | 1.69 | 0.0158 | 7.4 | 31 |
| Carbamazepine | 9-Anthroic acid (1:1) | 0.161 | 0.0849 | 0.168 | 6.8 | 32 |
| | Nicotinic acid.$H_2O$ (1:1:1) | | 500 | 0.304 | | |
| Efavirenz | Adipic acid (1:1) | 0.00546 | 14 | 0.00784 | - | 33 |
| | Lactic acid (1:1) | | 1000 | 0.00925 | | |
| Ethenzamide | 2,5-Dihydroxybenzoic acid (2:2) | 0.03 | 5 | 0.003 | 7.4 | 34 |
| | 2,6-Dihydroxybenzoic acid (1:1) | | 9.56 | 0.142 | | |
| | 3,4-Dihydroxybenzoic acid (1:1) | | 18.2 | 0.266 | | |
| | 3,5-Dihydroxybenzoic acid.$H_2O$ (1:3:2) | | 12 | 0.376 | | |
| Fenofibrate | Nicotinamide (1:1) | 0.0255 | 500 | 0.03097 | - | 35 |
| Fluconazole | Adipic acid (1:1) | 2.56 | 14 | 10.3 | - | 36 |
| | Dipicolinic acid (1:1) | | 5 | 7.464 | | |
| | Malic acid (1:1) | | 592 | 13.626 | | |
| | Fumaric acid.$H_2O$ (1:1:1) | | 7 | 13.95 | | |
| Flurbiprofen | Benzamide (1:1) | 1.927 | 13.5 | 3.42 | 6.8 | 37 |
| | Picolinamide (1:1) | | 179.5 | 7.572 | | |
| | Salicylamide (1:1) | | 2.06 | 1.612 | | |
| Furosemide | Anthranilamide (1:1) | 7.3 | 2.1 | 6.31 | 7.4 | 38 |

| | | | | | | |
|---|---|---|---|---|---|---|
| | Tetramethylpyrazine (1:1) | | 0.004 | 7.31 | | |
| | Caffeine (1:1) | | 21.7 | 2.7 | | |
| | Adenine (1:1) | | 1.03 | 4.96 | | |
| Gembibrozil | Isonicotinamide (1:1) | 23.64 | 191.7 | 33.04 | 7.4 | 39 |
| Gliclazide | Catechol (1:1) | 1.185 | 461 | 7.091 | 7.4 | 40 |
| | Resorcinol (1:1) | | 717 | 4.13 | | |
| | Piperazine (salt) (1:1) | | 1000 | 7.667 | | |
| Hesperetin | Caffeine (1:1) | 0.02378 | 21.7 | 0.0902 | 7.2 | 41 |
| | Nicotinamide (1:1) | | 500 | 0.09402 | | |
| | Picolinic acid (1:1) | | 960 | 0.06854 | | |
| Hydrochlorothiazide | 4-Aminobenzoic acid (1:2) | 0.994 | 6.11 | 2.396 | 7.4 | 42 |
| | Nicotinamide (1:1) | | 500 | 1.268 | | |
| | Nicotinic acid (1:1) | | 18 | 0.725 | | |
| | Resorcinol (1:1) | | 717 | 1.297 | | |
| | Succinamide (1:0.5) | | - | 0.212 | | |
| Ibuprofen | Nicotinamide (1:1) | 0.0495 | 500 | 0.347 | - | 43 |
| Leflunomide | 3-Hydroxybenzoic acid (1:1) | 0.03165 | 7.25 | 0.03658 | - | 44 |
| | Picolinic acid (1:1) | | 960 | 0.04011 | | |
| | Picolinic acid (1:2) | | 960 | 0.03445 | | |
| | Pyrogallol (1:1) | | 507 | 0.04463 | | |
| Melatonin | Pimelic acid (1:1) | 0.92 | 50 | 1.93 | 6.8 | 45 |
| Pirfenidone | Fumaric acid (1:1) | 18.29 | 7 | 8.1 | - | 46 |
| | Trimesic acid (1:1) | | 0.027 | 0.72 | | |
| Simvastatin | Saccharin (1:1) | 0.009 | 500 | 0.03 | - | 47 |
| | Nicotinamide (1:1) | | 4 | 0.083 | | 48 |
| Tegafur | 4-Hydroxybenzoic acid (1:1) | 23.3 | 5 | 16.8 | 6.8 | 49 |
| | Isonicotinamide (1:1) | | 191.7 | 53.9 | | |
| | Nicotinamide (1:1) | | 500 | 30 | | |
| | Pyrogallol (1:1) | | 507 | 28.6 | | |
| | Theophylline.$H_2O$ (1:1:1) | | 11.05 | 16.1 | | |
| Theophylline | Acesulfame (1:1) | 11.05 | 270 | 55.31 | 7.4 | 50 |
| | Saccharin (1:1) | | 4 | 22.42 | | |

### 3.3 Solid Dispersions

A solid dispersion refers to a material where one or more components are coated by, and molecularly dispersed, in an inert solid-state carrier or matrix [51]. Solid dispersions can be crystalline or amorphous and are seen as an effective strategy for enhancing physicochemical properties through changes to intermolecular interactions or stabilising high energy forms of APIs [52]. Crystalline solid dispersions are comprised of microcrystalline API particles dispersed in and coated by the matrix. By contrast, in amorphous solid dispersions, the API is molecularly mixed with the carrier in an amorphous state. Through these two methods, the carrier can be used to stabilise an amorphous form or metastable crystalline form to preserve a higher energy state [10].

Similar to co-crystals, solid dispersions with hydrophilic polymers have been shown to increase wettability and to stabilise a supersaturated form of the API in solution through a “spring and parachute” effect [53]. Supersaturation within the formulation generates an API concentration gradient which in turn leads to a further increase in API bioavailability. The extent and duration of this supersaturated state is dependent on the polymer used and is further influenced by using additional excipients such as precipitation inhibitors. Polymer selection dictates the rate of API release from the solid dispersion which can be tailored dependent on the administration route. For example, the use of ionic polymers which show higher water-solubility in certain pH environments can be used to target specific regions of the GIT [54]. Other polymers show sustained release properties for example, solid dispersion of API in cellulose-based polymers show controlled release due to gel formation in an aqueous environment [53, 55].

### 3.4 Coamorphous Forms

Coamorphous solids are a class of solid dispersion composed of a molecular mixture between two amorphous small molecules. Combined, both components stabilise each other in a single amorphous phase through local intermolecular bonding. These interactions can be ionic, like salts, or neutral, like co-crystals leading to further subclassification of these amorphous forms. Coamorphous forms display increased stability yet retain the advantageous of amorphous forms such as enhanced solubility and dissolution properties. Like co-crystals, by using a second small molecule as the coformer, this allows for the possibility of using another API leading to synergistic pharmacokinetic and pharmacodynamic effects through one formulation strategy. Coamorphous forms are an interesting formulation strategy and in recent years have been the subject of review [56].

## 4 Chemical Stability of Salts, Co-crystals, and Solid Dispersions

In addition to physical stability, many APIs are chemically unstable, meaning that they are labile to react or degrade. Common initiators of degradation include: moisture, pH, temperature and light. Of these, the interaction of atmospheric moisture with solid forms is most relevant to crystal engineering formulation strategies. Sorbed moisture from the atmosphere, becomes available for initiating chemical reactions within the formulation. The extent and nature of these reactions are directed by the coformers, counterions and excipients present [57].

The influence of different counterions on the chemical stability of an API is seen clearly in the case of amlodipine [58]. During stability testing, the maleic acid counterion was shown to initiate a Michael addition reaction within the compound in the presence of moisture. This resulted in the chemical degradation of amlodipine and as such, the besylate salt form was favoured as a less hygroscopic and therefore more stable alternative. In general, cocrystals are less hygroscopic than salts and seen as a viable strategy for increasing the chemical stability of hygroscopic APIs [57, 59]. The use of a neutral coformer which is fully incorporated into the crystal structure means there is a lack of available hydrogen bonding regions and no ionised functional groups for atmospheric moisture to interact with. This means that moisture driven chemical degradation is less likely to occur.

By contrast, solid dispersions with hydrophilic polymers can be especially sensitive to moisture sorption since there is likely to be many freely available hydrogen bonding regions [60]. The resulting presence of moisture within the solid dispersion can reduce the glass transition temperature of the amorphous form which increases the likelihood of formulation degradation through API re-crystallisation.

It is almost paradoxical that the increased wettability, and therefore better dissolving, of API solid forms brings with it a more hygroscopic and potentially more chemically unstable compound. It is vital that careful coformer, counterion and excipient selection is carried out in tandem with stability testing at stressed conditions particularly at high relative humidities.

## 5 Coformer, Counterion and Excipient Selection for Salts, Co-crystals, and Solid Dispersions

The selection of a suitable counterion, coformer or polymer carrier is often aided by theoretical models which quantify the molecular compatibility with the API. Molecular

compatibility works on the assumption that to generate a new solid form, molecules of API and excipients must be miscible on a molecular level, on the principle of “like attracting like”. One approach to quantify molecular miscibility is through the use of the total solubility parameter ($\delta_t$); a combination of Hansen Solubility Parameters (HSPs) that describes the total attractive forces for each molecule [61, 62]. Molecular miscibility can then be predicted on a principal that molecules with similar types of intermolecular interactions will have higher affinity for each other [63]. These models have been further adapted for in silico co-crystal coformer screening with high prediction accuracy [64].

Another example is the “Co-crystal design” function of the Cambridge Structural Database’s (CSD) Mercury program which screens an API molecule against a bank of coformers based on molecular compatibility [65]. The tool analyses the crystal structures of molecules and compares key molecule properties which are likely to influence the formation of a co-crystal. These include molecule size and shape, polarity, available hydrogen bond donors and acceptors determined through analysis known co-crystals [65]. Although there are limitations to this tool, it provides a useful starting point for assessing molecular compatibility during the coformer screening process.

Care must be taken when selecting excipients and coformers for pharmaceutical applications to ensure that they will not cause harm to a patient. Databases such as the US FDA’s GRAS (generally regarded as safe) database are a good reference. However, often FDA-approved excipients are required when formulating for specific routes e.g. for pulmonary delivery. Choice of excipients for inhalation is commented on later.

## 6 Preparation of Salts, Co-crystals and Solid Dispersions

Methods for API formulation through crystal engineering are based on generating an environment where intermolecular interactions *within* starting materials are overcome, followed by the formation of new intermolecular interactions *between* the starting materials [21, 66]. These methods can be split into two main categories: solvent-based methods and solid-state methods.

Solvents-based methods require formulation components to be in solution together and following this, saturation, and precipitation or recrystallisation are encouraged. This process can be achieved through solvent evaporation, antisolvent methods or the use of rapid drying techniques such as spray or freeze drying [67, 68]. The rate of recrystallisation and the solvents used direct the nature of the product formed. With solid-state methods, the energy required for the breaking and forming of interactions is added to the system through mechanical force or heat. Milling, extrusion methods and

high-sheer mixing have been shown to successfully produce new solid forms and are seen as a “green” alternative due to their limited use of solvents [69-71].

The milling-based solid-state approach, and the solvent-based spray drying approach are described in further detail below, as these are the most relevant methods for this thesis.

### 6.1 Solid State Preparation – Milling

Ball milling is a common solid-state method where the starting materials and some ball bearings are shaken within a sealed vessel. This method has been used extensively in pharmaceutical research for the generation of new solid forms (**Table 5**) [69, 72, 73].

Starting materials are exposed to mechanical force and a transfer of momentum takes place, initiated by excess kinetic energy, following impact between ball bearings and starting materials [74]. The mass and velocity of the ball bearings are therefore key to amount of energy transferred to the starting materials and thus these parameters dictate the rate and extent of reaction. Ball bearing velocity is directed by the ball bearing material as well as the frequency and duration of the milling process. Studies investigating the process parameters of ball milling show the correlations between frequency of milling, size/weight of balls and milling duration with the success and rate of product formation [74]. This is because the energy imparted by the ball mill needs to be sufficient to both overcome existing, and initiate new, intermolecular interactions.

Co-crystals, salts and polymeric solid dispersions have all been developed successfully through mechanochemical synthesis, but the exact mechanism for the formation of a single solid phase or a molecularly dispersed material has not yet been fully described. Studies suggest that the process is not a single step, but instead that mechanochemical activation leads to molecular diffusion within the starting materials via the formation of a solution, eutectic or amorphous phase [75, 76]. The addition of a small quantity of solvent (0 - 2 $\mu L mg^{-1}$) prior to milling can encourage the initiation of these processes and is known as liquid assisted milling or grinding (LAG) [75, 77]. During LAG, the formation of a new solid form seems to be most successful when API and coformer are both soluble in the solvent, suggesting that addition of solvent encourages miscibility [78]. There is some evidence to suggest that different solvents can drive the selective formation of a certain polymorph [79, 80].

It is important to note that the exact nature of mechanochemical activation will be unique for each set of staring materials and the success of solid dispersion formation is

strongly linked to the intermolecular compatibility of the starting materials for each other. It has also been shown that the addition of certain excipients to the mill with the starting materials can direct the formation of a crystalline or amorphous form and influence the purity of the final product [81].

### 6.1.1 Limitations of Milling

Ball milling is an attractive option for the formation of solid dispersion through a simple, controllable, solvent-free process. However, there are limitations to the method including poor scalability, incomplete starting material activation and risk of agglomeration or thermal degradation due to increased temperatures within the mill [82]. Developing a method with a high reaction rate and complete starting material transformation without over-milling is required, especially when considering large scale applications.

## 6.2 Solvent Based Preparation – Spray Drying

Spray drying is a rapid, single step, solvent-based preparation method where a solution or suspension is rapidly dried by spraying into a hot gas. As a method it is easily scalable and as such has been widely used in industry [83, 84]. Studies show that spray drying can be used for the generation of crystalline and amorphous salts, co-crystals and polymeric solid dispersions (**Table 5**).

The drying process can be summarised through these main processes; the atomisation of the feedstock into droplets, which are then sprayed into a hot gas drying chamber, causing the evaporation of solvent to form a dry solid product. Atomisation is largely directed by the size and type of nozzle used which leads to distinct droplet sizes and distributions. The temperature of the drying gas can also be adjusted to control the rate and extent of drying which in turn influences the solvent content in the final product. With respect to method optimisation, final product characteristics are strongly linked to feedstock composition, flow rate, drying temperatures and the spraying or atomisation process [85].

These process parameters influence the formation and composition of feedstock droplets within the drying chamber. In theory, each droplet will dry to become a powder particle; therefore the drying kinetics directly influence the nature of the particle formed. In general, solvent evaporation will first occur at the surface of the droplet forming a supersaturated region and eventually a solid shell. The drying kinetics following this initial step direct the resulting particle properties and morphology [86]. Drying kinetics

can be summarised through a balance of evaporation rate and solute diffusion motion within the droplet; the ratio of which can be described by the Péclet number [86].

With a low Péclet number (i.e. ≤ 1), solute within the droplet shows a faster or equal velocity to the evaporation rate, meaning the solute will diffuse away from the point of evaporation at the droplet surface to the centre. Since precipitation is likely to occur following solute migration to the droplet centre, the resultant particles are expected to have high density with limited void space. To ensure dense particles even with slow diffusion motion solutes, a low Péclet number can be encouraged by reducing the evaporation rate within the drying process through the formation of large droplets and using relatively low drying temperatures [87, 88].

By contrast, with a large Péclet number (i.e. > 1), the solute within the droplet shows diffusion motion less than the evaporation rate of the droplets during drying. Therefore, the droplet surface becomes enriched with solute, which will form a precipitated shell and then a hollow particle following solvent evaporation through the shell. Formation of hollow particles is therefore encouraged by a rapid drying process for example, when small droplets are formed and using drying temperatures at or above the boiling point of the solvent. This process tends to result in a particle similar to the size and shape of the original droplet, since rapid solvent evaporation prevents the shell from migrating towards the centre of the droplet. However, it is possible for this shell to buckle during the drying process leading to particles with non-spherical morphology. It has also been seen that using temperatures which are too high can result in particles breaking apart due to increased pressure build up within the outer shell from rapid evaporation of solvent. Therefore, the flexibility, permeability and stability of this shell during drying will determine the particle morphology during evaporation [86]. Péclet number can also be increased by changing the viscosity of the feedstock through addition of polymer excipients or increasing solute concentration. This will influence particle morphology by reducing the diffusion motion of molecules and within the solvent. An understanding of the solute kinetics within the droplet is vital for generation of suitable particles with unique morphologies. Composite particles which contain different proportions of API and excipients at the core compared to the surface have been developed through manipulating feedstock composition and drying conditions [87-89].

As such, spray drying is a highly controllable method for the preparation of solid dispersions through the alteration of key processing parameters, to yield specific particle sizes, densities and flowability. The addition of polymer or small molecule

excipients to the feedstock can generate solid dispersions with increased solution or aerodynamic properties for a variety of pharmaceutical applications (**Table 4**).

### 6.2.1 Spray Drying Limitations

Despite the many pharmaceutical and industrial applications, spray drying is limited by its reliance on large quantities of solvent, with the possibility of incomplete drying, as well as a relatively low production yield (approx. 40%) [84]. Another issue lies with generation of a uniform feedstock, especially when forming solid dispersions with multiple components which are soluble in different solvents. To overcome this, emulsion or suspension feedstocks can be used to combine the components prior to spray drying [90]. Another option is the use of a three-fluid nozzle which keeps the feedstocks separate until they are combined at the point of atomisation [89, 91]. The use of a three fluid nozzle can therefore be used to speed up formulation development since generating a uniform emulsion or suspension can be challenging.

**Table 4:** examples of solid dispersions generated through milling and spray drying.

| Method | API | Excipients | Final Product | Application | Ref. |
|---|---|---|---|---|---|
| Ball Milling | Sulphonamide | PVP<br>Soluplus® | Amorphous solid dispersion | - | [92] |
| Ball Milling | Acyclovir | Chitosan<br>HPMC | Amorphous solid dispersion | Enhanced dissolution, stable amorphous phase | [93] |
| Ball Milling | Olanzapine | Salicylic Acid<br>2ATPA<br>Anthranilic Acid<br>Resorcinol<br>Phenol | Crystalline salts and co-crystals | Salts showed enhanced solubility and dissolution | [94] |
| Ball Milling | Brexpiprazole | Succinic Acid<br>Catechol | Co-crystals | Enhanced solubility and dissolution | [95] |
| Spray Drying<br>(Two- Fluid Nozzle) | Theophylline | Urea<br>Saccharin<br>Nicotinamide | Co-crystals | Good aerosol performance compared to starting material. Lower surface energy compared to milling. | [96] |
| Spray Drying<br>(Two- Fluid Nozzle) | Dapsone | Caffeine | Co-crystal | Improved cell membrane permeability | [97] |
| Spray Drying<br>(Two- Fluid Nozzle) | Ibuprofen | PVP | Co-crystal within polymer matrix or co-amorphous solid dispersion | - | [71] |
| Spray Drying<br>(Two- Fluid Nozzle) | Ketoprofen | PVP | Amorphous solid dispersion | Enhanced dissolution | [98] |
| Spray Drying<br>(Two- Fluid Nozzle) | Indomethacin | L-Arginine<br>L-Histidine<br>L-Lysine | Co-amorphous salt formation | Enhanced dissolution | [99] |
| Spray Drying<br>(Three-Fluid Nozzle) | Resveratrol | Curcumin<br>CMC<br>SA | Encapsulation within SA/CMC microparticles | Resveratol core and Curcumin at the surface.<br>Controlled release of Resveratol | [89] |

PVP = Polyvinylpyrrolidone, HPMC = Hydroxypropyl methyl cellulose, 2ATPA =2-Aminoterephthalic acid, CMC = Carboxy methyl Cellulose, SA = Sodium Alginate.

## 7 Solid Form Characterisation Techniques

Careful characterisation is required following crystal engineering of APIs to determine the solid-state properties and whether multicomponent solid forms are present.

### 7.1 Solid Phase Identification

Solid phases and their nature, i.e. crystalline or amorphous can be clearly identified using X-ray diffraction and thermal analysis [100, 101].

#### 7.1.1 X-ray diffraction

Since crystalline materials are in a highly ordered state, when a single crystal is exposed to X-rays, diffraction spots of varying intensity occur at unique angles directly corresponding to the regular arrangement of atoms in the crystal structure. The relationship between atomic arrangement in a crystal and X-ray diffraction angle is explained through Bragg's Law, allowing access to interplanar spacings in the crystal [102]. Diffracted intensity is related to the types and positions of atoms within the unit cell of the crystal. Many computer programs have been developed to allow the conversion of angle and intensity information about diffraction features into a full 3D crystal structure. If single crystals of a material cannot be obtained, then powder X-ray diffraction (PXRD) can still be performed on the material. If the powdered material is crystalline, it is referred to as 'polycrystalline' and diffraction from it takes the form diffraction peaks occurring at particular 2θ angles (**Figure 1**).

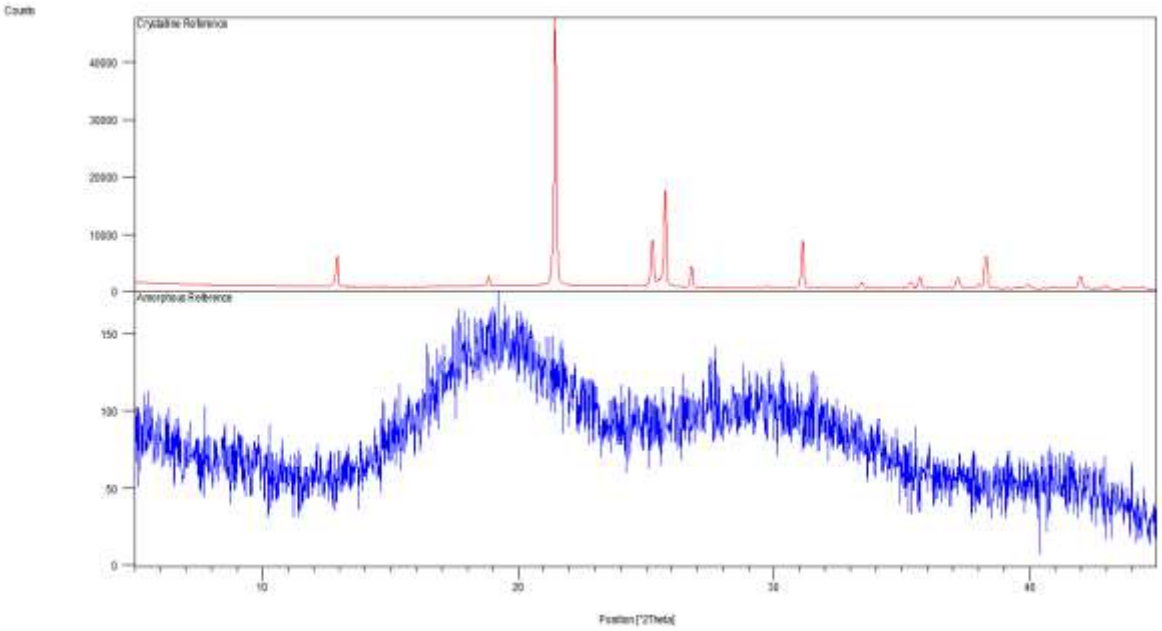


**Figure 1:** X-ray diffraction data comparing a crystalline material (Red) with an amorphous material (Blue).

In contrast, amorphous materials show no such sharp diffraction peaks, as there is no long-range order of molecules within the sample; rather, a so-called “amorphous hump” is seen (**Figure 1**).

Crystalline phases within a sample can also be identified through PXRD, since the diffraction pattern for a crystalline material is unique. If there has been the formation of a new crystalline phase, such as in salt or co-crystal formation, a unique PXRD pattern compared to those of starting materials will be seen. This comparison will also show if there is any residual starting material phases within the final product. If a novel composite phase has formed, crystal structure determination using single crystal X-ray diffraction can be used, provided that a single crystal of sufficient size (typically at least around 50 microns in each dimension) can be obtained. With a high-quality single crystal, often formed through a slow evaporation method, a crystal structure to atomic resolution can be obtained, and nature of intra/intermolecular interactions can be determined. When a new phase exists as a powder (as it generally the case for ball-milled samples), PXRD can be used to determine the crystal structure. Whilst the lower information content (relative to single-crystal diffraction data) of PXRD data means that crystal structures cannot be obtained with the same level of detail (e.g. they are lower resolution, and generally do not have anisotropic temperature factors), structure determination from powder diffraction data is a powerful approach [103, 104].

### 7.1.2 Thermal Analysis

A highly ordered crystalline state also gives a solid a distinct melting point during heating since the same amount of energy is required to overcome all bonds in the solid during the phase change. By contrast, on heating, an amorphous material will change from a glassy to rubbery state over a temperature range and this change of state is called a glass transition. Melting and glass transition can be observed using differential scanning calorimetry (DSC), which measures the heat flow for a material during thermal events. A melting point will be seen as a sharp endothermic peak compared to glass transition which is seen as a step [105] (**Figure 2**). DSC can be used to identify whether a new material has been formed through melting point analysis. If a new crystal structure is present, there will be a single crystalline melting point as opposed to multiple thermal events seen with physical mixtures.

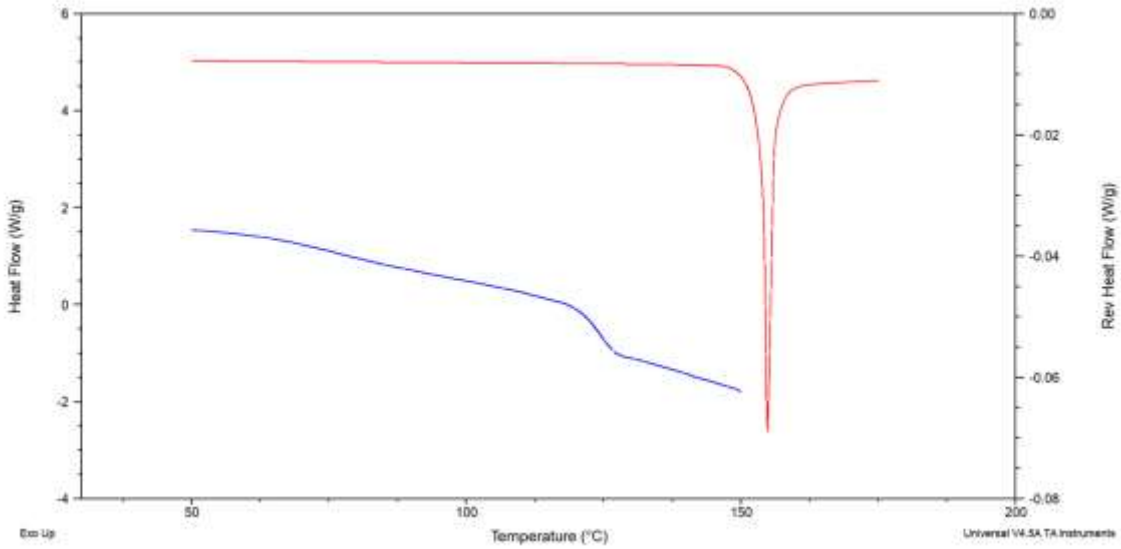


**Figure 2:** Differential scanning calorimetry data comparing a crystalline material melting point (Red) with an amorphous material glass transition (Blue).

7.2 Characterisation of Intermolecular Bonding via Spectroscopy

In the absence of a crystal structure, spectroscopy can be used to further understand the bonding within crystalline and amorphous solid forms. Fourier-transform infrared spectroscopy (FTIR) measures how much light a molecule absorbs over an IR range of wavelengths. Absorbed energy causes stretching and bending within molecules containing dipole moments, at specific frequencies corresponding to functional groups. Therefore, the quantity and frequency at which a molecule absorbs infrared radiation is directly linked to chemical structure. Specific functional groups can be identified by their absorption and whether or not they are involved in intermolecular bonding. For example, an ionised and unionised carboxylic acid group will display different absorption frequencies and for different polymorphs of the same API, absorption associated with the same functional group will often appear at slightly different wavelengths [106, 107]. Therefore, FTIR can be used to distinguish between physical mixtures and new solid forms, and to identify ionic or hydrogen bond formation.

When using FTIR for analysis of formulations with multiple components, for example with API and excipients, overlapping absorption can occur. This is a major limitation of the technique as key absorption bands can be masked by these components. In these situations, other spectroscopic techniques such as Raman spectroscopy can be used [108]. Raman spectroscopy focuses monochromatic light, usually in the form of a laser, onto a sample to cause excitation, and then measures the resulting scattering of photons. Scattering of a different energy to that of the original exciting photon is caused by the polarising of bonds within an excited molecule. Since polarisation is mostly seen in bonds

without existing dipole moments, functional groups which do not readily absorb infrared light are often Raman active. This can be useful particularly if an excipient absorbs infrared light at the same frequency as a key functional group. Raman spectroscopy can be used to map an area of sample to identify presence of API or excipients. This is particularly useful for assessing the uniformity of a solid dispersion or for quality control following tablet formation [109, 110].

### 7.3 Scanning Electron Microscopy (SEM) and Energy-Dispersive X-ray Analysis (EDX)

Sample morphology and chemical composition can be determined by using scanning electron microscopy (SEM) combined with energy-dispersive X-ray (EDX) analysis. During SEM analysis, a sample is exposed to a high energy electron beam, which causes two main types of responding signals: backscattered electrons and secondary electrons. These signals are related to the atomic number of atoms at the material surface and the general topography of the sample, and as such, high resolution images can be generated. The quality of these images is increased by coating samples with a thin layer of gold, which ensures a homogenous surface with respect to conductivity and emission of electrons. In addition to electron signals, X-rays of characteristic energy are also generated following ionisation by the SEM beam, relating to the unique number and arrangement of electrons within the atoms of a sample. The wavelengths of X-rays generated, and their relative proportions are analysed to give qualitative and quantitative information regarding the types of elements present in the sample. As such, surface coating with gold is not beneficial as X-ray emitted by gold atoms will cause interference. EDX is particularly useful for identifying compounds containing unique atoms within an amorphous solid dispersion. For example, the presence of indomethacin was detected within an amorphous solid dispersion using EDX by identifying X-rays associated with chlorine atoms, that could only be associated with the indomethacin molecule [111].

## 8 Applications of crystal engineering for Oral Drug Delivery

### 8.1 Solubility and Permeability for Oral Drug Delivery

Following oral administration, an API needs to dissolve in the GIT and then partition across epithelial membranes into systemic circulation. For most APIs the site of absorption is the small intestine where the API must be in aqueous solution as a prerequisite for partitioning out of the GIT through the intestinal wall [4]. Once in the blood stream, the API is transported to the site of action via bulk flow mechanisms; this process is not influenced by the chemical nature of the API. Therefore, aqueous solubility and epithelial permeability are key factors in determining the extent of absorption and therefore bioavailability of an API.

Amidon et al. first proposed a system (the Biopharmaceutical Classification System, BCS) to predict in-vivo bioavailability by categorising APIs based on their solubility and permeability and this system is now widely used [112, 113]. The BCS groups APIs into four classes of either high or low solubility and high or low permeability. Solubility is defined as the volume of aqueous media required to dissolve the highest dose at specified temperature and pH. Permeability is defined as the dose fraction absorbed to systemic circulation compared to an intravenous dose [112, 114]. APIs in classes 2 and 4, which exhibit low solubility with high and low permeability respectively, are prime targets for formulation development through solubility enhancement strategies. In recent years, projects such as the OrBiTo industry-academic collaboration have sought to further understand the processes of oral absorption of APIs [115]. Following this research, a greater emphasis has been put on how gut physiological differences influence permeability as well as the importance of using biologically relevant in-vitro solution testing [116-118].

## 9 Applications of crystal engineering for Pulmonary Drug Delivery

### 9.1 Solubility and Permeability for Pulmonary Drug Delivery

Like in oral drug delivery, the solubility and permeability of a molecule has great influence on the effectiveness of administration via the inhaled route. These factors have been shown to influence API retention time in either the lung lumen or tissue and then the extent of absorption into the systemic circulation [119]. For example, an API which shows high solubility and rapid dissolution in lung fluid will show greater partitioning into the systemic circulation with shorter retention time in the lung lumen and tissue. Formulation strategies to modify API solubility and dissolution can be implemented to encourage specific partitioning either residing in the lung tissue or entering systemic circulation, dependent on the API site of action.

Excipients have also been shown to enhance the absorption of APIs into lung tissues through the formation of ion-pair complexes. These complexes form between oppositely charged molecules in a saturated solution and although temporary species, possess distinct chemical properties. For example, Benaouda et al demonstrated that uptake of theophylline into the lung tissue was enhanced by preparing a formulation containing a polyamine transporter system substrate [120]. The theophylline and substrate were combined in solution as an ion-pair then delivered to the lung. *In-vivo* models demonstrated that the theophylline was being actively transported into the lung tissues through the polyamine transporter system in tandem with the substrate. Although this is in the liquid state, it is possible that ion-pairs will form when multicomponent crystals dissolve in small volumes of lung fluid.

To streamline and de-risk the formulation development process for inhaled products, the inhaled BCS (iBCS) [121, 122] classification system has been suggested. Operating in a similar vein to the oral BCS, APIs are separated into four categories depending on their solubility and permeability. Like the oral BCS, a category 1 iBCS API will display rapid absorption from the lung lumen and category 2 – 4 APIs will have reduced or incomplete absorption due to poor solubility or permeability. However, the principles from the oral model need to be adapted before they can be calculated for an inhaled context. Particular attention is made to how lung administration and physiology influences the rate and extent of absorption from the lung lumen into lung tissue.

Instead of solubility and permeability, calculated output parameters called $t_{1/2,lung}$ (API half-life in lung lumen) and $F_{abs,lung}$ (extent of available lung absorbed into lung tissue) are used as molecular descriptors in the context of the lung. These two parameters are strongly influenced by the dose and deposition pattern of API, the solubility and rate of API dissolution, and the rate of API clearance from the lung.

Dose calculation in the lung is not as simple as for the GIT and is often related to formulation design as commented upon in section 8.2. One key difference between dosing in the lungs and GIT is that all regions of the lung will receive API at the same time rather than through a “plug flow” model. Therefore, dissolution and absorption are taking place simultaneously in all areas of the lung rather than regionally as is the case in the GIT. Since physiology varies between regions of the lung (**Figure 3**), the extent and type of absorption will also differ. Therefore, an accurate prediction of the quantity of API depositing in each lung region is required for calculating the available dose in the lung.

Dissolution in the lungs also varies substantially compared to the GIT, due to the small volume of lung fluid present, the lack of pH variation, the presence of surfactants, the API dissolving on a surface (rather than being in bulk solution) and the lack of any “plug flow” through the lungs. In-vitro models must also consider the influence of deposited particle size, morphology, solid-state properties, and presence of excipients since dissolution will not occur in sink conditions. As such, the dissolution rate rather than the solubility can be the limiting factor for absorption into the lung tissue [123].

Clearance of API from the lungs occurs either through absorption into the lung tissues or via excretion mechanisms such as macrophage or mucociliary clearance, dependent on the lung region (**Figure 3**). Absorption clearance will mainly affect rapidly dissolving particles in the lower airways and mucociliary clearance will mainly affect slowly dissolving particles in the upper airways. Due to this close link between dissolving and clearance out of the lung or

into the lung tissue, it has been concluded that in contrast to the GIT, dissolution rate is a more significant factor for measuring API availability than solubility [123].

Adapting the parameters used in the original BSC to include regional dosing, dissolution rate and type of clearance allows the model to be adapted to the inhaled route and provide a quantifiable means of classification. Predictions can then be made whether an API will reside in the local tissue or partition into the systemic circulation and therefore direct formulation developments accordingly.

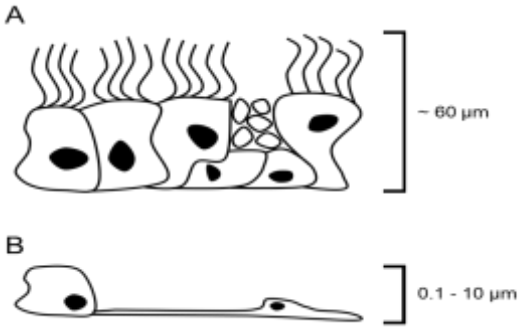


**Figure 3:** A schematic to show a cross section of epithelial cells in different regions of the lung. **A)** Upper airways (bronchi) showing ciliated, goblet and basal cells. **B)** Lower airways (alveoli) showing squamous epithelium with type I and type II cells.

9.2 Additional Considerations for Pulmonary Drug Delivery

When delivering API to the lungs, the formulation must be able to produce an inhalable aerosol. Early inhaler technology relied on the use of pressurised metered dose inhalers (pMDIs), which form an aerosol by releasing a fine spray of an API solution, or suspension, in a volatile propellent [124]. Due to the low dosing efficiency associated with pMDIs, dry powder inhaler (DPI) technology was developed [125, 126].

Traditionally, DPIs use a physical mixture of micronised API with large carrier particles which separate on inhalation to form a fine powder aerosol. On inhalation, the carrier and API particles separate, leaving the API to be inhaled and the carrier to impact into the throat and be swallowed. To achieve this, the API and carrier must be in a fixed ratio which puts a practical dose limit on the amount of powder and therefore API which can be inhaled [126, 127]. APIs delivered through these pMDI and DPI systems are the backbone of current asthma and COPD therapy. The development of carrier-free DPI technology has become a key area of research to achieve inhalable dry powders without the use of carrier particles. A carrier-free formulation will not have the dose limitations associated with current DPIs and as such will make the inhaled route more feasible for APIs requiring higher doses [127]. This is

particularly relevant for the development of locally acting inhaled antibiotics. Generating solid dispersions of API and excipients through a crystal engineering approach using spray drying has proved to be a promising area of research [128]. When formulating carrier free DPI formulations care must be taken in excipient selection. **Table 5** summarises the FDA-approved excipients for dry powder inhalation, which illustrates how limited this list is for excipients that are permitted in such licenced drug products. Potency per unit dose is described as the current highest quantity of excipient included in a marketed product per unit dose of that medication.

**Table 5:** Inactive ingredients in FDA approved dry powder inhalation products

| Excipient | Potency per Unit Dose | Maximum Daily Exposure | Literature Examples |
|---|---|---|---|
| Carrageenan | 0.42 mg | - | [129] |
| Ferric oxide yellow | 0.04 mg | - | - |
| Gelatin | 100 mg | - | [130] |
| Glycine | - | 2 mg | [131] |
| Hypromellose (4 mpa.S) | 45.67 mg | - | [132] |
| Lactose Monohydrate | - | 25 mg | [133] |
| Magnesium stearate | 0.08 mg | - | [134] |
| Mannitol | - | 6 mg | [135] |
| Potassium chloride | 0.18 mg | - | - |
| Titanium dioxide | 2 mg | - | - |
| Trisodium citrate dihydrate | - | 17 mg | - |

mpa.S = millipascal per second, dynamic viscosity measurement.

## 10 Aims and Objectives

Poor aqueous solubility has limited the application of many APIs through the oral route. Therefore, repurposing APIs for delivery through the inhaled route can be an effective option for increasing bioavailability. Any inhalable formulation will need to address the dose limitations of current dry powder inhalation technology through a carrier-free formulation strategy. These aims can be achieved through API formulation development, especially through the generation of new solid forms. Solid dispersions of API co-crystal and salt forms produced through a scalable process such as spray drying are an attractive option.

Therefore, it is the overall aim of this thesis to evaluate:

1. Whether salts and co-crystals of existing APIs can be formed to affect aqueous solubility and control of release.
2. Whether these salts and co-crystals can be prepared then formulated through a crystal engineering spray drying approach.

The organisation of this thesis is summarised in **Figure 4**. Chapters 1 and 2 are included as a general background to the area. Chapter 2 reviews the current advances in the generation of solid dispersions and co-crystals for high dose carrier-free dry powder inhalation. The review takes particular interest in the inhalation of antimicrobials and anticancer therapies, seen as model APIs which require high doses at the site of action to achieve their therapeutic effect.

The repurposing of the antibiotic ciprofloxacin to a controlled release inhaled formulation for local administration is then explored through Chapters 3 and 4. Four new salt forms of ciprofloxacin with biologically relevant organic acids were generated and fully characterised. These salt forms were then formulated into solid dispersions with hydroxypropyl methylcellulose (HPMC) using contrasting three-fluid spray drying methods and their *in vitro* inhalation and solution properties assessed as well as *in vivo* oral absorption.

The repurposing of the hormone progesterone into an inhaled formulation for systemic administration was explored in Chapter 5. A two-fluid spray drying method with the addition of L-leucine and hydroxypropyl methylcellulose acetate succinate (HPMCAS) was used to generate stabilised inhalable powders of the more water-soluble polymorph. The effect of the spray drying solvent system was also assessed with respect to the final product invitro inhalation properties. Chapter 6 follows on from this work by exploring a co-crystallisation approach for improving the solution properties of progesterone. The full structure of a co-crystal of progesterone and para-aminobenzoic acid is reported with preliminary aqueous solubility and dissolution data for a tablet formulation compared to a current marketed product.

In Chapter 7, the feasibility of the spray drying method to produce co-crystals through a rapid, single step method was assessed using the model system of salicylic acid and caffeine. Detailed are the comparison of two-fluid and three-fluid nozzle spray drying from a variety of solvent systems as well as initial tabletting studies.

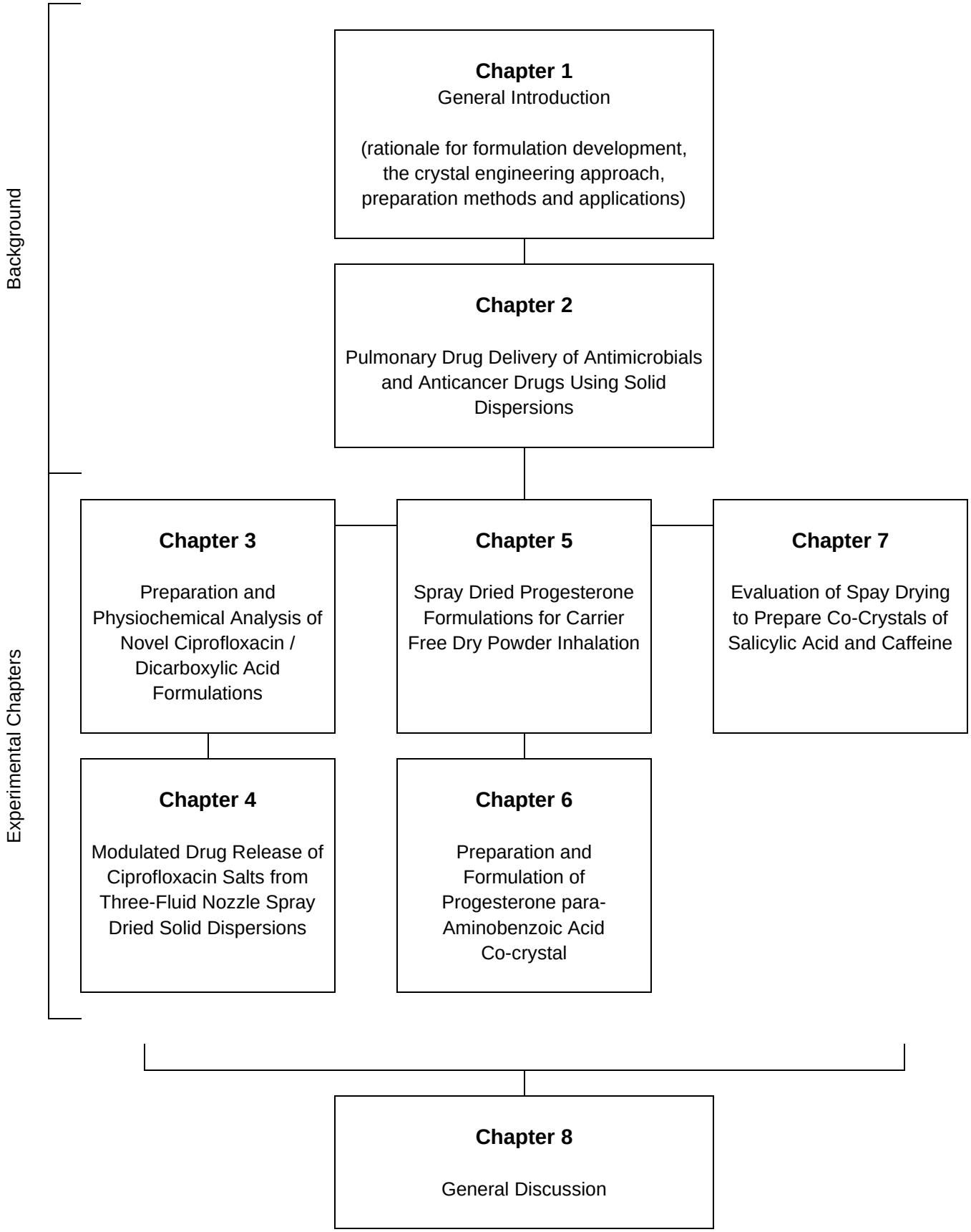


**Figure 4:** Schematic to represent the structure of this PhD Thesis

## References


1. Y. Kawabata, K. Wada, M. Nakatani, S. Yamada and S. Onoue, *International Journal of Pharmaceutics*, 2011, **420**, 1-10.
2. C. A. Lipinski, F. Lombardo, B. W. Dominy and P. J. Feeney, *Advanced Drug Delivery Reviews*, 1997, **23**, 3-25.
3. S. Jain, N. Patel and S. Lin, *Drug Development and Industrial Pharmacy*, 2015, **41**, 875-887.
4. M. S. Alqahtani, M. Kazi, M. A. Alsenaidy and M. Z. Ahmad, *Frontiers in Pharmacology*, 2021, **12**.
5. S. P. Newman, *Advanced Drug Delivery Reviews*, 2018, **133**, 5-18.
6. S. P. Newman, *Therapeutic Delivery*, 2017, **8**, 647-661.
7. H. Zhang, X. Huang, Y. Sun, G. Lu, K. Wang, Z. Wang, J. Xing and Y. Gao, *International Journal of Pharmaceutics*, 2015, **489**, 294-303.
8. A. Tronde, B. o. Nordén, H. Marchner, A. K. Wendel, H. Lennernäs and U. H. Bengtsson, *Journal of Pharmaceutical Sciences*, 2003, **92**, 1216-1233.
9. D. Gupta, D. Bhatia, V. Dave, V. Sutariya and S. Varghese Gupta, *Molecules*, 2018, **23**.
10. N. Blagden, M. de Matas, P. T. Gavan and P. York, *Advanced Drug Delivery Reviews*, 2007, **59**, 617-630.
11. Z. Gao, S. Rohani, J. Gong and J. Wang, *Engineering*, 2017, **3**, 343-353.
12. S. Saha, M. K. Mishra, C. M. Reddy and G. R. Desiraju, *Accounts of Chemical Research*, 2018, **51**, 2957-2967.
13. G. R. Desiraju, *Journal of the American Chemical Society*, 2013, **135**, 9952-9967.
14. A. J. Cruz-Cabeza, *CrystEngComm*, 2012, **14**, 6362-6365.
15. M. F. Pina, M. Zhao, J. F. Pinto, J. J. Sousa, C. S. Frampton, V. Diaz, O. Suleiman, L. Fábián and D. Q. M. Craig, *Crystal Growth & Design*, 2014, **14**, 3774-3782.
16. P. H. Stahl and C. G. Wermuth, *Pharmaceutical salts: Properties, selection and use*, John wiley & sons, 2002.
17. G. Kuminek, F. Cao, A. Bahia de Oliveira da Rocha, S. Gonçalves Cardoso and N. Rodríguez-Hornedo, *Advanced Drug Delivery Reviews*, 2016, **101**, 143-166.
18. M. Karimi-Jafari, L. Padrela, G. M. Walker and D. M. Croker, *Crystal Growth & Design*, 2018, **18**, 6370-6387.
19. N. Qiao, M. Li, W. Schlindwein, N. Malek, A. Davies and G. Trappitt, *International Journal of Pharmaceutics*, 2011, **419**, 1-11.
20. I. Sathisaran and S. V. Dalvi, *Pharmaceutics*, 2018, **10**.
21. G. Bolla, B. Sarma and A. K. Nangia, *Chemical Reviews*, 2022, **122**, 11514-11603.
22. J. F. Remenar, S. L. Morissette, M. L. Peterson, B. Moulton, J. M. MacPhee, H. R. Guzmán and Ö. Almarsson, *Journal of the American Chemical Society*, 2003, **125**, 8456-8457.
23. D. D. Bavishi and C. H. Borkhataria, *Progress in Crystal Growth and Characterization of Materials*, 2016, **62**, 1-8.
24. A. V. Trask, W. D. S. Motherwell and W. Jones, *Crystal Growth & Design*, 2005, **5**, 1013-1021.
25. S. L. Childs, G. P. Stahly and A. Park, *Molecular Pharmaceutics*, 2007, **4**, 323-338.
26. J. D. Loya, S. J. Li, D. K. Unruh and K. M. Hutchins, *Supramolecular Chemistry*, 2019, **31**, 558-564.

27. A. O. L. Évora, C. E. S. Bernardes, M. F. M. Piedade, A. C. L. Conceição and M. E. Minas da Piedade, *Crystal Growth & Design*, 2019, **19**, 5054-5064.
28. E. A. Losev and E. V. Boldyreva, *CrystEngComm*, 2018, **20**, 2299-2305.
29. K. V. Drozd, A. N. Manin, A. V. Churakov and G. L. Perlovich, *European Journal of Pharmaceutical Sciences*, 2017, **99**, 228-239.
30. S. Ketkar, S. K. Pagire, N. R. Goud, K. Mahadik, A. Nangia and A. Paradkar, *Crystal Growth & Design*, 2016, **16**, 5710-5716.
31. K. V. Drozd, A. N. Manin, A. V. Churakov and G. L. Perlovich, *CrystEngComm*, 2017, **19**, 4273-4286.
32. Q. Fu, Y. Han, Y.-f. Xie, N.-b. Gong and F. Guo, *Journal of Molecular Structure*, 2018, **1168**, 145-152.
33. V. G. Rajurkar, *Medicinal Chemistry*, 2015, **08**.
34. R. Khatioda, B. Saikia, P. J. Das and B. Sarma, *CrystEngComm*, 2017, **19**, 6992-7000.
35. S. Shewale, A. S. Shete, R. C. Doijad, S. S. Kadam, V. A. Patil and A. V. Yadav, *Indian J Pharm Sci*, 2015, **77**, 328-334.
36. B. C. Dayo Owoyemi, C. C. P. Da Silva, M. S. Souza, L. F. Diniz, J. Ellena and R. L. Carneiro, *Crystal Growth and Design*, 2019, **19**, 648-657.
37. A. O. Surov, A. N. Manin, A. P. Voronin, D. E. Boycov, O. V. Magdysyuk and G. L. Perlovich, *Crystal Growth & Design*, 2019, **19**, 5751-5761.
38. M. Banik, S. P. Gopi, S. Ganguly and G. R. Desiraju, *Crystal Growth & Design*, 2016, **16**, 5418-5428.
39. B. B. C. Holanda, R. T. Alarcon, C. Gaglieri, A. R. de Souza, R. A. E. Castro, P. C. P. Rosa, D. J. A. Tangerino and G. Bannach, *Journal of Thermal Analysis and Calorimetry*, 2019, **136**, 2049-2062.
40. A. Samie, G. R. Desiraju and M. Banik, *Crystal Growth & Design*, 2017, **17**, 2406-2417.
41. K. Chadha, M. Karan, Y. Bhalla, R. Chadha, S. Khullar, S. Mandal and K. Vasisht, *Crystal Growth and Design*, 2017, **17**, 2386-2405.
42. P. Sanphui, V. K. Devi, D. Clara, N. Malviya, S. Ganguly and G. R. Desiraju, *Molecular Pharmaceutics*, 2015, **12**, 1615-1622.
43. Y. Wei, L. Zhang, N. Wang, P. Shen, H. Dou, K. Ma, Y. Gao, J. Zhang and S. Qian, *Crystal Growth & Design*, 2018, **18**, 7343-7355.
44. J. Cadden, W. T. Klooster, S. J. Coles and S. Aitipamula, *Crystal Growth & Design*, 2019, **19**, 3923-3933.
45. Y. Yan, J.-M. Chen and T.-B. Lu, *CrystEngComm*, 2015, **17**, 612-620.
46. N. Kumari, B. Bhattacharya, P. Roy, A. A. L. Michalchuk, F. Emmerling and A. Ghosh, *Crystal Growth & Design*, 2019, **19**, 6482-6492.
47. I. Sopyan, A. Fudholi, M. Muchtaridi, I. Puspita Sari and A. Fudholi, *Journal of Young Pharmacists*, 2017, **9**, 183-186.
48. I. Sopyan, A. Fudholi, M. Muchtaridi and I. Puspita Sari, *Tropical Journal of Pharmaceutical Research*, 2017, **16**, 297-297.
49. S. Aitipamula, P. S. Chow and R. B. H. Tan, *Crystal Growth & Design*, 2014, **14**, 6557-6569.
50. S. Aitipamula, A. B. H. Wong and P. Kanaujia, *Journal of Pharmaceutical Sciences*, 2018, **107**, 604-611.
51. C. L.-N. Vo, C. Park and B.-J. Lee, *European Journal of Pharmaceutics and Biopharmaceutics*, 2013, **85**, 799-813.

52. B. J. Boyd, C. A. S. Bergström, Z. Vinarov, M. Kuentz, J. Brouwers, P. Augustijns, M. Brandl, A. Bernkop-Schnürch, N. Shrestha, V. Préat, A. Müllertz, A. Bauer-Brandl and V. Jannin, *European Journal of Pharmaceutical Sciences*, 2019, **137**, 104967.
53. A. Butreddy, *European Journal of Pharmaceutics and Biopharmaceutics*, 2022, **177**, 289-307.
54. T. Yoshida, T. C. Lai, G. S. Kwon and K. Sako, *Expert Opin Drug Deliv*, 2013, **10**, 1497-1513.
55. J. Siepmann and N. A. Peppas, *Advanced Drug Delivery Reviews*, 2001, **48**, 139-157.
56. J. Liu, H. Grohganz, K. Löbmann, T. Rades and N. J. Hempel, *Pharmaceutics*, 2021, **13**.
57. M. R. Dhondale, P. Thakor, A. G. Nambiar, M. Singh, A. K. Agrawal, N. R. Shastri and D. Kumar, *Pharmaceutics*, 2023, **15**.
58. C. J. Andres and R. L. Treanor, in *Annual Reports in Medicinal Chemistry*, ed. J. E. Macor, Academic Press, 2010, vol. 45, pp. 449-463.
59. P. Guerrieri, K. Jarring and L. S. Taylor, *Journal of Pharmaceutical Sciences*, 2010, **99**, 3719-3730.
60. N. G. Patel, S. Banella and A. T. M. Serajuddin, *International Journal of Pharmaceutics*, 2023, **636**, 122745.
61. C. M. Hansen, *Hansen Solubility Parameters: A User's Handbook*, CRC Press, 2007.
62. E. Stefanis and C. Panayiotou, *International Journal of Thermophysics*, 2008, **29**, 568-585.
63. X. Chen, I. Partheniadis, I. Nikolakakis and H. Al-Obaidi, *Polymers*, 2020, **12**.
64. M. A. Mohammad, A. Alhalaweh and S. P. Velaga, *International Journal of Pharmaceutics*, 2011, **407**, 63-71.
65. L. Fábián, *Crystal Growth & Design*, 2009, **9**, 1436-1443.
66. S. V. Bhujbal, B. Mitra, U. Jain, Y. Gong, A. Agrawal, S. Karki, L. S. Taylor, S. Kumar and Q. Zhou, *Acta Pharmaceutica Sinica B*, 2021, **11**, 2505-2536.
67. S. Jia, P. Yang, Z. Gao, Z. Li, C. Fang and J. Gong, *CrystEngComm*, 2022, **24**, 3122-3135.
68. J. Weng, S. N. Wong, X. Xu, B. Xuan, C. Wang, R. Chen, C. C. Sun, R. Lakerveld, P. C. L. Kwok and S. F. Chow, *Crystal Growth & Design*, 2019, **19**, 2736-2745.
69. L. M. Martínez, J. Cruz-Angeles, M. Vázquez-Dávila, E. Martínez, P. Cabada, C. Navarrete-Bernal and F. Cortez, *Journal*, 2022, **14**.
70. S. Korde, S. Pagire, H. Pan, C. Seaton, A. Kelly, Y. Chen, Q. Wang, P. Coates and A. Paradkar, *Crystal Growth & Design*, 2018, **18**, 2297-2304.
71. D. Walsh, D. R. Serrano, Z. A. Worku, A. M. Madi, P. O'Connell, B. Twamley and A. M. Healy, *International Journal of Pharmaceutics*, 2018, **551**, 241-256.
72. D. Tan, L. Loots and T. Friščić, *Chemical Communications*, 2016, **52**, 7760-7781.
73. X. Chen, I. Partheniadis, I. Nikolakakis and H. Al-Obaidi, *Polymers (Basel)*, 2020, **12**.
74. A. A. L. Michalchuk, I. A. Tumanov and E. V. Boldyreva, *CrystEngComm*, 2019, **21**, 2174-2179.
75. T. Friščić and W. Jones, *Crystal Growth & Design*, 2009, **9**, 1621-1637.
76. P. P. Mazzeo, M. Prencipe, T. Feiler, F. Emmerling and A. Bacchi, *Crystal Growth & Design*, 2022, **22**, 4260-4267.
77. P. Ying, J. Yu and W. Su, *Advanced Synthesis & Catalysis*, 2021, **363**, 1246-1271.
78. T. Friščić, S. L. Childs, S. A. A. Rizvi and W. Jones, *CrystEngComm*, 2009, **11**, 418-426.

79. F. Fischer, A. Heidrich, S. Greiser, S. Benemann, K. Rademann and F. Emmerling, *Crystal Growth & Design*, 2016, **16**, 1701-1707.
80. A. Chatziadi, E. Skořepová, J. Rohlíček, M. Dušek, L. Ridvan and M. Šoóš, *Crystal Growth & Design*, 2020, **20**, 139-147.
81. R. Shaikh, S. Shirazian, S. Guerin, E. Sheehan, D. Thompson, G. M. Walker and D. M. Croker, *International Journal of Pharmaceutics*, 2021, **601**, 120514.
82. S. Mateti, M. Mathesh, Z. Liu, T. Tao, T. Ramireddy, A. M. Glushenkov, W. Yang and Y. I. Chen, *Chemical Communications*, 2021, **57**, 1080-1092.
83. B. Wang, F. Liu, J. Xiang, Y. He, Z. Zhang, Z. Cheng, W. Liu and S. Tan, *International Journal of Pharmaceutics*, 2021, **594**, 120165.
84. R. Bellinghausen, *Drying Technology*, 2019, **37**, 612-622.
85. R. Vehring, *Pharmaceutical Research*, 2008, **25**, 999-1022.
86. J. Vicente, J. Pinto, J. Menezes and F. Gaspar, *Powder Technology*, 2013, **247**, 1-7.
87. A. Lechanteur and B. Evrard, Pharmaceutics, 2020, **12**.
88. J. Archer, J. S. Walker, F. K. A. Gregson, D. A. Hardy and J. P. Reid, *Langmuir*, 2020, **36**, 12481-12493.
89. M. Maria Leena, M. Gover Antoniraj, J. A. Moses and C. Anandharamakrishnan, *Journal of Drug Delivery Science and Technology*, 2020, **57**, 101678.
90. L. M. De Mohac, B. Raimi-Abraham, R. Caruana, G. Gaetano and M. Licciardi, *Journal of Drug Delivery Science and Technology*, 2020, **57**, 101750.
91. S. Focaroli, G. Jiang, P. Connell, J. V. Fahy and A.-M. Healy, *Pharmaceutics*, 2020, **12**.
92. V. Caron, Y. Hu, L. Tajber, A. Erxleben, O. I. Corrigan, P. McArdle and A. M. Healy, *AAPS PharmSciTech*, 2013, **14**, 464-474.
93. V. Nart, M. T. França, D. Anzilaggo, M. K. Riekes, J. M. Kratz, C. E. M. de Campos, C. M. O. Simões and H. K. Stulzer, *Materials Science and Engineering: C*, 2015, **53**, 229-238.
94. W. Gong, P. K. Mondal, S. Ahmadi, Y. Wu and S. Rohani, *International Journal of Pharmaceutics*, 2021, **608**, 121063.
95. M. R. Arabiani, B. R. K, S. Bhunia, P. K. Teja, A. Lodagekar, R. B. Chavan, N. R. Shastri, C. M. Reddy, P. Shelat and D. Dave, *CrystEngComm*, 2019, **21**, 6703-6708.
96. A. Alhalaweh, W. Kaialy, G. Buckton, H. Gill, A. Nokhodchi and S. P. Velaga, *AAPS PharmSciTech*, 2013, **14**, 265-276.
97. L. H. do Amaral, F. A. do Carmo, M. I. Amaro, V. P. de Sousa, L. C. R. P. da Silva, G. S. de Almeida, C. R. Rodrigues, A. M. Healy and L. M. Cabral, *AAPS PharmSciTech*, 2018, **19**, 2687-2699.
98. E. Browne, R. Charifou, Z. A. Worku, R. P. Babu and A. M. Healy, *International Journal of Pharmaceutics*, 2019, **566**, 173-184.
99. K. T. Jensen, L. I. Blaabjerg, E. Lenz, A. Bohr, H. Grohganz, P. Kleinebudde, T. Rades and K. Löbmann, *Journal of Pharmacy and Pharmacology*, 2016, **68**, 615-624.
100. X. Liu, X. Feng, R. O. Williams and F. Zhang, *Journal of Pharmaceutical Investigation*, 2018, **48**, 19-41.
101. S. Aitipamula and V. R. Vangala, *Journal of the Indian Institute of Science*, 2017, **97**, 227-243.
102. W. H. Bragg, *Philosophical Transactions of the Royal Society of London. Series A, Containing Papers of a Mathematical or Physical Character*, 1997, **215**, 253-274.

103. A. J. Florence, N. Shankland, K. Shankland, W. I. F. David, E. Pidcock, X. Xu, A. Johnston, A. R. Kennedy, P. J. Cox, J. S. O. Evans, G. Steele, S. D. Cosgrove and C. S. Frampton, *Journal of Applied Crystallography*, 2005, **38**, 249-259.
104. A. E. Watts, K. Maruyoshi, C. E. Hughes, S. P. Brown and K. D. M. Harris, *Crystal Growth & Design*, 2016, **16**, 1798-1804.
105. M. H. Chiu and E. J. Prenner, *J Pharm Bioallied Sci*, 2011, **3**, 39-59.
106. C. C. da Silva, F. F. Guimarães, L. Ribeiro and F. T. Martins, *Spectrochimica Acta Part A: Molecular and Biomolecular Spectroscopy*, 2016, **167**, 89-95.
107. R. Tripathi, S. V. Biradar, B. Mishra and A. R. Paradkar, *AAPS PharmSciTech*, 2010, **11**, 1493-1498.
108. D. Hurley, D. Carter, L. Y. Foong Ng, M. Davis, G. M. Walker, J. G. Lyons and C. L. Higginbotham, *Journal of Drug Delivery Science and Technology*, 2019, **53**, 101132.
109. C. Luebbert, C. Klanke and G. Sadowski, *International Journal of Pharmaceutics*, 2018, **535**, 245-252.
110. H. Carruthers, D. Clark, F. C. Clarke, K. Faulds and D. Graham, *Journal of Raman Spectroscopy*, 2022, **53**, 1115-1125.
111. A. Kapourani, E. G. Andriotis, K. Chachlioutaki, K. N. Kontogiannopoulos, P. A. Klonos, A. Kyritsis, E. Pavlidou, D. N. Bikiaris, D. G. Fatouros and P. Barmpalexis, *Molecular Pharmaceutics*, 2021, **18**, 4393-4414.
112. G. L. Amidon, H. Lennernäs, V. P. Shah and J. R. Crison, *Pharmaceutical Research*, 1995, **12**, 413-420.
113. A. Charalabidis, M. Sfouni, C. Bergström and P. Macheras, *International Journal of Pharmaceutics*, 2019, **566**, 264-281.
114. V. P. Shah and G. L. Amidon, *The AAPS Journal*, 2014, **16**, 894-898.
115. M. McAllister and P. Zane, *Molecular Pharmaceutics*, 2017, **14**, 4129-4131.
116. Z. Zhou, C. Dunn, I. Khadra, C. G. Wilson and G. W. Halbert, *Molecular Pharmaceutics*, 2017, **14**, 4132-4144.
117. B. E. Ainousah, J. Perrier, C. Dunn, I. Khadra, C. G. Wilson and G. Halbert, *Molecular Pharmaceutics*, 2017, **14**, 4170-4180.
118. C. Roos, D. Dahlgren, E. Sjögren, C. Tannergren, B. Abrahamsson and H. Lennernäs, *Molecular Pharmaceutics*, 2017, **14**, 4252-4261.
119. M. Karashima, N. Sano, S. Yamamoto, Y. Arai, K. Yamamoto, N. Amano and Y. Ikeda, *European Journal of Pharmaceutics and Biopharmaceutics*, 2017, **115**, 65-72.
120. F. Benaouda, S. A. Jones, J. Chana, B. M. Dal Corno, D. J. Barlow, R. C. Hider, C. P. Page and B. Forbes, *Molecular Pharmaceutics*, 2018, **15**, 861-870.
121. J. E. Hastedt, P. Bäckman, A. Cabal, A. Clark, C. Ehrhardt, B. Forbes, A. J. Hickey, G. Hochhaus, W. Jiang, S. Kassinos, P. J. Kuehl, D. Prime, Y.-J. Son, S. Teague, U. Tehler and J. Wylie, *Molecular Pharmaceutics*, 2022, **19**, 2032-2039.
122. P. Bäckman, A. Cabal, A. Clark, C. Ehrhardt, B. Forbes, J. Hastedt, A. Hickey, G. Hochhaus, W. Jiang, S. Kassinos, P. J. Kuehl, D. Prime, Y. J. Son, S. P. Teague, U. Tehler and J. Wylie, *Mol Pharm*, 2022, **19**, 2040-2047.
123. J. E. Hastedt, P. Bäckman, A. R. Clark, W. Doub, A. Hickey, G. Hochhaus, P. J. Kuehl, C.-M. Lehr, P. Mauser, J. McConville, R. Niven, M. Sakagimi and J. G. Weers, *AAPS Open*, 2016, **2**, 1.
124. P. B. Myrdal, P. Sheth and S. W. Stein, *AAPS PharmSciTech*, 2014, **15**, 434-455.
125. J. H. Bell, P. S. Hartley and J. S. G. Cox, *Journal of Pharmaceutical Sciences*, 1971, **60**, 1559-1564.
126. B. Chaurasiya and Y.-Y. Zhao, *Pharmaceutics*, 2021, **13**.

127. R. Scherließ and C. Etschmann, *International Journal of Pharmaceutics*, 2018, **548**, 49-53.
128. K. AboulFotouh, Y. Zhang, M. Maniruzzaman, R. O. Williams and Z. Cui, *International Journal of Pharmaceutics*, 2020, **587**, 119711.
129. M. L. Manca, D. Valenti, O. D. Sales, A. Nacher, A. M. Fadda and M. Manconi, *Int J Pharm*, 2014, **472**, 102-109.
130. H. Abdelrady, R. M. Hathout, R. Osman, I. Saleem and N. D. Mortada, *European Journal of Pharmaceutical Sciences*, 2019, **133**, 115-126.
131. A. G. Ogienko, E. G. Bogdanova, N. A. Trofimov, S. A. Myz, A. A. Ogienko, B. A. Kolesov, A. S. Yunoshev, N. V. Zubikov, A. Y. Manakov, V. V. Boldyrev and E. V. Boldyreva, *European Journal of Pharmaceutical Sciences*, 2017, **110**, 148-156.
132. N. A. Beinborn, J. Du, N. P. Wiederhold, H. D. C. Smyth and R. O. Williams, *European Journal of Pharmaceutics and Biopharmaceutics*, 2012, **81**, 600-608.
133. G. A. Hebbink, M. Jaspers, H. J. W. Peters and B. H. J. Dickhoff, *Advanced Drug Delivery Reviews*, 2022, **189**, 114527.
134. M. W. Jetzer, M. Schneider, B. D. Morrical and G. Imanidis, *Journal of Pharmaceutical Sciences*, 2018, **107**, 984-998.
135. T. Peng, X. Zhang, Y. Huang, Z. Zhao, Q. Liao, J. Xu, Z. Huang, J. Zhang, C.-y. Wu, X. Pan and C. Wu, *Scientific Reports*, 2017, **7**, 46517.

Chapter 2

# Pulmonary Drug Delivery of Antimicrobials and Anticancer Drugs Using Solid Dispersions

Publication Details:

Al-Obaidi, H.; Granger, A.; **Hibbard, T**.; Opesanwo, S. Pulmonary Drug Delivery of Antimicrobials and Anticancer Drugs Using Solid Dispersions. Pharmaceutics 2021, 13, 1056.

Chapter Summary:

In this chapter, current literature regarding the use of solid dispersions for high dose, carrier free dry powder inhalation is reviewed, with particular focus on inhaled antimicrobials and anticancer therapeutics.

Author Contributions:

Conceptualization, H.A.-O.; investigation, H.A.-O., A.G., T.H., S.O.; data curation, H.A.-O., A.G., T.H., S.O.; writing—H.A.-O., T.H.; writing—review and editing, H.A.-O.; supervision, H.A.-O.; project administration, H.A.-O.

TH contributions further details:

TH performed literature search, preparation of the original draft and initial editing particularly from Section 5 – Section 9 in addition to general reviewing and editing of whole manuscript.

*pharmaceutics*

MDPI

*Review*

# Pulmonary Drug Delivery of Antimicrobials and Anticancer Drugs Using Solid Dispersions

**Hisham Al-Obaidi *, Amy Granger, Thomas Hibbard and Sefinat Opesanwo**

The School of Pharmacy, University of Reading, Reading RG6 6AD, UK; a.granger@student.reading.ac.uk (A.G.); t.hibbard@pgr.reading.ac.uk (T.H.); s.t.opesanwo@student.reading.ac.uk (S.O.)
* Correspondence: h.al-obaidi@reading.ac.uk; Tel.: +44-1183-786-261

**Abstract:** It is well established that currently available inhaled drug formulations are associated with extremely low lung deposition. Currently available technologies alleviate this low deposition problem via mixing the drug with inert larger particles, such as lactose monohydrate. Those inert particles are retained in the inhalation device or impacted in the throat and swallowed, allowing the smaller drug particles to continue their journey towards the lungs. While this seems like a practical approach, in some formulations, the ratio between the carrier to drug particles can be as much as 30 to 1. This limitation becomes more critical when treating lung conditions that inherently require large doses of the drug, such as antibiotics and antivirals that treat lung infections and anticancer drugs. The focus of this review article is to review the recent advancements in carrier free technologies that are based on coamorphous solid dispersions and cocrystals that can improve flow properties, and help with delivering larger doses of the drug to the lungs.

**Keywords:** cocrystals; coamorphous; solubility; dry powder inhalers; pulmonary drug delivery

check for updates

**Citation:** Al-Obaidi, H.; Granger, A.; Hibbard, T.; Opesanwo, S. Pulmonary Drug Delivery of Antimicrobials and Anticancer Drugs Using Solid Dispersions. *Pharmaceutics* **2021**, *13*, 1056. https://doi.org/10.3390/pharmaceutics13071056

Academic Editor: Carsten Ehrhardt

Received: 14 June 2021
Accepted: 6 July 2021
Published: 10 July 2021

**Publisher's Note:** MDPI stays neutral with regard to jurisdictional claims in published maps and institutional affiliations.

**Copyright:** © 2021 by the authors. Licensee MDPI, Basel, Switzerland. This article is an open access article distributed under the terms and conditions of the Creative Commons Attribution (CC BY) license (https://creativecommons.org/licenses/by/4.0/).

## 1. Introduction

The respiratory tract is susceptible to a range of conditions, such as viral, bacterial and fungal infections [1], which in turn can result in an exacerbation of other existing conditions through inflammation [2]. Lower respiratory tract infections which include bronchitis, tuberculosis and pneumonia, are classed as two of the leading causes of death, while pneumonia is a leading cause of death in children globally [3]. While inflammation can affect the entire respiratory system, different pathogens will inhabit different parts of the respiratory tract. For example, tuberculosis causative microorganism *Mycobacterium tuberculosis* colonises the lungs, deep within, and also inside the lung's alveolar surfaces [4]. In cystic fibrosis (CF) patients, the bacterium, *Pseudomonas aeruginosa*, inhabits the conducting and respiratory zones of the lungs and is associated with recurrent infections. This is mainly caused by bacterial transformation to the biofilm producing mucoid strain, which exhibits increased resistance to both antibiotics and natural lung defence mechanisms, such as phagocytosis.

In addition to respiratory tract infections, lung cancer is a major cause of death. It is estimated that 1.6 million people die every year from lung cancer, making it one of the most fatal cancers [5]. Lung cancer remains difficult to cure using chemotherapy, as evident by the low long-term survival rate of patients [6]. Apart from the frequent low efficacy, cancer treatments have been associated with significant side effects. A study that included 449 cancer patients, revealed 86% of patients experienced at least one side effect from cancer chemotherapy, with 67% having experienced six or more side effects [7]. This calls for the exploration of new approaches, aimed at reducing the side effects, and in turn, improving patient tolerance [8], and further improve the quality of care provided to patients.

The pulmonary route has been used to treat different lung conditions, such as asthma and chronic obstructive pulmonary disease (COPD). Drugs delivered to the lungs are

typically formulated in low doses; however, there is an increasing clinical need to deliver higher doses. For example, when antimicrobials are delivered directly to the lungs, higher doses ensure optimum lung concentration for tackling the infection [9]. Hence, a major challenge is to formulate these drugs with efficient deposition, while maximising the delivered dose. Current technologies are based on formulating the required doses of the active pharmaceutical ingredient (API) with the addition of excipients (known as carrier particles) [10]. These carrier particles serve to minimise undesired deposition into the oropharyngeal region, as well as reducing loss in the inhalation device itself. Among approaches to deliver larger doses of the drug to the lungs is solid dispersions. These are molecular mixtures of the drug and a miscible carrier by which properties can be tailored to achieve optimum outcomes, such as improved solubility [11]. The carrier can be a small molecule known as a coformer or a polymeric carrier leading to the formation of crystalline or amorphous dispersions.

Although oral formulations have a more enhanced therapeutic profile when it comes to treating systemic diseases, inhaled drug formulations are better at targeting lung conditions, such as infections and cancer. The aim of this review article is to explore the respiratory route for drug delivery, highlighting its advantages and challenges to deliver larger doses. While there have been different approaches to maximise the dose that can be delivered, the focus of this review is on recent advancements in the delivery of particulates prepared as solid dispersions. The use of solid dispersions represents a novel approach to deliver larger amounts of the drug while maintaining enhanced physicochemical properties. These physical molecular complexes (i.e., solid dispersions) can be engineered to modify properties, such as adhesion, aerodynamic diameter and morphology, allowing enhanced pulmonary drug delivery.

*Physiology of the Lungs and Factors Affecting Particles Deposition*

The pulmonary alveoli exhibit a large surface area of over 100 $m^2$ and thin walls of less than 1 μm, allowing fast absorption of drugs into the rich blood supply for systemic effect [12]. This would be beneficial for a number of drugs as the fast absorption would result in a more rapid onset of action compared to other administration routes, such as oral administration. As well as being advantageous for drugs acting both locally and systemically, it also has reduced systemic side effects that are common with other administration routes [13]. It is considered a non-invasive form of drug administration and often require lower doses compared with other systemic drug delivery routes [14]. The local administration also avoids first pass liver metabolism, which is detrimental for some drugs. Thus, the pulmonary route may be favoured over other parenteral routes, or when absorption via the gastrointestinal (GI) tract is inappropriate or ineffective [12,15].

The respiratory system comprise 23 generations (G0–G23) which have varying sizes, structures and functions [16]. Each generation splits into two smaller daughter branches to give the next generation. Altogether, these generations are divided into two zones: Conducting and respiratory. The conducting zone includes the structures from the trachea to the bronchioles from G0 to G16. The main role of the conducting zone is to carry the air into the lungs. The respiratory zone includes structures from the respiratory bronchioles to the alveolar ducts and alveoli from G17 to G23. This zone contains functional tissues where gaseous exchange occurs [17].

As a result of the varying size and structure of the lungs, inhaled particle size affects how deep into the lungs the drug and excipients can penetrate. For example, particles with a mass median aerodynamic diameter (MMAD) of 10 μm or larger tend to be deposited in the oropharyngeal region, whereas smaller particles with an MMAD of less than 3 μm can penetrate much deeper through the lungs into the alveoli [18]. MMAD is a measurement used to define the size of aerosol particles. The aerodynamic diameter of a particle relates to a sphere with the same density as water (1 $g/cm^3$) which settles at the same velocity as the particle of interest in still air [19]. Using the mass median value, the aerosol size distribution is divided in half [20].

Particles intended for pulmonary drug delivery are categorised according to their size. The ideal particle size for inhalation is said to be <5 μm [21], with <3 μm having an 80% chance of reaching the lower airways and 50–60% chance of reaching the alveolar regions [22]. Particles > 5 μm are identified as coarse particles; fine particles range from 0.1–5 μm, and ultrafine particles are <0.1 μm. A monodisperse aerosol is said to be highly desirable for maximum deposition and specific targeting in the lungs [23]. However, there have been reports showing minimum differences in deposition between polydisperse and monodisperse aerosols [24]. The deposition of inhaled particles within the regions of the lungs is dependent on a number of physiological and pharmaceutical factors, such as particle shape, particle size, surface morphology, the breathing rate of the patient, lung volume and health condition of the patient. The physicochemical factors that affect particles deposition in the respiratory system are shown in Table 1. Particle deposition can occur through the following mechanisms: sedimentation, impaction and diffusion. Diffusion is a fundamental mechanism of particle deposition for particles < 0.5 μm. The process is influenced by Brownian motion—in other words, motion increases with decreasing particle size and particles move from a higher concentration to a lower concentration leading to the deposition upon contact with the airway walls. This mechanism heavily influences deposition in the lower regions of the lungs and the alveoli. Gravitational sedimentation can happen at a later region, typically within the tracheobronchial region (approximately the last six generations), as a result of the relatively low air velocity within this region [25]. In fact, as the residence time is longer, a combination of both sedimentation and free diffusion can occur. It is vital for drug absorption to occur, that the particles are deposited before exhalation takes place. Typical size depends on the aerodynamic diameter, which is approximately above 0.5 μm for sedimentation and below that for diffusion [26,27]. The bigger the particle and the lower the airflow rate, the faster the sedimentation in which inertial impaction plays a significant role for particles > 5 μm [28].

**Table 1.** Physicochemical factors to be considered when designing inhaled formulations. Each parameter influences both aerosolisation and deposition. Adapted from the work by the authors of [29–31].

| Property Type | Parameter |
|---|---|
| Aerosol | Air/Particle velocity<br>Mass median aerodynamic diameter<br>Fine particle fraction |
| Particle | Bulk density<br>Tap density<br>Shape<br>Charge<br>Surface energy *<br>Surface texture *<br>Surface composition * |
| Physicochemical | Solubility<br>Hygroscopicity |

Note—* Factors specifically affecting aerosolisation.

## 2. The Necessity to Deliver Larger Doses to Treat Lung Infections and Cancer

There are a variety of inhaled products for the treatment of conditions affecting the respiratory system (Table 2). As can be seen in Table 2, the maximum dose that has been successfully formulated for inhalation, thus far, is colistimethate sodium, with doses ranging from 80 to 125 mg, formulated as inhalation powder. Many of the higher inhalable doses are administered via the use of nebulisers, which may require guidance and can also be complicated for patients to use [32]. Desgrouas and Ehrmann reviewed the available evidence and called for developing inhaled antibiotics, especially for mechanically ventilated patients [33]. However, the majority of inhalable drug formulations are available in the dose range of micrograms and are indicated for conditions, such as asthma

and COPD. In addition, there is a limited number of inhaled medications available as combinations, which are again mostly limited for use in asthma and COPD.

**Table 2.** Examples of currently available inhaled products in the market.

| Drug | Quantity of API per Dose | Indication | Ref |
|---|---|---|---|
| Salbutamol | 100–200 μg | Asthma | [34] |
| Fluticasone propionate | 50–500 μg | Prophylaxis of asthma | [35] |
| Colistimethate sodium | 80–125 mg | Treatment of pneumonia | [36] |
| Tiotropium | 10–18 μg | Maintenance of COPD | [37] |
| Nedocromil sodium | 2 mg | Prophylaxis of asthma | [38] |
| Zanamivir | 5 mg | Treatment of influenza | [39] |
| Mannitol | 5–40 mg | Treatment of cystic fibrosis as add-on therapy to standard care | [40] |
| Budesonide with formoterol | 100–400 μg with 4.5–12 μg | Maintenance of asthma | [41] |
| Ciclesonide | 80–160 μg | Prophylaxis of asthma | [42] |

There are two major lung conditions that require high doses of medications, these being infections and malignancy. For lung infections, the causative bacteria and viruses can be found throughout the different structures of the lungs, which will alter the efficacy of treatment. The conducting zone of the respiratory system, which consists of the trachea, bronchi and bronchioles, plays a role in trapping microbes in mucus produced by goblet cells. The mucus is then transported by ciliated cells located on the epithelium to the oropharynx, where the mucus is either swallowed or removed via coughing [43]. However, in cases where the microbes go on to develop into infections, it is important to determine the specific site in the lungs where the infection has developed to effectively target and deliver the drug directly to the causative microbes. Table 3 lists common loci of prevalent microorganisms within the respiratory tract noting that several pathogens found in the respiratory tract are associated with the development of biofilms.

Upper respiratory tract infections typically occur in the conducting zone, examples of which include common cold, sinusitis and pharyngitis, whereas lower respiratory tract infections happen in the respiratory zone and include pneumonia and bronchitis. In addition, some microorganisms, such as *Haemophilus influenzae*, that are normally found in the conducting zone can go on to migrate to the respiratory zone, subsequently causing lower respiratory tract infections [44]. Some studies suggest that the conducting zone of the respiratory tract is the more common zone where bacteria and viruses are contained during infections. One study found that for *Pseudomonas aeruginosa* biofilms in cystic fibrosis patients, the majority of the bacteria were present in the conducting zone, which acted as a reservoir for the bacteria to multiply and form biofilms [45]. Consequently, it is important for inhaled formulations of antibacterials and antivirals to reach and deposit in the conducting zone of the respiratory tract to effectively treat the infections. With the ability to locally deliver antimicrobial drugs for treatment, there could also be a further advantage of reducing antimicrobial resistance. With oral and intravenous administration, there is a risk of an accumulation in infection-free sites, leading to the development of antimicrobial resistance. In addition, a number of antimicrobials, such as tobramycin, can be toxic when given in repeated high doses systemically, which can occur when antimicrobials are prescribed for recurrent infections [46]. Hence, utilising local drug delivery directly into the lungs could reduce the risk of toxicity.

**Table 3.** Location of infections causative microorganisms within the respiratory tract.

| Organism | Type | Location/Generation | Reference |
|---|---|---|---|
| **Bacteria** | *Pseudomonas aeruginosa* | Non-mucoid strain located mainly in the conduction airways<br>Mucoid strain present throughout the respiratory zone | [47] |
| | *Staphylococcus aureus* | Nasal cavity<br>Generation 0 | [48] |
| | *Mycobacterium tuberculosis*<br>*Chlamydia pneumonia* | Alveolar surfaces<br>Macrophages in lungs<br>Generation 20–22<br>Generation 21–23<br>Alveolar type 2 cells | [4]<br>[2] |
| **Fungi** | *Aspergillus* spp. | Terminal bronchioles, Terminal airways<br>Generation 16–23 | [49] |
| **Viruses** | Herpes Simplex Virus | Oropharynx–Generation 0 | [48] |

Similar to infectious conditions, lung cancer is another serious condition that requires large doses of drugs for treatment. Current survival rates for all stages of lung cancer include 40% of patients surviving for one year or more after diagnosis, 15% of patients surviving for five years or more after diagnosis and only 10% of patients surviving for 10 years or more after diagnosis [50]. The nature of lung cancer suggests that it is more effectively treated by direct delivery to the lungs. Sardeli et al., suggested the need to use inhaled immunotherapy as opposed to intravenous administration to avoid systemic side effects and achieve a localised effect [51]. Hence, pulmonary drug delivery provides a novel opportunity to avoid unwanted drug distribution and could achieve maximum deposition of the drug at the site of action. As such, there is the potential for higher concentrations of the drugs to reach the lungs compared with oral and intravenous administration. Lung cancer cells are prone to rapidly developing resistance to anticancer drugs, so higher doses are given to combat this challenge [52]. When administered systemically, chemotherapy drugs can cause toxic side effects affecting healthy organs, especially when administering large doses, which may be prevented by local administration of the drugs [53]. By targeting the lungs directly, this also means there is potential for an accumulation of the drug to build up in the tumour cells, rather than in the kidneys, liver and spleen, which is observed with systemic drug use [54]. This has the potential to beneficially impact patients' treatment and increase the likelihood of remission and survival.

## 3. Challenges Associated with Drug Delivery to the Lungs

Whilst pulmonary drug delivery has its advantages, to ensure advantageous deposition in the lungs, drug particles must be within the optimum size for lung deposition (Table 4 and Figure 1). If the particle size is relatively large, the deposition will occur in the larynx causing irritation, and if the particle size is relatively small, the particles will be immediately exhaled from the lungs and will not be deposited [55]. It is important to note that drug particles should be deposited in the lungs in a high enough proportion for the API to be absorbed and produce a therapeutic effect. Unsurprisingly, it has been shown that higher drug deposition in the lungs leads to enhanced clinical benefits [56]. As mentioned above, a common approach to improve the flow properties of powder for inhalation is to use carrier particles (such as lactose monohydrate). This is based on combining the drug with the larger lactose particles, which strip from the drug particles inside the device in response to the high velocity created by inhalation [57,58]. Any escaped lactose will deposit in the throat, leaving the drug particles to carry on with their journey towards the alveoli. Hence, the main challenge would be to deliver high doses of the API without significant loss in the oropharynx region. Another challenge is that inhalation devices do not have the capacity to accommodate high masses of powders [59].

As shown by the data collated and presented in Table 4, two different studies used a combination of beclomethasone dipropionate with formoterol labelled with technetium-99. The first dissolved the particles in hydrofluoroalkane to give an MMAD of 1.3 µm via pressurised metered-dose inhaler (pMDI) [60], the second delivered the solid particles with MMAD of 1.5 µm via a NEXThaler® dry powder inhaler (DPI) [61]. The lung deposition for the pMDI was 34.08% (standard deviation (SD) = 9.3%), and the DPI had a lung deposition of 55.2% (SD = 3.7%). This shows that even though the same APIs were used, and the particle sizes were similar, the way that the API is formulated plays a significant role in the lung deposition of the particles. It is apparent that the type of the API has an effect by comparing the lung deposition of albuterol and beclomethasone dipropionate with formoterol in the pMDI considered previously [62]. They both have an MMAD of 1.5 µm, are labelled with technium-99 and are administered using an pMDI; however, the lung deposition of albuterol was 56.3% (SD = 9.2%), which is considerably higher than the beclomethasone, which has a lung deposition of 34.08% (SD = 9.3%). This suggests that API type and formulation must also be carefully considered when formulating drugs for pulmonary drug delivery.

Furthermore, Table 4 shows that within the same administration device, the preparation method of the particle has an impact on the deposition within the lungs. One study compared two suspensions of beclomethasone dipropionate labelled with technetium-99 in a metered-dose inhaler, by which the first formulation was dissolved in hydrofluoroalkane, and the other was dissolved in chlorofluorocarbon [63], it demonstrated that the different preparation methods led to a difference in both MMAD and lung deposition. Therefore, this suggests that the type of excipients used must be carefully considered for optimum lung deposition.

**Table 4.** MMAD, lung deposition and preparation method of different inhaled APIs.

| API | MMAD (µm) | Lung Deposition (%) | Preparation of API | Ref |
|---|---|---|---|---|
| Formoterol | 0.8 | 31 ± 11 | Labelled with technetium-99 and dissolved in hydrofluoroalkane (HFA) in an pMDI | [64] |
| Beclomethasone dipropionate | 0.9 | 53 ± 7 | Labelled with technetium-99 and dissolved in HFA in an pMDI | [63] |
| Fluticasone propionate | 2 | 12 ± 7 | Labelled with technetium-99 and dissolved in chlorofluorocarbon (CFC) in an pMDI | |
| Beclomethasone dipropionate | 3.5 | 4 ± 11 | | |
| Albuterol (salbutamol) | 1.5 | 56.3 ± 9.2 | Labelled with technetium-99 in an pMDI | [62] |
| | 3 | 51 ± 8.9 | | |
| | 6 | 46 ± 13.6 | | |
| Beclomethasone dipropionate and formoterol | 1.3 | 34.08 ± 9.3 | Labelled with technetium-99 and dissolved in HFA in a pMDI | [60] |
| Ciclesonide | 1 | 52 ± 11 | Labelled with technetium-99 and dissolved in HFA in a pMDI | [65] |
| Beclomethasone dipropionate and formoterol fumarate | 1.5 | 55.2 ± 3.7 | Labelled with technetium-99 in a NEXThaler® DPI | [61] |

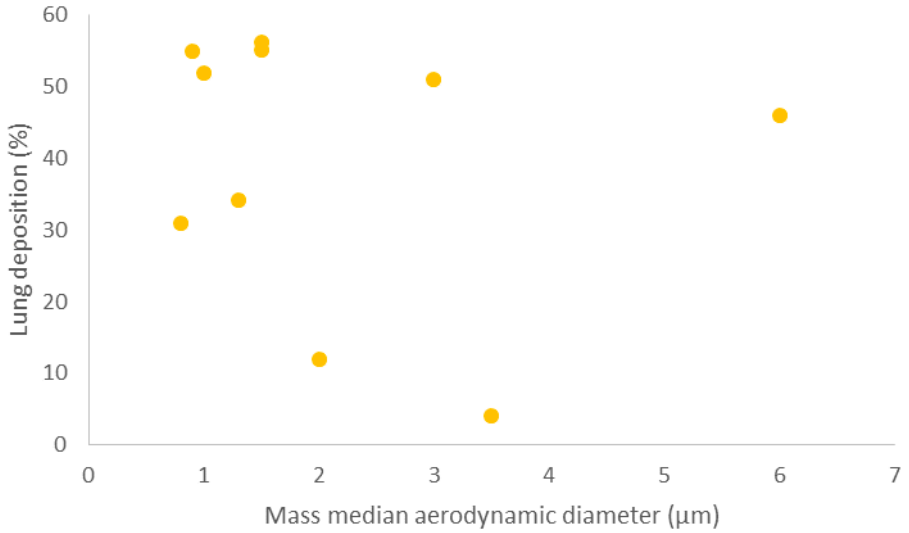


**Figure 1.** A scatter graph, comparing MMAD with corresponding lung deposition values in Table 4.

## 4. Impact of Drug Delivery Devices on the Extent of Pulmonary Drug Delivery

There are currently three major categories of delivery devices that are used for inhalation therapy: pressurised metered-dose inhalers (pMDIs), nebulisers and dry powder inhalers (DPIs). pMDIs are widely available, portable inhalers designed to releases a specific dose of the drug, following depression of an actuator, which the patient then inhales in a single inspiration or via a spacer device. Studies have found that many patients have difficulty in using these devices, due to the required coordination of pressing down on the actuator and inhaling the resultant mist simultaneously [66]. If patients do not have the required coordination to self-administer their medication using a pMDI, some of the drug is deposited in the mouth and at the back of the throat. As a result, less of the API will be inhaled than intended, so the correct dose will not be administered. This could potentially result in substandard treatment, leading to exacerbation or worsening of a patient's condition. pMDIs are formulated as a suspension or solution with one or more APIs along with a propellant. The propellant is used to generate the pressure required to form micron-scaled droplets for inhalation [67]. Furthermore, pMDIs deposit less of the drug into the lungs, due to the high particle exit velocity with the actuations [68]. This means that it is more difficult to formulate higher drug doses for use with this type of inhaler device.

DPIs are portable inhalers that operate by breath actuation, thus removing the need for coordination of inhalation with actuation required for pMDIs. Breath actuation involves the powder being released from the inhaler when the patient inhales with enough force, known as inspiratory flow. The inhalers are formulated to contain powder forms of drugs, and this solid-state gives the drug improved stability compared to pMDIs formulations [67]. The use of powders also allows for greater potential when formulating higher dose medications. Dry powder inhalers are available in three types: single-unit dose, multi-dose reservoir and multi-unit dose. The powder is stored in either capsules or sealed blisters that are broken during actuation. In general, patients tend to find that multi-dose DPIs are preferable to single-unit dose DPIs, due to the convenience of not having to replace the capsule or blisters with every use of the inhaler.

Nebulisers are less popular inhalation devices compared to the other two devices and are available in two forms. The most common nebuliser is the jet nebuliser, which works by passing a liquid formulation along with compressed air through a narrow tube into a wide chamber, which causes a reduction in pressure. This reduction in pressure then forms micron-sized droplets, which can then be inhaled. The alternative type of nebuliser is the ultrasonic nebuliser, which breaks down the solution of the drug into inhalable droplets by piezoelectric vibrations [68]. Both types of nebulisers require a face mask or

mouthpiece, which are bulkier and less portable than the other two devices, and therefore, less convenient for frequent and repeated use [69]. The way nebulisers are formulated are unsuitable for some drugs, particularly for drugs that are unstable when in solution [70]. Nebulisers also take longer to administer the drug when compared to other drug delivery devices, due to the time taken for the drug to pass through the chamber into the mouthpiece or mask, and with inhalation over a prolonged period. The use of nebulisers can also result in the administration of less precise doses as there can be deposition of the API particles in the chamber and mouthpiece or face mask. In general, nebulisers tend to be used by patients who cannot use the other devices, due to difficulties with coordination associated with pMDIs and/or the inability to produce adequate inspiratory flow associated with DPIs. The main patient groups these affect are young children, elderly populations, patients with COPD and patients with CF [71].

There is a limited number of licensed inhaled antimicrobials that are only available for patients suffering from recurrent infections as in CF (Table 5). Other antibiotics, such as gentamicin and amikacin, can be nebulised for pulmonary drug delivery by using the solution for injection if required; however, these cases are for unlicensed use in CF patients only and not for use for respiratory infections [72]. As can be seen in Table 5, nebuliser solutions and inhalation powders can be used to formulate higher doses of drugs, and hence, these are the devices currently used on the market. Tobramycin, colistimethate sodium and zanamivir are all available as dry powders for inhalation. Tobramycin inhalation powder is produced via an oil-in-water emulsion-based spray-drying process [69], and each particle consists of an amorphous tobramycin sulphate, and a gel-phase phospholipid 1,2-distearoyl-sn-glycero-3-phosphocholine (DSPC). Tobramycin inhalation powder comes in a device known as a TOBI® Podhaler®, which consists of the engineered dry powder, the hard capsule, which is the primary packaging of the powder, and the device to administer the powder [70]. Other excipients used in the capsules include calcium chloride, which is used to stabilise the emulsion droplets during the spray drying and sulphuric acid for pH adjustment [71,73]. Each inhalation delivers 28 mg of tobramycin from the capsule to the lungs; however, four capsules are required for each dose, and therefore, eight inhalations per day. Colistimethate sodium is an inactive prodrug of colistin (polymyxin E), and is formulated as such to reduce the toxicity, typically nephrotoxicity, that is often experienced by patients when taking colistin. It is formulated to be administered using a Turbospin® inhaler, under the brand name Colobreathe® [74]. The powder is micronised and filled in polyethylene glycol (PEG)-gelatin hard capsules, which also contain purified water and sodium lauryl sulphate as excipients [75,76]. Zanamivir is an antiviral drug used for the treatment and prevention of influenza. It is formulated under the brand name Relenza® for its inhalation powder, and is produced via air-jet milling to contain 5 mg of zanamivir and 20 mg of lactose monohydrate particles as carrier particles in each double-foil blister [77].

**Table 5.** Licensed inhaled antibacterials currently available on the market.

| Antibacterial Drug | Form | Available Strength | Ref |
|---|---|---|---|
| Tobramycin | Nebuliser liquid | 300 mg/5 mL, 300 mg/4 mL, 170 mg/1.7 mL | [78] |
| | Inhalation powder | 28 mg (1 dose = 4 × 28 mg inhalations) | |
| Colistimethate sodium | Inhalation powder | 1,662,500 IU ≈ 125 mg | [79,80] |
| | Powder for nebuliser solution | 1,000,000 IU ≈ 80 mg | |
| Aztreonam | Powder and solvent for nebuliser solution | 75 mg | [81] |

## 5. Pulmonary Drug Delivery Using Carrier Free Technology

Large carrier particles, such as alpha-lactose monohydrate, are added to the API to form an inhaled powder with enhanced formulation properties. These properties include

the flowability and aerosol dispersion of the powder to maximise the number of API particles reaching the site of action. Lactose is available in a variety of grades for inhalation, with median diameters ranging from <5 μm to 250 μm [82]. During formulation, micronised API particles with an MMAD of between 1 μm and 5 μm are attached to the surface of these much larger carrier particles. Physical interactions hold the API in place, which prevents agglomeration of micronised API, due to cohesive forces. On inhalation, API is detached from the carrier and aerosolised, due to force exerted by the inhaler design in the form of friction, inertia and drag [83]. By retaining micronised API particle size, maximum dispersion of powder into the lungs is seen, due to increased aerosolisation [84]. This influences the drug administration in addition to preventing problems during the manufacturing process of the powder [85].

Carrier-based DPIs are the most prevalent formulation of DPIs and tend to be used to deliver relatively higher doses of API compared to pMDIs. However, certain mass ratios of API to carrier particles must be maintained to prevent agglomeration, as for example these can vary depending on the type of the drug, ranging from 1:2 to 1:4 in some cases [86]. For example, Relenza® requires a 25 mg powder to be inhaled so that to deliver 5 mg of zanamivir (i.e., a mass ratio of 1:5). These ratios create a maximum practical dose that can be delivered to the lungs through dry powder inhalation, making high dose delivery even more challenging. Even with carrier particles enhancing aerosolisation, deposition in the lungs is still relatively low, and as a result, the amount of API to reach the site of action is low. Fine particle fraction (FPF) refers to the fraction of particles with a size smaller than the respirable size divided by the total emitted dose of the inhaled API [87]. DPIs that do not contain carrier particles, therefore, have greater potential for delivering higher doses to the lungs.

Carrier free DPIs are a new-generation system that use special excipients and technologies, such as crystal engineering, to formulate micronised API particles whilst addressing the limitations explained above. These methods can increase the amount of lung deposition, with some formulations reporting FPF values of 63% [88]. One of the benefits of developing carrier free DPI formulations is that there can be an increased mass of API without having to retain large masses of the carrier particles. Therefore, this can maximise the dose available in each inhalation through maximising the amount of API that is deposited in the lungs. There are several dry powder formulations that have been or are currently being investigated to produce carrier free dry powder inhalers, as shown below in Table 6. As can be seen, different doses have been tested with some formulations delivering doses up to 50 mg, as displayed in Figure 2.

Many different methods have been used to develop dry powders for inhalation, also shown in Table 6, and each method produces variation to yield, cost of production and manufacture time. This data shows the difference in the size of the doses able to be formulated in DPIs for inhalation, compared to current doses available for inhalation (Figure 2). This also suggests that the use of carrier free inhalation technology can play a key factor in addressing the challenge of increasing doses of drugs for pulmonary drug delivery. Also noted is the wide range of drug classes that are being considered with regards to delivery via dry powder inhalation, including non-steroidal anti-inflammatory drugs (NSAIDs, i.e., ibuprofen and indomethacin), antimicrobials (i.e., tobramycin and netilmicin), antihistamines (i.e., ketotifen), and phosphodiesterase type 5 inhibitors (i.e., sildenafil). It was also noted that for many antimicrobials, there is the possibility of creating drug combinations within the same device—a useful tool for patients who require complex antimicrobial treatment.

**Table 6.** Carrier free DPIs and the technology used to produce the powders.

| API | Dose in Capsule | Conditions Used | Ref |
|---|---|---|---|
| Indomethacin | 3 mg | Spray drying an aqueous-based feed to form microparticles | [89] |
| Ethionamide + moxifloxacin | 20 mg | Spray drying using a mini spray dryer | [90] |
| Ketotifen | 20 mg | Spray drying with different solvents (water, ethanol and water-ethanol mix) | [91] |
| Sildenafil | 5 mg | Spray drying using a mini spray dryer | [92] |
| Ibuprofen | 50 mg | Air-jet milling to produce micronised samples | [93] |
| Sodium cromoglycate | 20 mg | Pelletised | [94] |
| Tobramycin + clarithromycin | 22.72 mg tobramycin, 2.27 mg clarithromycin | Spray drying | [95] |
| Salbutamol sulphate | 5.1–7.1 mg | Gas-phase coating method to produce L-leucine coated powders | [96] |
| Tranexamic acid | 38 mg | Spray drying | [97] |
| Roflumilast | 20 mg | Spray drying with hydroxypropyl-β-cyclodextrin | [98] |
| Tobramycin | 28 mg | Micronised using a Labomill jet milling system | [99] |
| Meloxicam potassium | 1.3 mg | Cospray drying | [100] |
| Ciprofloxacin + colistin | 10 mg | Cospray drying | [101] |
| Netilmicin | 30 mg | Cospray drying | [102] |

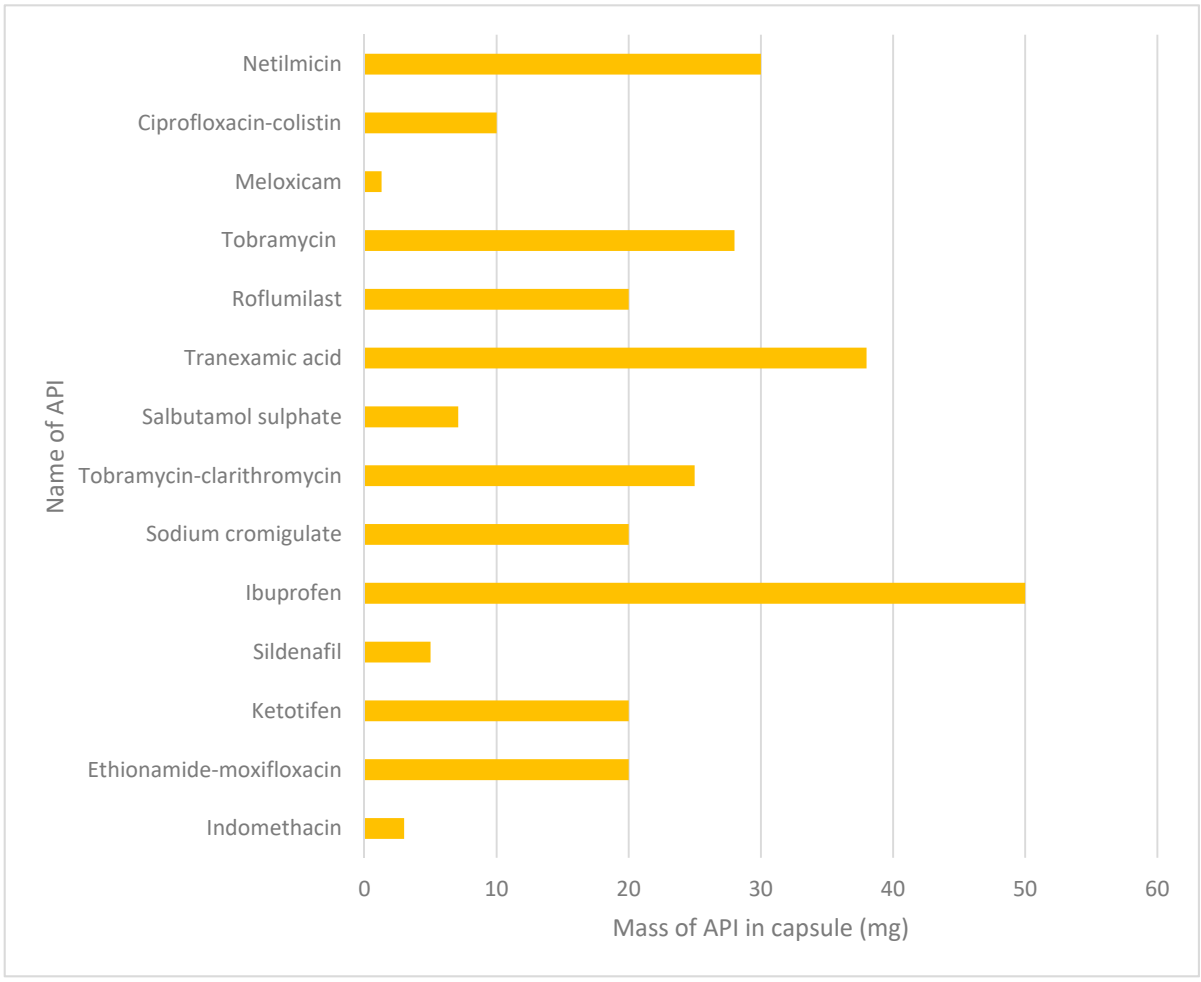


**Figure 2.** Bar graph for the weight of API in the capsule for each type of drug extracted from Table 6.

## 6. Pulmonary Drug Delivery on the Nanoscale

Nanoparticulate formulations maintain nanoscale particles of the drug through encapsulation within inhalable size particles to prevent aggregation and ensure deposition of nanoparticles in the lung. There are several particle engineering methods to achieve nanoparticle formulation, such as the use of liposomes, solid lipids and polymers, which have been reviewed elsewhere [103–105]. It is common for these formulations to be stored as suspensions then delivered to the lung through a nebuliser; however, carrier free, dry powder nanoparticle formulations are also being developed.

Zhu et al., described the formulation of poorly soluble ivacaftor (Iva) as bovine serum albumin nanoparticles, which were then spray freeze-dried with different ratios of soluble colistin (Co) matrix and L-leucine [106]. All subsequent formulations showed high emitted dose following inhalation for both APIs (>90%); however, a range of FPF values (%) were seen corresponding to initial solid content in the formulations. Dissolution rates of the best performing nanoformulation and a jet-milled physical mixture of Iva and Co were then compared. After 3 h, the nanoformulation showed three times greater dissolution of Iva compared to the physical mixture control, with the concentration of Iva dissolved equivalent to highly soluble Co. Enhanced dissolution of Iva was attributed to the albumin maintaining Iva nanoscale particle size and amorphous form. The use of Co as a water-soluble matrix both enhanced the dispersion of Iva nanoparticles, as well as broadening the formulation clinical scope for patients with cystic fibrosis.

Doxorubicin nanoparticles (DNPs) were formulated as a colloid through emulsion polymerisation then spray freeze-dried with lactose to form particles of inhalable size [107,108]. DNPs showed increased survival rates compared to IV doxorubicin controls (including IV DNPs) in a rat model and much lower cardiotoxicity compared to doxorubicin DPI control. DNPs were also formulated with sodium carbonate to enhance the release of doxorubicin from the formulation. When inhaled, the effervescent formulations showed increased survival rates compared to DNP controls showing the importance of an active release mechanism from the formulation. In a slightly different approach, often utilising nanoscale dimensions to enhance inhalation properties, the use of porous particles has been investigated and was shown to improve efficacy of inhalation [109–111].

## 7. The Design of Carrier Free Formulations Using Coamorphous Solid Dispersions (CACDs)

Most solid APIs exist in a crystalline state held together by strong intermolecular bonds, and therefore, display good stability profiles (Figure 3). However, the crystalline state often shows poor solubility, due to the high energy required to break the crystalline lattice which creates a major problem for developing new APIs [112,113]. There has been much interest in the process of 'drug amorphisation', to address poor solubility, which involves the conversion from a crystalline state to an amorphous solid state. The amorphous solid state offers an improved solubility and dissolution rates as a result of possessing higher entropy [114–116]. The advantages associated with higher energy forms are often negated, due to recrystallisation to a more thermodynamically stable form during processing and storage [117–119]. This can limit applications, and so the production and maintenance of amorphous drugs with adequate stability remain a challenge. Formulation strategies based on solid molecular dispersions are being explored, including polymeric amorphous solid dispersions (PASDs), and more recently, coamorphous solid dispersions (CASDs).

PASDs incorporate low API loading within a compatible polymer to maintain the solubility advantage of amorphous systems through the formation of strong intermolecular attractions [120]. Examples of PASDs applications are seen in the combination of paclitaxel and polyvinylpyrrolidone (PVP), ritonavir and PVP, ciprofloxacin and polyvinyl alcohol [121–123]. However, the main limitation of this approach is the low level of API loading within the formulation, requiring increased dosing. In addition, many polymeric carriers are hygroscopic, which can lead to API recrystallisation while in some cases polymers

can be unsuccessful in maintaining a good stability profile [123]. The applications and limitations of PASDs have been highlighted in a number of reviews [124–126].

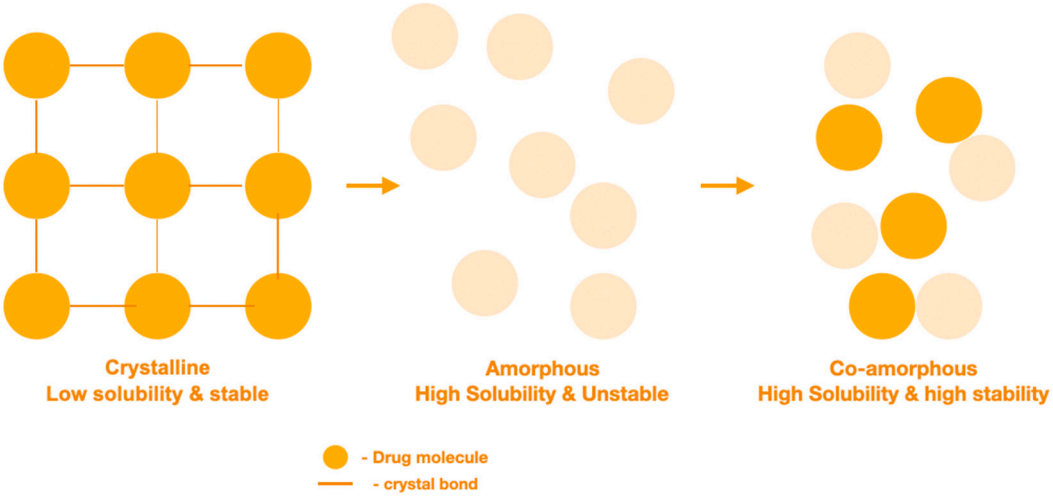


**Figure 3.** Illustration of the crystalline state, amorphous state and coamorphous state and their characteristics.

CASDs are a relatively new formulation approach through which the crystalline drug is amorphised thermally or mechanically and stabilised with a small molecular weight coformer. These systems are often stabilised through strong intermolecular hydrogen bonding and exhibit apparent stability, due to an increased glass transition temperature [124]. Glass transition temperature refers to the temperature at which below, the system exists in an unstable glassy state and above, the system exists in a rubbery state [125]. CASDs can be obtained through different preparation methods, such as freeze drying, quench cooling, milling and solvent evaporation methods [126,127]. Milling is an example of mechanical amorphisation where a direct mechanical impact on the drug causes a disturbance in the crystalline structure, forming an amorphous state. Quench cooling and solvent evaporation are examples of thermal amorphisation where a crystalline solid state is prevented from reforming, due to molecular level interactions. Here, the drug is either in a liquid state following melting or dissolved to form a solution then rapidly cooled, or solvent removed rapidly. CASDs are believed to be able to provide an increase in drug kinetic solubility thanks to the high energy of the amorphous state driving faster dissolution [128]. In addition, improved physical stability is offered through an increase in the glass transition temperature ($T_g$) and the presence of intermolecular interactions between the API and coformer, as reported by several research papers [124,129]. CASDs are said to reduce hygroscopicity, as API hydrogen bonding regions are strongly bound to the coformer. Therefore, hydrogen bonding with water is less favourable, which helps to maintain stability and particle integrity.

CASDs provide the opportunity for many types of formulations, such as drug-excipient and drug-drug combinations, and many have been reported as being successful. An example of a drug-drug combination is the spray drying of colistin with azithromycin to treat infections caused by multi-drug resistant bacteria [130]. A study conducted by Wang et al., showed an enhanced solubility profile between two APIs with low aqueous solubility: lacidipine and spironolactone [131]. Many other drug-excipient combinations are listed in Table 7, by which commonly used coformers in CASDs for pulmonary drug delivery include mannitol, sugars and amino acids, such as leucine [132,133].

The spray drying technique is based on solvent evaporation which uses the processes of liquid atomisation, gas/droplet mixing and drying to create microparticles [134]. First, a liquid feed consisting of mixed components, typically pure API, excipient and a common solvent, is converted into smaller droplets via atomisation. Next, the droplets are sprayed downwards into a vertical drying chamber exposed to air or nitrogen at a temperature

higher than the solvent boiling point [135]. Within this drying chamber, the droplets rapidly shrink in size to produce dry microparticles.

Through spray drying, aspects of particle morphology, such as shape, size and surface properties, can be highly controlled, which deems the technique appropriate for formulating inhalation powders. Many papers have controlled particle morphology through variations to the inlet temperature, the spray nozzle diameter and properties of the feed solution, such as concentration and viscosity [136]. The inlet temperature (also known as the drying temperature) and the feed rate are parameters of high importance as they control the rate of evaporation and drying load, which determine particle properties and product yield [137]. It is common to see outlet temperatures ranging from 70 °C to 105 °C with inlet temperatures ranging from 100 °C to 210 °C. A faster drying rate could lead to a higher product yield, as there are fewer particles adhering to the chamber walls, which may also implicate that solvent evaporation is not complete. The spray drying process is highly applicable for large scale manufacture, where the integrity of formulation is retained despite 'upscaling' [138]. Altogether, spray drying offers a great opportunity to incorporate a number of excipients into one formulation whilst improving the physical stability of the particles.

**Table 7.** Application of coamorphous solid dispersions prepared using different preparation methods. The inclusion of PASD of ciprofloxacin was shown to identify the apparent benefits of polymeric solid dispersions compared to coamorphous solid dispersions.

| API | Prime Excipient | Preparation Method | Fine Particle Fraction (FPF) (%) | Ref |
|---|---|---|---|---|
| Cyclosporin A (CsA) | Lactose, methylcellulose and erythritol | Jet-milling and freeze drying | 54 | [139] |
| Ciprofloxacin | Polyvinyl alcohol PVA | Spray drying | 25 ± 2.1 after 6 months | [121] |
| Ciprofloxacin | No excipient | Spray drying | 67.35 ± 1.1 after 6 months | [121] |
| Ciprofloxacin | Leucine | Spray drying | 79.78 ± 1.2 after 6 months | [121] |
| Ciprofloxacin | Hydroxypropyl-beta-cyclodextrin | Spray drying | 36.32 ± 1.3 after 6 months | [121] |
| Colistin | No excipient | Spray drying | 43.8 ± 4.6% | [140] |
| Colistin | No excipient | Jet milling | 28.4 ± 6.7 % | [140] |
| Colistin | L-leucine | Spray drying | 43.8 ± 4.6% (no difference from Spray dried alone) | [140] |
| Ciprofloxacin | No excipient | Spray drying | 28.0 ± 3.2% | [141] |
| Ciprofloxacin | Lactose, sucrose, trehalose, L-leucine | Spray drying | Lactose (43.5 ± 3.3%), sucrose (44.0 ± 4.3%), trehalose (44.0 ± 1.9%), L-leucine (73.5 ± 7.1%) | [141] |
| Thymopentin | Lactose/mannitol, Leucine, poloxamer 188 | Spray drying | 44.8%, 45.6%, 44.9%, 43.8% | [142] |
| CsA | Inulin | Spray freeze drying | >50 | [143] |
| Tacrolimus | Mannitol | Thin-film freeze-drying | 83.3 | [144] |
| Tacrolimus | Raffinose | Thin-film freeze-drying | 69.2 | [145] |
| Tacrolimus | Lactose | Thin-film freeze-drying | 68.7 | [145] |

## 8. Examples of Coformers as Components of CAMs

L-leucine has been widely used in many studies to improve the aerosolisation properties of particles, due to its antihygroscopic effect and its ability to generate coarse particles, following surface enrichment. Momin et al., formulated spray dried kanamycin with various concentrations of L-leucine, showing the 5% L-leucine formulation to have the best improvement in aerosolisation properties [146]. Likewise, significant increases in aerosoli-

sation properties were recorded for the other ratios of L-leucine. Other papers also reported L-leucine as a well-rounded excipient for improving the aerosolisation properties of powder particles. Interestingly Mangal et al., formulated spray dried azithromycin with various concentrations of L-leucine yet reported no significant change to powder morphology or FPF ($p > 0.05$) [132]. In addition, there was no significant increase seen in the percentage emitted dose ($p > 0.05$); however, an increased in vitro dissolution rate was reported. A lack of change to FPF and emitted dose can be explained when considering particle surface morphology and composition. It is believed that the more corrugated a particle surface is, the greater the resulting aerosolisation properties. This process is attributed to the success of L-leucine in improving aerosolisation. Chen et al., reported how changes to the composition of PASDs result in differences to the surface composition of particles, and therefore, flowability and aggregation [136]. Perhaps the surface enrichment of azithromycin with L-leucine for this formulation was poor, resulting in little change to particle surface morphology when compared to the control. When using L-leucine as a coformer, it is important that drying causes the distribution to the outer regions of droplets, causing recrystallisation of L-leucine on the particle surface, creating a corrugated effect [147]. This concept has also been documented by McShane et al. [138]. The impact of spray drying conditions on particles morphologies was recently highlighted in a different study by which spray dried coamorphous ciprofloxacin tartrate salt was shown to exhibit improved properties compared to ciprofloxacin alone [148].

The distribution of the components within the droplet during spray drying is said to be dependent on physicochemical properties of the components, such as solubility, the diffusivity of components and hydrophobicity [149]. These properties ultimately result in the final composition of the surface of spray dried particles. In the example mentioned above of azithromycin with L-leucine, the solubility of azithromycin is very low, and it likely had an impact on the distribution of L-leucine within the CASD. Li et al., conducted in vitro study to assess deposition, by which, spray drying azithromycin with mannitol resulted in low FPF values ranging between 38–42% [150]. Signifying the impact of preparation method and locality of excipients, Padhi et al., suggested that by increasing the ratio of L-leucine may improve surface enrichment, which would result in a substantial increase in the FPF [151]. In a different study, it was proposed that the presence of hydrophobic azithromycin helps to control humidity to prevent reduction in FPF [130].

Hassan et al., suggested that surface enrichment of spray dried materials is dependent on solvent evaporation rate and diffusion coefficients of the solutes [152]. Based on computational fluid dynamics, it was shown that the maximum rate of solvent evaporation proportionally affected MMAD [153]. It is believed the flow of the solute equates to that of the solvent; therefore, the movement of solute within a droplet is highly linked to solvent flow. Lower evaporation rates have a more significant impact on redistribution to droplet surface for solutes with high diffusion coefficients [149,152]. Shetty et al., when using water as a solvent, concluded that a low inlet temperature (<120 °C) was not considered, due to the possibility of it not being sufficient for drying [141]. Chen et al., also documented lower surface enrichment occurring, due to a reduction in the inlet temperature [136]. It is believed that the inlet temperature influences the particle shape, as well as surface enrichment. The inlet temperature indirectly affects the outlet temperature, and a lower outlet temperature is believed to result in a more spherical particle shape, which is detrimental to FPF [154,155].

Benke et al., reported spray dried meloxicam potassium (MXLspd) that was compared to the carrier-based meloxicam and lactose monohydrate InhaLac® (μMXL + IH70) [21]. As expected MXLspd showed an improvement in FPF < 5 μm (59.47%) compared to μMXL + IH70 with an FPF < 5 μm (24.99%). In addition, μMXL + IH70 had an MMAD of 7.18 μm, therefore unfavourable for pulmonary drug delivery. When assessing the impact of humidity on FPF, authors observed a significant decline ($p < 0.0001$) observed in the FPF (<4.9 μm) between cospray dried ciprofloxacin with lactose when stored at 20% RH and 50% RH after 10 days. This may be due to the caking observed, which led to larger powder

particles formed. Similar observations were reported by Guenette et al., which showed that larger lactose particles led to reduced flow properties [156]. The larger particle size may have occurred, due to particle agglomeration when stored at a higher RH. These examples highlight that for highly aerosolised powder, it is necessary to maintain the stability of spray dried CASDs when hygroscopic coformers are used. This is because of the presence of the excipient such as L-leucine, which has been reported to combat moisture-related stability issues, due to its hydrophobic nature [157]. Part of the reason why CASDs are successful is that the coformer changes from being a passive carrier to an essential constituent in the formulation [138].

In a separate study, Lababidi et al., further examined the success CASDs had in pulmonary drug delivery by which azithromycin and ciprofloxacin were spray dried with L-leucine and n-acetyl cysteine (NAC), an amino acid derivative and known mucolytic [129]. Mucolytics are used in combination with antibiotics to dissolve thick mucus found in the CF lung [157,158]. When mucolytics, such as NAC, are used as CASDs coformers, the formulation benefit becomes two-fold, creating a more effective treatment with better formulation characteristics. As mentioned before, the addition of L-leucine is aimed at reducing particle cohesion and increasing aerosolisation properties. However, in the study conducted by Lababidi et al., the main aim of adding NAC was to the formulation was to dissolve mucus, enhancing antibiotic effect against the bacteria. The authors showed that azithromycin/n-acetyl cysteine combination reduced *P. aeruginosa* biofilm by 25% at a concentration of 0.3 µm/mL compared to azithromycin and n-acetyl cysteine alone.

Forming amorphous dispersions composed of antimicrobials through complex formation with metal cations has been explored as a method for enhancing formulation characteristics of inhaled antimicrobials. Lamy et al., produced inhalable dry powder microparticles of ciprofloxacin, complexed with calcium or copper ions (Cip-Ca; Cip-Cu), through spray drying [159,160]. The resulting powders were amorphous, and both calcium and copper formulations showed similar shell-like morphology, characteristic of spray dried materials, and similar in vitro solution properties. When comparing pharmacokinetics in vivo, both formulations showed enhanced lung retention compared to the ciprofloxacin control, suggesting that forming metal counterion complexes can reduce the rate of transcellular diffusion from the lung fluid. It was also seen that the ratio of ciprofloxacin in epithelial lining fluid to plasma was five times greater for the Cip-Cu than Cip-Ca formulations. The authors linked this with the strength of complex which had formed, corresponding to: The enhanced stability of the Cip-Cu, a slower rate of absorption into plasma and longer elimination half-life. Thus, antibiotic lung retention can be controlled depending on the metal ion selected, leading to an optimised concentration in lung fluid.

The influence of metal salts on the inhalation properties of levofloxacin has also been analysed. Barazesh et al., cospray dried levofloxacin with four metal chloride salts with and without leucine [161]. Sodium (Na) and potassium (K) monovalent salts were compared with magnesium (Mg) and calcium (Ca) divalent salts. When measuring aerosol properties, most effects was seen for formulations containing the highest measured percentage of metal ion (i.e., 20% *w*/*w*). It was also observed that the addition of divalent salts reduced the FPF of formulations and caused higher water retention post spray drying. The authors concluded that the highly hygroscopic divalent metal salts are likely to uptake more water, leading to local crystallisation and particle aggregation. Monovalent salts at 20% *w*/*w* showed a higher FPF compared to lower concentrations. With respect to leucine formulations, FPF was significantly higher, corresponding to the characteristic corrugated effect seen when spray drying with leucine.

## 9. The Design of Carrier Free Formulations Using Cocrystals

The formulation of carrier free dry powders can be achieved by a variety of methods. These include the formation of salts, such as the generation of a sildenafil-citrate salt [92], forming complexes with cationic groups, such as the generation of indomethacin

and polylysine microparticles [89], and forming CASDs, such as with ciprofloxacin and colistin [101]. Another route being investigated is the generation of cocrystals and seems to be a promising method of improving physicochemical properties if other methods are not suitable. For example, with the formation of salts, if the API is neutral, and therefore, does not contain an acidic or basic group that can be ionised, salts cannot be practically formed [162]. Cocrystallisation may also be seen as a more desirable method of physicochemical enhancement than others, for example, CASDs, due to enhanced physical and chemical stability [163].

Pharmaceutical cocrystals are multicomponent crystals formed between an API and pharmaceutically acceptable coformer. API and coformer exist in a fixed stoichiometric ratio held together through [164] non-covalent and non-ionic interactions. These interactions are intermolecular in nature and include hydrogen bonding, halogen bonding, π-π stacking and van der Waal forces [165]. Hydrogen bonds are considered the 'key interaction' for cocrystallisation, due to their strength, directionality and being commonly found in organic molecules [166]. Therefore, cocrystals are distinct from polymorphs, due to multiple components, and salts, due to lack of ionisation, and CASDs, due to their crystalline nature. The formulation of APIs as cocrystals is regarded as a physical modification to improve physicochemical properties, which maintains the API pharmacodynamic profile [167]. Since the cocrystal is a unique crystalline entity, it has unique physical properties, including solubility, dissolution, flowability and stability. In general, coformers are chosen based on molecular compatibility, as well as possession of desired physical property change. For example, to improve an API's solubility, one would choose a coformer with compatible functional groups, as well as high solubility [168].

Cocrystallisation is currently attracting considerable interest, due to the improved physicochemical properties that can be introduced to the API [169,170]. For example, cocrystals of meloxicam–succinic acid were combined with PEG 4000 to enhance aqueous solubility [171]. Cocrystals have largely been studied with a focus on improving oral drug delivery, and it is only recently that studies have begun to explore how cocrystals can be used for other administration routes, including pulmonary drug delivery. It is important to focus on all changes to API physical properties rather than flowability and dispersion alone. For example, altering solubility and dissolution will influence retention and epithelium wall permeation which will determine either a local or systemic effect. Selecting the correct coformer can increase aerosolisation properties, as well as maintaining the balance between API retention in the lung and API clearance through various mechanisms [172].

M Karashima et al., produced micronised powder formulations of itraconazole for inhalation using cocrystallisation and jet-milling [163]. These cocrystal formulations showed superior aerodynamics compared with itraconazole control put through the same processing and amorphous itraconazole spray dried with mannitol corresponding with reduced particle size. Also tested were the intrinsic dissolution rates of cocrystal formulations compared to itraconazole and amorphous itraconazole in mock lung surfactant. After 1 h, the dissolved concentration of itraconazole from cocrystal formulations were between 5 and 10 times higher than itraconazole and the amorphous form. The authors reported higher plasma concentrations ($C_{max}$) compared to itraconazole and the amorphous form of itraconazole. Comparing this finding with intrinsic dissolution data, supports the conclusion that the extent of dissolution in the lungs influences the extent of systemic partitioning.

Alhalaweh et al., produced several inhalable powders of theophylline through cocrystallisation with nicotinamide, urea and saccharin [173]. These were compared against theophylline control, but also against cocrystals formulated with lactose carrier. The authors comment that cocrystal formulations showed more favourable aerosolisation with less API loss, due to impaction. However, not all cocrystal formulations were better aerodynamically compared to the control. This highlights the unpredictable nature of coformer selection in cocrystal formation and the importance of considering all aspects of physical property changes. Tanaka et al., produced a theophylline:oxalic acid cocrystal through a combination of spray and freeze drying [174]. When compared to the control,

the resulting formulation showed resistance to hygroscopicity and polymorphic transition whilst maintaining good pulmonary delivery. The authors attribute this stability to the low recorded energy state and close intermolecular interactions within the cocrystal.

API solution properties are a key component to determining API destination following inhalation. One study investigated how the properties of 5-fluorouracil differ from three different cocrystals created with gentisic acid (FUGA), 4,5 dihydroxybenzoic acid (FUBA) and 4-aminopyridine (FUPN). This study determined that the intrinsic dissolution of all three cocrystals were increased compared to pure 5-fluorouracil in both pHs of 1.2 and 6.8, with the largest difference being between 5-fluoruracil and FUPN. 5-fluorouracil had an intrinsic dissolution rate (IDR) of 0.12 mg $cm^{-2}$/s in pH 1.2 and 0.18 $cm^{-2}$/s in pH 6.8, whereas FUPN had an IDR of 0.7 mg $cm^{-2}$/s in pH 1.2 and 0.92 mg $cm^{-2}$/s in pH 6.8, showing more rapid dissolution from the cocrystal forms of 5-fluoruracil than the pure API [175]. Increased dissolution has also been observed in three diacerein cocrystals with isonicotinamide, nicotinamide and theophylline (DA-ISO), (DA-NIC) and (DA-THE). Diacerein had an IDR of 0.065 mg $cm^{-2}$/min compared to 0.216 mg $cm^{-2}$/min, 0.284 mg $cm^{-2}$/min and 0.137 mg $cm^{-2}$/min for DA-ISO, DA-NIC and DA-THE, respectively. This again shows that each cocrystal had a higher IDR value than the pure API molecule, suggesting a faster rate of dissolution [176].

Another study demonstrated the effects that cocrystals have on the pharmacokinetic profile of a drug. Daidzein and three cocrystals, with isonicotinamide (DIS), cytosine (DCYT) and theobromine (DTB) as the coformers, were compared. It was found that all three cocrystals had higher Cmax values, than daidzein (870.5 ng/mL), with DIS possessing the highest Cmax (1848.7 ng/mL). In addition, the time taken to reach the Cmax (Tmax) values for each cocrystal was 3 h compared to 4 h for pure daidzein [177]. Table 8 summarises a variety of cocrystal formulations, the method of manufacture used and the difference between API and coformer molecular weight. Shown is that cocrystallisation applied to a great variety of different APIs produced through a wide range of different production methods. Of note are the studies which use methods applicable for producing inhalable dry powders, such as spray drying, spray freeze drying and jet milling. It also gives an example of the wide variety of successful coformers available for cocrystallisation, suggesting a great variety in physical property variations even for the same API. Examples of drug:drug cocrystals are listed to show the possibility of creating synergistic therapies through a single phase crystalline powder, i.e., cocrystals. As shown in Table 8 and Figure 4, all coformers have molecular weights lower than alpha-lactose monohydrate (342.3 g/mol) and either much smaller or similar molecular weight to the API. This demonstrates how formulations containing coformers take up less volume in comparison to carrier-based delivery systems. As discussed earlier, the volume which lactose particles take up in formulations restricts the quantity of API that can be practically delivered. By avoiding the use of carrier particles, through coformer based methods, greater amounts of API particles can be formulated within a DPI device, possibly increasing the dose of API per actuation.

**Table 8.** Cocrystalline APIs, their coformers, technology used and molecular weights.

| API | Coformer | Technology Used | Molecular Weight (g/mol) | | |
|---|---|---|---|---|---|
| | | | API | Coformer | Ref |
| Itraconazole | Succinic acid | Jet-milling | 705.63 | 118.09 | [163] |
| | L-tartaric acid | | | 150.09 | |
| Levofloxacin | Metacetamol | Grinding and heating | 361.37 | 151.16 | [178] |
| Pyrazinamide | 3-Hydroxy benzoic acid | Slow evaporation and neat grinding | 123.11 | 138.12 | [179] |
| Dapsone | Caffeine | Slow evaporation, liquid-assisted grinding, spray drying | 248.30 | 194.19 | [180] |
| Nitrofurantoin | Melamine | Slow evaporation | 238.16 | 126.12 | [181] |
| Telaprevir | 4-aminosalicylic acid | Ball milling | 679.85 | 153.14 | [182] |
| Trimethoprim | Glutarimide | Slow evaporation | 290.32 | 113.11 | [183] |
| Telmisartan | Gentisic acid | Slurry approach | 514.62 | 154.12 | [184] |
| | Maleic acid | | | 116.07 | |
| Sulfadimidine | 4-aminosalicylic acid | Liquid-assisted comilling | 278.33 | 153.14 | [185] |
| Isoniazid | Ferulic acid | Liquid-assisted grinding | 137.14 | 194.18 | [186] |
| | Caffeic acid | | | 180.16 | |
| | Vanillic acid | | | 168.15 | |
| Adefovir | Stearic acid | Antisolvent precipitation | 273.19 | 284.50 | [187] |
| Acyclovir | Fumaric acid | Liquid-assisted grinding | 225.20 | 116.07 | [188] |
| Meloxicam | Aspirin | Solution, slurry and solvent drop methods | 351.40 | 180.16 | [189] |
| Theophylline | Oxalic acid | Spray freeze drying | 180.16 | 90.03 | [174] |
| Niclosamide | Nicotinamide | Spray drying | 327.12 | 122.12 | [190] |
| Lomefloxacin | Barbituric acid | Slow evaporation | 351.35 | 128.09 | [191] |
| | Isophthalic acid | | | 166.13 | |
| Enoxacin | Oxalic acid | Slow evaporation | 320.32 | 90.03 | [192] |
| | Malonic acid | | | 104.06 | |
| | Fumaric acid | | | 116.07 | |
| Sulfaguanidine | Thiobarbutaric acid | Slow evaporation | 214.24 | 144.15 | [193] |
| | 1,10-phenanthroline | | | 180.20 | |

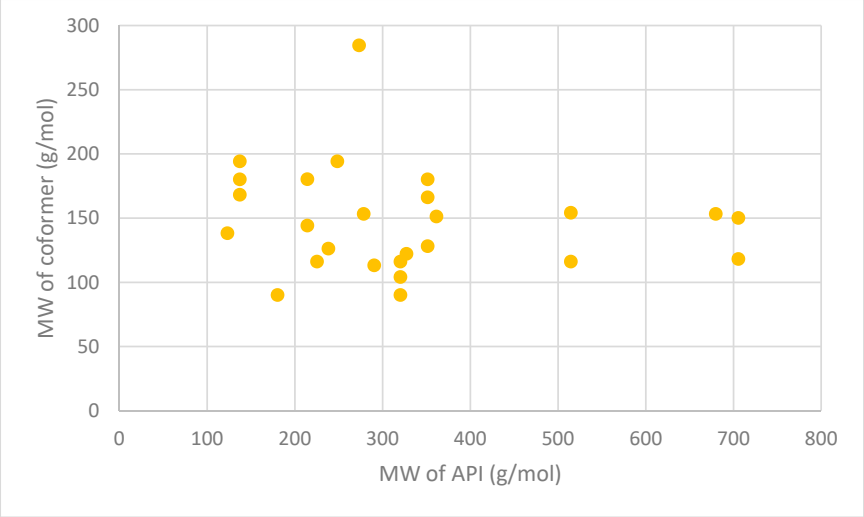


**Figure 4.** A scatter graph of the data from Table 8 comparing the molecular weights of the APIs and their coformers.

## 10. Conclusions

Coamorphous solid dispersions and cocrystals are attractive physical structures that have been used to improve the physicochemical properties of inhaled APIs to target infections and lung cancer. When developing pharmaceutical cocrystals/coamorphous for inhalation, careful selection of the coformer should be followed to improve the efficacy to deliver drugs to the lungs. It is likely that by creating cocrystals/coamorphous dispersions, the need for carrier particles in DPIs can be eliminated, and therefore, a greater amount of the API can be delivered. This would result in an increased dose in each inhalation, allowing lower potency drugs that require higher doses to be formulated for inhalation. It is important to understand the complexities of pulmonary drug delivery when considering the formulation of drugs for inhalation to ensure the drug particles have adequate aerosolization properties. This is necessary to ensure the particles can reach deep into the lungs at the site of action, without being aggregated or immediately exhaled from the lungs. It is important to consider all steps throughout drug development process, including the excipients that are used and the devices to administer the drug, because some of the devices have shown clear advantages when it comes to overcoming the challenges with formulating inhaled APIs. The complexity of diseases imposes greater challenges demanding more studies to optimise particles properties for better deposition. Ultimately, it is crucial to match the properties of the particles to the desired site of action, such as the case when targeting bacterial biofilms and cancer.

**Author Contributions:** Conceptualization, H.A.-O.; investigation, H.A.-O., A.G., T.H., S.O.; data curation, H.A.-O., A.G., T.H., S.O.; writing—H.A.-O., T.H.; writing—review and editing, H.A.-O.; supervision, H.A.-O.; project administration, H.A.-O. All authors have read and agreed to the published version of the manuscript.

**Funding:** This research received no external funding.

**Institutional Review Board Statement:** Not applicable.

**Informed Consent Statement:** Not applicable.

**Data Availability Statement:** Not applicable.

**Conflicts of Interest:** The authors declare no conflict of interest.

## References

1. Moss, N.H.; Thompson, S.D.; Bauer, H.C.; Clark, J.J.; Clark, W.R. Diseases of the Respiratory System. *New Complet. Med. Health Encycl.* **1997**, *2*, 474–476.
2. Rupp, J.; Droemann, D.; Goldmann, T.; Zabel, P.; Solbach, W.; Vollmer, E.; Branscheid, D.; Dalhoff, K.; Maass, M. Alveolar epithelial cells type II are major target cells for C. pneumoniae in chronic but not in acute respiratory infection. *FEMS Immunol. Med. Microbiol.* **2004**, *41*, 197–203. [CrossRef]
3. Goyal, K.A.; Garg, T.; Bhandari, S.; Rath, G. Advancement in pulmonary drug delivery systems for treatment of tuberculosis. In *Nanostructures for Drug Delivery*; Andronescu, E., Grumezescu, M.A., Eds.; Elsevier: Amsterdam, The Netherlands, 2017; pp. 669–695.
4. Smith, I. Mycobacterium tuberculosis pathogenesis and molecular determinants of virulence. *Clin. Microbiol. Rev.* **2003**, *16*, 463–496. [CrossRef] [PubMed]
5. Forum of International Respiratory Societies. *Global Impact of Respiratory Disease*; Forum of International Respiratory Societies: Sheffield, UK, 2017; pp. 12–26.
6. Goel, A.; Baboota, S.; Sahni, J.K.; Ali, J. Exploring targeted pulmonary delivery for treatment of lung cancer. *Int. J. Pharm. Investig.* **2013**, *3*, 8–14. [CrossRef]
7. Pearce, A.; Haas, M.; Viney, R.; Pearson, S.A.; Haywood, P.; Brown, C.; Ward, R. Incidence and severity of self-reported chemotherapy side effects in routine care: A prospective cohort study. *PLoS ONE* **2017**, *12*, e0184360. [CrossRef]
8. Nurgali, K.; Jagoe, R.T.; Abalo, R. Editorial: Adverse Effects of Cancer Chemotherapy: Anything New to Improve Tolerance and Reduce Sequelae? *Front. Pharmacol.* **2018**, *9*, 245. [CrossRef]
9. Rangaraj, N.; Pailla, S.; Sampathi, S. Insight into pulmonary drug delivery: Mechanism of drug deposition to device characterization and regulatory requirements. *Pulm. Pharmacol. Ther.* **2019**, *54*, 1–21. [CrossRef]
10. Chaurasiya, B.; Zhao, Y.-Y. Dry powder for pulmonary delivery: A comprehensive review. *Pharmaceutics* **2021**, *13*, 31. [CrossRef]
11. Al-Obaidi, H.; Buckton, G. The characterization and dissolution properties of griseofulvin solid dispersions with HPMCAS. *J. Pharm. Pharmacol.* **2006**, *1*, A18–A19.

12. Newman, S. Drug delivery to the lungs: Challenges and opportunities. *Ther. Deliv.* **2017**, *8*. [CrossRef]
13. Islam, N.; Ferro, V. Recent Advances in Chitosan-Based Nanoparticulate Pulmonary Drug Delivery. *Nanoscale* **2016**, *8*, 14341–14358. [CrossRef]
14. Luczak-Wozniak, K.; Dabrowska, M.; Domagala, I.; Miszczuk, M.; Lubanski, W.; Leszczynski, A.; Krenke, R. Mishandling of pMDI and DPI inhalers in asthma and COPD- repetitive and non-repetitive errors. *Pulm. Pharmacol. Ther.* **2018**, *51*, 65–72. [CrossRef] [PubMed]
15. Parumasivam, T.; Chang, R.; Abdelghany, S.; Ye, T.; Britton, W.; Chan, H. Dry powder inhalable formulations for anti-tubercular therapy. *Adv. Drug Deliv. Rev.* **2016**, *102*, 83–101. [CrossRef] [PubMed]
16. Patwa, A.; Shah, A. Anatomy and physiology of respiratory system relevant to anaesthesia. *Indian J. Anaesth* **2015**, *59*, 533–541. [CrossRef] [PubMed]
17. Hakim, A.; Usmani, O.S. Structure of the Lower Respiratory Tract. In *Reference Module in Biomedical Sciences*; Elsevier: Amsterdam, The Netherlands, 2014.
18. Carvalho, T.; Peters, J.; Williams, R.r. Influence of particle size on regional lung deposition- What evidence is there? *Int. J. Pharm.* **2011**, *406*, 1–10. [CrossRef]
19. DeCarlo, P.; Slowik, J.; Worsnop, D.; Davidovits, P.; Jimenez, J. Particle Morphology and Density Characterization by Combined Mobility and Aerodynamic Diameter Measurements. Part 1: Theory. *Aerosol Sci. Technol.* **2004**, *38*, 1185–1205. [CrossRef]
20. Laube, B.; Janssens, H.; de Jongh, F.; Devadason, S.; Dhand, R.; Diot, P.; Everard, M.; Horvath, I.; Navalesi, P.; Voshaar, T.; et al. What the pulmonary specialist should know about the new inhalation therapies. *Eur. Respir. J.* **2011**, *37*, 1308–1417. [CrossRef]
21. Benke, E.; Farkas, Á.; Szabó-Révész, P.; Ambrus, R. Development of an Innovative, Carrier-Based Dry Powder Inhalation Formulation Containing Spray-Dried Meloxicam Potassium to Improve the In Vitro and In Silico Aerodynamic Properties. *Pharmaceutics* **2020**, *12*, 535. [CrossRef]
22. Labiris, N.R.; Dolovich, M.B. Pulmonary drug delivery. Part I: Physiological factors affecting therapeutic effectiveness of aerosolized medications. *Br. J. Clin. Pharmacol.* **2003**, *56*, 588–599. [CrossRef]
23. Verma, K.R.; Ibrahim, M.; Garcia-Contreras, L. *Lung Anatomy and Physiology and Their Implications for Pulmonary Drug Delivery*; Wiley: Chichester, UK, 2015; pp. 2–14.
24. Kim, C.S.; Rosati, J.A. Comparison of Monodisperse and Polydisperse Aerosol Deposition in a Packed Bed. Available online: https://cfpub.epa.gov/si/si_public_record_Report.cfm?Lab=NHEERL&dirEntryID=62538 (accessed on 18 April 2021).
25. Patton, J.S. Mechanisms of macromolecule absorption by the lungs. *Adv. Drug Deliv. Rev.* **1996**, *19*, 3–36. [CrossRef]
26. Heyder, J. Deposition of inhaled particles in the human respiratory tract and consequences for regional targeting in respiratory drug delivery. *Proc. Am. Thorac. Soc.* **2004**, *1*, 315–320. [CrossRef]
27. Cheng, Y.S. Mechanisms of pharmaceutical aerosol deposition in the respiratory tract. *AAPS PharmSciTech* **2014**, *15*, 630–640. [CrossRef] [PubMed]
28. Weers, J.; Clark, A. The Impact of Inspiratory Flow Rate on Drug Delivery to the Lungs with Dry Powder Inhalers. *Pharm. Res.* **2017**, *34*, 507–528. [CrossRef]
29. Ibrahim, M.; Verma, R.; Garcia-Contreras, L. Inhalation drug delivery devices: Technology update. *Med. Devices* **2015**, *8*, 131–139. [CrossRef]
30. Momin, M.A.M.; Tucker, I.G.; Das, S.C. High dose dry powder inhalers to overcome the challenges of tuberculosis treatment. *Int. J. Pharm.* **2018**, *550*, 398–417. [CrossRef] [PubMed]
31. Sallam, A.S.; Nazzal, S.; AlKhatib, S.H.; Darwazeh, N. *Quality by Design: Concept for Product Development of Dry-Powder Inhalers*, 1st ed.; Wiley: Chichester, UK, 2015; pp. 322–324.
32. Alhaddad, B.; Smith, F.; Robertson, T.; Watman, G.; Taylor, K. Patients' practices and experiences of using nebuliser therapy in the management of COPD at home. *BMJ Open Respir. Res.* **2015**, *2*, e000076. [CrossRef]
33. Desgrouas, M.; Ehrmann, S. Inhaled antibiotics during mechanical ventilation—Why it will work. *Ann. Transl. Med.* **2020**, *9*, 598. [CrossRef]
34. NICE. Salbutamol. Available online: https://bnf.nice.org.uk/medicinal-forms/salbutamol.html (accessed on 5 November 2020).
35. NICE. Fluticasone. Available online: https://bnf.nice.org.uk/drug/fluticasone.html (accessed on 4 November 2020).
36. Kalil, A.; Metersky, M.; Klompas, M.; Muscedere, J.; Sweeney, D.; Palmer, L.; Napolitano, L.; O'Grady, N.; Bartlett, J.; Carratalà, J.; et al. Management of Adults with Hospital-Acquired and Ventilator-Associated Pneumonia: 2016 Clinical Practice Guidelines by the Infectious Diseases Society of America and the American Thoracic Society. *Clin. Infect. Dis.* **2016**, *63*, e61–e111. [CrossRef]
37. NICE. Tiotropium. Available online: https://bnf.nice.org.uk/medicinal-forms/tiotropium.html (accessed on 5 November 2020).
38. NICE. Nedocromil Sodium. Available online: https://bnf.nice.org.uk/drug/nedocromil-sodium.html#medicinalForms (accessed on 5 November 2020).
39. NICE. Zanamivir. Available online: https://bnf.nice.org.uk/medicinal-forms/zanamivir.html (accessed on 5 November 2020).
40. NICE. Mannitol. Available online: https://bnf.nice.org.uk/drug/mannitol.html#medicinalForms (accessed on 5 November 2020).
41. NICE. Budesonide with Formoterol. Available online: https://bnf.nice.org.uk/drug/budesonide-with-formoterol.html (accessed on 28 March 2021).
42. NICE. Ciclesonide. Available online: https://bnf.nice.org.uk/drug/ciclesonide.html (accessed on 28 March 2021).
43. Rogers, D.F. Physiology of Airway Mucus Secretion and Pathophysiology of Hypersecretion. *Respir. Care* **2007**, *52*, 1134–1149.
44. Paul, K. Haemophilus influenzae and the lung (Haemophilus and the lung). *Clin. Transl. Med.* **2012**, *1*, 10. [CrossRef]
45. Bjarnsholt, T.; Jensen, P.; Fiandaca, M.; Pedersen, J.; Hansen, C.; Andersen, C.; Pressler, T.; Givskov, M.; Høiby, N. Pseudomonas aeruginosa biofilms in the respiratory tract of cystic fibrosis patients. *Paediatr. Pulmonol.* **2009**, *44*, 547–558. [CrossRef] [PubMed]

46. Ho, D.; Nichols, B.; Edgar, K.; Murgia, X.; Loretz, B.; Lehr, C. Challenges and strategies in drug delivery systems for treatment of pulmonary infections. *Eur. J. Pharm. Biopharm.* **2019**, *144*, 110–124. [CrossRef] [PubMed]
47. Cramer, N.; Wiehlmann, L.; Tümmler, B. Clonal epidemiology of Pseudomonas aeruginosa in cystic fibrosis. *Int. J. Med. Microbiol.* **2010**, *300*, 526–533. [CrossRef] [PubMed]
48. Robinson, J. Colonization and infection of the respiratory tract: What do we know? *Paediatr Child. Health* **2004**, *9*, 21–24. [CrossRef] [PubMed]
49. Carpagnano, G.E.; Lacedonia, D.; Palladino, G.P.; Logrieco, G.; Crisetti, E.; Susca, A.; Logrieco, A.; Foschino-Barbaro, M.P. Aspergillus spp. colonization in exhaled breath condensate of lung cancer patients from Puglia Region of Italy. *BMC Pulm Med.* **2014**, *14*, 22. [CrossRef] [PubMed]
50. Cancer Research UK. Survival. Available online: https://www.cancerresearchuk.org/about-cancer/lung-cancer/survival (accessed on 8 April 2021).
51. Sardeli, C.; Zarogoulidis, P.; Kosmidis, C.; Amaniti, A.; Katsaounis, A.; Giannakidis, D.; Koulouris, C.; Hohenforst-Schmidt, W.; Huang, H.; Bai, C.; et al. Inhaled chemotherapy adverse effects: Mechanisms and protection methods. *Lung Cancer Manag.* **2020**, *8*, LMT19. [CrossRef]
52. Garbuzenko, O.; Saad, M.; Pozharov, V.; Reuhl, K.; Mainelis, G.; Minko, T. Inhibition of lung tumor growth by complex pulmonary delivery of drugs with oligonucleotides as suppressors of cellular resistance. *Proc. Natl. Acad. Sci. USA* **2010**, *107*, 10737–10742. [CrossRef]
53. Garbuzenko, O.; Mainelis, G.; Taratula, O.; Minko, T. Inhalation treatment of lung cancer: The influence of composition, size and shape of nanocarriers on their lung accumulation and retention. *Cancer Biol. Med.* **2014**, *11*, 44–55. [CrossRef]
54. Lee, W.; Loo, C.; Ghadiri, M.; Leong, C.; Young, P.; Traini, D. The potential to treat lung cancer via inhalation of repurposed drugs. *Adv. Drug Deliv. Rev.* **2018**, *133*, 107–130. [CrossRef]
55. Gandhimathi, C.; Venugopal, J.; Sundarrajan, S.; Sridhar, R.; Tay, S.; Ramakrishna, S.; Kumar, S. Breathable Medicine: Pulmonary Mode of Drug Delivery. *J. Nanosci. Nanotechnol.* **2015**, *15*, 2591–2604. [CrossRef]
56. Reychler, G.; San Miguel-Pagola, M.; Aubriot, A.; Herrero-Cortina, B.; Lecocq, V.; Hesse, M.; Liistro, G.; Jamar, F. Targeted Lung Deposition from Nebulization Is Not Improved in the Lateral Decubitus Position in Healthy Volunteers. *Respir. Care* **2019**, *64*, 1537–1544. [CrossRef]
57. Healy, A.M.; Amaro, M.I.; Paluch, K.J.; Tajber, L. Dry powders for oral inhalation free of lactose carrier particles. *Adv. Drug Deliv. Rev.* **2014**, *75*, 32–52. [CrossRef]
58. Kaialy, W.; Martin, G.P.; Larhrib, H.; Ticehurst, M.D.; Kolosionek, E.; Nokhodchi, A. The influence of physical properties and morphology of crystallised lactose on delivery of salbutamol sulphate from dry powder inhalers. *Colloids Surf. B Biointerfaces* **2012**, *89*, 29–39. [CrossRef]
59. Sibum, I.; Hagedoorn, P.; de Boer, A.; Frijlink, H.; Grasmeijer, F. Challenges for pulmonary delivery of high powder doses. *Int. J. Pharm.* **2018**, *548*. [CrossRef] [PubMed]
60. De Backer, W.; Devolder, A.; Poli, G.; Acerbi, D.; Monno, R.; Herpich, C.; Sommerer, K.; Meyer, T.; Mariotti, F. Lung Deposition of BDP/Formoterol HFA pMDI in Healthy Volunteers, Asthmatic, and COPD Patients. *J. Aerosol Med. Pulm. Drug Deliv.* **2010**, *23*, 137–148. [CrossRef]
61. Virchow, J.; Poli, G.; Herpich, C.; Kietzig, C.; Ehlich, H.; Braeutigam, D.; Sommerer, K.; Häussermann, S.; Mariotti, F. Lung Deposition of the Dry Powder Fixed Combination Beclometasone Dipropionate Plus Formoterol Fumarate Using NEXThaler Device in Healthy Subjects, Asthmatic Patients and, COPD Patients. *J. Aerosol Med. Pulm. Drug Deliv.* **2018**, *31*, 269–280. [CrossRef] [PubMed]
62. Usmani, O.; Biddiscombe, M.; Barnes, P. Regional Lung Deposition and Bronchodilator Response as a Function of $\beta_2$-Agonist Particle Size. *Am. J. Respir. Crit. Care Med.* **2005**, *172*, 1497–1504. [CrossRef]
63. Leach, C.; Davidson, P.; Hasselquist, B.; Boudreau, R. Lung Deposition of Hydrofluoroalkane-134a Beclomethasone is Greater Than That of Chlorofluorocarbon Fluticasone and Chlorofluorocarbon Beclomethasone: A Cross-Over Study in Healthy Volunteers. *Chest* **2002**, *122*, 510–516. [CrossRef] [PubMed]
64. Häussermann, S.; Acerbi, D.; Brand, P.; Herpich, C.; Poli, G.; Sommerer, K.; Meyer, T. Lung deposition of formerol HFA (Atimos/Forair) in healthy volunteers, asthmatic and COPD patients. *J. Aerosol Med.* **2007**, *20*, 331–341. [CrossRef] [PubMed]
65. Leach, C.; Bethke, T.; Boudreau, R.; Hasselquist, B.; Drollmann, A.; Davidson, P.; Wurst, W. Two-dimensional and three-dimensional imaging show ciclesonide has high lung deposition and peripheral distribution: A nonrandomized study in healthy volunteers. *J. Aerosol Med.* **2006**, *19*, 117–126. [CrossRef] [PubMed]
66. Javadzadeh, Y.; Yaqoubi, S. Therapeutic nanostructures for pulmonary drug delivery. In *Nanostructures for Drug Delivery*; Andronescu, E., Grumezescu, A.M., Eds.; Elsevier: Amsterdam, The Netherlands, 2017; pp. 619–638.
67. Peng, T.; Lin, S.; Niu, B.; Wang, X.; Huang, Y.; Zhang, X.; Li, G.; Pan, X.; Wu, C. Influence of physical properties of carrier on the performance of dry powder inhalers. *Acta Pharm. Silica B* **2016**, *4*, 308–318. [CrossRef] [PubMed]
68. Martin, A.; Finlay, W. Nebulizers for Drug Delivery to the Lungs. *Expert Opin. Drug Deliv.* **2015**, *12*, 889–900. [CrossRef] [PubMed]
69. Hamed, K.; Debonnett, L. Tobramycin inhalation powder for the treatment of pulmonary *Pseudomonas aeruginosa* in patients with cystic fibrosis: A review based on clinical evidence. *Ther. Adv. Respir. Dis.* **2017**, *11*, 193–209. [CrossRef] [PubMed]
70. Miller, D.; Tan, T.; Nakamura, J.; Malcolmson, R.; Tarara, T.; Weers, J. Physical Characterization of Tobramycin Inhalation Powder. II. State Diagram of an Amorphous Engineered Particle Formulation. *Mol. Pharm.* **2017**, *14*, 1950–1960. [CrossRef]
71. Emc. Tobi Podhaler 28 mg Inhalation Powder, Hard Capsules. Available online: https://www.medicines.org.uk/emc/product/4757 (accessed on 19 November 2020).

72. Quon, B.; Goss, C.; Ramsey, B. Inhaled Antibiotics for Lower Airway Infections. *Annu. Am. Thorac. Soc.* **2014**, *11*, 425–434. [CrossRef]
73. Miller, D.; Tan, T.; Tarara, T.; Nakamura, J.; Malcolmson, R.; Weers, J. Physical Characterization of Tobramycin Inhalation Powder. I. Rational Design of a Stable-Engineered Particle Formulation for Delivery to the Lungs. *Mol. Pharm.* **2015**, *12*. [CrossRef]
74. Conole, D.; Keating, G. Colistimethate Sodium Dry Powder for Inhalation: A Review of Its Use in the Treatment of Chronic *Pseudomonas aeruginosa* Infection in Patients with Cystic Fibrosis. *Drugs* **2014**, *74*, 377–387. [CrossRef]
75. Emc. Colobreathe. Available online: https://www.medicines.org.uk/emc/product/3063 (accessed on 19 November 2020).
76. Schwarz, C. Colobreathe for the Treatment of Cystic Fibrosis-Associated Pulmonary Infections. *Pulm. Ther.* **2015**, *1*, 19–30. [CrossRef]
77. Cai, X.; Yang, Y.; Xie, X.; Yu, F.; Yang, Y.; Yang, Z.; Zhang, T.; Mei, X. Preparation, characterization and pulmonary pharmacokinetics of a new inhalable zanamivir dry powder. *Drug Deliv.* **2016**, *23*, 1962–1971. [CrossRef]
78. NICE. Tobramycin. Available online: https://bnf.nice.org.uk/medicinal-forms/tobramycin.html (accessed on 5 November 2020).
79. Emc. Colomycin 1 Million International Units (IU) Powder for Solution, Injection, Infusion or Inhalation. Available online: https://www.medicines.org.uk/emc/product/1094/smpc (accessed on 5 November 2020).
80. NICE. Colistimethate Sodium. Available online: https://bnf.nice.org.uk/medicinal-forms/colistimethate-sodium.html (accessed on 5 November 2020).
81. NICE. Aztreonam. Available online: https://bnf.nice.org.uk/medicinal-forms/aztreonam.html (accessed on 5 November 2020).
82. Pharma, D. Dry Powder Inhalation. Available online: https://dfepharma.com/Excipients/Expertise/Dry-Powder-Inhalation (accessed on 31 March 2021).
83. Demoly, P.; Hagedoorn, P.; De Boer, A.H.; Frijlink, H.W. The clinical relevance of dry powder inhaler performance for drug delivery. *Respir. Med.* **2014**, *108*, 1195–1203. [CrossRef]
84. Tan, B.M.J.; Chan, L.W.; Heng, P.W.S. Improving Dry Powder Inhaler Performance by Surface Roughening of Lactose Carrier Particles. *Pharm. Res.* **2016**, *33*. [CrossRef]
85. Lee, H.; Lee, H.; Kwon, Y.; Kim, J.; Rhee, Y.; Chon, J.; Park, E.; Kim, D.; Park, C. The role of lactose carrier on the powder behaviour and aerodynamic performance of bosentan microparticles for dry powder inhalation. *Eur. J. Pharm. Sci.* **2018**, *117*, 279–289. [CrossRef]
86. Yeung, S.; Traini, D.; Tweedie, A.; Lewis, D.; Church, T.; Young, P. Limitations of high dose carrier based formulations. *Int. J. Pharm.* **2018**, *544*, 141–152. [CrossRef] [PubMed]
87. Pacławski, A.; Szlęk, J.; Lau, R.; Jachowicz, R.; Mendyk, A. Empirical modeling of the fine particle fraction for carrier-based pulmonary delivery formulations. *Int J. Nanomed.* **2015**, *10*, 801–810. [CrossRef]
88. Ambrus, R.; Benke, E.; Farkas, Á.; Balásházy, I.; Szabó-Révész, P. Novel dry powder inhaler formulation containing antibiotic using combined technology to improve aerodynamic properties. *Eur. J. Pharm. Sci.* **2018**, *123*, 20–27. [CrossRef] [PubMed]
89. Ceschan, N.; Bucalá, V.; Mateos, M.; Smyth, H.; Ramírez-Rigo, M. Carrier free indomethacin microparticles for dry powder inhalation. *Int. J. Pharm.* **2018**, *549*, 169–178. [CrossRef] [PubMed]
90. Momin, M.; Sinha, S.; Tucker, I.; Das, S. Carrier-free combination dry powder inhaler formulation of ethionamide and moxifloxacin for treating drug resistant tuberculosis. *Drug Dev. Ind. Pharm.* **2019**, *45*, 1321–1331. [CrossRef] [PubMed]
91. Azari, F.; Ghanbarzadeh, S.; Safdari, R.; Yaqoubi, S.; Adibkia, K.; Hamishehkar, H. Development of a Carrier Free Dry Powder Inhalation Formulation of Ketotifen for Pulmonary Drug Delivery. *Drug Res.* **2020**, *70*, 26–32. [CrossRef]
92. Nguyen, T.; Yi, E.; Hwang, K.; Cho, C.; Park, C.; Kim, J.; Rhee, Y.; Park, E. Formulation and evaluation of carrier-free dry powder inhaler containing sildenafil. *Drug Deliv. Transl. Res.* **2019**, *9*, 319–333. [CrossRef]
93. Yazdi, A.; Smyth, H. Carrier-free high-dose dry powder inhaler formulation of ibuprofen: Physicochemical characterization and in vitro aerodynamic performance. *Int. J. Pharm.* **2016**, *511*, 403–414. [CrossRef]
94. Edwards, A.; Chambers, A. Comparison of a lactose-free formulation of sodium cromoglycate and sodium cromoglycate plus lactose in the treatment of asthma. *Curr. Med. Res. Opin.* **1989**, *11*, 283–292. [CrossRef] [PubMed]
95. Pilcer, G.; De Bueger, V.; Traina, K.; Traore, H.; Sebti, T.; Vanderbist, F.; Amighi, K. Carrier-free combination for dry powder inhalation of antibiotics in the treatment of lung infections in cystic fibrosis. *Int. J. Pharm.* **2013**, *451*, 112–120. [CrossRef]
96. Raula, J.; Lahde, A.; Kauppinen, E. Aerosolization behaviour of carrier-free L-leucine coated salbutamol sulphate powders. *Int. J. Pharm.* **2009**, *365*, 18–25. [CrossRef] [PubMed]
97. Haghi, M.; van den Oetelaar, W.; Moir, L.; Zhu, B.; Phillips, G.; Crapper, J.; Young, P.; Traini, D. Inhalable tranexamic acid for haemoptysis treatment. *Eur. J. Pharm. Biopharm.* **2015**, *93*, 311–319. [CrossRef]
98. Suzuki, É.; Amaro, M.; de Almeida, G.; Cabral, L.; Healy, A.; de Sousa, V. Development of a new formulation of roflumilast for pulmonary drug delivery to treat inflammatory lung conditions. *Int. J. Pharm.* **2018**, *550*, 89–99. [CrossRef]
99. Zhu, B.; Padroni, M.; Colombo, G.; Phillips, G.; Crapper, J.; Young, P.; Traini, D. The development of a single-use, capsule-free multi-breath tobramycin dry powder inhaler for the treatment of cystic fibrosis. *Int. J. Pharm.* **2016**, *514*, 392–398. [CrossRef] [PubMed]
100. Chvatal, A.; Farkas, Á.; Balásházy, I.; Szabó-Révész, P.; Ambrus, R. Aerodynamic properties and in silico deposition of meloxicam potassium incorporated in a carrier-free DPI pulmonary system. *Int. J. Pharm.* **2017**, *520*, 70–78. [CrossRef]
101. Shetty, N.; Ahn, P.; Park, H.; Bhujbal, S.; Zemlyanov, D.; Cavallaro, A.; Mangal, S.; Li, J.; Zhou, Q. Improved Physical Stability and Aerosolization of Inhalable Amorphous Ciprofloxacin Powder Formulations by Incorporating Synergistic Colistin. *Mol. Pharm.* **2018**, *15*, 4004–4020. [CrossRef]
102. Cui, Y.; Zhang, X.; Wang, W.; Huang, Z.; Zhao, Z.; Wang, G.; Cai, S.; Jing, H.; Huang, Y.; Pan, X.; et al. Moisture-Resistant Co-Spray-Dried Netilmicin with l-Leucine as Dry Powder Inhalation for the Treatment of Respiratory Infections. *Pharmaceutics* **2018**, *10*, 252. [CrossRef] [PubMed]

103. Kumar, R.; Dalvi, S.V.; Siril, P.F. Nanoparticle-Based Drugs and Formulations: Current Status and Emerging Applications. *ACS Appl. Nano Mater.* **2020**, *3*, 4944–4961. [CrossRef]
104. Mangal, S.; Gao, W.; Li, T.; Zhou, Q. Pulmonary delivery of nanoparticle chemotherapy for the treatment of lung cancers: Challenges and opportunities. *Acta Pharmacol. Sin.* **2017**, *38*, 782–797. [CrossRef]
105. Huang, Z.; Kłodzińska, S.N.; Wan, F.; Nielsen, H.M. Nanoparticle-mediated pulmonary drug delivery: State of the art towards efficient treatment of recalcitrant respiratory tract bacterial infections. *Drug Deliv. Transl. Res.* **2021**, *11*, 1634–1654. [CrossRef]
106. Zhu, C.; Chen, J.; Yu, S.; Que, C.; Taylor, L.S.; Tan, W.; Wu, C.; Zhou, Q.T. Inhalable Nanocomposite Microparticles with Enhanced Dissolution and Superior Aerosol Performance. *Mol. Pharm.* **2020**, *17*, 3270–3280. [CrossRef]
107. Roa, W.H.; Azarmi, S.; Al-Hallak, M.H.D.K.; Finlay, W.H.; Magliocco, A.M.; Löbenberg, R. Inhalable nanoparticles, a non-invasive approach to treat lung cancer in a mouse model. *J. Control. Release* **2011**, *150*, 49–55. [CrossRef]
108. Azarmi, S.; Tao, X.; Chen, H.; Wang, Z.; Finlay, W.H.; Löbenberg, R.; Roa, W.H. Formulation and cytotoxicity of doxorubicin nanoparticles carried by dry powder aerosol particles. *Int. J. Pharm.* **2006**, *319*, 155–161. [CrossRef] [PubMed]
109. Indermun, S.; Govender, M.; Kumar, P.; Choonara, Y.E.; Pillay, V. Porous particulate platforms for enhanced pulmonary delivery of bioactives. In *Targeting Chronic Inflammatory Lung Diseases Using Advanced Drug Delivery Systems*; Elsevier: Amsterdam, The Netherlands, 2020; pp. 359–373.
110. Chvatal, A.; Ambrus, R.; Party, P.; Katona, G.; Jójárt-Laczkovich, O.; Szabó-Révész, P.; Fattal, E.; Tsapis, N. Formulation and comparison of spray dried non-porous and large porous particles containing meloxicam for pulmonary drug delivery. *Int. J. Pharm.* **2019**, *559*, 68–75. [CrossRef] [PubMed]
111. Ogienko, A.G.; Bogdanova, E.G.; Trofimov, N.A.; Myz, S.A.; Ogienko, A.A.; Kolesov, B.A.; Yunoshev, A.S.; Zubikov, N.V.; Manakov, A.Y.; Boldyrev, V.V.; et al. Large porous particles for respiratory drug delivery. Glycine-based formulations. *Eur. J. Pharm. Sci.* **2017**, *110*, 148–156. [CrossRef]
112. Al-Obaidi, H.; Majumder, M.; Bari, F. Amorphous and crystalline particulates: Challenges and perspectives in drug delivery. *Curr. Pharm. Des.* **2016**, *23*, 350–361. [CrossRef]
113. Al-Obaidi, H.; Lawrence, M.J.; Buckton, G. Atypical effects of incorporated surfactants on stability and dissolution properties of amorphous polymeric dispersions. *J. Pharm. Pharmacol.* **2016**, *68*, 1373–1383. [CrossRef]
114. Hancock, B.C.; Parks, M. What is the true solubility advantage for amorphous pharmaceuticals? *Pharm. Res.* **2000**, *17*, 397–404. [CrossRef] [PubMed]
115. Bhanderi, A.; Bari, F.; Al-Obaidi, H. Evaluation of the impact of surfactants on miscibility of griseofulvin in spray dried amorphous solid dispersions. *J. Drug Deliv. Sci. Technol.* **2021**, *64*, 102606. [CrossRef]
116. Baghel, S.; Cathcart, H.; O'Reilly, N.J. Polymeric Amorphous Solid Dispersions: A Review of Amorphization, Crystallization, Stabilization, Solid-State Characterization, and Aqueous Solubilization of Biopharmaceutical Classification System Class II Drugs. *J. Pharm. Sci.* **2016**, *105*, 2527–2544. [CrossRef]
117. Grzybowska, K.; Paluch, M.; Wlodarczyk, P.; Grzybowski, A.; Kaminski, K.; Hawelek, L.; Zakowiecki, D.; Kasprzycka, A.; Jankowska-Sumara, I. Enhancement of amorphous celecoxib stability by mixing it with octaacetylmaltose: The molecular dynamics study. *Mol. Pharmacol.* **2012**, *9*, 894–904. [CrossRef]
118. Al-Obaidi, H.; Brocchini, S.; Buckton, G. Anomalous properties of spray dried solid dispersions. *J. Pharm. Sci.* **2009**, *98*, 4724–4737. [CrossRef]
119. Al-Obaidi, H.; Buckton, G. Evaluation of griseofulvin binary and ternary solid dispersions with HPMCAS. *AAPS PharmSciTech* **2009**, *10*, 1172–1177. [CrossRef]
120. AboulFotouh, K.; Zhang, Y.; Maniruzzaman, M.; Williams, R.O.; Cui, Z. Amorphous solid dispersion dry powder for pulmonary drug delivery: Advantages and challenges. *Int. J. Pharm.* **2020**, *587*, 119711. [CrossRef]
121. Karimi, K.; Katona, G.; Csóka, I.; Ambrus, R. Physicochemical stability and aerosolization performance of dry powder inhalation system containing ciprofloxacin hydrochloride. *J. Pharm. Biomed. Anal.* **2018**, *148*, 73–79. [CrossRef] [PubMed]
122. Moes, J.; Koolen, S.; Huitema, A.; Schellens, J.; Beijnen, J.; Nuijen, B. Development of an oral solid dispersion formulation for use in low-dose metronomic chemotherapy of paclitaxel. *Eur. J. Pharm. Biopharm.* **2013**, *83*, 87–94. [CrossRef] [PubMed]
123. Purohit, H.S.; Taylor, L.S. Phase Behavior of Ritonavir Amorphous Solid Dispersions during Hydration and Dissolution. *Pharm. Res.* **2017**, *34*, 2842–2861. [CrossRef] [PubMed]
124. Mizoguchi, R.; Waraya, H.; Hirakura, Y. Application of Co-Amorphous Technology for Improving the Physicochemical Properties of Amorphous Formulations. *Mol. Pharm.* **2019**, *16*, 2142–2152. [CrossRef] [PubMed]
125. Newman, A.; Zografi, G. Commentary: Considerations in the Measurement of Glass Transition Temperatures of Pharmaceutical Amorphous Solids. *Am. Assoc. Pharm. Sci.* **2019**, *21*, 26. [CrossRef]
126. Wostry, M.; Plappert, H.; Grohganz, H. Preparation of Co-Amorphous Systems by Freeze-Drying. *Pharmaceutics* **2020**, *12*, 941. [CrossRef]
127. Lim, A.W.; Löbmann, K.; Grohganz, H.; Rades, T.; Chieng, N. Investigation of physical properties and stability of indomethacin-cimetidine and naproxen-cimetidine co-amorphous systems prepared by quench cooling, coprecipitation and ball milling. *J. Pharm. Pharmacol.* **2016**, *68*, 36–45. [CrossRef]
128. Karagianni, A.; Kachrimanis, K.; Nikolakakis, I. Co-Amorphous Solid Dispersions for Solubility and Absorption Improvement of Drugs: Composition, Preparation, Characterization and Formulations for Oral Delivery. *Pharmaceutics* **2018**, *10*, 98. [CrossRef]

129. Lababidi, N.; Ofosu Kissi, E.; Elgaher, W.A.M.; Sigal, V.; Haupenthal, J.; Schwarz, B.C.; Hirsch, A.K.H.; Rades, T.; Schneider, M. Spray-drying of inhalable, multifunctional formulations for the treatment of biofilms formed in cystic fibrosis. *J. Control. Release* **2019**, *314*, 62–71. [CrossRef]
130. Zhou, Q.T.; Loh, Z.H.; Yu, J.; Sun, S.P.; Gengenbach, T.; Denman, J.A.; Li, J.; Chan, H.K. How Much Surface Coating of Hydrophobic Azithromycin Is Sufficient to Prevent Moisture-Induced Decrease in Aerosolisation of Hygroscopic Amorphous Colistin Powder? *Am. Assoc. Pharm. Sci.* **2016**, *18*, 1213–1224. [CrossRef]
131. Wang, Z.; Sun, M.; Liu, T.; Gao, Z.; Ye, Q.; Tan, X.; Hou, Y.; Sun, J.; Wang, D.; He, Z. Co-amorphous solid dispersion systems of lacidipine-spironolactone with improved dissolution rate and enhanced physical stability. *Asian J. Pharm. Sci.* **2019**, *14*, 95–103. [CrossRef] [PubMed]
132. Mangal, S.; Nie, H.; Xu, R.; Guo, R.; Cavallaro, A.; Zemlyanov, D.; Zhou, Q.T. Physico-Chemical Properties, Aerosolization and Dissolution of Co-Spray Dried Azithromycin Particles with L-Leucine for Inhalation. *Pharm. Res.* **2018**, *35*. [CrossRef] [PubMed]
133. Kasten, G.; Löbmann, K.; Grohganz, H.; Rades, T. Co-former selection for co-amorphous drug-amino acid formulations. *Int. J. Pharm.* **2019**, *557*, 366–373. [CrossRef]
134. Su, M.; Xia, Y.; Shen, Y.; Heng, W.; Wei, Y.; Zhang, L.; Gao, Y.; Zhang, J.; Qian, S. A novel drug–drug coamorphous system without molecular interactions: Improve the physicochemical properties of tadalafil and repaglinide. *RSC Adv.* **2020**, *10*, 565–583. [CrossRef]
135. Carvahlo, R.S.; Watts, B.A.; Peters, I.J.; Williams, O.R. *Dry Powder Inhalation for Pulmonary Delivery: Recent Advances and Continuing Challenges*; Wiley: Chichester, UK, 2015; pp. 36–48.
136. Chen, Z.; Yang, K.; Huang, C.; Zhu, A.; Yu, L.; Qian, F. Surface Enrichment and Depletion of the Active Ingredient in Spray Dried Amorphous Solid Dispersions. *Pharm. Res.* **2018**, *35*, 38. [CrossRef]
137. Al-Obaidi, H.; Ke, P.; Brocchini, S.; Buckton, G. Characterization and stability of ternary solid dispersions with PVP and PHPMA. *Int. J. Pharm.* **2011**, *419*, 20–27. [CrossRef]
138. Vehring, R. Pharmaceutical particle engineering via spray drying. *Pharm. Res.* **2008**, *25*, 999–1022. [CrossRef]
139. Onoue, S.; Sato, H.; Kawabata, Y.; Mizumoto, T.; Hashimoto, N.; Yamada, S. In vitro and in vivo characterization on amorphous solid dispersion of cyclosporine A for inhalation therapy. *J. Control. Release* **2009**, *138*, 16–23. [CrossRef]
140. Jong, T.; Li, J.; Morton, D.A.; Zhou, Q.T.; Larson, I. Investigation of the Changes in Aerosolization Behavior Between the Jet-Milled and Spray-Dried Colistin Powders Through Surface Energy Characterization. *J. Pharm. Sci.* **2016**, *105*, 1156–1163. [CrossRef]
141. Shetty, N.; Park, H.; Zemlyanov, D.; Mangal, S.; Bhujbal, S.; Zhou, Q.T. Influence of excipients on physical and aerosolization stability of spray dried high-dose powder formulations for inhalation. *Int. J. Pharm.* **2018**, *544*, 222–234. [CrossRef] [PubMed]
142. Wang, L.; Zhang, Y.; Tang, X. Characterization of a new inhalable thymopentin formulation. *Int. J. Pharm.* **2009**, *375*, 1–7. [CrossRef] [PubMed]
143. Zijlstra, G.S.; Rijkeboer, M.; Jan van Drooge, D.; Sutter, M.; Jiskoot, W.; van de Weert, M.; Hinrichs, W.L.; Frijlink, H.W. Characterization of a cyclosporine solid dispersion for inhalation. *AAPS J.* **2007**, *9*, E190–E199. [CrossRef] [PubMed]
144. Wang, Y.-B.; Watts, A.B.; Peters, J.I.; Liu, S.; Batra, A.; Williams, R.O., 3rd. In vitro and in vivo performance of dry powder inhalation formulations: Comparison of particles prepared by thin film freezing and micronization. *AAPS PharmSciTech* **2014**, *15*, 981–993. [CrossRef]
145. Watts, A.B.; Wang, Y.-B.; Johnston, K.P.; Williams, R.O. Respirable Low-Density Microparticles Formed In Situ from Aerosolized Brittle Matrices. *Pharm. Res.* **2013**, *30*, 813–825. [CrossRef]
146. Momin, M.A.M.; Sinha, S.; Tucker, G.I.; Doyle, C.; Das, C.S. Dry powder formulation of kanamycin with enhanced aerosolization efficiency for drug-resistant tuberculosis. *Int. J. Pharm.* **2017**, *528*, 107–117. [CrossRef]
147. McShane, P.J.; Weers, J.G.; Tarara, T.E.; Haynes, A.; Durbha, P.; Miller, D.P.; Mundry, T.; Operschall, E.; Elborn, J.S. Ciprofloxacin Dry Powder for Inhalation (ciprofloxacin DPI): Technical design and features of an efficient drug-device combination. *Pulm. Pharmacol. Ther.* **2018**, *50*, 72–79. [CrossRef]
148. Mohammed, A.; Zurek, J.; Madueke, S.; Al-Kassimy, H.; Yaqoob, M.; Houacine, C.; Ferraz, A.; Kalgudi, R.; Zariwala, M.G.; Hawkins, N.; et al. Generation of High Dose Inhalable Effervescent Dispersions against Pseudomonas aeruginosa Biofilms. *Pharm. Res.* **2020**, *37*, 150. [CrossRef]
149. Porowska, A.; Dosta, M.; Fries, L.; Gianfrancesco, A.; Heinrich, S.; Palzer, S. Predicting the surface composition of spray-dried particle by modelling component reorganisation in a drying droplet. *Chem. Eng. Res. Des.* **2016**, *110*, 131–140. [CrossRef]
150. Li, X.; Vogt, F.G.; Hayes, D.; Mansour, H.M. Design, characterization, and aerosol dispersion performance modeling of advanced co-spray dried antibiotics with mannitol as respirable microparticles/nanoparticles for targeted pulmonary delivery as dry powder inhalers. *Pharm. Drug Deliv. Pharm. Technol.* **2014**, *103*, 2937–2949. [CrossRef] [PubMed]
151. Padhi, B.K.; Chougule, M.B.; Misra, A. Optimization of formulation components and characterization of large respirable powders containing high therapeutic payload. *Pharm. Dev. Technol.* **2006**, *11*, 465–475. [CrossRef] [PubMed]
152. Hassan, A.; Farkas, D.; Longest, W.; Hindle, M. Characterization of excipient enhanced growth (EEG) tobramycin dry powder aerosol formulations. *Int. J. Pharm.* **2020**, *591*, 120027. [CrossRef]
153. Longest, P.W.; Farkas, D.; Hassan, A.; Hindle, M. Computational Fluid Dynamics (CFD) Simulations of Spray Drying: Linking Drying Parameters with Experimental Aerosolization Performance. *Pharm. Res.* **2020**, *37*, 101. [CrossRef] [PubMed]
154. Yu, J.; Chan, H.K.; Gengenbach, T.; Denman, J.A. Protection of hydrophobic amino acids against moisture-induced deterioration in the aerosolization performance of highly hygroscopic spray-dried powders. *Eur. J. Pharm. Biopharm.* **2017**, *119*, 224–234. [CrossRef] [PubMed]

155. Maa, Y.F.; Costantino, H.R.; Nguyen, P.A.; Hsu, C.C. The effect of operating and formulation variables on the morphology of spray-dried protein particles. *Pharm. Dev. Technol.* **1997**, *2*, 213–223. [CrossRef]
156. Guenette, E.; Barrett, A.; Kraus, D.; Brody, R.; Harding, L.; Magee, G. Understanding the effect of lactose particle size on the properties of DPI formulations using experimental design. *Int. J. Pharm.* **2009**, *380*, 80–88. [CrossRef]
157. Tulane University. Mucolytics. Available online: https://tmedweb.tulane.edu/pharmwiki/doku.php/mucolytics (accessed on 14 April 2021).
158. British National Formulary (Online). Cystic Fibrosis. Available online: https://bnf.nice.org.uk/treatment-summary/cystic-fibrosis.html (accessed on 18 April 2021).
159. Lamy, B.; Tewes, F.; Serrano, D.R.; Lamarche, I.; Gobin, P.; Couet, W.; Healy, A.M.; Marchand, S. New aerosol formulation to control ciprofloxacin pulmonary concentration. *J. Control. Release* **2018**, *271*, 118–126. [CrossRef]
160. Tewes, F.; Brillault, J.; Lamy, B.; O'Connell, P.; Olivier, J.-C.; Couet, W.; Healy, A.M. Ciprofloxacin-Loaded Inorganic–Organic Composite Microparticles To Treat Bacterial Lung Infection. *Mol. Pharm.* **2016**, *13*, 100–112. [CrossRef] [PubMed]
161. Barazesh, A.; Gilani, K.; Rouini, M.; Barghi, M.A. The effect of metal salts on aerosol performance of spray dried carrier-free formulations of levofloxacin. *Daru* **2020**, *28*, 75–85. [CrossRef] [PubMed]
162. Walsh, D.; Serrano, D.; Worku, Z.; Norris, B.; Healy, A. Production of cocrystals in an excipient matrix by spray drying. *Int. J. Pharm.* **2018**, *536*, 467–477. [CrossRef]
163. Karashima, M.; Sano, N.; Yamamoto, S.; Arai, Y.; Yamamoto, K.; Amano, N.; Ikeda, Y. Enhanced pulmonary absorption of poorly soluble itraconazole by micronized cocrystal dry powder formulations. *Eur. J. Pharm. Biopharm. Off. J. Arb. Pharm. Verfahr. EV* **2017**, *115*, 65–72. [CrossRef]
164. Emami, S.; Adibkia, K.; Barzegar-Jalali, M.; Siahi-Shadbad, M. Piroxicam cocrystals with phenolic coformers: Preparation, characterisation and dissolution properties. *Pharm. Dev. Technol.* **2018**, *24*, 199–210. [CrossRef] [PubMed]
165. Wicker, J.; Crowley, L.; Robshaw, O.; Little, E.; Stokes, S.; Cooper, R.; Lawrence, S. Will they cocrystallize? *CrysEngComm* **2017**, *19*, 5336–5340. [CrossRef]
166. Fukte, S.; Wagh, M.; Rawat, S. Coformer selection: An important tool in cocrystal formation. *Int. J. Pharm. Pharm. Sci.* **2014**, *6*, 9–14.
167. Cvetkovski, A.; Ferretti, V.; Bertolasi, V. New Pharmaceutical Salts Containing Pyridoxine. *Acta Crystallogr. Sect. C Struct. Chem.* **2017**, *73*, 1064–1070. [CrossRef]
168. Chadha, R.; Bhalla, Y.; Nandan, A.; Chadha, K.; Karan, M. Chrysin Cocrystals: Characterization and Evaluation. *J. Pharm. Biomed. Anal.* **2017**, *134*, 361–371. [CrossRef] [PubMed]
169. Perlovich, G.L. Thermodynamic characteristics of cocrystal formation and melting points for rational design of pharmaceutical two-component systems. *CrysEngComm* **2015**, *17*, 7019–7028. [CrossRef]
170. Panzade, P.; Shendarkar, G. Superior Solubility and Dissolution of Zaltoprofen via Pharmaceutical Cocrystals. *Turk. J. Pharm. Sci.* **2019**, *16*, 310–316. [CrossRef]
171. Ogienko, A.G.; Myz, S.A.; Ogienko, A.A.; Nefedov, A.A.; Stoporev, A.S.; Mel'gunov, M.S.; Yunoshev, A.S.; Shakhtshneider, T.P.; Boldyrev, V.V.; Boldyreva, E.V. Cryosynthesis of Co-Crystals of Poorly Water-Soluble Pharmaceutical Compounds and Their Solid Dispersions with Polymers. The "Meloxicam–Succinic Acid" System as a Case Study. *Cryst Growth Des.* **2018**, *18*, 7401–7409. [CrossRef]
172. Zellnitz, S.; Roblegg, E.; Pinto, J.; Fröhlich, E. Delivery of Dry Powders to the Lungs: Influence of Particle Attributes from a Biological and Technological Point of View. *Curr. Drug Deliv.* **2019**, *16*, 180–194. [CrossRef]
173. Alhalaweh, A.; Kaialy, W.; Buckton, G.; Gill, H.; Nokhodchi, A.; Velaga, S.P. Theophylline cocrystals prepared by spray drying: Physicochemical properties and aerosolization performance. *AAPS PharmSciTech* **2013**, *14*, 265–276. [CrossRef]
174. Tanaka, R.; Hattori, Y.; Otsuka, M.; Ashizawa, K. Application of spray freeze drying to theophylline-oxalic acid cocrystal engineering for inhaled dry powder technology. *Drug Dev. Ind. Pharm.* **2020**, *46*, 179–187. [CrossRef]
175. Gautam, M.; Besan, M.; Pandit, D.; Mandal, S.; Chadha, R. Cocrystal of 5-Fluorouracil: Characterization and Evaluation of Biopharmaceutical Parameters. *AAPS PharmSciTech* **2019**, *20*, 149. [CrossRef]
176. Tomar, S.; Chakraborti, S.; Jindal, A.; Grewal, M.; Chadha, R. Cocrystals of diacerein: Towards the development of improved biopharmaceutical parameters. *Int. J. Pharm.* **2020**, *574*, 118942. [CrossRef]
177. Bhalla, Y.; Chadha, K.; Chadha, R.; Karan, M. Daidzein cocrystals: An opportunity to improve its biopharmaceutical parameters. *Heliyon* **2019**, *5*, e02669. [CrossRef]
178. Shinozaki, T.; Ono, M.; Higashi, K.; Moribe, K. A Novel Drug-Drug Cocrystal of Levofloxacin and Metacetamol: Reduced Hygroscopicity and Improved Photostability of Levofloxacin. *J. Pharm. Sci.* **2019**, *108*, 2383–2390. [CrossRef]
179. Wang, Q.; Xue, J.; Hong, Z.; Du, Y. Pharmaceutical Cocrystal Formation of Pyrazinamide with 3-Hydroxybenzoic Acid: A Terahertz and Raman Vibrational Spectroscopies Study. *Molecules* **2019**, *24*, 488. [CrossRef]
180. do Amaral, L.; do Carmo, F.; Amaro, M.; de Sousa, V.; da Silva, L.; de Almeida, G.; Rodrigues, C.; Healy, A.; Cabral, L. Development and Characterization of Dapsone Cocrystal Prepared by Scalable Production Methods. *AAPS PharmSciTech* **2018**, *19*, 2687–2699. [CrossRef]
181. Khan, E.; Shukla, A.; Jhariya, A.; Tandon, P.; Vangala, V. Nitrofurantoin-melamine monohydrate (cocrystal hydrate): Probing the role of H-bonding on the structure and properties using quantum chemical calculations and vibrational spectroscopy. *Spectrochim. Acta Part. A Mol. Biomol. Spectrosc.* **2019**, *221*, 117170. [CrossRef]

182. Stavropoulos, K.; Johnston, S.; Zhang, Y.; Rao, B.; Hurrey, M.; Hurter, P.; Topp, E.; Kadiyala, I. Cocrystalline Solids of Telaprevir with Enhanced Oral Absorption. *J. Pharm. Sci.* **2015**, *104*, 3343–3350. [CrossRef]
183. Ton, Q.; Egert, E. Cocrystals of the antibiotic trimethoprim with glutarimide and 3,3-dimethylglutarimide held together by three hydrogen bonds. *Acta Crystallogr. Sect. C Struct. Chem.* **2015**, *71*, 75–79. [CrossRef]
184. Haneef, J.; Arora, P.; Chadha, R. Implication of Coformer Structural Diversity on Cocrystallization Outcomes of Telmisartan with Improved Biopharmaceutical Performance. *AAPS PharmSciTech* **2019**, *21*, 10. [CrossRef] [PubMed]
185. Serrano, D.; Persoons, T.; D'Arcy, D.; Galiana, C.; Dea-Ayuela, M.; Healy, A. Modelling and shadowgraph imaging of cocrystal dissolution and assessment of in vitro antimicrobial activity for sulfadimidine/4-aminosalicylic acid cocrystals. *Eur. J. Pharm. Sci.* **2016**, *89*, 125–136. [CrossRef] [PubMed]
186. Swapna, B.; Maddileti, D.; Nangia, A. Cocrystals of the Tuberculosis Drug Isoniazid: Polymorphism, Isostructurality, and Stability. *Cryst. Growth Des.* **2014**, *14*, 5991–6005. [CrossRef]
187. Seo, J.; Hwang, K.; Lee, S.; Kim, D.; Park, E. Preparation and characterization of adefovir dipivoxil-stearic acid cocrystal with enhanced physicochemical properties. *Pharm. Dev. Technol.* **2017**, *23*, 890–899. [CrossRef]
188. Cai, Q.; Xue, J.; Wang, Q.; Du, Y. Solid-state cocrystal formation between acyclovir and fumaric acid: Terahertz and Raman vibrational spectroscopic studies. *Spectrochim. Acta Part. A Mol. Biomol. Spectrosc.* **2017**, *186*, 29–36. [CrossRef] [PubMed]
189. Cheney, M.; Weyna, D.; Shan, N.; Hanna, M.; Wojtas, L.; Zaworotko, M. Coformer selection in pharmaceutical cocrystal development: A case study of a meloxicam aspirin cocrystal that exhibits enhanced solubility and pharmacokinetics. *J. Pharm. Sci.* **2011**, *100*, 2172–2181. [CrossRef] [PubMed]
190. Ray, E.; Vaghasiya, K.; Sharma, A.; Shukla, R.; Khan, R.; Kumar, A.; Verma, R. Autophagy-Inducing Inhalable Co-crystal Formulation of Niclosamide-Nicotinamide for Lung Cancer Therapy. *AAPS PharmSciTech* **2020**, *21*, 260. [CrossRef] [PubMed]
191. Zhang, Z.; Zhang, Q.; Zhang, Q.; Chen, C.; He, M.; Chen, Q.; Song, G.; Xuan, X.; Huang, X. From a binary salt to salt co-crystals of antibacterial agent lomefloxacin with improved solubility and bioavailability. *Acta Crystallogr. Sect. B Struct. Sci. Cryst. Eng. Mater.* **2015**, *71*, 437–446. [CrossRef]
192. Liu, L.; Zou, D.; Zhang, Y.; Zhang, Q.; Feng, Y.; Guo, Y.; Liu, Y.; Zhang, X.; Cheng, G.; Wang, C.; et al. Pharmaceutical salts/cocrystals of enoxacin with dicarboxylic acids: Enhancing in vitro antibacterial activity of enoxacin by improving the solubility and permeability. *Eur. J. Pharm. Biopharm.* **2020**, *154*, 62–73. [CrossRef] [PubMed]
193. Abidi, S.; Azim, Y.; Khan, S.; Khan, A. Sulfaguanidine cocrystals: Synthesis, structural characterization and their antibacterial and hemolytic analysis. *J. Pharm. Biomed. Anal.* **2018**, *149*, 351–357. [CrossRef]

Chapter 3

# Preparation and Physiochemical Analysis of Novel Ciprofloxacin / Dicarboxylic Acid Salts

Publication Details:
**Hibbard T**, Nyambura B, Scholes P, Totolici M, Shankland K, Al-Obaidi H. Preparation and
Physiochemical Analysis of Novel Ciprofloxacin / Dicarboxylic Acid Salts. *J Pharm Sci*. 2023;112(1):195-203.

Chapter Summary:

In this chapter, four new salt forms of ciprofloxacin were reported including full crystal structures analysis and physicochemical characterisation. All salt forms showed increased solubility compared to ciprofloxacin base form and the glutaric acid salt showed a substantial increase in solubility compared to ciprofloxacin hydrochloride monohydrate. All four salt forms retained antimicrobial activity *in vivo*.

Author Contributions:

TH: conceptualisation, investigation, methodology, writing – original draft, review & editing; BN, PS: conceptualisation, review & editing; MT: review & editing; KS: crystallographic investigation, writing – original draft, review & editing; HAO: conceptualisation, investigation, methodology, project administration, writing – original draft, review & editing.

Journal of Pharmaceutical Sciences 112 (2023) 195–203

Contents lists available at ScienceDirect

Journal of Pharmaceutical Sciences

journal homepage: www.jpharmsci.org

Pharmaceutics, Drug Delivery and Pharmaceutical Technology

# Preparation and Physiochemical Analysis of Novel Ciprofloxacin / Dicarboxylic Acid Salts

Thomas Hibbard[a], Bildad Nyambura[b], Peter Scholes[b], Mihaela Totolici[b], Kenneth Shankland[a,*], Hisham Al-Obaidi[a,*]

[a] School of Pharmacy, University of Reading, Reading, RG6 6AD, UK
[b] Quotient Sciences, 5 Boulton Road, Reading, RG2 0NH, UK

ARTICLE INFO

*Article history:*
Received 19 April 2022
Revised 27 July 2022
Accepted 5 August 2022
Available online 8 August 2022

*Keywords:*
Mechanochemical activation
Crystalline salts
Ciprofloxacin
Single crystal
Thermal analysis
Solubility

ABSTRACT

The crystal structures of four novel dicarboxylic acid salts of ciprofloxacin (CFX) with modified physicochemical properties, prepared by mechanochemical synthesis and solvent crystallization, are reported. A series of dicarboxylic acids of increasing molecular weight was chosen, predicted to interact via a carboxylic acid:secondary amine synthon. These were succinic (SA), glutaric (GA), adipic (AA) and pimelic (PA) acids (4, 5, 6, 7 carbon atoms respectively). Characterized by single crystal and powder X-ray diffraction, Fourier-Transform Infrared Spectroscopy, thermogravimetric analysis, differential scanning calorimetry, scanning electron microscopy and aqueous solubility measurements, these salts showed distinct physicochemical properties relative to ciprofloxacin base. Searches of the Cambridge Structural Database (CSD) confirmed CFX-SA, CFX-GA, CFX-AA and CFX-PA to be novel crystal structures. Furthermore, the GA salt has substantially higher solubility than the widely available hydrochloride monohydrate salt (CFX-HCl·$H_2O$). CFX-SA, CFX-GA and CFX-AA showed minimum inhibitory concentration (MIC) of 0.008 g/L and CFX-PA showed MIC of 0.004 g/L. The prepared CFX salts retained antibacterial activity exhibiting equivalent antimicrobial activity to CFX-HCl·$H_2O$. These salts have positive implications for increasing the application of CFX beyond conventional oral formulations and highlight mechanochemical activation as suitable production method.

© 2022 The Authors. Published by Elsevier Inc. on behalf of American Pharmacists Association. CCBYLICENSE
This is an open access article under the CC BY IGO license (http://creativecommons.org/licenses/by/3.0/igo/)

## Introduction

Aqueous solubility of active pharmaceutical ingredients (APIs) can be improved through the discovery of new solid forms. Common examples of different solid forms used are salts, polymorphs, amorphous and coamorphous forms, cocrystals, solvates and hydrates; these are the subject of several extensive reviews and studies.[1-7] In each of these cases, the same API can exhibit different physiochemical properties without change to the chemical structure.[8-10] Novel solid forms have a variety of applications[11,12] in oral and pulmonary drug delivery, and cocrystals, organic salts and inorganic salts showing a variety of physicochemical properties have previously been reported.[13-17]

Fluoroquinolone antibiotics, such as ciprofloxacin (CFX), have been the subject of a great deal of solid-state research due to their poor aqueous solubility.[18,19] CFX is classified as class IV drug exhibiting poor aqueous solubility and permeability limiting its absorption and bioavailability.[20] Recent application of CFX to target lung infections has showed significant improvement when delivered as dry powder directly to the lungs.[21] Nevertheless, the problem of poor solubility remains a challenge and a problem that requires crystal engineering approach. Salt formation is the most well-established among other methods and has brought many APIs to market, usually through increasing API solubility.[22,23] Although the hydrocholoride salt is often the preferred candidate, it is also associated with increased hygroscopicity leading to problems with manufacturing.[24,25] This can have a negative impact on applications in drug delivery to the lungs when dry powders are desired. Whilst there has been diverse research on inorganic counterions, the use of organic counterions remains relatively limited.

In this work, a series of four potential dicarboxylic acid counterions with increasing molecular weight was selected for study. Similar molecules have also been investigated for their synergistic antibacterial, antibiofilm effects. For example, Bahamondez-Canas et al. showed that succinic acid stimulated degeneration of biofilm, allowing enhanced killing of *P. aeruginosa*.[26,27] Selecting a series of counterions with increasing carbon chain length allows for a comparison between counterions and final product physicochemical properties.

* Corresponding authors.
*E-mail addresses:* k.shankland@reading.ac.uk (K. Shankland), h.al-obaidi@reading.ac.uk (H. Al-Obaidi).

https://doi.org/10.1016/j.xphs.2022.08.008
0022-3549/© 2022 The Authors. Published by Elsevier Inc. on behalf of American Pharmacists Association. CCBYLICENSE This is an open access article under the CC BY IGO license (http://creativecommons.org/licenses/by/3.0/igo/)

Of the counterions selected, only hydrated forms of ciprofloxacin: succinic acid and ciprofloxacin:adipic acid have previously been reported.[13,28] Crystal structures for four CFX salts are reported, as are their physicochemical properties, thermal behaviour, aqueous solubility and antimicrobial activity.

## Experimental Section

**Materials**: Ciprofloxacin base, ciprofloxacin hydrochloride monohydrate, succinic acid, glutaric acid, adipic acid and pimelic acid were obtained from Sigma-Aldrich (Dorset, UK). Methanol was obtained from Fisher-Scientific Limited (Leicestershire, UK). All chemicals were used as received.

## Methods

### *Counterion Selection*

Compatibility screening of CFX against a bank of coformers was performed using the "Co-crystal design" function of Mercury[29] and this yielded approximately 100 potential matches. A series of dicarboxylic acids of increasing molecular weight was chosen, predicted to interact via a carboxylic acid:secondary amine synthon. These were succinic (SA), glutaric (GA), adipic (AA) and pimelic (PA) acids (4, 5, 6, 7 carbon atoms respectively). The 2D structure formulas and physicochemical properties of CFX and the counterions are summarised in Fig. 1. The $\Delta pK_a$ ($pK_a$ (base) – $pK_a$ (acid)) values are greater than 3 in each case,[30] suggesting salt formation between the acid-base pairs.

### *Preparation of CFX Salts*

Equimolar quantities of CFX and counterion (1:1 molar ratio) were milled using a Retsch MM400 ball mill. A 25 mL vessel was shaken at 30 Hz for 30 mins with two 7.5 mm stainless steel balls and 20 $\mu$L of methanol. This approach to multicomponent crystal synthesis was tested successfully on a known theophylline:nicotinamide system.[31] CFX and counterions were also mixed in a MeOH/ACN (1:1 molar ratio) solvent system at 45°C for 4 to 6 hours. The resultant suspensions were filtered through a 0.22 $\mu$m syringe filter (Ministart®) and the filtrates left to saturate by solvent evaporation at 25°C. Resultant crystals were harvested for single crystal X-ray diffraction (SC-XRD). CFX and counterions were also dissolved in aqueous solution at 70°C. Resultant solutions were filtered through a 0.22 $\mu$m syringe filter (Ministart®) and left to saturate at 25°C. Resulting crystals were harvested for SC-XRD.

### *Powder X-ray Diffraction (PXRD)*

Transmission capillary PXRD data were collected for all powders post-milling, using a Bruker D8 Advance diffractometer equipped with a monochromatic Cu$K\alpha_1$ source. Samples were packed into 0.7 mm borosilicate glass capillaries then scanned in the range 4° to 45° 2$\theta$ using a step size of 0.0171° and a count time of 1.4 seconds per step. PXRD patterns were compared to reference data collected from starting materials using the same settings.

### *Single Crystal X-ray Diffraction (SC-XRD)*

Single crystals showing birefringence under polarised light were isolated in Paratone-N oil, then mounted on a suitable crystal mounting loop. Diffraction data at 100K were collected using a Rigaku Synergy diffractometer equipped with a Cu microsource, a HyPix detector and an Oxford Cryosystems Cryostream device. Crystal structures were solved using ShelXT[32] and refined using ShelXL[33] (running as part of the Olex2[34] system) and crosschecked with the Cambridge Structural Database (CSD) database[35] then rendered using Mercury.[36] The positions of hydrogen atoms were determined directly from the observed electron density. Hydrogen atoms attached to carbons were treated with a riding ('AFIX') model, whilst hydrogen atoms attached to O or N atoms were allowed to refine freely, ensuring that the co-crystal or salt nature of the materials was directly determined.

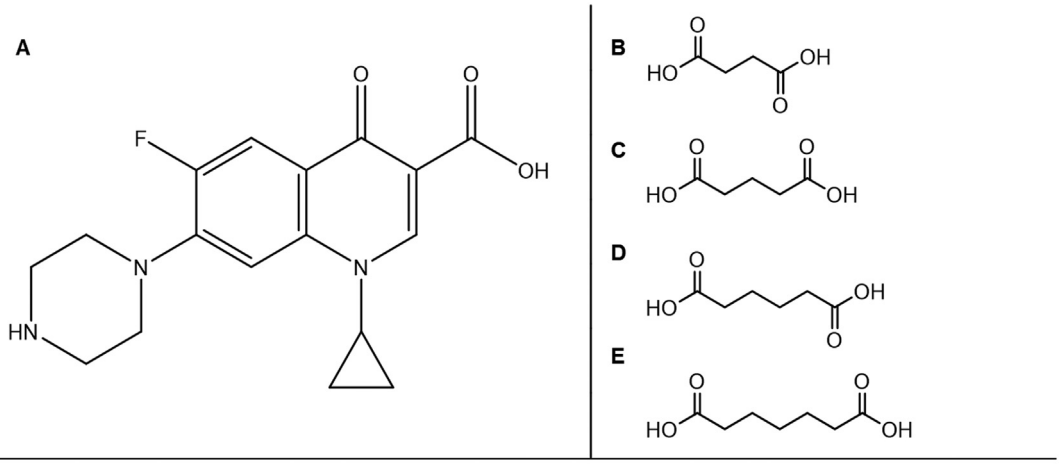


| | MWt / gmol$^{-1}$ | MPt / °C | log*P* | p$K_a$ | Water Solubility / mgml$^{-1}$ |
|---|---|---|---|---|---|
| **Succinic Acid (B)** | 118.09 | 188 | -0.59 | 4.21 | 83.2 |
| **Glutaric Acid (C)** | 132.11 | 96.9 | -0.29 | 4.34 | 1600 |
| **Adipic Acid (D)** | 146.14 | 153.2 | 0.08 | 4.44 | 30.8 |
| **Pimelic Acid (E)** | 160.17 | 106 | 0.61 | 4.51 | 50 |
| **Ciprofloxacin Base (A)** | 331.35 | 259 | 0.28 | 8.74 | 1.35 |

**Fig. 1.** The structures of ciprofloxacin base and the potential counterions used in this work. Key known physiochemical properties are listed.

*Fourier-Transform Infrared Spectroscopy (FTIR)*

FTIR spectra were collected using a Perkin-Elmer 100 FTIR Spectrometer equipped with a diamond attenuated total reflectance (ATR) accessory (Shelton, Connecticut, USA). 16 scans were made, with transmission recorded over the range 650–4000 $cm^{-1}$ with a resolution of 4 $cm^{-1}$.

*Thermal Analysis*

Melting point analysis was performed for all samples using a TA-Q2000 Differential Scanning Calorimetry (DSC) instrument (TA instruments, New Castle, USA). Samples were hermetically sealed in an aluminium pan and allowed to equilibrate at 30°C before heating at 10°C/min to 280°C in an $N_2$ atmosphere. Pierced lids were used to avoid issues relating to pressure build up during heating. Thermogravimetric Analysis (TGA) using TA-TGA Q50 instrument (New Castle, USA) was performed by weighing approximately 5-10mg of the samples and heated from ambient temperature at a heating rate of 10°C/min. TA Universal Analysis software was used to describe thermal events and to calculate melting points using onset temperature.

*Saturation Solubility Measurement*

Excess solid was added to 1 mL of phosphate buffers (0.1M and 0.2M, pH 6.8) and mixed at 25°C (± 1°C) using rotary mixer for 72 hours. Supernatant was removed following centrifugation and filtered through a 0.2 $\mu$m syringe filter (Ministart®). CFX concentration was determined using UV-Vis HPLC analysis (see SI for details) at 278 nm following calibration with stock CFX solutions.

*Determination of Minimum Inhibitory Concentration (MIC)*

MICs for all milled samples were measured against *Escherichia coli* ATCC 25922 using broth microdilution technique according to CLSI and EUCAST guidelines. Milled samples were diluted with deionised water in 7 progressive concentrations ranging from 0.064 to 0.001 $\mu$g $mL^{-1}$ CFX. Identification of bacterial growth was aided with the addition of resazurin dye, which changes colour in the presence of viable bacteria.

**Scanning electron microscopy (SEM)**. Images of the samples were obtained using an FEI Quanta 600F scanning electron microscope (Oregon, USA). Samples were attached to carbon tabs, mounted on aluminium pins, then sputter-coated with gold for 3 min at 30 mA, using an Emitech K550. Images were recorded under high vacuum, then enhanced using brightness, contrast and astigmatism correction to assess particle size and morphology.

## Results and Discussion

*CFX Organic Salt Characterization*

*Powder X-ray Diffraction (PXRD)*

Milled products, later identified as ciprofloxacin:succinic acid (CFX-SA), ciprofloxacin:glutaric acid (CFX-GA), ciprofloxacin:adipic acid (CFX-AA) and ciprofloxacin:pimelic acid (CFX-PA), were synthesised by ball milling. PXRD analysis of the milled products indicated formation of novel, crystalline materials. When compared to reference diffraction patterns of the starting materials, novel powder patterns exhibiting sharp diffraction peaks were seen for all four CFX: dicarboxylic acid systems. Notably, diffraction features at low $2\theta$ suggest the presence of large unit cells, as expected for crystalline materials composed of multiple different molecules (Figs. S1 – S4).

*Single Crystal X-ray Diffraction (SC-XRD)*

Solid phases later identified as CFX-SA, CFX-GA, CFX-AA, CFX-PA CFX-SA hydrate (CFX-SA·$H_2O$), and CFX-AA hydrate (CFX-AA·$H_2O$) and were obtained as suitable single crystals by crystallization from aqueous and organic solvents. In each case, proton transfer was confirmed, in line with the agreed understanding of ionization and $\Delta pK_a$ in multicomponent crystals.[14] CSD searches showed CFX-SA, CFX-GA, CFX-AA and CFX-PA to be novel crystal structures; the crystal structures of both CFXSA·$H_2O$ and CFXAA·$H_2O$ have previously been reported.[13,28] Whilst the existence of CFX-SA has also been reported,[28] its structure has not. Table 1 summarizes the crystal information for each of the materials and complete, solved structures are included in supplementary information.

CFX-SA crystallizes in space group $P\overline{1}$ with one CFX ion and one SA ion in the asymmetric unit. The positively charged $N^+H_2$ groups of the piperazinium rings form a centrosymmetric $R_4^4(18)$ motif with the C=O groups of the carboxylates. O5 and O6 of adjacent SA ions are relatively closely spaced at 2.438(2) Å apart; atom H6 lies a somewhat distant 1.09(3) Å from its parent O6, and only 1.35(3) Å through space from O5, leading to interpretation of the structure by OLEX2 as polymeric (Fig. 2; Figs. S5A, S5B; Table S1).

CFX-GA crystallizes in space group $P\overline{1}$ with two CFX ions and two GA ions in the asymmetric unit, with the unique ions in a pseudo-centrosymmetric arrangement. These GA ions form a central $R_2^2(16)$ motif, whilst the positively charged $N^+H_2$ groups of the piperazinium rings of centrosymmetrically related CFX ions form an $R_4^2(8)$ motif with the carboxylate $O^-$ atoms of two centrosymmetrically related GA ions. In the pseudo-centrosymmetric GA pair: O6 and O12 lie 2.515(1) Å apart, with atom H6 0.95(2) Å from its parent O6 and 1.58 (2) Å through space from O12; O5 and O13 lie 2.502(1) Å apart, with atom H13 0.94(2) Å from its parent O13 and 1.57(2) Å through space from O5. (Figs. S6A, S6B, Table S2)

CFX-AA crystallizes in space group $P2_1/c$ with one CFX ion and one AA ion in the asymmetric unit. Two $D_1^1(2)$ motifs link the positively charged $N^+H_2$ group of the piperazinium ring to O4 of an AA at $x,y,z$ and to O5 of AA at $x,{}^1/_2\text{-}y,-{}^1/_2\text{+}z$. O6 of the AA at $x,y,z$ lies 2.508(2) Å from O5 of the AA at $-1\text{+}x,{}^1/_2\text{-}y,{}^1/_2\text{+}z$, forming a $C_1^1(9)$ motif, with H6 0.93(3) Å from its parent O6 and 1.58(3) Å through space from O5. (Figs. S7A, S7B, Table S3)

CFX-PA crystallizes in space group *Pbca* with one CFX ion and one PA ion in the asymmetric unit. The PA ions form a chain running parallel to the *c* axis, with O5 and O6 of adjacent PA ions are relatively closely spaced at 2.428(1) Å; atom H6 lies a somewhat distant 1.20 (2) Å from its parent O6, and only 1.23(2) Å through space from O5, leading to interpretation of the structure by OLEX2 as polymeric. Two $D_1^1(2)$ motifs link the positively charged $N^+H_2$ group of the piperazinium ring to O4 of the PA at $x,y,z$ and to O5 of the PA at ${}^1/_2\text{-}x,2\text{-}y,-{}^1/_2\text{+}z$. (Figs. S8A, S8B; Table S4).

*Comparison of CFX Salts from Milled and Solution Crystallization Methods*

That single crystals obtained from solution were representative of the bulk materials obtained by ball milling was confirmed by two approaches. Firstly, single crystals of each of the CFX salts were lightly ground in a mortar and pestle, and the resultant powder subjected to DSC, FT-IR, and PXRD; these characterization methods returned the same results as those obtained from the milled products. Secondly, PXRD data from the bulk materials produced by milling were Pawley fitted in TOPAS,[37] starting from the SC-XRD unit cells. For CFX-GA, CFX-PA and CFX-AA, the unit cell parameters were able to be refined to their room-temperature values and account for all observed diffraction features; for CFX-SA, cell refinement was again successful, leaving only four very weak unaccounted-for diffraction features (Figs. S9 – S12).

**Table 1**
SC-XRD data for CFX salts generated in this work.

| Identification code | CFX-AA | CFX-GA | CFX-PA | CFX-SA |
|---|---|---|---|---|
| Moiety formula | $(C_{17}H_{19}FN_3O_3)^+$ $(C_6H_9O_4)^-$ | $(C_{17}H_{19}FN_3O_3)^+$ $(C_5H_7O_4)^-$ | $(C_{17}H_{19}FN_3O_3)^+$ $(C_7H_{11}O_4)^-$ | $(C_{17}H_{19}FN_3O_3)^+$ $(C_4H_5O_4)^-$ |
| Formula weight | 477.48 | 463.46 | 491.51 | 449.43 |
| Temperature / K | 100.00 | 100.00 | 100.00 | 100.00 |
| Crystal system | monoclinic | triclinic | orthorhombic | triclinic |
| Space group | $P2_1/c$ | $P$-1 | $Pbca$ | $P$-1 |
| a / Å | 6.94330(10) | 7.12370(10) | 23.4190(3) | 7.2812(3) |
| b / Å | 35.2390(5) | 16.3289(2) | 8.44410(10) | 9.1428(4) |
| c / Å | 9.7722(2) | 18.7813(2) | 23.5428(3) | 16.1257(7) |
| $\alpha$ / ° | 90 | 93.1360(10) | 90 | 75.627(4) |
| $\beta$ / ° | 108.113(2) | 99.1070(10) | 90 | 85.627(3) |
| $\gamma$ / ° | 90 | 91.2250(10) | 90 | 77.389(3) |
| Volume/Å$^3$ | 2272.53(7) | 2152.91(5) | 4655.64(10) | 1014.53(8) |
| Z | 4 | 4 | 8 | 2 |
| $\rho_{calc}$ g/cm$^3$ | 1.396 | 1.430 | 1.402 | 1.471 |
| $\mu$/mm$^{-1}$ | 0.921 | 0.955 | 0.915 | 0.995 |
| F(000) | 1008.0 | 976.0 | 2080.0 | 472.0 |
| Crystal size / mm | 0.04 × 0.13 × 0.20 | 0.05 × 0.06 × 0.15 | 0.06 × 0.12 × 0.12 | 0.14 × 0.16 × 0.20 |
| Radiation | Cu K$\alpha$ | Cu K$\alpha$ | Cu K$\alpha$ | Cu K$\alpha$ |
| 2$\Theta$ range for data / ° | 5.016 to 152.206 | 4.774 to 157.494 | 7.51 to 152.38 | 5.66 to 154.206 |
| Reflections collected | 26381 | 89162 | 28006 | 22601 |
| Independent reflections | 4611 $R_{int}$ = 0.0486 | 9172 $R_{int}$ = 0.0707 | 4724 $R_{int}$ = 0.0294 | 4089 $R_{int}$ = 0.0669 |
| Data/restraints/parameters | 4611/0/323 | 9172/0/627 | 4724/0/332 | 4089/0/308 |
| Goodness-of-fit on F$^2$ | 1.064 | 1.074 | 1.049 | 1.070 |
| Final R indexes [I>=2$\sigma$ (I)] | $R_1$ = 0.0417 $wR_2$ = 0.1150 | $R_1$ = 0.0352 $wR_2$ = 0.0954 | $R_1$ = 0.0324 $wR_2$ = 0.0827 | $R_1$ = 0.0515 $wR_2$ = 0.1422 |
| Final R indexes [all data] | $R_1$ = 0.0456 $wR_2$ = 0.1189 | $R_1$ = 0.0404 $wR_2$ = 0.0992 | $R_1$ = 0.0351 $wR_2$ = 0.0846 | $R_1$ = 0.0600 $wR_2$ = 0.1487 |
| Largest diff peak/hole /eÅ$^{-3}$ | 0.37/-0.30 | 0.25/-0.25 | 0.20/-0.23 | 0.32/-0.38 |

*Fourier-Transform Infrared Spectroscopy (FTIR)*

FTIR spectra were taken for CFX salts from milled and solution methods, physical mixtures of the starting materials and CFX HCl·$H_2O$. CFX salts show differences in stretches compared to reference spectra and physical mixtures, particularly around carboxylic acid carbonyl region (~1700 cm$^{-1}$) and in the fingerprint region (1500-500 cm$^{-1}$). This analysis was used to verify salt formation in milled samples in the absence of SC-XRD. Firstly, FTIR spectra of milled materials and crystals obtained from solution were compared and showed identical spectra. FTIR spectra for CFX-SA·$H_2O$ and CFX-AA·$H_2O$ were distinct from those of milled CFX-SA and CFX-AA. The absence of the characteristic ~3200 cm$^{-1}$ signal of -OH bond stretch in bound water suggested that the milled materials do not contain water (Fig. 3). Also seen were differences at the carboxylic acid carbonyl stretch (~1700 cm$^{-1}$) i.e. a shift from 1720 cm$^{-1}$ to 1700 cm$^{-1}$. Such changes can be interpreted in terms of different intermolecular bonding as shown in the single-crystal structures.

The reference spectra for CFX base starting material shows a zwitterionic (betaine) form, with ionised carboxylic acid and secondary amine groups. There is an absence of a carboxylic acid carbonyl stretch at ~1700 cm$^{-1}$ and the presence of characteristic asymmetric stretching for carboxylate ion (−COO$^-$) at ~1600 cm$^{-1}$ and ~1400 cm$^{-1}$ (Fig. 4A). FT-IR spectra for CFX-HCl·$H_2O$ confirms this, as a carboxylic acid carbonyl stretch at ~1700 cm$^{-1}$ is present and CFX-HCl·$H_2O$ is known to exist with a neutral carboxylic acid (confirmed experimentally by SC-XRD, Fig. 4B). The FT-IR spectrum for CFX-HCl·$H_2O$ was used as a reference for interpreting bonding in the carbonyl region.

Fig. 5 compares the spectra for CFX-GA with CFX-HCl·$H_2O$, and GA. For CFX-GA, there are peaks at 1726 cm$^{-1}$ and 1702 cm$^{-1}$ corresponding to neutral carboxylic acid carbonyl stretching in GA and CFX, respectively. The GA peak at 1726 cm$^{-1}$ is also shifted from 1683 cm$^{-1}$ suggesting presence of bonding. There are also strong peaks present in CFX-GA at 1627 cm$^{-1}$ and 1470 cm$^{-1}$, characteristic of asymmetric stretching for carboxylate ion (−COO$^-$). This mirrors the complex bonding between carboxylic acids seen in SC-XRD data. All milled materials display these characteristic carbonyl peaks confirming formation of salts through milling (Fig. S13 – S16).

*Thermal Analysis*

DSC analysis showed single sharp endothermic peaks corresponding to crystalline melt for all milled CFX salts, with no exothermic events (Fig. S17 – S20). All CFX salts displayed melting distinct from that of CFX and the corresponding counterion, and all melting points lie between CFX and the counterion melts (Table 2). Melting points increase with molecular weight of coformer, with CFX-PA as an exception; it possesses the lowest melting point of all the four salts. TGA analysis showed no weight loss for any of the milled CFX salts between 30°C and 150°C which confirms the absence of bound water hypothesised from the FT-IR data.

*Solubility Measurements*

The measured solubilities, starting from each of the CFX salts, are substantially greater than the measured solubility starting from CFX base (Table 3**)**. Interpretation of these solubility measurements is, however, not straightforward. As can be seen, even with 0.2 M phosphate buffer, the pH of the supernatant has shifted away from 6.8 by the end of the 72 hr period. Furthermore, an examination by PXRD of the excess solids recovered at the end of the dissolution experiments shows a complex picture; the excess solids starting from CFX base, CFX-GA, CFX-PA, CFX-SA and CFX-HCl·$H_2O$ all exhibit broadly similar PXRD patterns (Fig. S21) that cannot be explained in terms of the excesses comprising the starting crystalline salt forms being tested. Closer examination, however, reveals some important differences that are apparent in Fig 6, which shows the low angle region of the PXRD patterns. Of particular note is that the excess from the CFX-GA starting material does not exhibit any of the four distinct

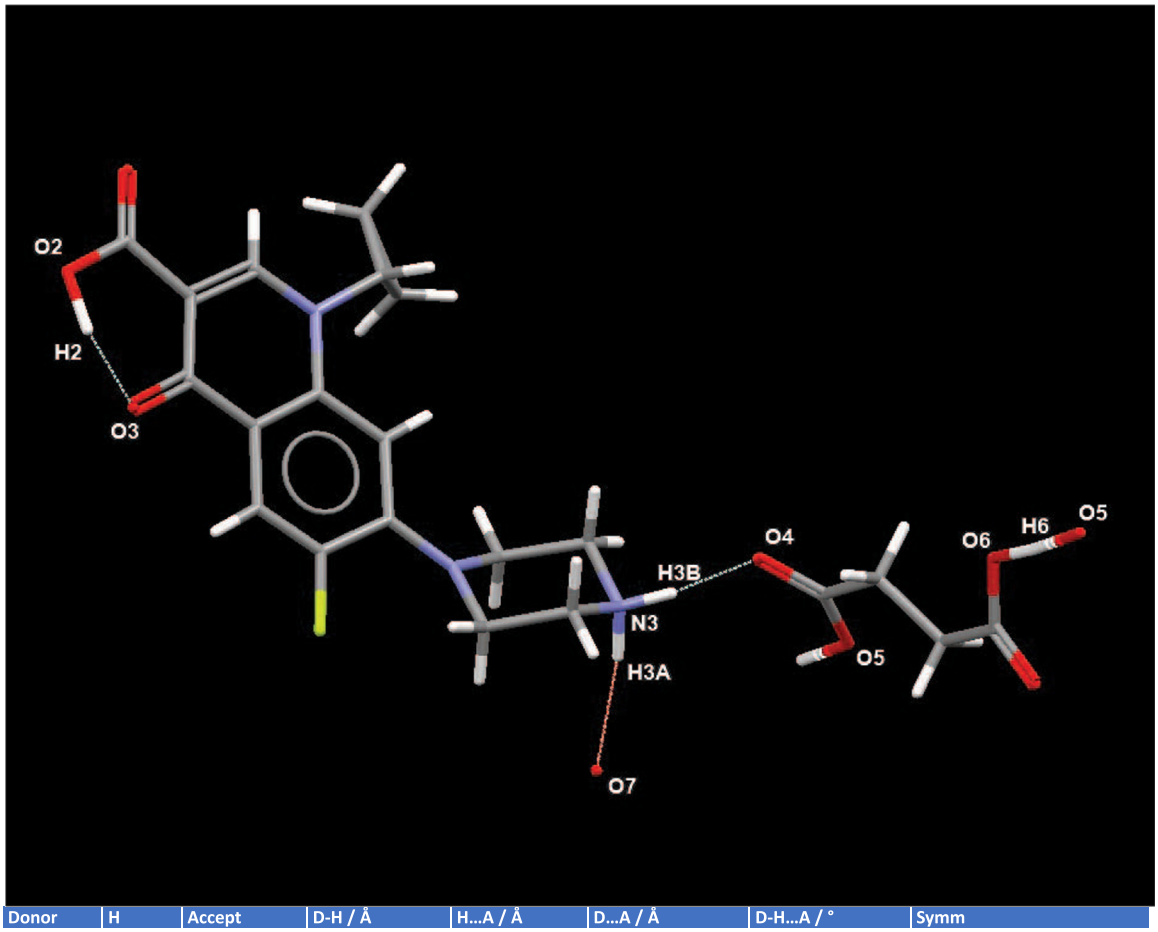


| Donor | H | Accept | D-H / Å | H...A / Å | D...A / Å | D-H...A / ° | Symm |
|---|---|---|---|---|---|---|---|
| O2 | H2 | O3 | 1.04(4) | 1.53(4) | 2.545(2) | 163(3) | x,y,z |
| N3 | H3A | O7 | 0.94(3) | 1.98(3) | 2.8703(19) | 157(2) | -x+1,-y+2,-z |
| N3 | H3B | O4 | 0.92(2) | 1.75(2) | 2.654(2) | 167(2) | x,y,z |
| O6 | H6 | O5 | 1.09(3) | 1.35(3) | 2.4384(17) | 175(2) | x-1,y,z |

**Fig. 2.** A Mercury diagram for the asymmetric unit of CFX-SA, showing the unique set of hydrogen bonds (dashed lines) and the associated bond distances and angles. Note the long O6—H6 bond, which places H6 at a point where it is interpreted as being "shared" with O5, leading to classification of the structure as "polymeric".

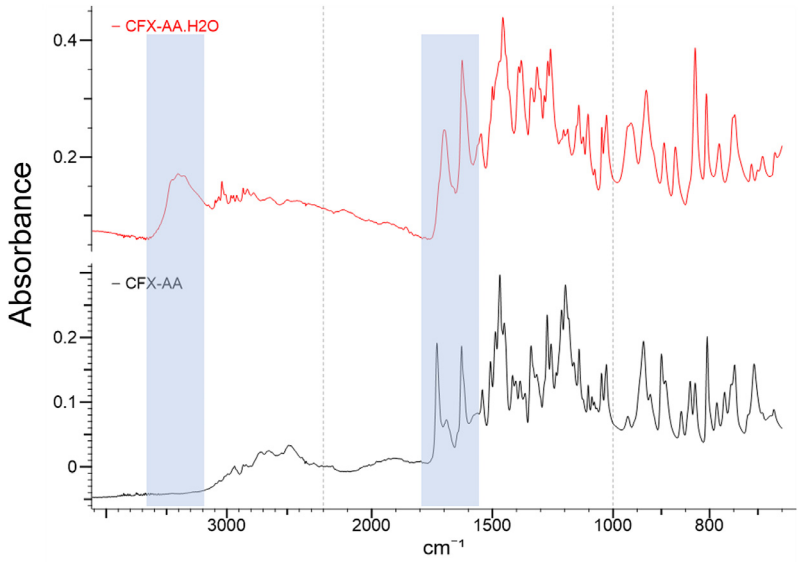


**Fig. 3.** FTIR spectra of CFX-AA·$H_2O$ (red) and CFX-AA (black) between wavenumbers 600 $cm^{-1}$ and 4000 $cm^{-1}$ with highlighted bound water and carboxylic acid stretching regions. (For interpretation of the references to color in this figure legend, the reader is referred to the web version of this article.)

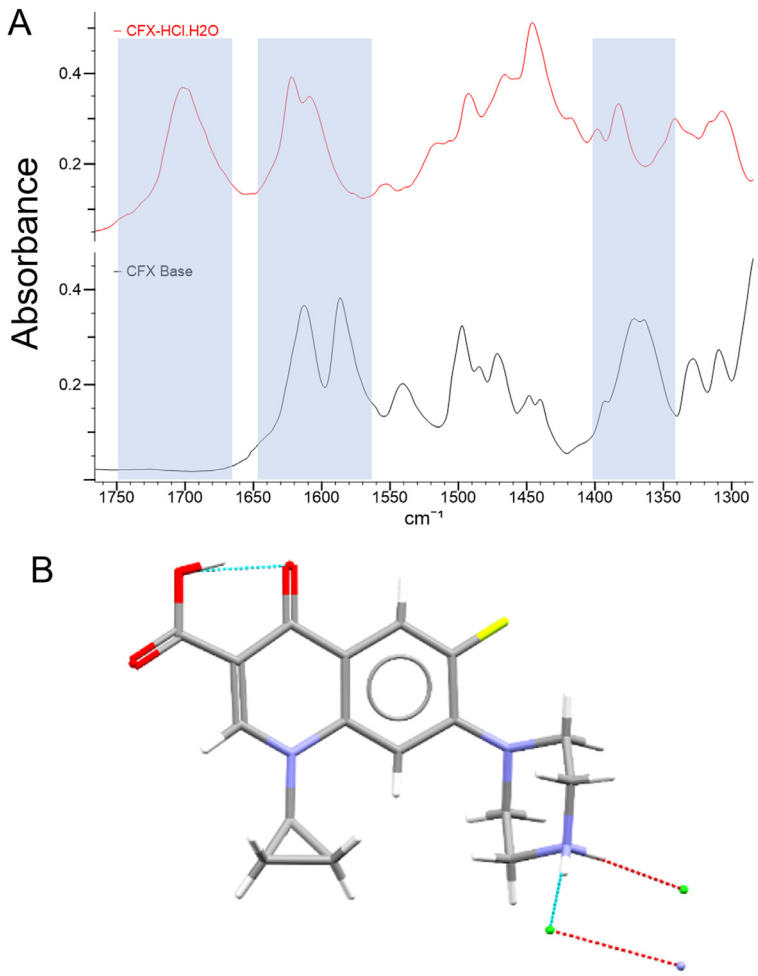


**Fig. 4.** **(A)** FTIR spectra of CFX-HCl·$H_2O$ (red) and CFX base (black) between wavenumbers 1300 $cm^{-1}$ and 1750 $cm^{-1}$ with highlighted carboxylic acid stretching regions. **(B)** Single-crystal structure of CFX-HCl·$H_2O$. Ionization of secondary amine and neutral carboxylic acid is seen. (For interpretation of the references to color in this figure legend, the reader is referred to the web version of this article.)

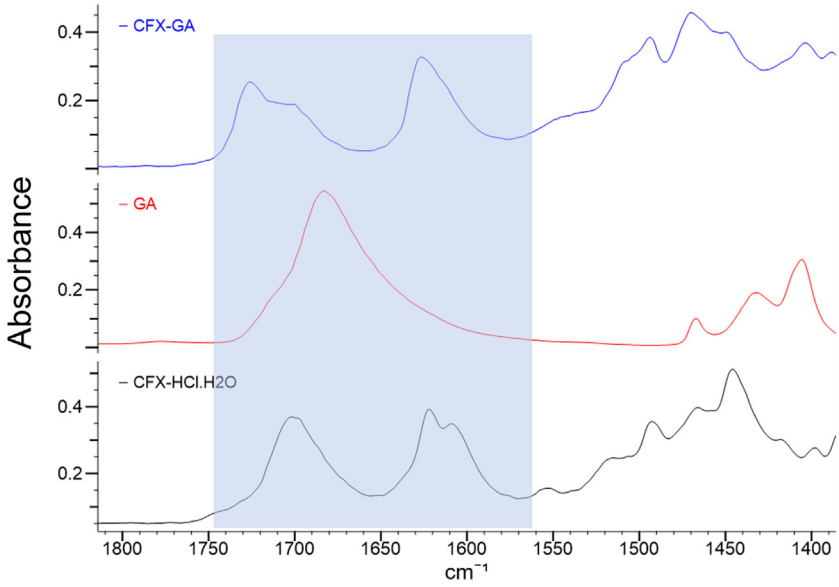


**Fig. 5.** FTIR spectra of CFX-GA milled (blue) with GA (red) and CFX-HCl·$H_2O$ references (black) between wavenumbers 1350 $cm^{-1}$ and 1800 $cm^{-1}$ with highlighted carboxylic acid stretching regions. (For interpretation of the references to color in this figure legend, the reader is referred to the web version of this article.)

**Table 2**
DSC data for CFX and CFX salts compared to counterion MWt and MPt.

| | MP (°C) | Counterion MWt ($g.mol^{-1}$) | Counterion MPt (°C) |
|---|---|---|---|
| CFX base | 273.24 | n/a | n/a |
| CFX-SA | 218.44 | 118.09 | 192.08 |
| CFX-GA | 222.05 | 132.12 | 99.63 (75.58) |
| CFX-AA | 234.53 | 146.14 | 154.50 |
| CFX-PA | 191.25 | 160.17 | 107.38 |

peaks in the range 6-8° 2$\theta$ shown by CFX base, CFX-PA, CFX-SA and CFX-HCl·$H_2O$, whilst the excess of the CFX-Base starting material does not exhibit the peak at ca. 11.5° 2$\theta$ that is shared by the excesses from all of the other starting salt forms shown. It is thus likely that the excesses consist of phase mixtures, and that the composition of the excess starting from CFX-GA is markedly different from that of the others, this latter observation being the cause of its higher observed solubility. We have not as yet been successful in explaining the observed PXRD data for these excesses in terms of reported forms of CFX, its salts and its hydrates. However, in the case of the excess solid from the CFX-AA starting material experiment, which gives rise to a significantly different PXRD pattern (Fig. S22) from the other starting materials, we conclude that it is largely composed of ciprofloxacin hemikis(adipate) dihydrate [CSD refcode QUKHOV] (Fig. S23). This conclusion is supported by the fact that a small single crystal, whose experimental cell dimensions matched those of QUKHOV, was retrieved from the excess, and by the strong level of agreement between the observed PXRD data and a calculated PXRD pattern for QUKHOV.

Overall, it is unclear exactly what physical forms the saturation solubility values determined in the work pertain to. Nevertheless, it is noteworthy that CFX-GA, whose solid excess does not match those of the other salts, does give rise to the highest solubility of any of the salts examined.

*Minimum Inhibitory Concentration (MIC)*

Following incubation, plates were analysed to determine lowest concentration of ciprofloxacin salt which completely inhibited *E. coli* growth. All CFX salts showed an MIC within the acceptable range for CFX-HCl·$H_2O$ as validated by EUCAST (i.e. Target = 0.008 g/L; Range = 0.004 g/L to 0.016 g/L) (Fig. S24). CFX-SA, CFX-GA and CFX-AA showed MIC of 0.008 g/L and CFX-PA showed MIC of 0.004 g/L.

**Table 3**
Solubility measurements for CFX base, CFX-HCl·H2O, and the salt forms generated in this work.

| | 0.1 M Phosphate Buffer pH 6.8 | | 0.2 M Phosphate Buffer pH 6.8 | |
|---|---|---|---|---|
| Formulation | Final pH | Solubility ($mg\ mL^{-1}$) | Final pH | Solubility ($mg\ mL^{-1}$) |
| CFX Base | - | 0.04 | 6.93 | 1.20 |
| CFX-HCl·$H_2O$ | - | 14.36 | 5.20 | 5.55 |
| CFX-SA | 5.32 | 8.43 | 5.64 | 5.81 |
| CFX-GA | 5.22 | 107.83 | 5.43 | 13.55 |
| CFX-AA | 5.62 | 4.28 | 5.61 | 4.02 |
| CFX-PA | 5.61 | 13.79 | 5.90 | 5.15 |

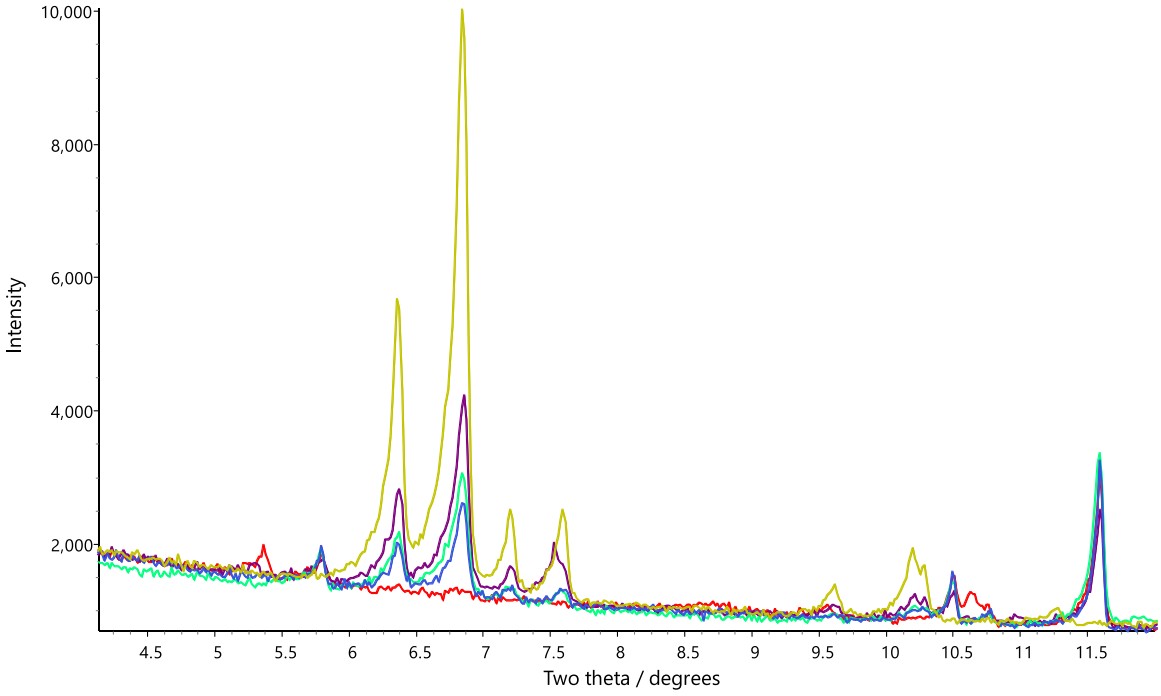


**Fig. 6.** The low-angle region of PXRD patterns for excess solids recovered at the end of the dissolution experiments. Starting materials: CFX-GA (red), CFX-SA (green), CFX-PA (purple), CFX-Base (mustard) and CFX-HCl·$H_2O$ (blue). (For interpretation of the references to color in this figure legend, the reader is referred to the web version of this article.)

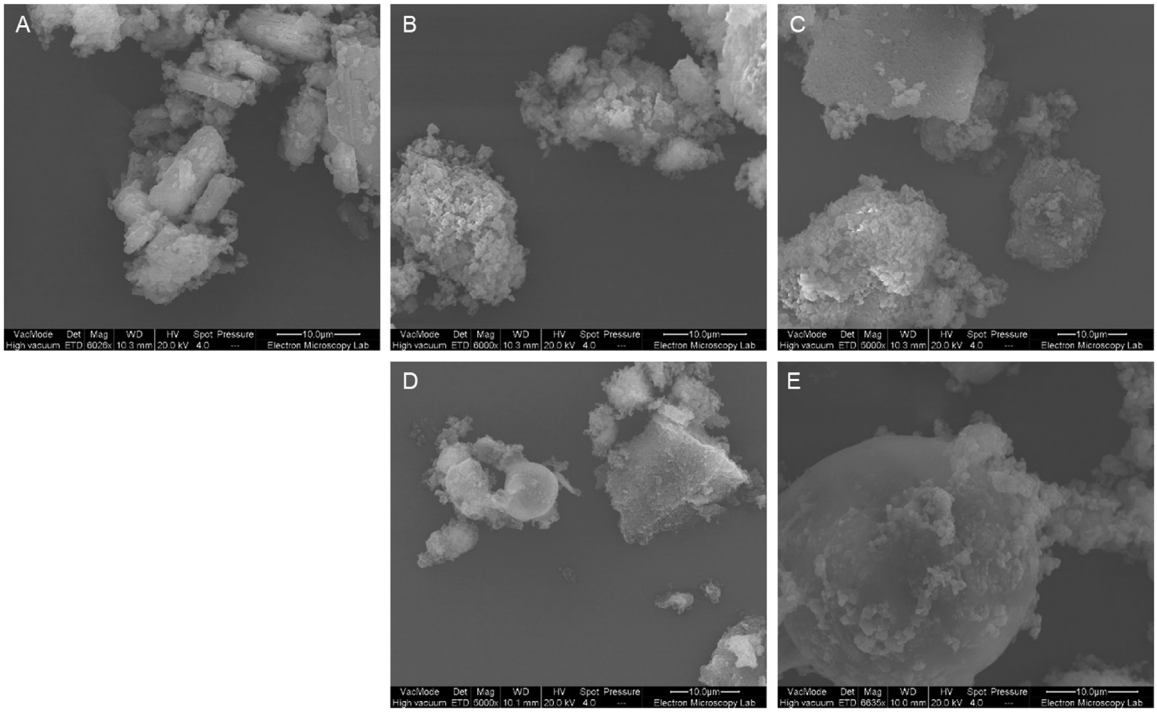


**Fig. 7.** SEM images for CFX base (A) compared to CFX-SA (B), CFX-GA (C), CFX-AA (D), CFX-PA (E) milled salts. Milled CFX salts appear to have lost needle crystal habit of CFX base and show some signs of agglomeration. Approximate particles size appears to be greater than 10 $\mu$m, although irregular shapes exist.

CFX salts did not show a detrimental impact on antibacterial activity showing equivalent results to CFX-HCl·$H_2O$. This confirms that in this case, physicochemical property change does not alter antimicrobial activity.

*Scanning Electron Microscopy (SEM)*

SEM micrographs of milled CFX salts are shown in Fig. 7. The powders showed a wide range of particle sizes and surface morphologies. The semi-regular "needle like" crystal habit of CFX base has been removed by ball milling. Furthermore, CFX salt particles appear more aggregated than CFX base raw material, which is common for ball milled powders. It is well known that reduced average particle size can be advantageous for a variety of pharmaceutical physicochemical properties e.g. dissolution and aerodynamic properties.[38,39] SEM images showed the presence of some large (> 10 $\mu$m) particles and as such, the next stage in formulation development for these CFX salts would most likely need to consider particle size reduction and control.

## Conclusion

Crystalline CFX salts with distinct physicochemical properties have been successfully produced by ball milling and solution crystallization. Proton transfer between CFX and acid counterions was confirmed through SC-XRD and FTIR analysis. Melting point analysis showed single crystalline melts located between CFX and corresponding acids. However, neither counterion molecular weight nor melting point seem to have an influence on observed melting points. Saturation solubility experiments, coupled with PXRD analysis of excess solids, reveal a complex picture of phase transformations and a CFX-GA salt form that results in a markedly higher solubility than that of CFX-HCl·$H_2O$. Antibacterial activity of all the novel salt forms against free bacteria has been confirmed. The existence of novel solid forms of CFX may help extend its pharmaceutical use beyond that of the traditional oral formulation with CFX-HCl·$H_2O$. Further studies to assess the key properties of these CFX salts are required, especially focusing on explaining physical form transformations in solution and observing counterion activity against bacterial biofilms.

## Funding Sources

This work was supported by Quotient Sciences and the Engineering and Physical Sciences Research Council (EPSRC UK) [grant number 2266759].

## Conflict of Interest Disclosure

The authors declare no conflict of interest.

## Acknowledgments

The authors would like to thank the Chemical Analysis Facility (CAF) at the University of Reading for providing essential access to instruments used in this study. We are grateful to the UK Materials & Molecular Modelling Hub for computational resources, which is partially funded by EPSRC (EP/P020194/1 and EP/T022213/1), for DFT-D calculations used to verify H atom locations in the CFX salts. We are also grateful to Dr. Norman Shankland, for useful discussions on solubility measurements and the PXRD data obtained from the excess solids.

## Supplementary Materials

Supplementary material associated with this article can be found, in the online version, at doi:10.1016/j.xphs.2022.08.008.

## References

1. Sathisaran I, Dalvi SV. Engineering cocrystals of poorlywater-soluble drugs to enhance dissolution in aqueous medium. *Pharmaceutics*. 2018;10(3):108.

2. Williams H, Trevaskis N, Charman S, et al. Strategies to address low drug solubility in discovery and development. *Pharmacol Rev*. 2013;65:315–499.
3. Shi Q, Moinuddin SM, Cai T. Advances in coamorphous drug delivery systems. *Acta Pharm Sinica B*. 2019;9(1):19–35.
4. Blagden N, de Matas M, Gavan PT, York P. 2007. Crystal engineering of active pharmaceutical ingredients to improve solubility and dissolution rates. ed. p 617-630.
5. Duggirala NK, Perry ML, Almarsson Ö, Zaworotko MJ. Pharmaceutical cocrystals: along the path to improved medicines. *Chem Commun*. 2016;52(4):640–655.
6. Al-Obaidi H, Majumder M, Bari F. Amorphous and crystalline particulates: challenges and perspectives in drug delivery. *Curr Pharm Des*. 2017;23(3):350–361.
7. Al-Obaidi H, Lawrence MJ, Buckton G. Atypical effects of incorporated surfactants on stability and dissolution properties of amorphous polymeric dispersions. *J Pharm Pharmacol*. 2016;68(11):1373–1383.
8. Xiong X, Du Q, Zeng X, He J, Yang H, Li H. Solvates and polymorphs of rebamipide: preparation, characterization, and physicochemical analysis †. *RSC Adv*. 2017;7:23279–23286.
9. Hu Y, Gniado K, Erxleben A, McArdle P. Mechanochemical reaction of sulfathiazole with carboxylic acids: formation of a cocrystal, a salt, and coamorphous solids. *Cryst Growth Des*. 2014;14(2):803–813.
10. Al-Obaidi H, Kowalczyk RM, Kalgudi R, Zariwala MG. Griseofulvin solvate solid dispersions with synergistic effect against fungal biofilms. *Colloids Surf B*. 2019;184:110540.
11. McShane PJ, Weers JG, Tarara TE, et al. *Ciprofloxacin Dry Powder for Inhalation (Ciprofloxacin DPI): Technical Design and Features of an Efficient Drug–Device Combination*. Academic Press; 2018:72–79.
12. Florindo C, Costa A, Matos C, et al. Novel organic salts based on fluoroquinolone drugs: Synthesis, bioavailability and toxicological profiles. *Int J Pharm*. 2014;469(1):179–189.
13. Surov AO, Manin AN, Voronin AP, et al. Pharmaceutical salts of ciprofloxacin with dicarboxylic acids. *Eur J Pharm Sci*. 2015;77:112–121.
14. Gunnam A, Suresh K, Ganduri R, Nangia A. Crystal engineering of a zwitterionic drug to neutral cocrystals: a general solution for floxacins. *Chem Commun*. 2016;52:12610–12613.
15. Basavoju S, Boström D, Velaga SP. Pharmaceutical cocrystal and salts of norfloxacin. *Cryst Growth Des*. 2006;6(12):2699–2708.
16. de Almeida AC, Torquetti C, Ferreira PO, et al. Cocrystals of ciprofloxacin with nicotinic and isonicotinic acids: Mechanochemical synthesis, characterization, thermal and solubility study. *Thermochim Acta*. 2020;685: 178346.
17. Chen X, Partheniadis I, Nikolakakis I, Al-Obaidi H. Solubility improvement of progesterone from solid dispersions prepared by solvent evaporation and co-milling. *Polymers*. 2020;12(4):854.
18. Uhljar LE, Kan SY, Radacsi N, Koutsos V, Szabo-Revesz P, Ambrus R. In vitro drug release, permeability, and structural test of ciprofloxacin-loaded nanofibers. *Pharmaceutics*. 2021;13(4).
19. Mesallati H, Conroy D, Hudson S, Tajber L. Preparation and characterization of amorphous ciprofloxacin-amino acid salts. *Eur J Pharm Biopharm*. 2017;121:73–89.
20. Olivera ME, Manzo RH, Junginger HE, et al. Biowaiver monographs for immediate release solid oral dosage forms: ciprofloxacin hydrochloride. *J Pharm Sci*. 2011;100(1):22–33.
21. Mohammed A, Zurek J, Madueke S, et al. Generation of high dose inhalable effervescent dispersions against pseudomonas aeruginosa biofilms. *Pharm Res*. 2020;37(8):150.
22. Paulekuhn GS, Dressman JB, Saal C. Trends in active pharmaceutical ingredient salt selection based on analysis of the orange book database. *J Med Chem*. 2007;50(26):6665–6672.
23. Kawabata Y, Wada K, Nakatani M, Yamada S, Onoue S. *Formulation Design for Poorly Water-Soluble Drugs Based on Biopharmaceutics Classification System: Basic Approaches and Practical Applications*. Elsevier B.V; 2011:1–10.
24. Berge SM, Bighley LD, Monkhouse DC. Pharmaceutical salts. *J Pharm Sci*. 1977;66(1):1–19.
25. Carvalho Jr P, Diniz L, Tenorio J, et al. 2019. Pharmaceutical paroxetine-based organic salts of carboxylic acids with optimized properties: the identification and characterization of potential novel API solid forms. 21:3668−3678.
26. Bahamondez-Canas T, Smyth HDC. Influence of excipients on the antimicrobial activity of tobramycin against pseudomonas aeruginosa biofilms. *Pharm Res*. 2018;35(1):10.
27. Dayo Owoyemi BC, Da Silva CCP, Souza MS, Diniz LF, Ellena J, Carneiro RL. Fluconazole: synthesis and structural characterization of four new pharmaceutical cocrystal forms. *Cryst Growth Des*. 2019;19(2):648–657.
28. Paluch KJ, McCabe T, Müller-Bunz H, Corrigan OI, Healy AM, Tajber L. Formation and physicochemical properties of crystalline and amorphous salts with different stoichiometries formed between ciprofloxacin and succinic acid. *Mol Pharmaceutics*. 2013;10(10):3640–3654.
29. Fábián L. Cambridge structural database analysis of molecular complementarity in cocrystals. *Cryst Growth Des*. 2009;9(3):1436–1443.
30. Childs SL, Stahly GP, Park A. The salt−cocrystal continuum: the influence of crystal structure on ionization state. *Mol Pharmaceutics*. 2007;4(3):323–338.
31. Lu J, Rohani S. Preparation and characterization of theophylline−nicotinamide cocrystal. *Org Process Res Dev*. 2009;13(6):1269–1275.
32. Sheldrick G. SHELXT - Integrated space-group and crystal-structure determination. *Acta Crystallogr, Sect A*. 2015;71(1):3–8.
33. Sheldrick G. Crystal structure refinement with SHELXL. *Acta Crystallogr Section C*. 2015;71(1):3–8.
34. Dolomanov OV, Bourhis LJ, Gildea RJ, Howard JAK, Puschmann H. OLEX2: a complete structure solution, refinement and analysis program. *J Appl Crystallogr*. 2009;42(2):339–341.
35. Groom CR, Bruno IJ, Lightfoot MP, Ward SC. The Cambridge structural database. *Acta Crystallogr Section B*. 2016;72(2):171–179.
36. Macrae CF, Sovago I, Cottrell SJ, et al. Mercury 4.0: from visualization to analysis, design and prediction. *J Appl Crystallogr*. 2020;53(1):226–235.
37. Coelho AA. TOPAS and TOPAS-Academic: an optimization program integrating computer algebra and crystallographic objects written in C++. *J Appl Crystallogr*. 2018;51(1):210–218.
38. Savjani KT, Gajjar AK, Savjani JK. Drug solubility: importance and enhancement techniques. *ISRN Pharmaceutics*. 2012;2012:1–10.
39. Chow AHL, Tong HHY, Chattopadhyay P, Shekunov BY. *Particle Engineering for Pulmonary Drug Delivery*. 20072007:411–437.

Chapter 4

# Modulated Drug Release of Ciprofloxacin Salts from Three-Fluid Nozzle Spray Dried Solid Dispersions

**Thomas Hibbard[1]**, Twana Mohammed M. Ways[2], Sadat A. Aziz[3], Vasiliki Virvili[1], Muhammad Yaqoob[4], Kenneth Shankland[1], Hisham Al-Obaidi[1]

[1] School of Pharmacy, University of Reading, Reading, RG6 6AD, UK
[2]*College of Pharmacy, University of Sulaimani, Iraq*
[3]*College of Vet. Medicine, University of Sulaimani, Iraq*
[4]*Interaction ChemPharm Ltd, Reading RG2 0QX, UK*

Chapter Summary:
In this chapter, solid dispersions of ciprofloxacin dicarboxylic acid salts were prepared by three-fluid nozzle spray drying either from solution or suspension feedstocks. Solid dispersions showed modified ciprofloxacin release kinetics and suitable aerosolisation properties for dry powder inhalation. Suspension formulations showed biphasic release of ciprofloxacin *in vitro* and better absorption following oral delivery, in rabbits.

Author Contributions:
TH: conceptualisation, investigation, methodology, writing – original draft, review & editing.
TW, SA: *in vivo* investigation; VV: cascade impaction investigation; MY: HPLC Methodology; KS: writing – original draft, review & editing; HAO: conceptualisation, investigation, methodology, project administration, writing – original draft, review & editing.

**Abstract**

Predominantly amorphous solid dispersions of ciprofloxacin dicarboxylic acid salts within a HPMC matrix are reported. These solid dispersions were generated through two contrasting 3-fluid nozzle spray drying methods which incorporated the salts and polymer via a solution or suspension process. Ciprofloxacin salts without polymer were also generated through spray drying and used as a control.

Powder X-ray diffraction, energy dispersive X-ray spectroscopy, Fourier-transform infrared spectroscopy and Raman spectroscopy were used to characterise the dispersions and confirmed the generation of ciprofloxacin salts in a predominantly amorphous state. Following characterisation, the solubility and dissolution properties of the dispersions were tested *in vitro* which showed clear differences in sink and non-sink conditions. Solid dispersions from suspension showed enhanced solubility compared to the solution-based formulations in low solvent volumes, as well as a bi-phasic dissolution release profile in sink conditions. Testing bioavailability *in vivo* showed a substantial increase in the ciprofloxacin plasma concentration for rabbits treated with the suspension-based solid dispersion formulation rather than solution-based solid dispersion.

Solid dispersion formulations also showed improved inhalation properties *in vitro* compared to spray dried salt control formulations, with decreased MMAD and increased FPF and FPD.

This study highlights the utility of the 3-fluid spray drying method for co-spraying feed stocks of different compositions to generate solid dispersions with valuable properties and therefore potential applications.

## 1. Introduction

Crystal engineering approaches have been used to modify drug physicochemical properties with the aim of enhancing the solution properties of poorly soluble drugs [1, 2]. The formation of solid dispersions is one strategy which has proved to be effective for overcoming solubility issues. Solid dispersions are novel materials comprising a drug, molecularly mixed within an inert carrier molecule, and these materials often exhibit improved formulation properties [3]. When a drug is dispersed in the amorphous state within a large carrier molecule (e.g. a polymer), the resulting material is known as an amorphous solid dispersion with the potential to become a solid solution if miscibility is maximised [4]. Moreover, when the drug is dispersed with a small molecule, the resulting dispersion is known as a co-amorphous solid dispersion as both the drug and the co-former are completely miscible with one another in a stabilised amorphous state. Stabilising a drug in the amorphous state via the addition of polymer or co-former has the potential to enhance properties such as dissolution, kinetic solubility, and surface properties [5].

Applications such as oral and pulmonary drug delivery often require modified release of the drug through prolonged dissolution and enhanced kinetic solubility [6, 7]. This helps to achieve an extended-release profile which reduces the dosing requirements in oral delivery and can achieve localised drug action with minimised lung clearance for pulmonary delivery. Surface properties are of particular importance for drug delivery to the lungs as these determine powder flow properties, which in turn determine powder deposition in the lungs, when using a dry powder inhalation system [8]. Localised drug delivery and extended-release profile are particularly useful for inhaled antibiotics as continual exposure of lung tissue to the antibiotic is desirable for treatment of infections [9].

We recently reported the formation of novel ciprofloxacin (CFX) salts which show modulated solubility compared to CFX base and the commercially available hydrochloride salt [10]. To formulate these salts for pulmonary delivery, good aerodynamic properties and sustained release of drug must be achieved and one way to achieve this is through the generation of amorphous solid dispersions [11-14]. Spray drying is a commonly used preparation method for generating amorphous solid dispersions with polymers and small molecule co-formers. By spraying drug-coformer-polymer solutions into a hot drying gas, amorphous homogenous molecular mixtures of the starting materials can be formed. In a different setup, the drug solution can be pumped through a different nozzle to the polymer/co-former solution which causes the separate solutions to meet at the point of atomisation in the spray drying process. This is known as three-fluid nozzle spray drying and is particularly useful for producing solid dispersions if the drug and excipients do not

dissolve in a mutual solvent [15, 16]. The three-fluid nozzle set up may also be used to generate a salt form of the drug and a solid dispersion simultaneously *in situ* via the ionisation of species and molecular mixing happening when the separate fluids merge at atomisation. This method is explored through this study, with the aim of preparing an amorphous matrix of the polymer embedded with co-amorphous salt of CFX/counter ion. As a contrast, we also suspended CFX salt particles which were then spray dried with a polymer solution to form an amorphous polymer matrix embedded with the CFX salt particles. The preparation, characterisation, *in vitro* and *in vivo* testing of these contrasting solid dispersions is reported in this paper.

The reported crystal engineering approach aims to better control drug release from solid dispersions and increase the control of dissolution kinetics through a method with reduced processing variables. The use of three-fluid nozzle spray drying for *in situ* formation of salts within solid dispersions is a novel application and the findings of this work will help exploit the use of crystal engineering to improve drug properties that can affect oral and pulmonary drug delivery.

## 2. Material and methods

### 2.1. Materials

Ciprofloxacin base (CFX), succinic acid (SA), glutaric acid (GA), adipic acid (AA), pimelic acid (PA) and hypromellose (HPMC) were obtained from Sigma-Aldrich (Dorset, UK). Acetic acid, HPLC water, hydrochloric acid (HCl), acetonitrile and propan-2-ol were obtained from Fisher-Scientific Limited (Leicestershire, UK). All chemicals were used as received.

### 2.2. Synthesis of CFX Salts

Equimolar quantities of CFX and counterion (1:1 molar ratio) were milled using a Retsch MM400 ball mill as per methodology described in previous work [10]. These salts were used as reference materials for formulations containing CFX with SA, GA, AA and PA. The milled salts were also used in the generation of suspension formulations.

### 2.3. Preparations of Spray Dried Solid Dispersions

Spray drying experiments were performed using a B-290 spray dryer (Büchi, Labortechnik AG Switzerland) operated in closed loop mode with a nitrogen atomising gas and nitrogen drying atmosphere. The aspirator was set to 100% generating a vacuum pressure of -100 mbar with the atomising gas flow valve set to 40 mm corresponding to 660 L/hr flow rate. For each experiment the inlet temperature was set to 130 °C and

experiments were started when the outlet temperature stabilised to 70 °C. A 3-fluid nozzle with nozzle diameter 0.5 mm was used, which allowed the simultaneous spray drying of two feedstocks called internal and external feeds. The rate of the internal and external pumps was quantified using fixed volumes of solvent then synced to pump at 5 mL·min$^{-1}$ and combine at the tip of the nozzle as per Fig 1.

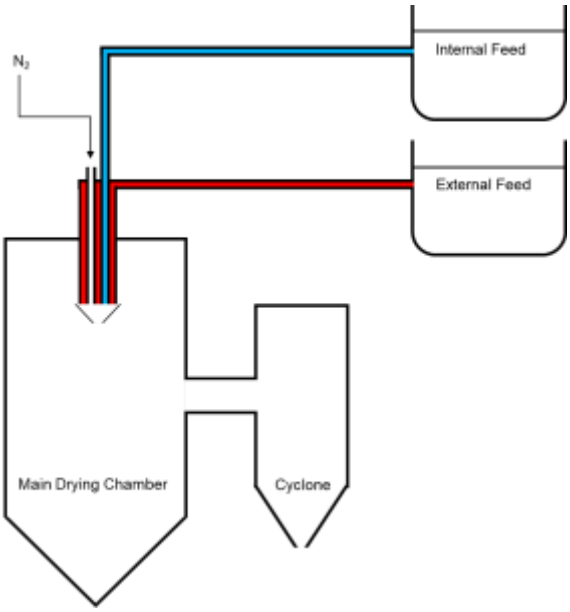


**Fig 1:** Diagram detailing mechanism of three-fluid nozzle spray-drying process i.e. atomising gas ($N_2$), internal and external feeds.

Feedstocks were prepared according to Table 1 to contain CFX and coformer in a 1:1 molar ratio. HPMC was added to feedstocks in a 1:1 mass ratio to CFX, when applicable as per Table 1. All feedstocks were prepared to a final concentration of 1% w/v. To generate suspensions, milled salt with equivalent CFX proportion was added to propan-2-ol at 1% w/v. Suspended CFX salt particles were reduced in size to separate milled agglomerates using a high sheer mixer at 20,000 rpm for 10 mins (MXBAOHENG, RCD-1A) followed by sonication for a further 10 mins (Fisher Scientific, FB 15047). Following spray drying, collected powder was transferred to a vial, weighed, and stored in a desiccator at room temperature.

**Table 1:** 3-fluid nozzle spray-drying methods for salt, solution and suspension formulations. Internal and external feeds were solutions in 3% acetic acid, except for the internal feed of SUS formulations where CFX salt was suspended in propan-2-ol.

| **Salt Formulation (SALT)** | **CSA** | **CGA** | **CAA** | **CPA** |
|---|---|---|---|---|
| Internal Feed | CFX | | | |
| External Feed | SA | GA | AA | PA |
| **Solution Formulation (SOL)** | **CSAH-sol** | **CGAH-sol** | **CAAH-sol** | **CPAH-sol** |
| Internal Feed | CFX + HPMC | | | |
| External Feed | SA + HPMC | GA + HPMC | AA + HPMC | PA + HPMC |
| **Suspension Formulation (SUS)** | **CSAH-sus** | **CGAH-sus** | **CAAH-sus** | **CPAH-sus** |
| Internal Feed | CFX-SA Salt | CFX-GA Salt | CFX-AA Salt | CFX-PA Salt |
| External Feed | HPMC | | | |

### 2.4. Powder X-ray Diffraction (PXRD)

Transmission capillary PXRD data were collected for all spray dried formulations using a Brucker D8 Advance diffractometer equipped with a monochromatic $CuK\alpha_1$ source. Samples were packed into a 0.7 mm borosilicate glass capillary then scanned in the range 4° to 45° 2θ using step size 0.0171° with a count time of 1.4 seconds per step. Data for the starting materials and milled samples were also collected using the same settings to be used as references.

### 2.5. Scanning Electron Microscopy (SEM)

Images of spray dried powders were obtained using a Quanta 600F scanning electron microscope under high vacuum. Samples were attached to carbon tabs, mounted on

aluminium pins, then sputter-coated with gold for 3 min at 30 mA (Emitech K550). Elemental analysis was performed using an Energy Dispersive X-ray spectroscopy (EDX) system (INCA Energy System).

### 2.6. Fourier -Transform Infrared Spectroscopy (FTIR)

FTIR spectra were collected using a Perkin-Elmer 100 FTIR Spectrometer equipped with a diamond attenuated total reflectance (ATR) accessory (Shelton, Connecticut, USA). Transmission was recorded from an average of 16 scans over the range 650 – 4000 $cm^{-1}$ with a resolution of 4 $cm^{-1}$. Physical mixtures of HPMC with either CFX Base + dicarboxylic acid or CFX-Salt were generated using a tumble mixer.

### 2.7. Raman Spectroscopy

Raman measurements were performed on spray dried samples and references using a Renishaw inVia$^{TM}$ Dispersive Raman Microscope equipped with enhanced CCD array detector (Gloucestershire, UK). Spectra were collected using a 785 nm diode laser at 50% power from a 3 s accumulation in the 600 – 1700 $cm^{-1}$ spectral range.

### 2.8. High Performance Liquid Chromatography Analysis (UV-HPLC) for *In Vitro* Experiments

CFX separation was achieved with ACE 3 C18 column (75 x 4.6mm, 3 µm) and isocratic elution with 3% acetic acid:acetonitrile mobile phase (80:20). The UV detector was set to 278 nm. A linear calibration curve was generated ($r^2$ > 0.99) from CFX Base in 3% acetic acid over a range of 0.1 $mg \cdot mL^{-1}$ to 200 $mg \cdot mL^{-1}$.

### 2.9. CFX Content Analysis

50 mg of each formulation was weighed then dissolved completely in 100 mL of 3% acetic acid using a volumetric flask in triplicate. On complete dissolving, samples were filtered with 0.22 µm syringe filter (Ministart®) and CFX concentration was determined through UV-HPLC analysis. The proportion of CFX was then calculated as a percentage of total mass. These values were used as a reference for future experiments where equivalent CFX content was required.

### 2.10. Saturation solubility measurements

Formulations with equivalent mass of CFX (1 mg) were added to 1 mL of phosphate buffer (0.1M, pH 6.8) and mixed at 37.5 °C (± 1 °C) using a rotary mixer for 24 hours. Following centrifugation, 50 µL of supernatant was removed at time intervals of 10 mins,

1 hour, 3 hours and 24 hours then diluted with 3% acetic acid. The CFX concentration in each sample was determined using UV-HPLC analysis.

### 2.11. *In Vitro* Powder Dissolution Study

Dissolution experiments were carried out using a Copley Scientific DIS 8000 instrument (Nottingham, UK) fitted with paddle apparatus. All experiments were performed at 37.5 °C (± 0.5 °C) with stirring speed of 50 rpm using 900 mL of degassed 0.2N HCl (pH 1.2) to ensure sink conditions, as per previously recorded CFX salt solubility values [10]. Formulations with equivalent mass of CFX (20 mg) were loaded into a size 0 gelatine capsule and placed in a stainless-steel capsule sinker. During the experiments, 5 mL of dissolution media was removed from dissolution baths at 5, 15, 30, 60 and 120 mins and filtered using a 0.22 µm syringe filter (Ministart®). CFX concentration was then determined using UV-HPLC analysis. Following removal of samples, 5 mL of fresh dissolution media was replaced to maintain sink conditions. For the SALT formulations, sampling times were 2, 5, 10, 12, 15 and 30 mins to accommodate for their faster dissolution rate.

### 2.12. High Performance Liquid Chromatography Analysis (UV-HPLC) for *In Vivo* Experiments

The serum and plasma ciprofloxacin concentration were determined using HPLC. The analysis was conducted using a UHPLC instrument (Thermo) which consisted of a degasser, a quaternary pump (UPLC), an autosampler, a column oven, and a UV detection system. Chromeleon software 6 was used to process the data. Reverse phase chromatography was used with an XBridge® C18 HPLC column (4.6 × 25 mm, 5µm). The mobile phase was acetonitrile:0.025 M phosphoric acid (pH 3 adjusted with trimethylamine, 13:87 volume ratio). An isocratic mode with a 1.5 mL/min flow rate and a UV detection wavelength of 278 nm were used. The injection volume was 50 µL and the analysis was conducted at 30 ºC.

### 2.13. Determination of Pharmacokinetic Parameters in Albino Rats

The bioavailability of the formulations was evaluated in albino rats. A total of 27 male rats (average weight of 120 g) were acclimatised by housing in a standard environment (12 hours light–dark cycle, 25 ± 1°C) and fed a standard rats' diet with free access to water. The rats were divided into 8 treatment groups and one control group (3 rats per group). All four salt varieties of SOL and SUS formulations were dispersed in 1% acetic acid to obtain 9.6 $mg \cdot mL^{-1}$ dispersions. 1 mL of each dispersion (equivalent to a CFX dose of 28 mg/Kg) was administered orally to the corresponding treatment group of rats, and the control group were treated with 1 mL 1% acetic acid. Two hours later, a whole

blood sample was collected by heart puncture from each rat after being euthanised (using chloroform). An equal volume of the serum (750 µL) and acetonitrile (750 µL) were mixed thoroughly and centrifuged twice at 13000 RPM for 10 minutes at temperature of at 25 °C. The supernatant (1 mL) was transferred to high performance liquid chromatography (HPLC) vials after being filtered using filter syringe and analysed using HPLC. The serum ciprofloxacin concentration was calculated using a calibration curve ($r^2 > 0.99$) prepared from standard solutions of ciprofloxacin in serum at a concentration range of (1.56 to 200 $mg \cdot mL^{-1}$).

### 2.14. Determination of Pharmacokinetic Parameters in Albino Rabbits

The bioavailability of ciprofloxacin powders was also studied in male rabbits (850 g). The rabbits were acclimatised by housing in a standard environment (12 hours' light–dark cycle, 25 ± 1°C) and fed with standard rabbits' diet and had free access to water. The rabbits were divided into 2 treatment groups and 1 control group (3 rabbits per group); Group-1 was treated with CGAH-sol formulation, and Group-2 was treated with CGAH-sus formulation. 51 mg of sample (equivalent to 21 mg CFX) of either CGAH-sol or CGAH-sus was filled into hard gelatine capsules (size 3). The capsules were then orally administered to their corresponding groups while empty capsules were used as treatment for the control group. 3.5 hours later, blood samples were collected from each rabbit from the lateral saphenous vein. Plasma samples were separated from the whole blood and mixed with acetonitrile. Equal volumes of the plasma (750 µL) and acetonitrile (750 µL) were mixed thoroughly and centrifuged twice at 13000 RPM and 25 °C for 10 minutes. The supernatant (1 mL) was transferred to a HPLC vial after being filtered using filter syringe and analysed using HPLC analysis. The plasma CFX concentration was calculated using a calibration curve ($r^2 > 0.99$) prepared from standard solutions of ciprofloxacin in plasma at a concentration range of (0.019 to 20 µg/mL).

### 2.15. Ethical Approval of *in vivo* Studies

*In vivo* studies were conducted according to the relevant guidelines and regulations, and were approved by the Ethics and Research Registration Committee (No. PH81-22)) at the College of Pharmacy, University of Sulaimani, Iraq.

### 2.16. Cascade Impaction

The aerodynamic properties of the spray dried powders were determined using an Andersen Cascade Impactor (ACI) (Copley Scientific, Nottingham, UK). The device was fitted with a pre-separator and 8 stages with cut off size: 8.6, 6.5, 4.4, 3.3, 2, 1.1, 0.54 and 0.25 µm at 60 L/min. Formulations equivalent to 10 mg of CFX were loaded into a

size 3 gelatine capsule and dispersed through the apparatus from a RS01 DPI device. The instrument operated at 60 L/min over 4s and was verified with a flow meter prior to testing. Following each run, particles were collected from each stage by dissolving contents in 20 mL of 3% acetic acid. These were then filtered with 0.22 µm syringe filter (Ministart®) and CFX concentration was determined through UV-HPLC analysis.
Emitted dose (ED) was calculated as % of original CFX dose collected from all stages following the pre-separator. Mass median aerodynamic diameter (MMAD) was calculated as the aerodynamic particle size at which 50% of the ED is larger and 50% of the ED is smaller. Geometric standard deviation (GSD) was calculated to describe the spread of data around the MMAD using equation 1.

$$GSD = \sqrt{\frac{Quantity\ with\ Size < 84\ \mu m}{Quantity\ with\ Size < 16\ \mu m}}$$

**Equation 1:** Formula used to calculate geometric standard deviation for the formulations [17].

Fine particle fraction (FPF) was calculated as the % of ED which has an aerodynamic diameter < 5 µm. Fine particle dose (FPD) was calculated as the mg of CFX found in the FPF.

### 2.17. Statistical Analysis

Statistical analysis was carried out using SPSS software (IBM SPSS version 27.0, SPSS Inc.). Data were compared with appropriate test following test for normality and variance. In each case, statistical significance was defined as $p < 0.05$ with significance levels: *** = $p < 0.001$, ** $p < 0.01$, * = $p < 0.05$ and NS = $p > 0.05$.

## 3. Results

### 3.1. Preparation of Spray Dried formulations

12 spray dried formulations were generated according to the Table 1 and the production yields are recorded in Fig 2. In general, the SUS formulations showed the lowest yield of the three formulation types. This is clearly seen for the SA and GA formulations where the SUS formulation shows approximately 75% reduction in yield compared to the SALT and SOL. This effect is not mirrored with the AA and PA formulation types which showed the SOL method to be the most efficient. Despite this, all AA and PA formulations have a very low yield at less than 25%.

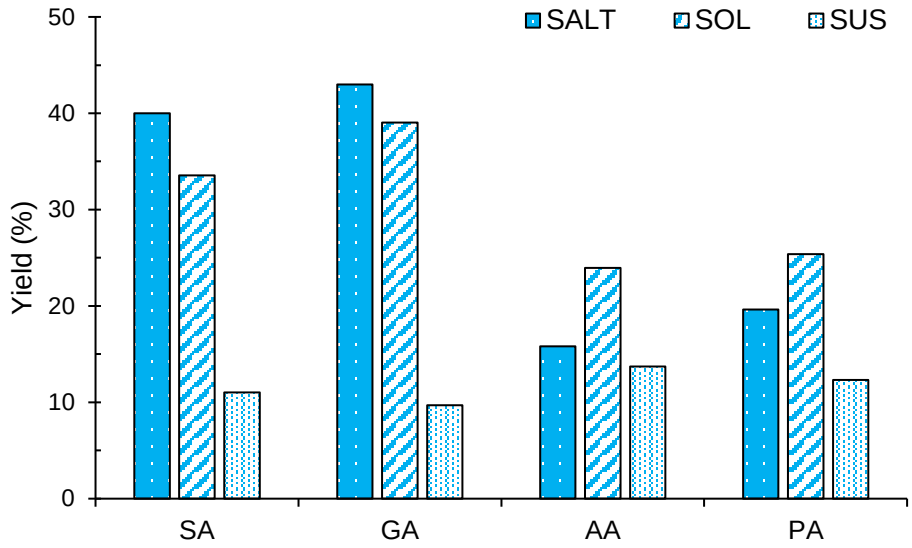


**Fig 2:** Spray drying yields for all salt, solution, and suspension formulations from collected powder as a % of total solid in feedstocks.

## 3.2. Physical Characterisation of Spray Dried Formulations

### 3.2.1. Powder X-ray diffraction (PXRD)

PXRD was used to characterise the solid-state nature of the spray dried materials with respect to crystallinity and to identify any crystalline solid phases formed (Fig 3, Fig S1-S3).

Firstly, comparing CFX salt milled references with spray dried SALT formulations, comparable diffraction patterns can be seen, especially for CSA and CGA, although the peaks show a much lower intensity and broader peak width, corresponding to reduced crystallinity. For the CAA formulation (Fig S2) there appears to be the presence of one or more new phases in addition to the CFX-AA salt form, which we hypothesise may be a new solid form of the CFX-AA salt since there is no evidence of starting material or any known CFX-AA hydrate (CSD refcode QUKHOV) in the spray dried product.

However, for the CPA formulation, there is no agreement with the milled reference for CFX-PA salt or the starting material references (i.e. CFX and PA). From this it can be concluded that a new solid form has been produced through the spray drying process (Fig S3). These observations confirm that salts of CFX can be generated in situ through spray drying, although with much reduced crystallinity, with the implication that salt formation is also likely to take place for spray dried formulations containing HPMC.

With respect to all SUS and SOL formulations, generation of a largely amorphous product has occurred, as shown through the lack of sharp diffraction peaks compared to milled references. (Fig S1-S4). To check whether the shear mixing and sonication step for SUS formulations had caused the crystalline salt to become amorphous prior to spray

drying, the solid phase of a CFX-GA suspension was separated and analysed by PXRD. Sharp diffraction patterns were seen following sheer mixing and sonication indicating that the amorphous phase is generated during the spray drying process (Fig S5). It feasible that at the point of atomisation, when the suspended particles meet the aqueous solution of HPMC, dissolution occurs, followed by crystallisation / precipitation within the polymer matrix. The resulting solid dispersion has an even lower crystallinity than that seen in the SOL formulations, where some low intensity diffraction peaks are associated with a small amount of residual crystalline CFX salt. This is particularly notable for CSAH-sol and CGAH-sol where peaks (e.g. at ~5° 2θ and ~24° 2θ) matching the milled references are seen (Fig 3, Fig S1).

In general, CFX salts appear to be highly miscible with HPMC especially with following suspension and particle size reduction, whereas generating the salt in situ (as in SOL method) increases the likelihood of generating a larger proportion of crystalline CFX salt.

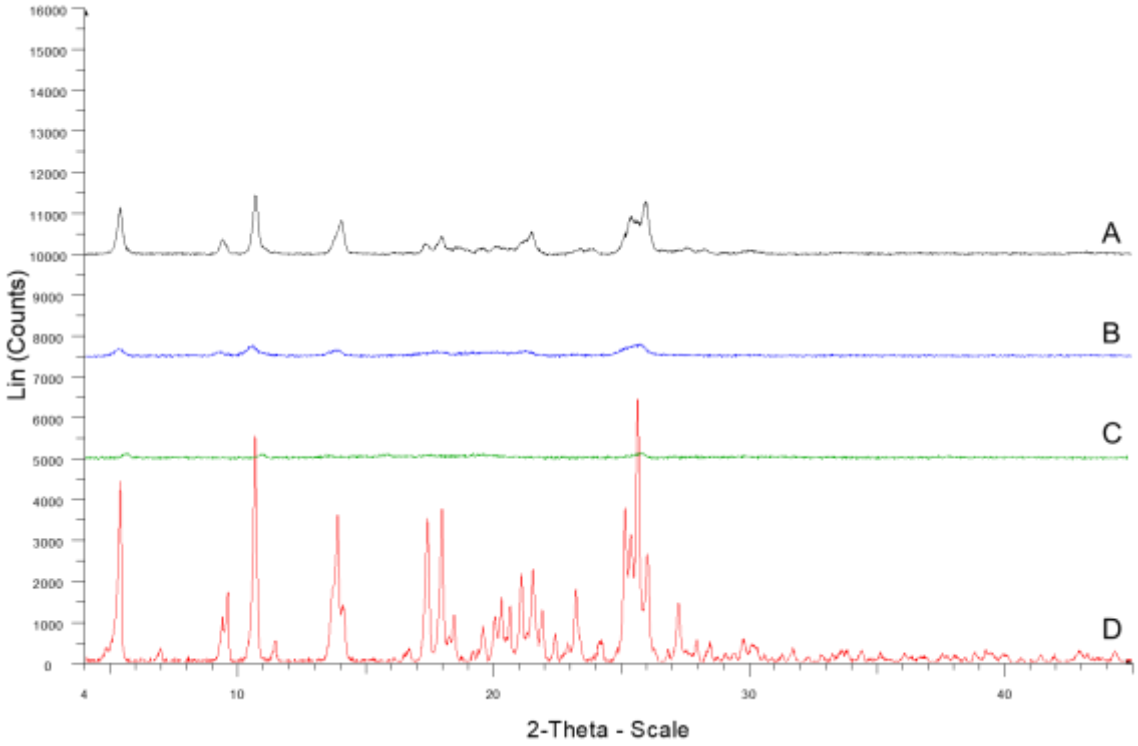


**Fig 3:** PXRD patterns with background scattering removed showing spray drying formulations of **A)** Salt (black), **B)** Solution (blue) and **C)** Suspension (green) compared to **D)** CFX salt reference (red) for ciprofloxacin glutaric acid formulations.

### 3.2.2. Scanning Electron Microscopy (SEM) imaging

SEM micrographs comparing SOL and SUS formulations are shown in Fig 4. All formulations appear to show a range of particle sizes and surface morphologies. Particles show characteristics of a large Péclet number drying process (i.e., large, sunken particles with wrinkled surfaces) which is more likely with viscous polymer containing feedstocks [18].

There appears to be the presence of different particle shapes particularly in the CGAH-sus and CAAH-sus formulations. These “needle-like” particles could correspond to come milled CFX salts crystals which have not completely dispersed in the polymer. This may be the cause of the small low intensity peaks seen in CGAH-sus and CAAH-sus PXRD patterns (Fig 3, Fig S2).

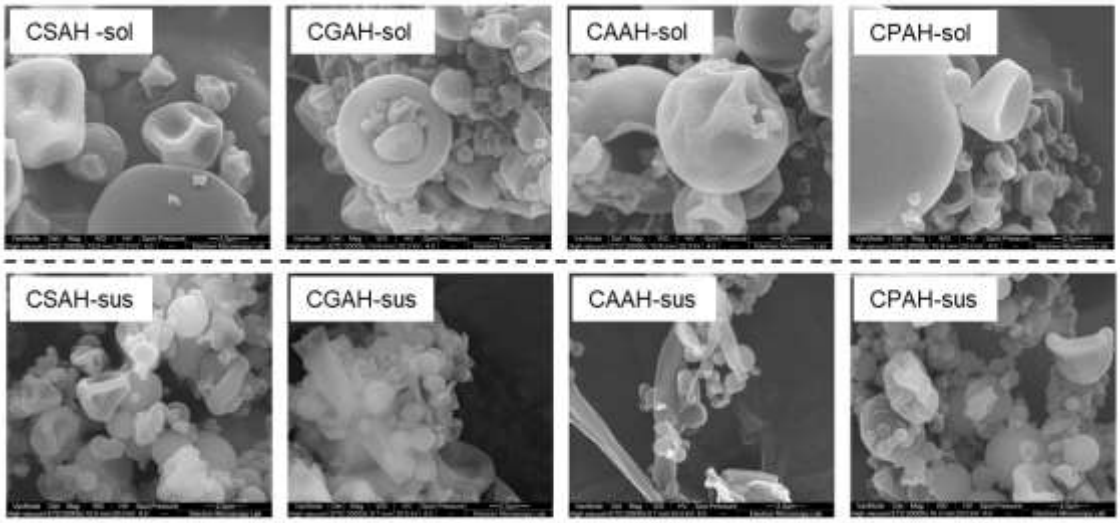


**Fig 4:** SEM images comparing SOL formulations to SUS formulations for each salt form. Images taken at 20,000x magnification.

## 3.3. Analysis of Intermolecular Interactions Within Solid Dispersions

### 3.3.1. FTIR Spectroscopy

FTIR spectra were taken for all solid dispersions from both SOL and SUS methods and compared to physical mixtures of CFX Base, CFX milled salts and HPMC references (Fig 5, Fig S6 – S9).

All solid dispersions showed evidence of a change from CFX Base to CFX salt formation as shown through changes in the stretching frequencies at the carbonyl region. These shifts are typically from ~1610 $cm^{-1}$ and ~1585 $cm^{-1}$ to ~1720 $cm^{-1}$ and ~1625 $cm^{-1}$ and are known to be characteristic of a change in CFX ionisation state as seen in salt for-

mation [10]. During ionisation, CFX switches from a zwitterionic form with ionised carboxylic acid group to a cationic form with neutral carboxylic acid form. It is this change which is observed here on the FT-IR spectrum.

There are slight differences in the positioning and shape of these carbonyl peaks between the different salt forms and between the SOL and SUS formulations. This is likely to be due to the formation of intermolecular interactions between CFX and HPMC which would influence the carbonyl stretching frequencies particularly with the formation of hydrogen bonds.

SOL and SUS formulations show peaks at ~2900 $cm^{-1}$ and ~1050 $cm^{-1}$ which are characteristic for HPMC, corresponding to –OH and –CO stretching in alcohol groups (Fig S6 – S9). These peaks are more prominent than the corresponding regions in physical mixtures which indicates a uniform mixture or solid dispersion of CFX salt and polymer generated through spray drying rather than physical mixing.

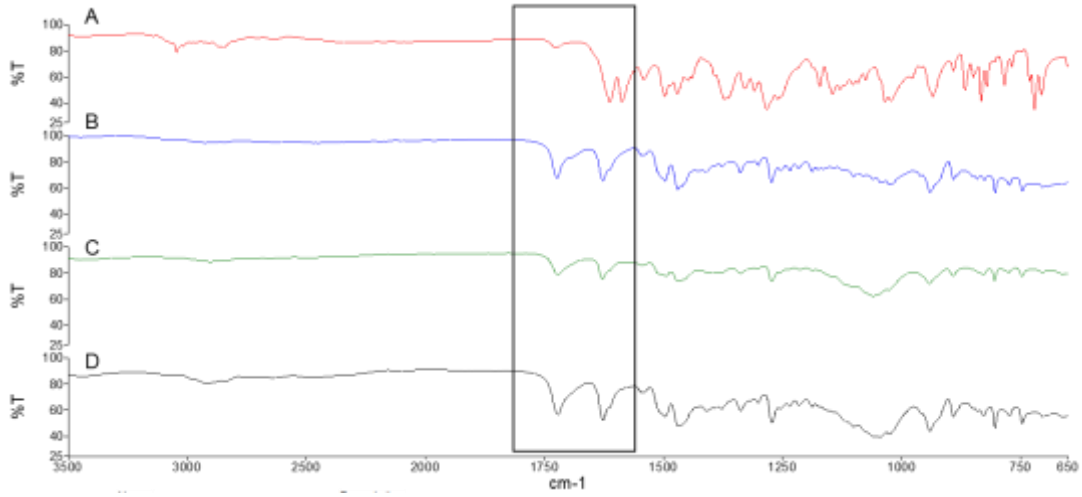


**Fig 5:** FTIR data comparing physical mixtures of **A)** CFX Base + SA + HPMC (red), **B)** CFX-SA + HPMC (blue) and spray dried formulations of **C)** CSAH-sol (green) and **D)** CSAH-sus (black). Carbonyl region highlighted.

### 3.3.2. Raman Spectroscopy

Raman spectra were collected for all spray dried powders and compared to CFX salt milled references. This analysis was chosen in addition to FTIR since HPMC is relatively Raman inactive compared to CFX. As such any spectra collected can be largely attributed to the nature of, and interactions between, CFX, the acid counterion and their environment without interference from peaks associated with the polymer.

All spray dried materials show good agreement with the CFX salt references. Most interestingly is the nature of the peak stretches between 1700 $cm^{-1}$ and 1600 $cm^{-1}$ which

are commonly associated with the carboxylic acid region in CFX. Like FTIR, this region changes distinctly dependent on whether CFX is existing in salt form, with neutral carboxylic acid group (-COOH), or in zwitterionic base form, with a carboxylate ion ($-COO^-$). Fig 6 shows CFX base and SA references compared to CFX-SA salt form where this change to unionised -COOH is clearly seen. Also of note is the absence of a SA peak at ~925 $cm^{-1}$ in the CFX-SA salt form. This peak most likely corresponds to a carboxylic acid dimer which would be lost during salt formation with CFX. Since all spray dried materials possess the neutral carboxylic acid peak, it can be inferred that salt formation has occurred or been maintained, for SOL and SUS formulations respectively, and that no CFX base starting material remains. Also, the absence of any peaks associated with dicarboxylic acids (e.g. carboxylic acid dimer) suggests that there is no counter ion existing independently of CFX.

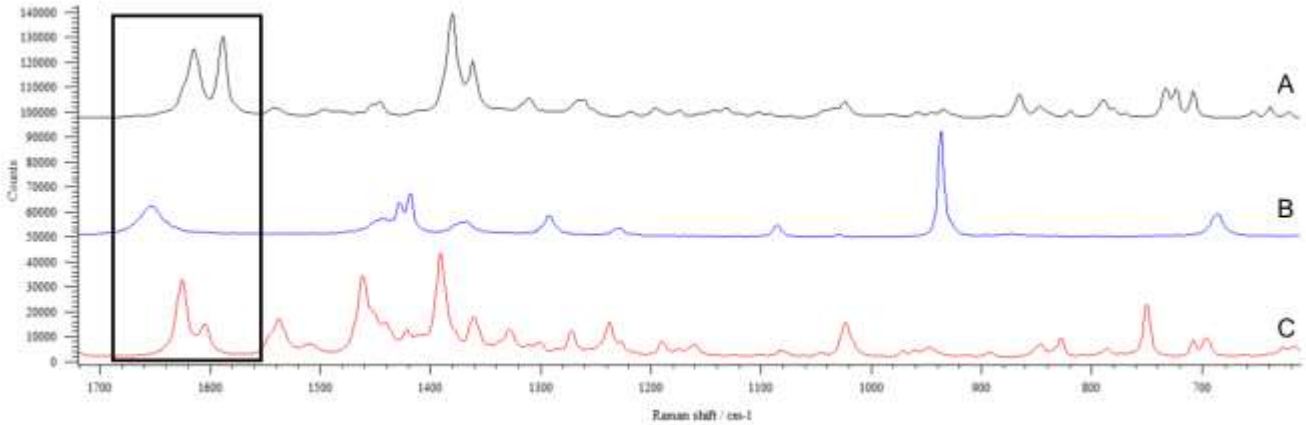


**Fig 6:** Raman data comparing A) CFX Base (black), B) Succinic Acid (blue), C) CFX-SA salt (red) references with -COOH region highlighted.

Some differences between the milled reference and spray dried materials are seen (Fig 7, Fig S10 – S12). In general, there is a reduction in peak intensity and peak broadening from SUS to SOL to SALT which is often associated with increased disorder [19]. Since PXRD analysis showed SUS formulations to be more amorphous than SOL formulation, these differences must be due to the nature of the local interactions between CFX, counter ion and their environment. For the SOL formulations it is likely that CFX and counter-ion are existing in a co-amorphous salt state within the polymer matrix, with the addition of small regions of more crystalline salt. By contrast it is likely that for the SUS formulations, the CFX salt particles have become fully dissolved in the HPMC matrix and in so doing, have formed a more uniform solid dispersion with crystalline CFX salt in solid solution.

Of the three formulation classes, the SALT formulations without HPMC, show the largest differences from the salt reference in terms of peak definition but also positioning. This hints at the utility of HPMC in the spray drying process for encouraging uniform salt formation.

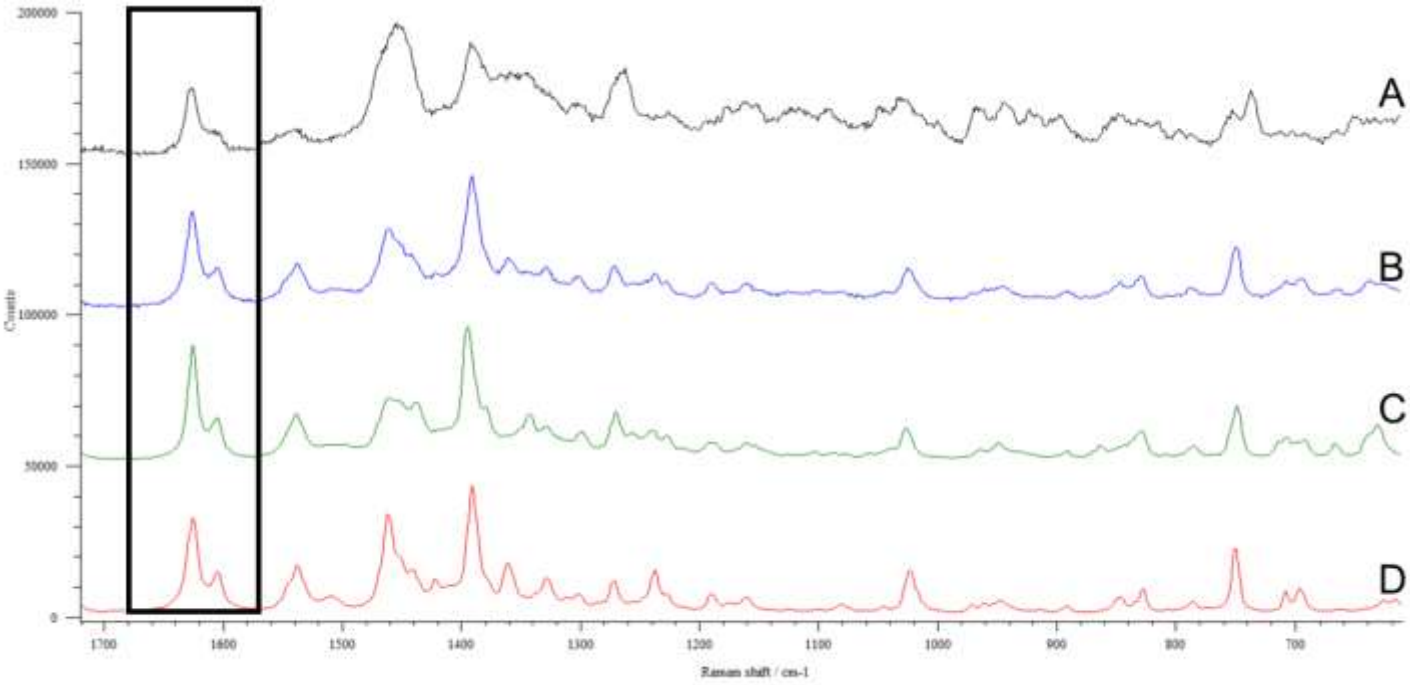


**Fig 7:** Raman data comparing A) CSA (black), B) CSAH-sol (blue), C) CSAH-sus (green) and D) CFX-SA reference (red).

### 3.4. CFX Content Within Solid Dispersions

#### 3.4.1. Energy Dispersive X-ray Analysis (EDX)

EDX and EDX-spot analysis were used to quantify and compare the percentage weight of surface fluorine atoms between the samples as well as between different particle morphologies. Fluorine (F) atoms are used as a marker for CFX in all samples since this atom is unique to CFX. All SUS formulations showed a higher mean surface F weight percentage than SOL formulations as shown in Fig 8. CSAH-sol, CGAH-sol and CPAH-sol are all significantly less than the corresponding SUS formulations (ANOVA, $p < 0.05$). F weight % is equivalent between CAAH-sol and CAAH-sus. CSAH-sus, CGAH-sus and CPAH-sus show a similar F weight % which is ~ 1% higher than the value for CAAH-sus.

For the SOL formulations, there is much more variation in the mean F weight % values between the salt forms, however, these differences are not significant (ANOVA, $p > 0.05$).

When using spot analysis to compare between different particle morphologies seen in the SEM analysis, there was no detectable difference in F weight %. This suggests that there is no difference between surface CFX content in “needle like” and spherical particles confirming the generation of a uniform solid dispersion for SUS formulations.

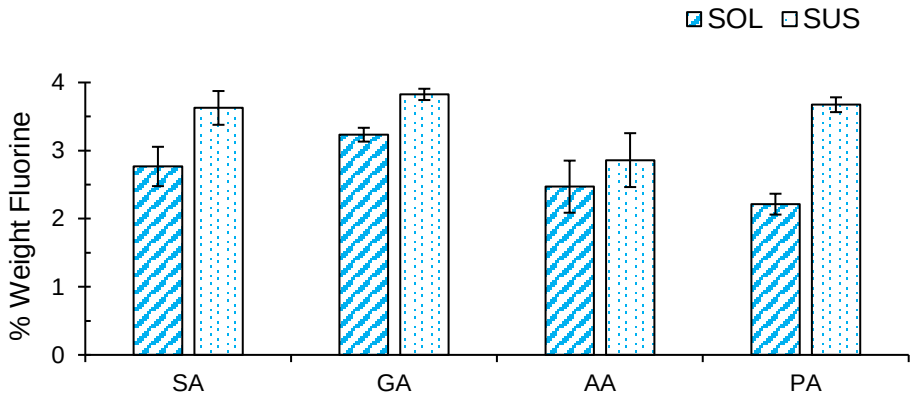


**Fig 8:** EDX data comparing Fluorine weight % as an average over three data points between solution and suspension formulations.

### 3.4.2. Solution Concentration Analysis

In comparison to EDX analysis, % CFX in SOL and SUS formulations was calculated through a solution concentration method (Fig 9). All formulations showed CFX content different to the theoretical CFX value as calculated from starting material solid content in feedstocks (~ 40 %, see method 2.3). Most SUS formulations contain higher than the predicted CFX content, which is also higher than the equivalent SOL formulations, except for CAAH-sus. SUS formulations also show much less variability between the different salt forms.

When correlating CFX concentration values with the F weight % there is good agreement for both SOL and SUS formulations ($R^2$ = 0.97 and $R^2$ = 0.95 respectively). This implies that the proportion of CFX on the particle surface is broadly similar to the proportion of CFX in the bulk powder, suggesting complete miscibility between CFX salt and HPMC during spray drying.

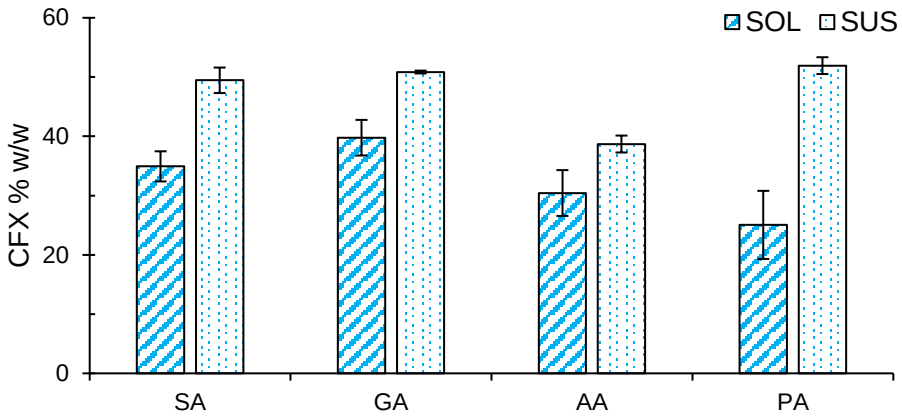


**Fig 9:** CFX content analysis for SOL and SUS formulations as a % of total formulation weight.

### 3.5. In Vitro Solution Properties

3.5.1. Aqueous Solubility Study

Solubility measurements in saturated solution showed there to be differences between the formulations, formulation types and CFX concentration in solution over time.

These effects are most pronounced in the formulations containing CFX-GA, which has been shown to have the highest solubility of the four CFX salts [10] (Fig 10D). Looking at the milled salt reference there is a fluctuation in the CFX solution concentration over the course of the experiment with an overall reduction in concentration. However, this is not mirrored in the formulations which contain HPMC. Notably, CGAH-sus, which shows a slower release of CFX into solution up to 1 hour time point, followed by a downward trend. This trend is seen in all SUS formulations with max solubility at 1 hour for CSAH-sus and CGAH-sus and at 3 hours for CAAH-sus and CPAH-sus (Fig 10A ii).

Comparing spray dried formulations with HPMC (Fig 10A i and 10A ii), SUS formulations appear to be able to sustain a higher CFX concentration in solution than the SOL formulations. The order of maximum solubility for SUS formulations is as follows: CGAH-sus (1.42 µg) > CPAH-sus (1.27 µg) > CAAH-sus (1.13 µg) > CSAH-sus (1.07 µg) compared to SOL formulations: CGAH-sol (0.42 µg) > CAAH-sol (0.34 µg) > CPAH-sol (0.19 µg) > CSAH-sol (0.069 µg). When comparing the 24-hour concentrations for CGAH-sol/CGAH-sus and CAAH-sol/CAAH-sus, the difference in CFX concentration is much less pronounced, suggesting that any difference seen between the SOL and SUS formulations is kinetic in nature. This change is most clearly seen with CGAH-sus formulation, where the difference is reduced by more than 50% from 1 hour to the 24 hours (Fig 10B). Differences in solubility kinetics are likely due to the differences between in solid dispersion composition with respect to residual crystallinity and salt particle size within the polymer matrix.

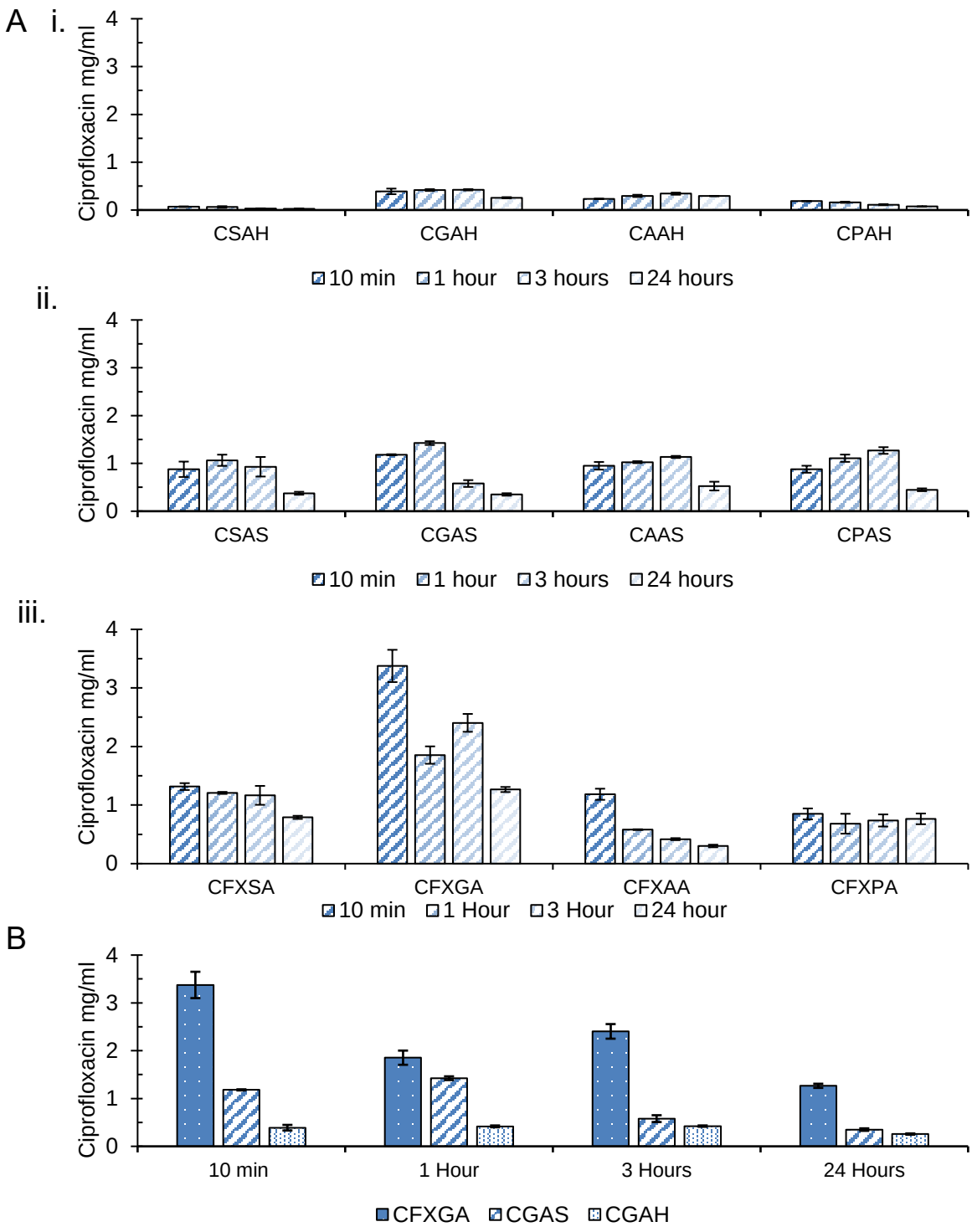


**Fig 10:** A) Comparison of solubilities over 24 hours in fixed volume of solution i) Solution formulations grouped by salt form, ii) Suspension formulations grouped by salt form, iii) Salt formulations grouped by salt form, B) Comparison of glutaric acid salt, suspension, and solution formulations over 24 hours.

### 3.5.2. In Vitro Dissolution Study

#### 3.5.2.1. Dissolution of SALT formulation references

All SALT formulations achieved over 90% dissolution by 10 mins although this is seen at different rates (Fig 11). The difference in rate is most clearly seen at the 5 min time point, where there is a significant difference between all four salts ($p < 0.001$). The % release of CFX into solution at the 5 min time point is as follows: CFX-GA > CFX-SA > CFX-PA > CFX-AA. CFX-GA has released almost double the amount of CFX into solution that CFX-AA has at the 5 min time point. This trend is broadly similar to the trends seen with saturated solubility analysis from a previous work although using different media [10].

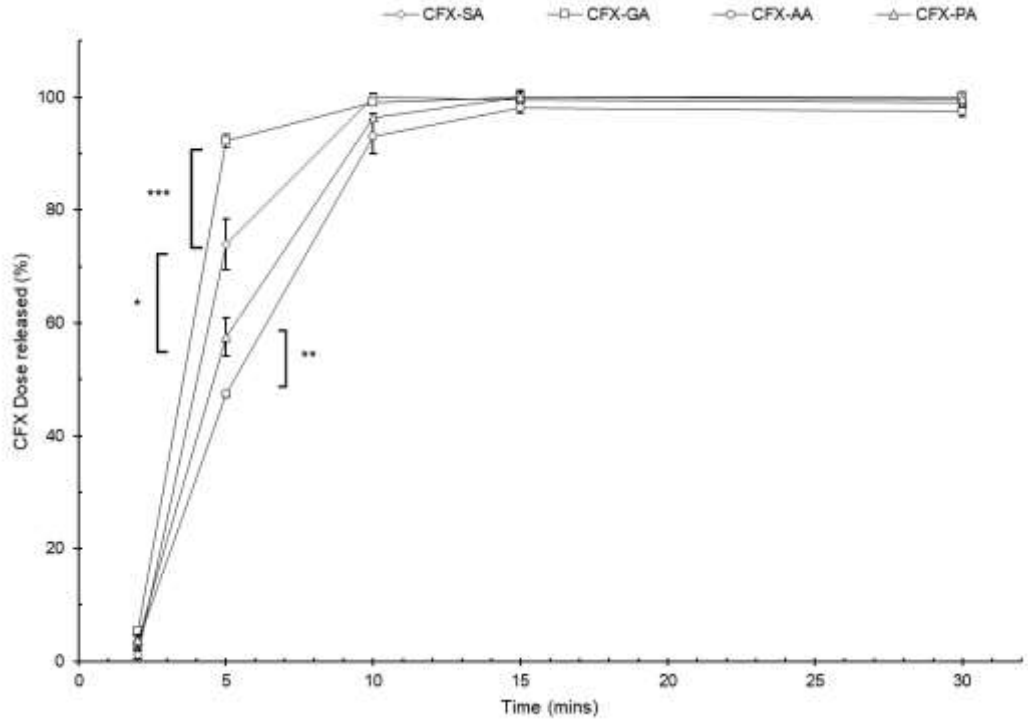


**Fig 11:** In-vitro dissolution data for spray dried CFX Salt formulations. [ANOVA: *** = $p < 0.001$, ** $p < 0.01$, * $p < 0.05$].

#### 3.5.2.2. Comparison of SALT, SOL and SUS *In Vitro* Dissolution

Mean dissolution values for all four salts of each formulation were calculated then plotted to compare the differences between SALT, SOL and SUS formulations (Fig 12). Mean values were used since no significant difference was found between the time points for the different salt forms of SOL and SUS formulations (ANOVA, $p > 0.05$ for all time points within SOL and SUS formulations).

Comparing polymer formulations to the SALT formulations shows how the formation of solid dispersion with HPMC slows the dissolution rate of CFX into solution (Fig 12). At the 15 min time point, formulations with HPMC show ~20% CFX release compared to

full dissolution of the free salts. HPMC is known to swell and gel with the addition of water, and this gelling is likely to cause the reduced release rate of CFX from the formulation. Diffusion of CFX out of the HPMC gel into the dissolution media will become the rate controlling step for dissolution.

SOL and SUS formulations approach full dissolution over the course of the experiment and at the 2-hour point show ~60% and ~80% CFX release respectively. The SOL formulations show a smooth release curve compared to the SUS formulations which appear to show a more bi-phasic release pattern. From time 0 to 15 mins the SUS release pattern is the same as for the SOL formulations; from 30 mins until the 2-hour time point, the rate increases significantly, to the point where SUS formulations have released ~25% more CFX into solution than the SOL formulations. Since CFX content analysis showed both SOL and SUS formulations to have uniform CFX distribution between the bulk powder and particle surface, differences in dissolution profiles must be due to the nature of the solid dispersion formed.

The gradual single phase release profile seen for the SOL formulations points to the formation of a solid dispersion with HPMC, where dissolution will be defined by CFX diffusion out of the hydrated polymer matrix. Whereas, for SUS formulations, it is likely that dissolution is initially led by the carrier before becoming predominantly API controlled. The higher proportion of amorphous CFX salt within the polymer leads to increased dissolution following the hydration and dispersion of polymer into the dissolution medium.Since there is thorough dispersion of CFX salt throughout the polymer matrix, no “dose dumping” is seen; rather, there is  a gradual release approaching 100% dissolution at the 2-hour time point.

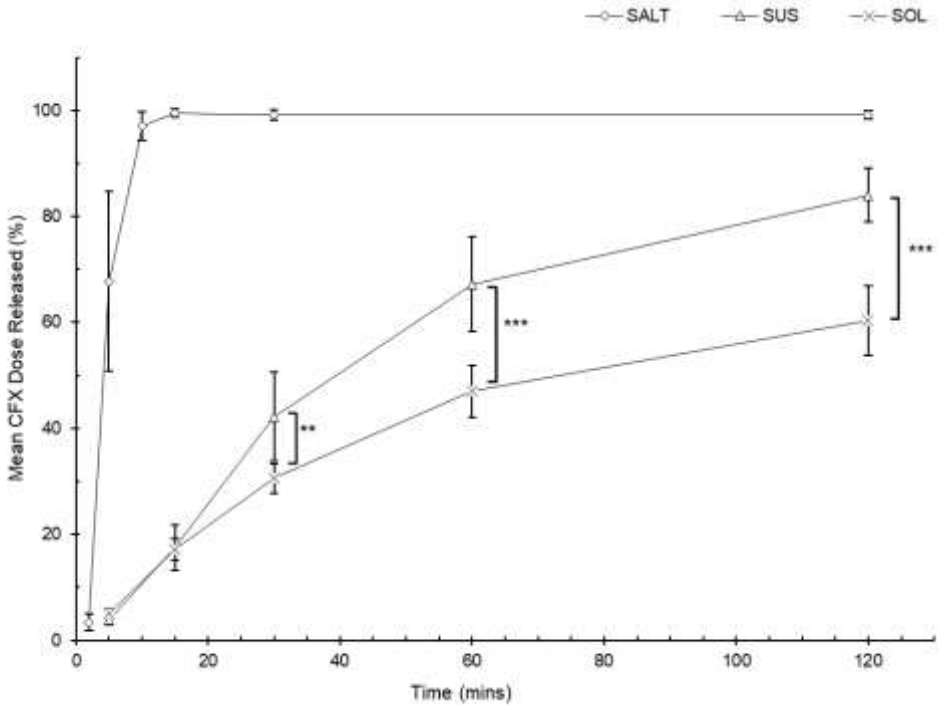


**Fig 12:** In-vitro dissolution data for Salt, Solution and Suspension formulation types expressed as a mean of the four salt forms. [ANOVA: *** = $p < 0.001$, ** = $p < 0.01$].

The comparison of the three formulation types per salt form is shown in Fig S13. CFX-SA and CFX-GA formulations display the trend seen in the mean formulation values most clearly, as does CFX-PA but to a lesser extent. The bi-phasic release pattern is seen in CAAH-sus; however, the rate appears to be less than the CAAH-sol release profile initially and only exceeds CAAH-sol significantly at the 2-hour time point. This difference in release profile could be due to the lower drug loading seen in CAAH-sus, compared to other SUS formulations. To gain an equivalent quantity of CFX, there will be a higher amount of HPMC in the delivery system. At the 2-hour mark, all SUS formulations show significantly higher dissolution than the equivalent SOL formulations (ANOVA, $p < 0.05$ for all salt forms).

### 3.6. In Vivo Pharmacokinetic Study

#### 3.6.1. CFX Oral Bioavailability Study in Rats

To assess the physiological impact of SOL and SUS formulations, bioavailability was assessed in rodents and rabbits. The first set of experiments involved testing all formulations by reconstituting the powders in 1% acetic acid solution. This is to assess whether the formed particles are equivalent in terms of dose size and to ensure that any differences are attributed to the nature of the solid dispersions. As can be seen in Table 2, the pharmacokinetic data showed that most formulations were similar in terms of oral

bioavailability. This trend was expected as dissolving prior to administration will remove the effect of crystal engineering on the dissolution kinetics and subsequently any difference will likely to be due to differences in quantity absorbed. CSAH-sol and CSAH-sus showed statistically different serum CFX concentration following administration which we attribute to genetic and physiological factors. The differences seen between the different CFX salt forms may be due to the influence of the counter ion on CFX absorption. However, the influence of counter ion on bioavailability requires further investigation in the absence of polymer.

**Table 2:** Concentration of ciprofloxacin in rats' serum 2 hours after oral administration of different formulations, mean ± SD, n=3-8, P=0.01.

| **Formulation** | **Serum conc. (ng·mL$^{-1}$)** |
|---|---|
| CSAH-sol | 1410 ± 593$^{A}$ |
| CSAH-sus | 757 ± 118$^{B}$ |
| CGAH-sol | 590 ± 297$^{B}$ |
| CGAH-sus | 731 ± 296$^{B}$ |
| CAAH-sol | 561 ± 760$^{B}$ |
| CAAH-sus | 486 ± 196$^{B}$ |
| CPAH-sol | 647 ± 338$^{B}$ |
| CPAH-sus | 475 ± 281$^{B}$ |

3.6.2. Solid Dispersion Oral Bioavailability Study in Rabbits

In the second set of experiments, rabbits were treated with CGAH-sol and CGAH-sus in capsules and CFX bioavailability was evaluated. These two formulations were selected because of their high solubility compared to other formulations. It was expected that a similar pattern to the *in vitro* findings would be observed (Fig 10D, Fig S11B) which showed that CGAH-sus had delivered a larger quantity of CFX than the CGAH-sol. As can be seen in Fig 13, the data showed agreement with this observation in that plasma concentrations were significantly higher than the SOL formulations. However, contrary to expectation, the data showed that there was no detected CFX following treatment with CGAH-sol. This finding highlights the necessity of *in vivo* work to assess formulation performance and points to the requirement of more detailed pharmacokinetic studies monitoring concentration over time to investigate this finding further.

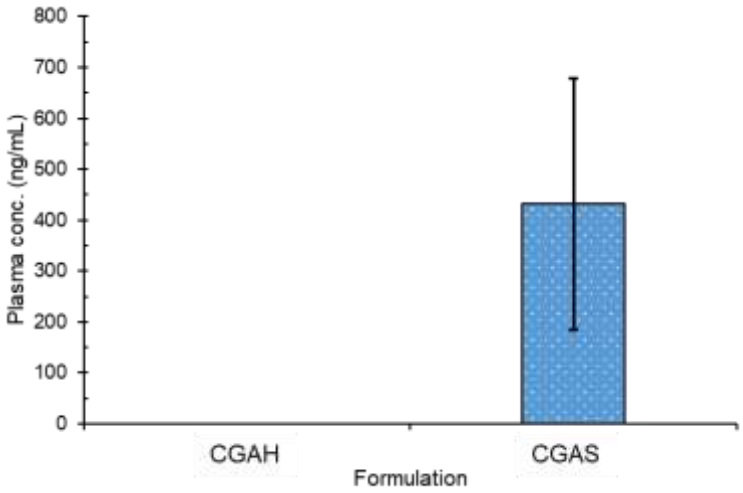


**Fig 13:** Plasma concentration of ciprofloxacin in rabbits, 3.5 hours after oral administration of G1 and G2, (mean ± SD, n=3, p=0.039).

### 3.7. In Vitro Lung Deposition Study (ACI)

All spray dried formulations, except for CAA show an MMAD of less than 5 µm, which generally suggests that the powders will have good inhalation properties in vivo. Comparing the formulation types, MMAD decreases with the addition of polymer, and again through spray drying from SUS. This trend is most pronounced in the AA based formulations where there is a statistically significant decrease in MMAD from 5.47 µm to 2.88 µm across the three formulation types. Taking the average of the MMAD across all formulation categories shows that SUS formulations display a significant reduction in MMAD compared to SOL and salt (Fig 14A). Since the overall aerodynamic diameter is smaller, it can be inferred that addition of polymer and using a SUS based formulation will give a powder with better lung deposition and with less loss in the throat and upper airways. One exception to this trend is for glutaric acid formulations where the is no significant difference between the SOL and SUS methods. CSAH-sus shows the lowest MMAD of the formulations at 2.71 µm.

All spray dried formulations display a GSD of greater than 1.2 µm and as such are classified as heterodisperse aerosols (Fig 14C). It is advantageous to have an aerosol which as close to monodisperse as possible to deliver a precise dose. For these formulations, GSD decreases with the addition of polymer and again through spray drying from SUS, apart from glutaric SUS and pimelic SOL formulations. Since the range of particle size is reduced, it can be inferred that the addition of polymer, especially using a SUS formulation gives a more uniform inhalation powder. CAAH-sus formulation has shown the lowest GSD of the formulations at 1.78 µm.

The fraction of powder in the fine particle range (FPF) (i.e. < 5 µm aerodynamic diameter) consistently increases with the addition of polymer and again from spray drying from SUS (Fig 14B). This increase is highly significant for all formulations. The effect is most pronounced for the adipic and pimelic salt forms which show a doubling of FPF with the addition of polymer then a further doubling between SOL and SUS formulations. For all SUS formulations most of the emitted dose is of a size range acceptable for inhalation (i.e., < 5 µm) compared to SOL and pure salt forms where FPF is less than 50%. CAAH-sus shows the highest FPF of the formulations at 63%.

When comparing the CFX dose within the FPF the difference in drug loading of the solid dispersions is clear (Fig 14D). Except for adipic, the SUS formulations show significantly lower CFX content compared to pure salt and SOL formulations. This is particularly seen for succinic where the SUS formulation contains ~7 times less CFX than the pure salt and SOL formulation. This fits the hypothesis of HPMC encapsulation for SUS formulations since it is likely that smaller particles will contain differing proportions of CFX compared to larger particles. These smaller particles will reach the fine particle range of the Andersen cascade impactor.

Steps to standardise drug loading within the SUS formulations would be required perhaps by increasing the concentration and uniformity of the suspensions. CGAH-sol shows the highest FPD of the polymer formulations at 2.24 mg and CSA shows the highest FPD of all formulations at 2.5 mg.

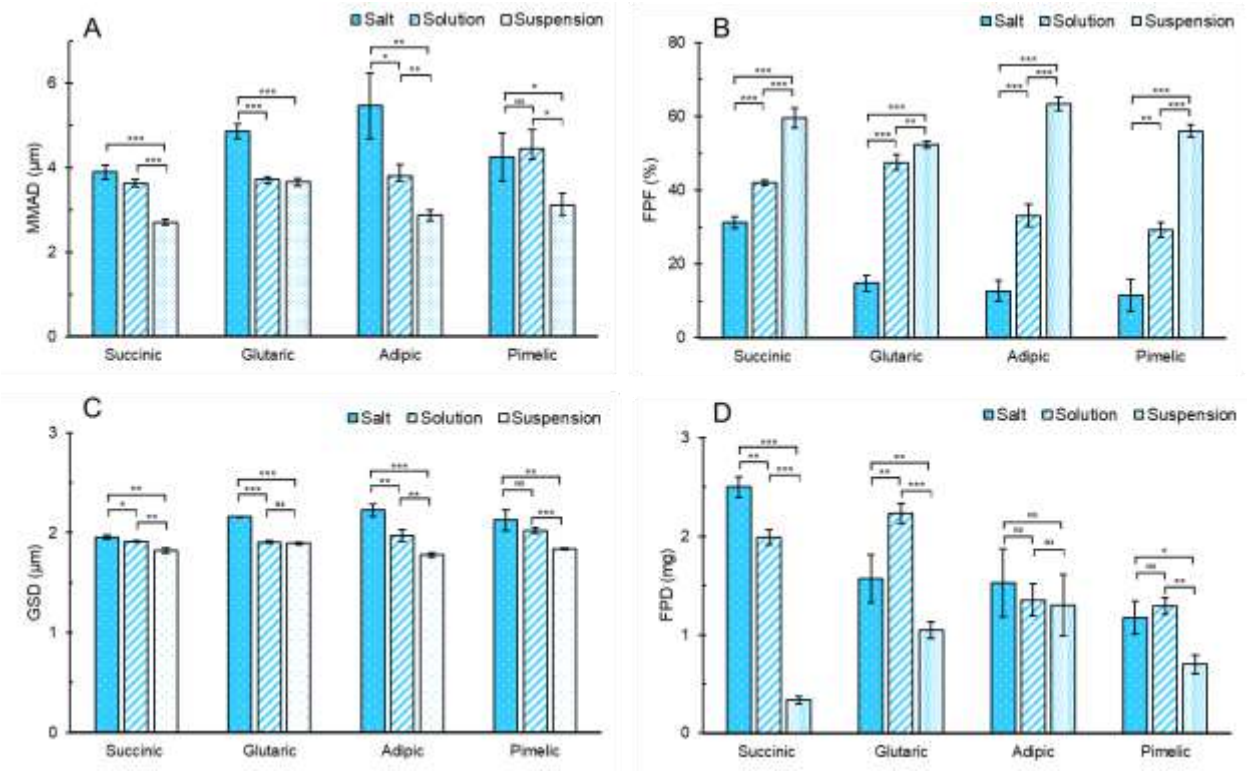


**Fig 14:** Comparison of inhalation parameters between formulation types grouped by salt form. A) Mass Median Aerodynamic Diameter (MMAD), B) Fine Particle Fraction (FPF), C) Geometric Standard Deviation (GSD), D) Fine Particle Dose (FPD).

## 4. Conclusion

Solid dispersions of CFX salts with distinct solution and inhalation properties have been produced through contrasting 3-fluid spray drying methods. The presence of CFX salt within the solid dispersions was confirmed through FT-IR and Raman spectroscopy by comparison to known salt reference spectra. Solubility and dissolution experiments reveal significant differences in release kinetics between the two formulations linked to the nature of the CFX-polymer solid dispersion. When assessing the oral bioavailability of these formulations *in vivo*, clear differences are seen between the two classes of formulation. Assessment of inhalation properties showed how the addition of HPMC to formulations enhanced the aerodynamic powder performance, especially with respect to MMAD and FPF. The generation of these CFX solid dispersions in single-step spray drying method, with the dispersions showing different release kinetics and enhanced powder aerodynamic properties, may help extend use of CFX beyond its existing oral formulations. Further studies focusing on fine-tuning the spray drying process parame-

ters to ensure exact drug loading and higher yield (especially within the SUS formulations) and the assessment of CFX stability within the formulations are required. Further *in vivo* pharmacokinetic studies are also needed.

## References


1. N. Blagden, M. de Matas, P. T. Gavan and P. York, *Advanced Drug Delivery Reviews*, 2007, **59**, 617-630.
2. S. Saha, M. K. Mishra, C. M. Reddy and G. R. Desiraju, *Accounts of Chemical Research*, 2018, **51**, 2957-2967.
3. C. L.-N. Vo, C. Park and B.-J. Lee, *European Journal of Pharmaceutics and Biopharmaceutics*, 2013, **85**, 799-813.
4. Y. He and C. Ho, *Journal of Pharmaceutical Sciences*, 2015, **104**, 3237-3258.
5. J. Liu, H. Grohganz, K. Löbmann, T. Rades and N. J. Hempel, *Pharmaceutics*, 2021, **13**.
6. J. E. Hastedt, P. Bäckman, A. R. Clark, W. Doub, A. Hickey, G. Hochhaus, P. J. Kuehl, C.-M. Lehr, P. Mauser, J. McConville, R. Niven, M. Sakagimi and J. G. Weers, *AAPS Open*, 2016, **2**, 1.
7. G. L. Amidon, H. Lennernäs, V. P. Shah and J. R. Crison, *Pharmaceutical Research*, 1995, **12**, 413-420.
8. R. Scherließ and C. Etschmann, *International Journal of Pharmaceutics*, 2018, **548**, 49-53.
9. H. Al-Obaidi, A. Granger, T. Hibbard and S. Opesanwo, *Journal*, 2021, **13**.
10. T. Hibbard, B. Nyambura, P. Scholes, M. Totolici, K. Shankland and H. Al-Obaidi, *Journal of Pharmaceutical Sciences*, 2023, **112**, 195-203.
11. K. AboulFotouh, Y. Zhang, M. Maniruzzaman, R. O. Williams and Z. Cui, *International Journal of Pharmaceutics*, 2020, **587**, 119711.
12. G. Yildiz Türkyilmaz, K. V. Özdokur, L. Alparslan and E. Karasulu, *Pharmaceutical Development and Technology*, 2023, 1-8.
13. W. Lu, T. Rades, J. Rantanen, H.-K. Chan and M. Yang, *International Journal of Pharmaceutics*, 2019, **572**, 118724.
14. H. Wang, G. George, S. Bartlett, C. Gao and N. Islam, *European Journal of Pharmaceutics and Biopharmaceutics*, 2017, **113**, 118-131.
15. S. Focaroli, G. Jiang, P. Connell, J. V. Fahy and A.-M. Healy, *Pharmaceutics*, 2020, **12**.
16. A. Kauppinen, J. Broekhuis, N. Grasmeijer, W. Tonnis, J. Ketolainen, H. W. Frijlink and W. L. J. Hinrichs, *European Journal of Pharmaceutics and Biopharmaceutics*, 2018, **123**, 50-58.
17. W. H. Finlay and C. Darquenne, *Journal of Aerosol Medicine and Pulmonary Drug Delivery*, 2020, **33**, 178-180.
18. J. Archer, J. S. Walker, F. K. A. Gregson, D. A. Hardy and J. P. Reid, *Langmuir*, 2020, **36**, 12481-12493.
19. G. Gouadec and P. Colomban, *Progress in Crystal Growth and Characterization of Materials*, 2007, **53**, 1-56.

Chapter 5

# Spray Dried Progesterone Formulations for Carrier Free Dry Powder Inhalation

**Thomas Hibbard**[1], Hannah Mitchell[1], Yoonha Kim[1], Kenneth Shankland[1], Hisham Al-Obaidi[1]

[1]School of Pharmacy, University of Reading, Reading, RG6 6AD, UK

Chapter Summary:

In this chapter, spray dried formulations containing progesterone and excipients in a variety of solvent systems were generated for dry powder inhalation. Following spray drying, the Form II progesterone polymorph was found to be exclusively present in a crystalline state, independent of feedstock solvent or excipients. When HPMCAS was added to formulations, no temperature induced phase change back to Form I was observed before melting and increased kinetic solubility and fine particle fraction were seen.

Author Contributions:

TH: conceptualisation, investigation, methodology, writing – original draft, review & editing.

HM, YK: cascade impaction and spray drying experimentation; KS: writing – original draft, review & editing; HAO: conceptualisation, investigation, methodology, project administration, writing – original draft, review & editing.

**Abstract**

Inhalable formulations of progesterone, L-leucine and hydroxypropyl methylcellulose acetate succinate (HPMCAS) are reported following spray drying from a variety of aqueous:organic feedstocks. PXRD, FTIR and DSC were used to characterise these formulations and confirmed that progesterone crystallises as the Form II polymorph during spray drying regardless of the solvent used.

The resultant formulations showed higher aqueous solubility than progesterone Form I starting material and the addition of HPMCAS was shown to temporarily enable a supersaturated state.

All formulations showed suitable lung deposition profiles (mass median aerodynamic diameter, MMAD < 5 μm) with significant variation depending on the organic solvent used and the ratio of organic to aqueous phase in the feedstock. The addition of HPMCAS was seen to increase the deposition in the lower lung and therefore formed a formulation with a lower fine particle fraction and MMAD.

Thermal analysis was used to show that the Form II polymorph was sensitive to transformation to Form I during heating. The addition of L-leucine to the formulations reduced the temperature for the polymorphic transformation by ~10 °C. However, when HPMCAS was added to the formulation, the Form II polymorph was prevented from transforming to the Form I polymorph. Therefore, HPMCAS is suggested as a suitable excipient to improve solubility, inhalation properties and prevent polymorphic transformation of spray dried progesterone formulations.

This study highlights the use of spray drying to form inhalable progesterone powders with higher solubility which may broaden the application of this medicine.

## 1. Introduction

Hormone replacement therapy (HRT) is required for many women suffering from obstetric and gynaecological conditions. Progestogens, such as progesterone (PROG) are a major component of these therapies due to their high efficacy and reduced side-effect profile compared to other hormones. Other therapies use oestrogens which are associated with many side effects including an increase in breast cancer rate [1, 2].

Currently, formulations of PROG are available for oral, vaginal, or transdermal routes of drug administration, with the oral route preferred. These oral formulations contain micronised PROG in the form of a soft gel capsule to enhance the poor absorption from the GI tract by improving water solubility [3]. Following oral administration, PROG is extensively metabolised in the digestive tract, lumen wall and liver [4]. This limits the overall bioavailability and makes multiple dosing throughout the day necessary [5]. In addition, by-products of this metabolism are pharmacologically active and associated with side effects [4].

As such, alternative routes of administration are being explored, for example delivery of PROG through the inhaled route [6]. The lungs have great potential for systemic drug delivery due to high levels of vascularisation, a very thin diffusion pathway and minimal pH or enzymatic activity [7, 8]. Dry powder inhalers (DPI) are a key delivery system for the inhaled route but since their conception have largely relied on the use of a coarse carrier, such as lactose, to ensure good aerosolisation and lung deposition [9, 10]. Limitations associated with the use of coarse carrier use have initiated a shift in technology towards carrier-free formulations generated through technologies such as spray drying [11, 12]. At the time of writing, no previous research with respect to developing PROG for inhalation using a carrier free spray drying method exists.

The addition of small molecule and polymer excipients can increase stability and modify solution properties and the aerosolisation performance of inhaled powders [13-15]. Leucine (LEU) is one such small molecule which significantly increases aerosol performance, therefore, formulation with PROG would be beneficial [16]. A formulation containing PROG and hydroxypropyl methylcellulose acetate succinate (HPMCAS) has been shown to increase aqueous solubility, which is a significant property in developing inhaled formulations for systemic delivery [17].

One challenge of formulating PROG, LEU and HPMCAS through spray drying comes from their different solubility profiles, especially since PROG and LEU favour organic and aqueous solvents respectively [18]. Therefore, the spray drying feedstock needs to be

a mixture of miscible organic and aqueous phases allowing PROG and LEU to be in solution together. In this work, the solvent type and aqueous to organic ratio in the feedstock was varied to investigate the influence on inhalation properties for the spray dried product with or without HPMCAS. PROG LEU formulations with and without HPMCAS are contrasted to investigate the influence of excipients on formulation stability, solubility and aerosolisation performance. Physicochemical properties, thermal behaviour, aqueous solubility measurements and in-vitro aerodynamic performance are reported. It is the aim of this research to explore the utility of a carrier free spray drying method to enable the development of a PROG DPI formulation. In this work we systematically varied spray drying feedstock parameters to prepare different carrier free spray dried inhalable formulations of PROG. The organic solvents acetone, ethanol and propan-2-ol were selected to investigate the difference boiling point has on product drying and physical properties.

## 2. Material and methods

### 2.1. Materials

Progesterone (PROG) and L-leucine (LEU) (Fig 1) were obtained from Sigma-Aldrich (Dorset, UK). Ethanol (EtOH), HPLC water, acetone (ACE), acetonitrile and propan-2-ol (IPA) were obtained from Fisher-Scientific Limited (Leicestershire, UK). Hydroxypropyl methylcellulose acetate succinate HG grade (HPMCAS) grade was obtained from Shin-Etsu Chemical Co (Tokyo, Japan) (Fig 1). Gamble's solution was obtained from Pickering Laboratories (Mountain View, California). All chemicals were used as received.

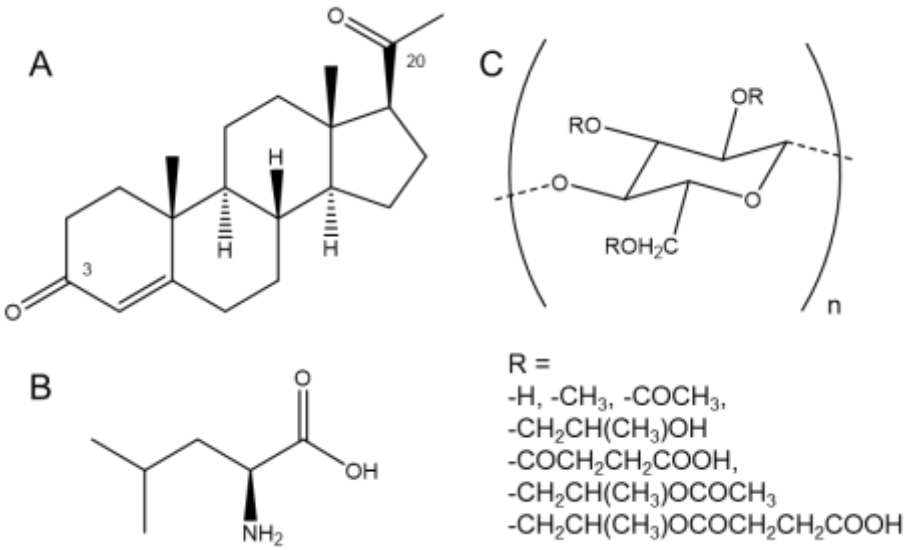


**Figure 1:** Structures of progesterone (A), L-leucine (B) and HPMCAS (C). Key progesterone carbon atoms are numbered.

## 2.2. Preparations of spray dried formulations

Spray drying experiments were performed using a B-290 spray dryer (Büchi, Labo-retechnik AG Switzerland) operated in closed loop mode with a nitrogen atomising gas and nitrogen drying atmosphere. The aspirator was set to 100% generating a vacuum of -100 mbar with the atomising gas flow valve set to 40 mm which corresponds to a 660 L/hr flow rate. For each experiment the inlet temperature was set to 110 °C and experiments were started when the outlet temperature stabilised to 60 °C. A two-fluid nozzle with nozzle diameter 0.5 mm was used at a 5 mL/min pump rate.

Feedstocks were prepared according to Table 1 to contain PROG and LEU in a 9:1 mass ratio with varying types and proportions of organic phase. Initially, PROG and LEU were dissolved separately in organic and aqueous solvents respectively. Organic and aqueous phases were then combined to create one feedstock with total final concentration of 1% w/v. Combining the two phases resulted in a clear solution following stirring. A PROG sample without LEU was generated, to be used as a reference, from a 1% w/v acetone solution using the same spray drying conditions (PROG-SD).

Following spray drying, collected powder was transferred to vials, weighed, and stored in a desiccator.

**Table 1:** Spray-drying methods for PROG-LEU formulations

| Experiment | Organic Solvent | Solvent Ratio % v/v (Aqueous:Organic) |
|---|---|---|
| 1 | EtOH | 50:50 |
| 2 | EtOH | 70:30 |
| 3 | EtOH | 60:40 |
| 4 | IPA | 60:40 |
| 5 | IPA | 70:30 |
| 6 | IPA | 50:50 |
| 7 | ACE | 70:30 |
| 8 | ACE | 50:50 |
| 9 | ACE | 60:40 |

Following initial analysis of processing yields and formulation composition, run 7 was chosen for re-run with the addition of 20% w/w HPMCAS grade. The method was similar except for the HPMCAS was added to the aqueous phase with LEU. Organic and aqueous phases were combined in the same way to produce a feedstock with 1% w/v solid content containing 10% w/v LEU, 20% w/v HPMCAS and 70% w/v PROG.

## 2.3. Physicochemical Analysis

### 2.3.1. Powder X-ray Diffraction (PXRD)

Transmission capillary PXRD data were collected for all spray dried formulations using a Brucker D8 Advance diffractometer equipped with a monochromatic $CuK\alpha_1$ source. Samples were packed into a 0.7 mm borosilicate glass capillary then scanned in the range 4° to 45° 2θ using step size 0.0171° with a count time of 1.4 seconds per step. Data for the starting materials and PROG-SD were also collected using the same settings to be used as a reference.

### 2.3.2. Variable temperature PXRD (VT-PXRD)

PXRD data were also collected over a range of 100 – 130 °C to monitor the polymorphic transformation of PROG. Temperature control was achieved using an Oxford Cryosystems Cryostream Compact device. The same data collection parameters as previous PXRD experiments were used.

### 2.3.3. Fourier -Transform Infrared Spectroscopy (FTIR)

FTIR spectra were collected using a Perkin-Elmer 100 FTIR Spectrometer equipped with a diamond attenuated total reflectance (ATR) accessory (Shelton, CT, USA). Transmission was recorded from an average of 16 scans over the range 650 – 4000 $cm^{-1}$ with a resolution of 4 $cm^{-1}$.

### 2.3.4. Thermogravimetric Analysis (TGA)

Thermal degradation of formulations was analysed using TGA. Samples were heated to 400 °C at 20 °C/min in a $N_2$ atmosphere (TGA, TA Q50) (New Castle, DE, USA). Results were analysed using TA Universal Analysis to identify degradation temperature.

### 2.3.5. Differential Scanning Calorimetry (DSC)

Thermal properties of samples were analysed using DSC following identification of degradation point using TGA. For DSC experiments, samples were hermetically sealed into aluminium pans with pierced lids to allow for any pressure release. All samples were heated to 150 °C at 10 °C/min in a $N_2$ atmosphere using a TA Q2000 DSC instrument (New Castle, DE USA). Results were analysed using TA Universal Analysis to identify thermal events.

2.3.6. Scanning Electron Microscopy (SEM)

Images of samples were obtained using a Quanta 600F scanning electron microscope (Hillsboro, ORE, USA) under high vacuum. Samples were attached to carbon tabs, mounted on aluminium pins, then sputter-coated with gold for 3 min at 30 mA (Emitech K550).

## 2.4. Physical property analysis

2.4.1. UV-HPLC

PROG separation was achieved with ACE 3 C18 column (75 x 4.6mm, 3 µm) and gradient elution with water:acetonitrile mobile phase. The UV detector was set to 245 nm. A linear calibration curve was generated ($r^2 > 0.99$) from a stock solution of PROG in 50:50 acetonitrile:water over a range of 0.1 mg $mL^{-1}$ to 200 mg $mL^{-1}$.

2.4.2. In-vitro aerodynamic performance – Andersen Cascade Impaction (ACI)

Aerodynamic properties of the samples were determined using an Andersen Cascade Impactor (Copley Scientific, Nottingham, UK). The device was fitted with a pre-separator and 8 stages with cut off size: 8.6, 6.5, 4.4, 3.3, 2, 1.1, 0.54 and 0.25 µm. Formulations equivalent to 20 mg of PROG were loaded into a size 3 gelatine capsule and dispersed through the apparatus from a RS01 DPI device. The instrument operated at 60 L/min over 4 sec and the flow rate was verified with a flow meter prior to testing. Following each run, particles were collected from each stage by washing with 20 ml of absolute ethanol. These were then filtered with 0.22 µm syringe filter (Ministart®) and PROG concentration was determined through UV-HPLC analysis.

Emitted dose (ED) was calculated as % of original PROG dose collected from all stages following the pre-separator. Mass median aerodynamic diameter (MMAD) was calculated as the aerodynamic particle size at which 50% of the ED is larger and 50% of the ED is smaller. Geometric standard deviation (GSD) was calculated to describe the spread of data around the MMAD using Equation 1.

$$GSD = \sqrt{\frac{Quantity\ with\ Size < 84.1\ \mu m}{Quantity\ with\ Size < 15.8\ \mu m}}$$

**Equation 1:** Formula used to calculate geometric standard deviation for the formulations

Fine particle fraction (FPF) was calculated as the % of ED which has an aerodynamic diameter < 5 µm. Fine particle dose (FPD) was calculated as the mg of PROG found in the FPF.

#### 2.4.3. In-Vitro Solubility Analysis

The solubility of the samples was assessed in deionised water over a period of 24 hours. 5 mg of each sample was added to 5 mL of solvent in triplicate, which was a sufficient quantity to prevent complete dissolving. Three sets of experiments were mixed on a mechanical mixer for 1 hour, 3 hours or 24 hours at 25 °C. At the required time point, samples were centrifuged at 13,000 rpm for 5 mins then the supernatant was diluted, and PROG concentration determined using UV-Vis spectroscopy at 245 nm, following generation of a calibration curve ($r^2 > 0.99$). A repeat experiment was conducted comparing the saturated solubility of PROG-LEU and PROG-HPMCAS with PROG Form I reference in simulated lung fluid (SLF, Gamble's solution) at 24 hours.

### 2.5. Statistical Analysis

Statistical analysis was carried out using SPSS software (IBM SPSS version 27.0, SPSS Inc.). Data were compared with appropriate test following test for normality and variance. In each case, statistical significance was defined as $p < 0.05$ with significance levels: *** = $p < 0.001$, ** $p < 0.01$, * = $p < 0.05$ and NS = $p > 0.05$.

## 3. Results

### 3.1. Preparation of spray dried (SD) formulations

Spray dried formulations were prepared following the method outlined in section 2.2 and the % yield was calculated (Fig 2). All formulations showed over 50% yield with the maximum yield being ~ 80%.

The results show that the spray drying yield was mostly affected by the ratio of organic to aqueous solvents rather than the organic solvent used. Taking the mean of each solvent ratio, the 50:50 solvent ratio showed a significantly lower yield than both 60:40 and 70:30. There was no significant difference between the yield of the 60:40 and 70:30 solvent ratios; the 60:40 ratio is considered to be the most suitable due to high yield and reduced use of organic solvent.

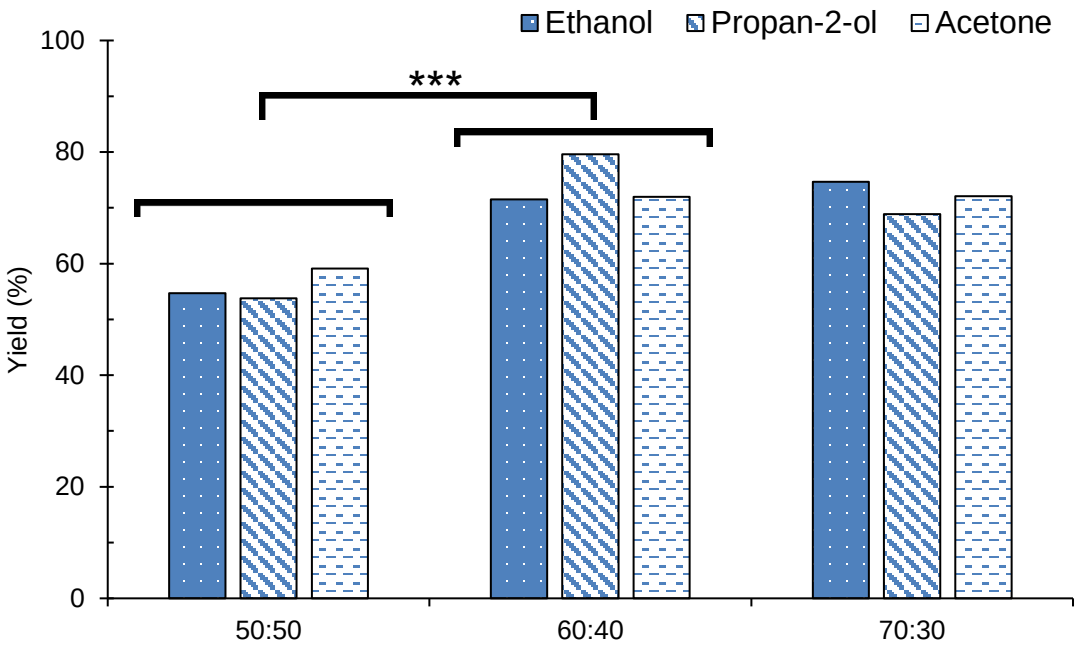


**Figure 2:** % yield for spray dried PROG-LEU formulations calculated as collected mass from the total solid content in the feedstock.

### 3.2. Effect of the Spray Drying Process on Progesterone

#### 3.2.1. Progesterone Polymorphism

PXRD analysis of all spray dried powders showed the presence of PROG Form II rather than the PROG I starting material (Sigma Aldrich). Figure 3 shows the comparison of starting material with PROG-SD, PROG-LEU and PROG-LEU-HPMCAS. Form II is present exclusively in all experiments regardless of feedstock solvent composition. This is most clearly seen by the loss of peaks at 9.48 °2θ and 12.80 °2θ and the appearance of peaks at 10.55 °2θ and 13.73 °2θ. Spray drying PROG from solution is the cause of the Form II polymorph being exclusively present in all formulations since the diffraction differences are seen regardless of excipients or solvents used (Fig S1).

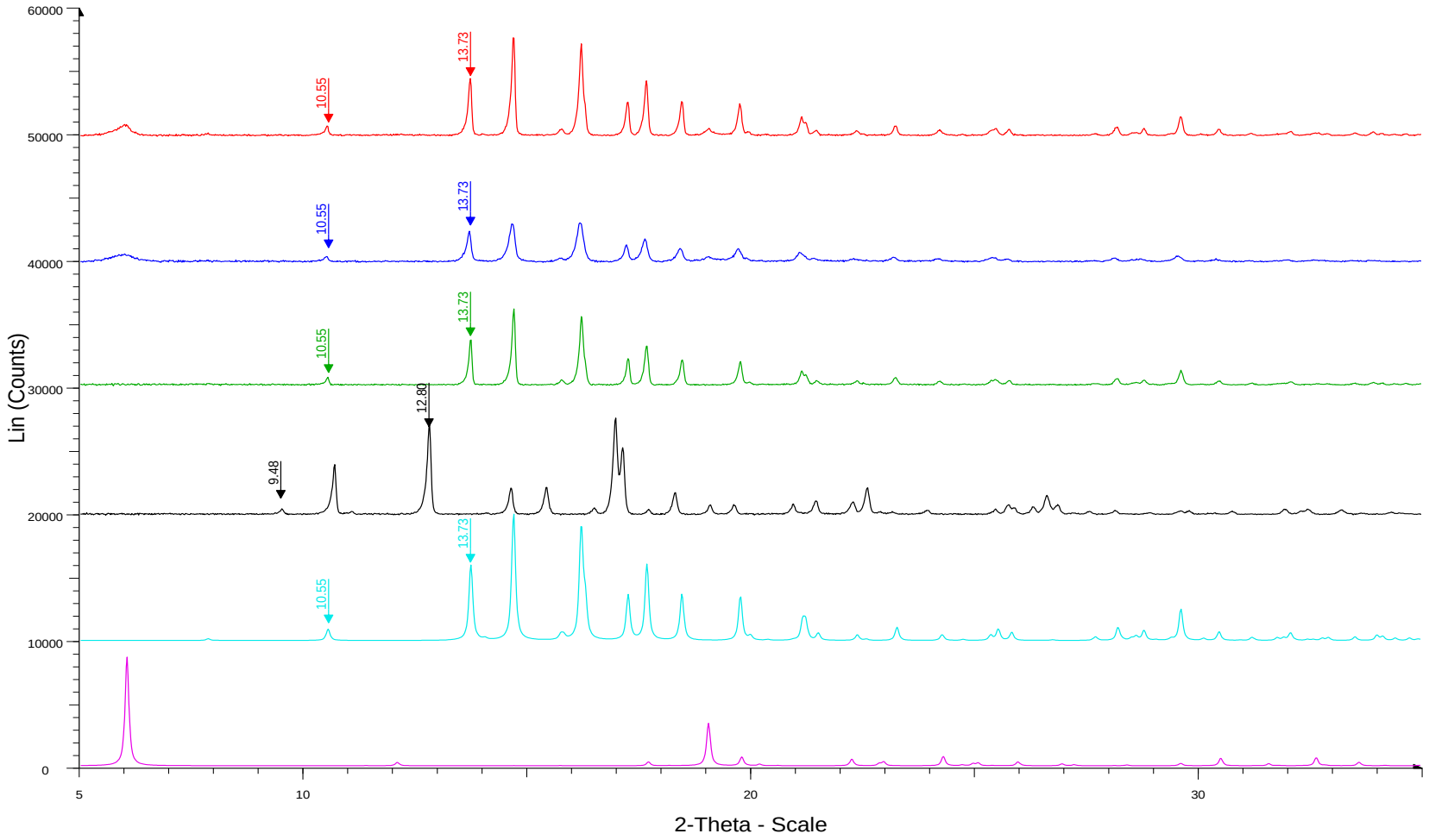


**Figure 3:** PXRD data comparing A) PROG-LEU (red), B) PROG-LEU-HPMCAS (blue), C) PROG-SD (green), D) PROG starting material (Form I, black), E) PROG Form II (light blue) and E) L-leucine (pink).

Similar observations are also seen when analysing FTIR data for the spray dried formulations. Comparing the PROG-SD, PROG-LEU and PROG-LEU-HPMCAS to PROG Form I reference shows a slight difference in the positioning of both ketone carbonyl stretching frequencies at ~1700 $cm^{-1}$ ($C_{20}$) and ~1660 $cm^{-1}$ ($C_3$). For the spray dried materials, these peaks have shifted to a higher wavenumber by ~5 $cm^{-1}$ (Fig 4a) and there is also a clear difference between PROG-SD and PROG Form I at in the fingerprint region, where the Form I polymorph shows a peak at 871 $cm^{-1}$ compared to PROG-SD which shows a peak at 862 $cm^{-1}$ (Fig 4B). These changes indicate that PROG-SD is indeed Form II [19] and so FTIR can be used to differentiate between the formulations regardless of excipients present.

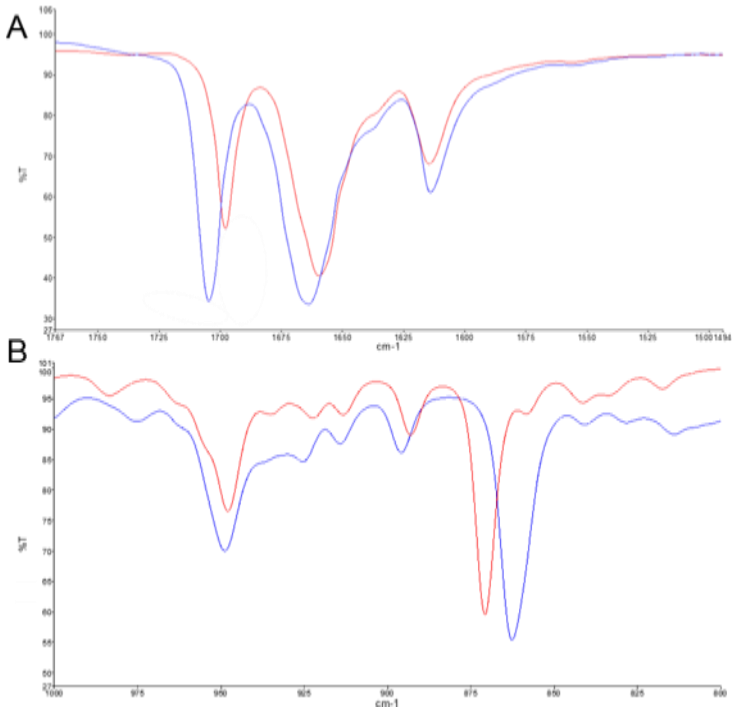


**Figure 4:** FTIR data comparing PROG-SD (Blue) and PROG starting material (Red, Form I). PROG-SD does not match PROG Form I for either of the characteristic regions.

The presence of PROG form II following spray drying fits with the current theory that PROG Form II is encouraged through fast evaporation of solvent, as proposed by Sarkar et al [20] and by Tripathi et al. [21] in their studies of polymorphism of PROG.

### 3.2.2. Progesterone – Excipient Interactions

PXRD confirms that PROG-LEU and PROG-LEU-HPMCAS formulations are physical mixtures of PROG Form II and excipients rather than having formed solid dispersions or polymeric solid dispersions. Physical mixtures can be identified through comparison with PROG and LEU reference patterns which confirm the presence of two crystalline phases in the final product (Fig S1). Crystalline material is produced through the spray drying process regardless of feedstock composition and there is no significant difference between the full width at half maximum values for equivalent PROG Form II peaks in PROG-LEU and PROG-LEU-HPMCAS. The presence of LEU as a separate phase is most clearly identified by peaks at ~ 6 °2θ and ~ 19 °2θ. For the PROG-LEU-HPMCAS formulation, no additional diffraction peaks are seen, confirming that HPMCAS remains in an amorphous state, as per the starting material reference (Fig S2, S3).

Figure 5 shows FTIR data for PROG-SD, PROG-LEU and PROG-LEU-HPMCAS compared LEU reference and all are clear composites of PROG Form II and LEU. There is no difference in the carbonyl region where peaks are present for PROG Form II at ~1705 $cm^{-1}$ and ~1670 $cm^{-1}$ and for LEU at ~1575 $cm^{-1}$. There would likely be shifting in these peaks if there was hydrogen bonding between PROG and LEU through the carbonyl regions. This composite spectrum is true for all the other PROG-LEU formulations, showing their uniformity in intermolecular interactions despite the use of different solvent systems (Fig S4). An additional peak at ~1740 $cm^{-1}$ is attributable to the amorphous HPMCAS in the PROG-LEU-HPMCAS formulation.

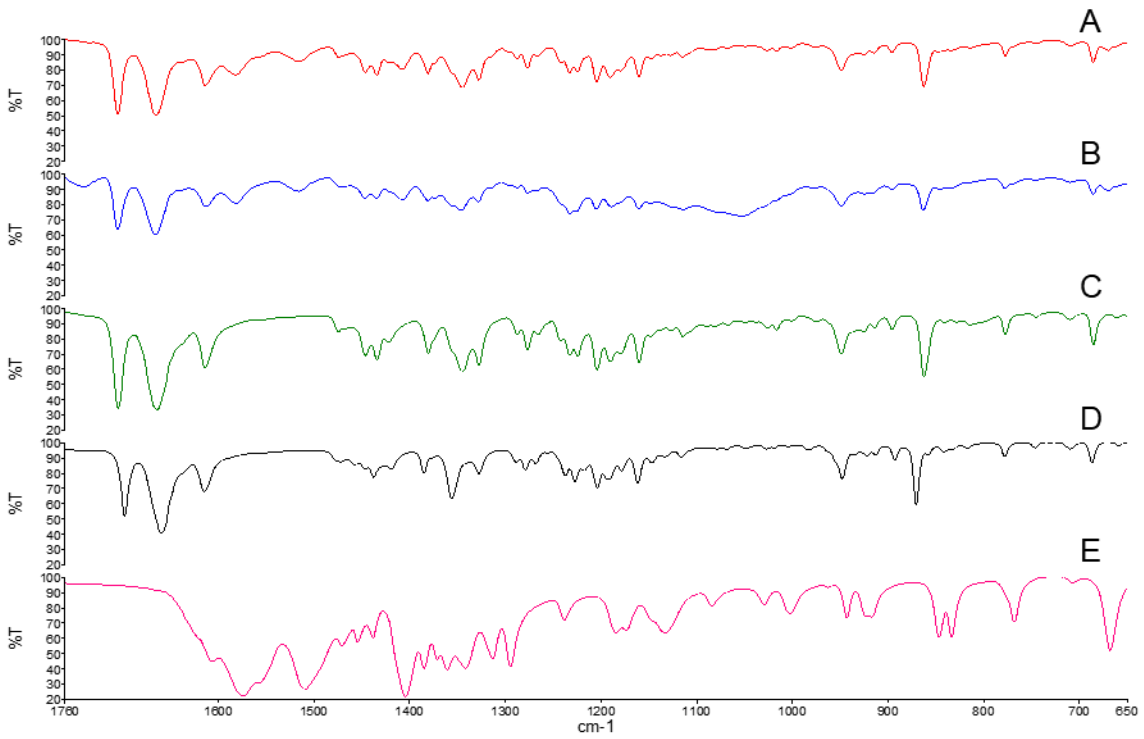


**Figure 5:** FTIR spectra for A) PROG-LEU, B) PROG-LEU-HPMCAS, C) PROG-SD, D) PROG Form I reference and E) L-leucine reference.

### 3.3. Effect of Spray Drying Process on Physical Properties

#### 3.3.1. In Vitro Solubility Study

The effect of spray drying on solution properties was investigated. Figure 6A shows the mean solubility values for the PROG-LEU formulations, compared to the solubility data for PROG-LEU-HPMCAS in water. There was no significant difference between the solubilities of PROG-LEU formulations produced from different solvent systems, so a mean value of all nine samples was used as the PROG-LEU solubility value.

When comparing PROG-LEU and PROG-LEU-HPMCAS formulations there is a significant difference in solubility at the 3-hour time point (ANOVA, $p < 0.05$). PROG-LEU-HPMCAS shows an ~ 7 $\mu gmL^{-1}$ increase in solubility which then reverts to the starting solubility by the 24-hour time point. This result indicates that the addition of polymer to the system was able to facilitate a temporary increase in PROG solubility during the experiment.

A further 24-hour solubility experiment was conducted using simulated lung fluid (SLF) to compare PROG-LEU and PROG-LEU-HPMCAS to the PROG Form I reference (Fig 6B). For the spray dried formulations, there is a significant increase in PROG solubility compared to the reference but no difference with the addition of HPMCAS. Therefore, differences in saturated

solubility can be attributed to the different PROG polymorphs. This finding is in line with literature which reports PROG Form I to have a lower aqueous solubility than Form II (Table S1).

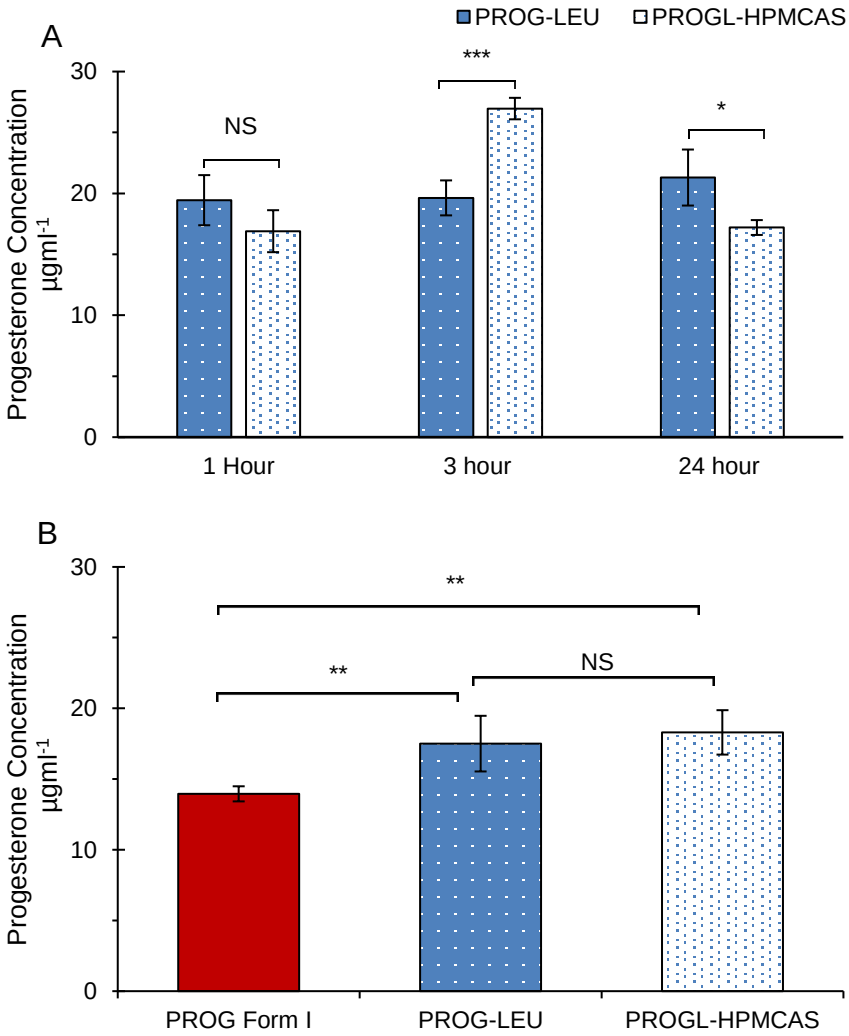


**Figure 6:** Solubility data comparing the solubility of PROG-LEU formulation with PROG-LEU-HPMCAS over the course of 24-hours at 20 °C. **A)** Solubility data in $H_2O$, **B)** Solubility data at 24 hours in SLF. Significance levels: *** = $p < 0.001$, ** $p < 0.01$, * = $p < 0.05$, NS = $p > 0.05$.

A variety of solubility values for PROG Form I and II have been reported in literature depending on temperature and media composition (Table S1). In general, the results presented here are comparable with previous literature values which show Form II to have a higher solubility that Form I.

### 3.3.2. Cascade Impaction – in vitro lung deposition study

The effect of spray drying on particle aerodynamic properties was investigated and results of cascade impaction data summarised in Table 2. All PROG-LEU formulations showed a Mass median aerodynamic diameter (MMAD) of close to 5 µm which is an indicator for good aerosol

performance and lung deposition in vivo. Ideally, an MMAD of < 5 µm is most advantageous, which is the case for IPA 60:40 and 70:30 formulations. The influence of changing the solvent ratio is only significant for the IPA formulations where the 50:50 ratio has a significantly higher MMAD than the 60:40 and 70:30 ratios (5.83 µm compared to 4.5 µm and 4.58 µm). These 60:40 and 70:30 formulations from IPA showed the smallest MMAD of all the solvent systems which suggests that their deposition will occur deepest in the lung.

When considering geometric standard deviation (GSD) values there are significant difference for all solvents formulations. Each formulation showed a GSD value greater than 1.2 µm and so was classed as being aerodynamically heterodisperse. A monodisperse aerosol is advantageous for clinical administration of API since it leads to much more precise dosing. Fine tuning of spray drying parameters and the addition of excipients would be required to produce a more monodisperse aerosol. Although still greater than 1.2 µm, EtOH 70:30 and IPA 50:50 show the smallest GSDs for all the formulations.

Viewing the scanning electron microscopy (SEM) images for PROG-LEU formulations confirms the MMAD and GSD findings (Fig S5) although aerodynamic diameter and physical diameter are different. SEM shows particles with a diameter of less than 10 µm and a range of particle sizes can be seen. The IPA formulation also appears to have a different particle morphology than EtOH and ACE. Many of the particles appear to have “winkled surfaces” which is often seen with the addition of LEU to formulations, especially when LEU has dried on the surface of the particles [16]. Presence of LEU on the surface is believed to improve inhalation properties [16].

Fine particle fraction (FPF) values range from 42% to 57% across the formulations and the formulations from IPA show the highest values. In general, a higher FPF corresponds to deposition deeper in the lung. In the case of the IPA formulations the 50:50 ratio shows a significantly lower FPF than the 60:40 and 70:30 ratios (42% compared to 57% and 56%). This trend in FPF mirrors the trends seen in the MMAD data confirming that a lower MMAD usually corresponds to a higher FPF.
Significant differences exist when considering the emitted dose (ED; % Dose delivered to the impactor) and fine particle dose (FPD; mg PROG < 5 µm) between the ratios for all solvents. Since ED and FPD describe the amount of drug delivered to the lungs, these values were used to compare the inhalation performance between the solvent ratios.

For EtOH, the 60:40 ratio shows the highest FPD values at 4.1 mg and 45% which is an increase of ~20% from the 50:50 ratio and an ~30% increase from the 70:30 ratio. These increases are mirrored in the ED fractions. For EtOH, the 60:40 ratio shows the best aerodynamic performance was selected for further analysis.

For IPA, the 70:30 ratio shows the highest values at 6.27 mg and 56% which for the FPD correspond to an ~45% increase from 50:50 ratio and ~20% increase from the 60:40 ratio. This increase is also mirrored in the ED fraction. Therefore, the IPA 70:30 ratio shows the best aerodynamic performance and was selected for further analysis.

For ACE, the 50:50 ratio shows the highest values at 7.28 mg and 81.73% which corresponds to an ~35% increase from the 70:30 ratio and ~40% increase from the 60:40 ratio with respect to FPD. For ED, the increase from 60:40 and 70:30 to 50:50 is similar at ~35%. This could indicate that for the 60:40 formulation a much larger proportion of the ED is deposited in the upper airways compared to the 50:50 and 70:30 formulations. Therefore, the ACE 50:50 formulation shows the best aerodynamic performance and was selected for further analysis.

From these data there is not an obvious trend between solvent ratio and inhalation characteristics for each solvent. For IPA, it seems that increasing the proportion of organic solvent in the feedstock consistently improves the inhalation properties. However, this is not the case for ACE and EtOH where no relationships between solvent ratio and inhalation properties exist.

**Table 2:** Inhalation statistics for PROG-LEU formulations

| Solvent | Ratio | MMAD (µm) | GSD (µm) | FPF (%) | FPD (mg) | ED (%) |
|---|---|---|---|---|---|---|
| Ethanol | 50:50 | 5.81 ± 0.21 (NS) | 2.01 ± 0.21 (***) | 42.47 ± 1.57 (NS) | 3.16 ± 0.25 (*) | 37.10 ±1.79 (**) |
| | 60:40 | 5.41 ± 0.31 (NS) | 1.90 ± 0.02 (***) | 45.62 ± 3.06 (NS) | 4.10 ± 0.45 (*) | 44.75 ±2.06 (*) |
| | 70:30 | 5.52 ± 0.22 (NS) | 1.40 ± 0.02 (***) | 44.14 ± 2.00 (NS) | 2.78 ± 0.30 (*) | 31.43 ± 2.09 (*) |
| Propan-2-ol | 50:50 | 5.83 ± 0.18 (**) | 1.40 ± 0.02 (***) | 41.77 ± 0.95 (**) | 3.44 ± 0.31 (*) | 41.16 ± 2.73 (*) |
| | 60:40 | 4.50 ± 0.08 (**) | 1.76 ± 0.01 (***) | 56.83 ± 0.73 (**) | 4.99 ± 0.53 (*) | 44.01 ± 5.19 (*) |
| | 70:30 | 4.58 ± 0.27 (**) | 1.78 ± 0.02 (***) | 55.69 ± 3.68 (**) | 6.27 ± 0.62 (*) | 56.16 ± 2.20 (*) |
| Acetone | 50:50 | 5.49 ± 0.12 (NS) | 1.85 ± 0.01 (***) | 44.53 ± 1.15 (NS) | 7.28 ± 0.20 (***) | 81.73 ± 1.32 (***) |
| | 60:40 | 5.72 ± 0.25 (NS) | 1.99 ± 0.02 (***) | 43.53 ± 2.21 (NS) | 4.45 ± 0.53 (***) | 50.95 ± 3.53 (***) |
| | 70:30 | 5.59 ± 0.23 (NS) | 1.89 ± 0.01 (***) | 43.74 ± 2.58 (NS) | 4.64 ± 0.47 (***) | 52.91 ± 2.33 (***) |

ANOVA: NS $p > 0.05$, * $p < 0.05$, ** $p < 0.01$, *** $p < 0.001$

MMAD = Mass Median Aerodynamic Diameter, GSD = Geometric Standard Deviation,

FPF = Fine Particle Fraction (% < 5µm of ED), FPD = Fine Particle Dose (mg < 5µm),

ED = Emitted Dose (%)

### 3.3.3. Cascade Impaction – Comparison of Best Organic Solvent Ratios

The deposition profile for the solvent ratio which showed the best aerodynamic properties for each solvent was compared. Fig 7 shows there to be clear differences between the deposition of these three formulations. IPA and ACE formulations appear to show a normal distribution like curve with maximum deposition in stages 1 - 2 and stages 2 - 3 respectively. By contrast the ethanol formulation gives steady deposition in stages 0 – 2 then shows a gradual decline throughout the impactor.

The ACE formulation delivers a higher proportion of PROG to the lung than IPA and EtOH (82% compared to 56% and 45% respectively). However, much of this is delivered into the upper airways (stage 0 – 2) meaning that the IPA formulation delivers a higher percentage of PROG into the lower lung (24% compared to 20%). This is mirrored in the MMAD values where IPA (2.80 µm) shows a significantly lower value than ACE (3.47 µm) (ANOVA, $p<0.001$).

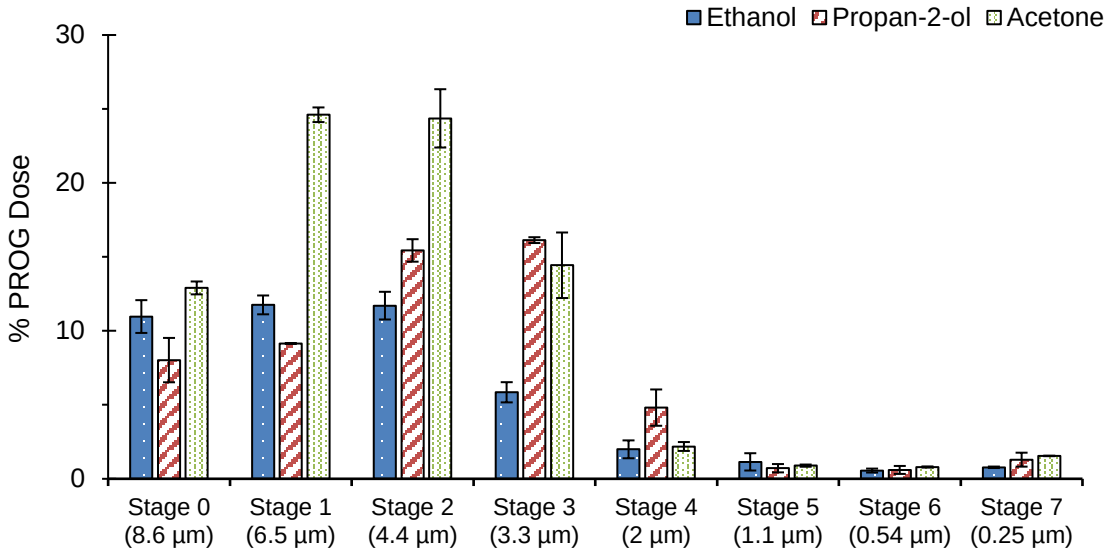


**Figure 7:** Andersen Cascade Impactor data comparing the best ratio of each solvent based on FPD (mg) and ED (%).

The ACE 60:40 system was reformulated with additional HPMCAS to increase the deep lung deposition of PROG. ACE 60:40 was chosen on a balance of spray drying yield and low FPF. The inhalation performance of the PROG-LEU-HPMCAS powder was then assessed through ACI (FIG 8, Table 3). There is no significant difference between the GSD, FPD or ED values for these two formulations. However, there is a significant difference between the MMAD and FPF values. The addition of HPMCAS has increased the FPF from 44% to 52% ($p = < 0.05$, ANOVA) and reduced the MMAD by 15 % to less than 5 µm. These changes can be seen when comparing the deposition profiles (Fig 8). While the formulations have a similar looking

deposition profile, the PROG-LEU-HPMCAS formulation appears to show much higher deposition in from stages 4 onwards (corresponding to < 2µm aerodynamic diameter). This equals 10% PROG deposition in the lower airways compared to 5% for the PROG-LEU formulation. Therefore, with correct optimisation, the addition of HPMCAS may generate a formulation with much better deep lung deposition.

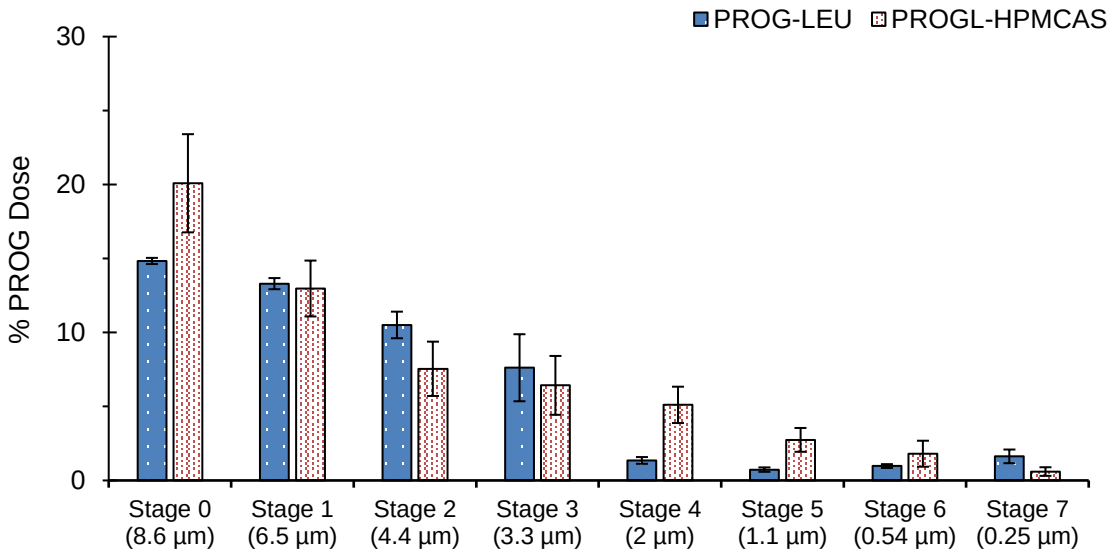


**Figure 8:** ACI data comparing PROG-LEU formulation with PROG-LEU-HPMCAS

**Table 3:** Inhalation statistics comparing PROG-LEU with PROG-LEU-HPMCAS

| Solvent | Ratio | MMAD (µm) | GSD (µm) | FPF (%) | FPD (mg) | ED (%) |
|---|---|---|---|---|---|---|
| Acetone 60:40 | PROG-LEU | 5.72 ± 0.25 (**) | 1.99 ± 0.03 (NS) | 43.53 ± 2.70 (**) | 4.45 ± 0.65 (NS) | 50.95 ± 4.32 (NS) |
| | PROG-LEU-HPMCAS | 4.87 ± 0.22 (**) | 1.96 ± 0.16 (NS) | 51.57 ± 3.32 (**) | 5.90 ± 1.08 (NS) | 57.29 ± 10.73 (NS) |

ANOVA: NS $p > 0.05$, * $p < 0.05$, ** $p < 0.01$, *** $p < 0.001$

MMAD = Mass Median Aerodynamic Diameter, GSD = Geometric Standard Deviation,

FPF = Fine Particle Fraction (% < 5µm of ED), FPD = Fine Particle Dose (mg < 5µm),

ED = Emitted Dose (%)

### 3.4. Polymorphic Transformation Studies

To further understand the stability of PROG Form II within these formulations, DSC was carried out. Firstly, the DSC data for all PROG-LEU formulations show two endothermic peaks present at ~121 °C and ~ 129 °C (Table 4, Fig S6). These temperatures correspond to the reported melting points for PROG Form II and I respectively. A temperature-induced polymorphic transition has occurred during the DSC experiment, since PXRD data showed the spray dried formulations to be exclusively Form II rather than a physical mixture of the two (section 3.2.1)

In comparison, there is only one thermal event seen for PROG-LEU-HPMCAS over the range 100 – 150 °C. This event has a slightly lower onset temperature than the other formulations but results in the same peak temperature as shown in Fig 9. This event is most likely attributed to Form II melting and in the absence of any thermal event at ~ 129 °C indicates that no polymorphic transition has taken place. It is most likely that following melting of Form II, HPMCAS has prevented the recrystallisation of PROG to Form I.

**Table 4:** DSC results for all experiments showing melting endotherm onset and heat of fusion values.

| **Solvent** | **Ratio** | **Peak Onset (°C)** | **$\Delta H_{fus}$ ($Jg^{-1}$)** | **Peak Onset (°C)** | **$\Delta H_{fus}$ ($Jg^{-1}$)** |
|---|---|---|---|---|---|
| Acetone | 50:50 | 121.41 | 40.74 | 128.82 | 23.68 |
| | 60:40 | 121.66 | 46.49 | 129.07 | 9.985 |
| | 70:30 | 121.7 | 46.58 | 129.17 | 15.74 |
| Ethanol | 50:50 | 121.35 | 62.49 | 129.02 | 4.512 |
| | 60:40 | 121.23 | 57.79 | 128.9 | 12.81 |
| | 70:30 | 121.83 | 53.78 | 129.45 | 2.212 |
| Propan-2-ol | 50:50 | 121.53 | 49.71 | 129.1 | 15.71 |
| | 60:40 | 120.53 | 48.59 | 128.9 | 8.457 |
| | 70:30 | 121.14 | 50.53 | 128.89 | 12.66 |
| Acetone (+ HPMCAS) | 60:40 | 120.27 | 41.53 | n/a | n/a |

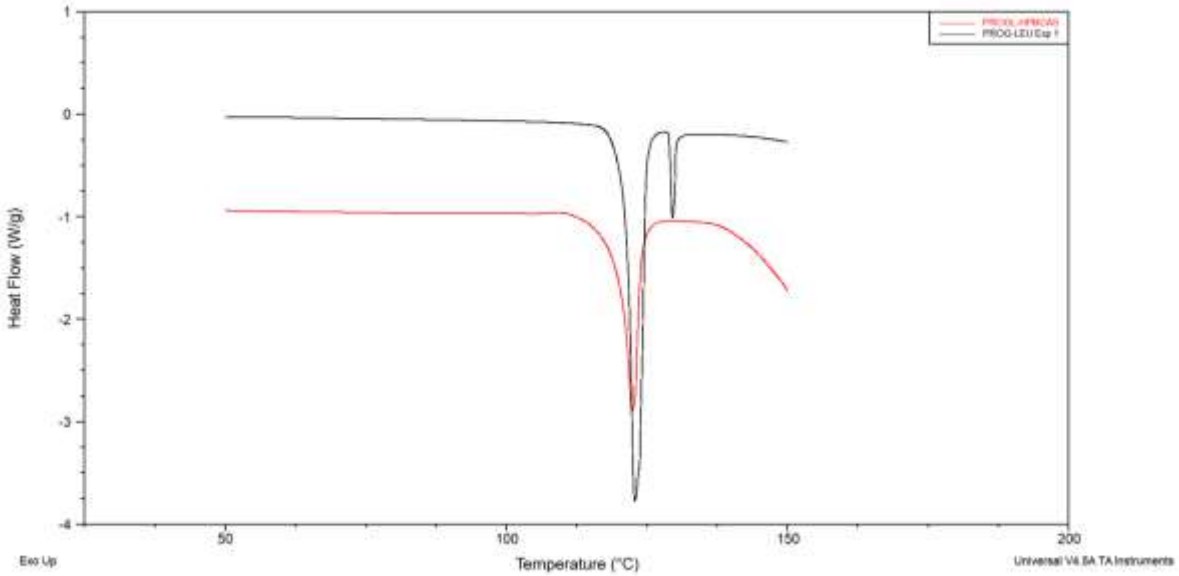


**Figure 9:** DSC data comparing a typical PROG-LEU thermogram (Black, Experiment 1) against PROG-LEU-HPMCAS (Red). Note the two melting points in PROG-LEU corresponding to Form II (~121 °C) and Form I (~129 °C) respectively.

To further test hypotheses with respect to polymorphic transformation, PROG-SD, PROG-LEU and PROG-LEU-HPMCAS formulations were investigated using a VT-PXRD method. A series of PXRD measurements were made over the temperature range identified in DSC experiments i.e. 100 – 130 °C. Through this experiment, PROG-SD clearly showed a transition from Form II to Form I over the temperature range, proceeding via a physical mixture of the two solid forms (Fig S7). When the temperature reached 130 °C, all Form II peaks disappeared from the diffraction pattern, an observation which agrees with the DSC data.

Repeating the same experiment with the PROG-LEU formulations showed the thermal transformation to take place at a lower temperature than for PROG-SD (~110°C vs ~120°C) with full transformation to Form I before the melting point (Fig S8). However, when heating the PROG-LEU-HPMCAS formulation there is no evidence of any change to Form I before the formulation melts (Fig S9). This confirms that the presence of polymer is preventing recrystallisation of Form I on heating and a solid dispersion with PROG and HPMCAS is formed on melting. Fig 10 compares PROG-LEU and PROG-LEU-HPMCAS at 120°C where the difference in polymorph can be clearly seen.

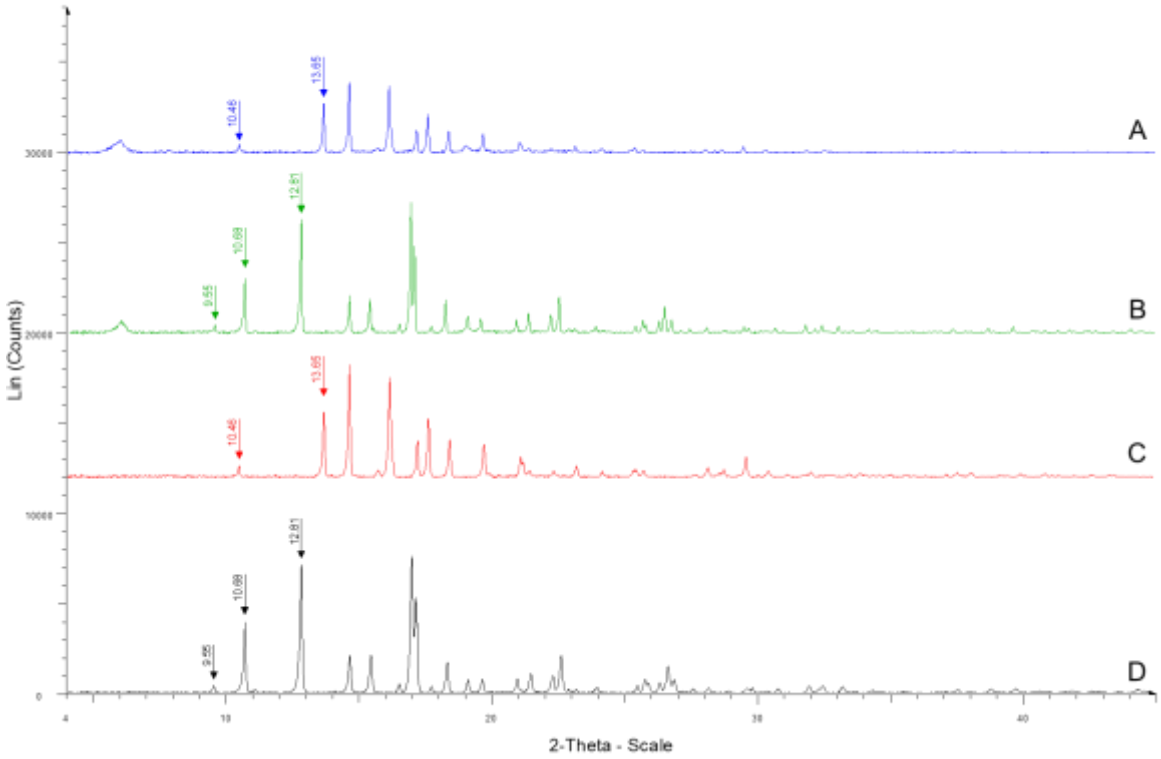


**Figure 10:** VT-PXRD data at 120 °C for A) PROG-LEU-HPMCAS (Blue) and B) PROG-LEU (Green). Compared to C) PROG Form II reference (Red) and D) PROG Form I Reference (Black).

## 4. Conclusion

Inhalable formulations of PROG have been generated through a spray drying method which caused the complete transformation of PROG to the Form II polymorph regardless of the solvent system used. The effect of solvent and organic:aqueous solvent ratio in the spray drying feedstock was investigated showing these to influence the aerodynamic properties of the formulations. Spray drying with the addition of HPMCAS and LEU showed a beneficial effect on the solubility of the PROG and changed the lung deposition profile of PROG with a higher proportion depositing in the lower airways. The addition of HPMCAS to the formulation was also shown to prevent PROG Form II polymorph from recrystallisation to Form I polymorph on heating. The generation of these formulations may assist in the generation of a PROG DPI as an alternative to traditional oral formulations. Further studies are required to focus on generating a more uniform formulation with respect to GSD through adjusting spray drying parameters or the addition of excipients. Furthermore, understanding the mechanism for preventing Form II to Form I transformation and the temporary increase in solubility with the addition of HPMCAS will need future study.

**References**


1. N. Asi, K. Mohammed, Q. Haydour, M. R. Gionfriddo, O. L. Vargas, L. J. Prokop, S. S. Faubion and M. H. Murad, *Syst Rev*, 2016, **5**, 121.
2. S. Furness, H. Roberts, J. Marjoribanks and A. Lethaby, *Cochrane Database Syst Rev*, 2012, **2012**, CD000402.
3. G. N. Wagh, K. M. Kundavi Shankar and S. Bachani, *Drugs Context*, 2021, **10**.
4. L. A. Fitzpatrick and A. Good, *Fertility and Sterility*, 1999, **72**, 389-397.
5. F. Z. Stanczyk, J. P. Hapgood, S. Winer and D. R. Mishell, Jr., *Endocrine Reviews*, 2013, **34**, 171-208.
6. D. Ragab, S. Rohani, M. W. Samaha, F. M. El-Khawas and H. A. El-Maradny, *Journal of Pharmaceutical Sciences*, 2010, **99**, 1123-1137.
7. H. Zhang, X. Huang, Y. Sun, G. Lu, K. Wang, Z. Wang, J. Xing and Y. Gao, *International Journal of Pharmaceutics*, 2015, **489**, 294-303.
8. S. P. Newman, *Therapeutic Delivery*, 2017, **8**, 647-661.
9. R. Scherließ and C. Etschmann, *International Journal of Pharmaceutics*, 2018, **548**, 49-53.
10. J. H. Bell, P. S. Hartley and J. S. G. Cox, *Journal of Pharmaceutical Sciences*, 1971, **60**, 1559-1564.
11. H. Al-Obaidi, A. Granger, T. Hibbard and S. Opesanwo, *Pharmaceutics*, 2021, **13**.
12. B. Chaurasiya and Y.-Y. Zhao, *Journal*, 2021, **13**.
13. K. AboulFotouh, Y. Zhang, M. Maniruzzaman, R. O. Williams and Z. Cui, *International Journal of Pharmaceutics*, 2020, **587**, 119711.
14. A. D. Brunaugh, L. Ding, T. Wu, M. Schneider, R. Khalaf and H. D. C. Smyth, *Journal of Pharmaceutical Sciences*, 2022, **111**, 403-416.
15. M. I. Amaro, F. Tewes, O. Gobbo, L. Tajber, O. I. Corrigan, C. Ehrhardt and A. M. Healy, *International Journal of Pharmaceutics*, 2015, **483**, 6-18.
16. N. Alhajj, N. J. O'Reilly and H. Cathcart, *Drug Discovery Today*, 2021, **26**, 2384-2396.
17. J. E. Hastedt, P. Bäckman, A. Cabal, A. Clark, C. Ehrhardt, B. Forbes, A. J. Hickey, G. Hochhaus, W. Jiang, S. Kassinos, P. J. Kuehl, D. Prime, Y.-J. Son, S. Teague, U. Tehler and J. Wylie, *Molecular Pharmaceutics*, 2022, **19**, 2032-2039.
18. W. Shen, W. Sun, W. Yang, H. Xu, G. Hu, G. Zhao, Z. Deng, J. Feng, F. Li and Y. Hu, *Journal of Molecular Liquids*, 2021, **324**, 114715.
19. X. Chen, I. Partheniadis, I. Nikolakakis and H. Al-Obaidi, *Polymersl*, 2020, **12**.
20. A. Sarkar, D. Ragab and S. Rohani, *Crystal Growth & Design*, 2014, **14**, 4574-4582.
21. R. Tripathi, S. V. Biradar, B. Mishra and A. R. Paradkar, *AAPS PharmSciTech*, 2010, **11**, 1493-1498.

Chapter 6

# Preparation and Formulation of Progesterone para-Aminobenzoic Acid Co-crystal

**Thomas Hibbard**[1], Kenneth Shankland[1], Hisham Al-Obaidi[1]

[1]School of Pharmacy, University of Reading, Reading, RG6 6AD, UK

Chapter Summary:

In this chapter, a new co-crystal of progesterone is detailed following *in silico* and experimental screening against a series of co-formers. Full characterisation using X-ray diffraction, thermal and spectroscopic analysis is detailed. Three scale up methods were trialled with milling selected as the most suitable. The co-crystal showed enhanced dissolution compared to progesterone starting material and when formulated into a tablet, showed enhanced dissolution compared to Utrogestan® soft capsule formulation.

Author Contributions:

TH: conceptualisation, investigation, methodology, writing – original draft, review & editing.

KS: crystallographic investigation, writing – original draft, review & editing; HAO: conceptualisation, investigation, methodology, project administration, writing – original draft, review & editing.

**Abstract**

The crystal structure of a new Progesterone (PROG) co-crystal with para-aminobenzoic acid (PABA) showing enhanced solution properties is reported. PROG-PABA co-crystal was first identified though an in silico coformer screening process using the CSD Co-crystal deign function, then confirmed through a solution evaporation crystallisation experiment. The resulting co-crystal was characterized using single crystal X-ray diffraction, differential scanning calorimetry and Fourier-transform infrared spectroscopy.

Milling was shown to be a successful scale up method compared to spray drying and antisolvent methods. Following scale up, aqueous solubility, stability and dissolution measurements were carried out. PROG-PABA showed increased distinct aqueous solubility and dissolution compared to PROG starting material and was shown to be stable at 75% relative humidity for 3 months.

Tablets containing co-crystal were produced then compared to the Utrogestan® soft gel capsule formulation through a dissolution experiment. PROG-PABA tablets showed a substantial increase in dissolution over the course of the experiment with over 30x the amount of PROG dissolved at the 3-hour time point.

This co-crystal shows positive implications for developing an improved oral PROG formulation.

## 1. Introduction

Progesterone (PROG) is a commonly used drug for the treatment of obstetric and gynaecological conditions available in oral, vaginal and transdermal formulations [1, 2]. To ensure adequate bioavailability, oral formulations must increase PROG aqueous solubility and this is currently attempted by using micronised PROG formulated into a soft gel capsule (e.g. Utrogestan®) [3]. However, solubility remains low for PROG through formulating in this way and as such bioavailability is poor. Moreover, soft gelatine capsules are costly to develop and are often associated with sensitivity to heat, moisture and microbial contamination [4]. Therefore, other options such as tabletting, and the co-crystal crystal engineering approach have been trialled for increasing aqueous solubility.

Co-crystallisation is favoured for PROG as opposed to salt formation since PROG is a relatively neutral molecule without any readily ionisable functional groups. Co-crystals of PROG prepared through evaporation and grinding experiments have been reported previously and these co-crystals show a variety of physical properties compared to PROG [5-8]. To further develop PROG co-crystals for pharmaceutical applications, it is necessary to discover new co-crystals of PROG to ensure the solid form with the most advantageous physical properties can be used.

Detailed in this publication is a screening process which was used to discover a new co-crystal of PROG with para-aminobenzoic acid. The resultant co-crystal was fully characterised through X-ray diffraction, thermal and spectroscopy analysis. Once a new co-crystal is discovered, the development of a reliable scaleup method is also required, so to this end, PROG-PABA preparation was also explored through spray drying, antisolvent and milling techniques. Following scale up, the stability, aqueous solubility and invitro dissolution are assessed including a comparison of dissolution between a co-crystal tablet formulation and Utrogestan® marketed PROG formulation.

To our knowledge this co-crystal has not been reported before or formulated into a tablet for comparison with current oral PROG formulations.

## 2. Material and methods

### 2.1. Materials

Progesterone (PROG), para-aminobenzoic acid (PABA), α-lactose monohydrate, Polyplasdone™ XL (crospovidone), magnesium stearate and sodium lauryl sulphate were obtained from Sigma-Aldrich (Dorset, UK). HPLC water, acetonitrile, ethanol and propan-2-ol were obtained from Fisher-Scientific Limited (Leicestershire, UK). Utrogestan®

capsules (UTRO) were used as a comparison for dissolution studies. All chemicals were used as received.

## 2.2. Preparation of PROG Co-crystal and Formulations

### 2.2.1. Co-crystal Screening

An in silico co-crystal screen was performed using the “co-crystal design” function of Mercury [9]. Following the generation of 32 matches, 6 coformers were chosen for crystallisation experiments to cover a range of coformer molecular characteristics. These were: para-aminobenzoic acid, caffeine, hippuric acid, methylparaben, pimelic acid and tartaric acid (Figure 1).

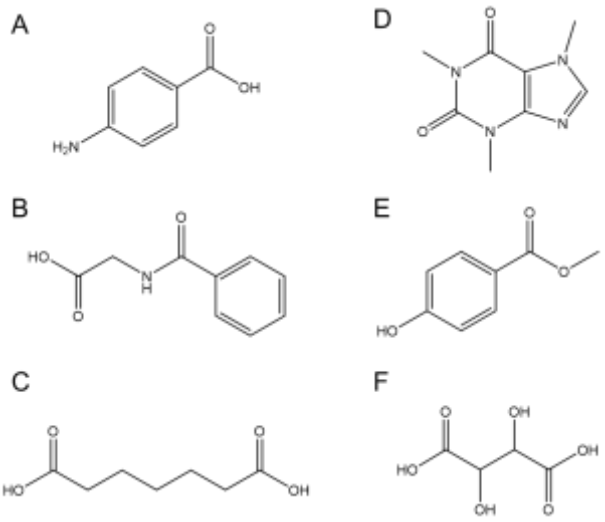


**Figure 1:** Chemical structures of molecules selected for experimental coformer screening. **A)** para-aminobenzoic acid, **B)** hippuric acid, **C)** pimelic acid, **D)** caffeine, **E)** methylparaben, **F)** tartaric acid.

PROG and coformers were dissolved in separate vials to a concentration of 10 mg/ml using propan-2-ol. PROG and a coformer solution containing an equimolar quantity of coformer were then filtered and pipetted into a single well of a 24-well plate. This process was repeated with the each coformer and then the plate was sealed, and the solutions left to crystalise in a temperature-controlled incubator over 3 days. Resulting crystals were isolated and analysed through single crystal X-ray diffraction.

### 2.2.2. Milling Experiments

Equimolar quantities of PROG and PABA were milled using a Retsch MM 500 nano mill with the addition of 20 µL of ethanol [10]. All experiments were performed for 30 mins at

25 Hz with 2.5 mm stainless steel ball bearings in a 1:20 mass ratio to the starting materials. The milled powder was transferred to a vial and stored in a desiccator.

### 2.2.3. Antisolvent Experiments (AS)

Equimolar quantities of PROG and PABA were added to a vial and dissolved in the minimal volume of propan-2-ol to form a saturated solution. This solution was then pumped dropwise into an antisolvent solution of 200 ml ultrapure water at 2 ml/min. Any precipitate formed was isolated using vacuum filtration and dried in an incubator at 25 °C, transferred to a vial then stored in a desiccator.

### 2.2.4. Spray drying Experiments (SD)

Spray drying experiments were performed using a B-290 spray dryer (Büchi, Laboretechnik AG Switzerland) which used a nitrogen atomising gas and nitrogen drying atmosphere operated in a closed loop mode. The aspirator was set to 100%, the inlet temperature at 120 °C and experiments were started when the outlet temperature stabilised at 60 °C. A two-fluid nozzle with nozzle diameter 0.5 mm was used and the feedstock was pumped at 5 ml/min. The feedstock was composed of PROG and PABA dissolved in propan-2-ol at a 1:1 molar ratio to a concentration of 2% w/v. Spray dried powder was transferred to a vial and stored in a desiccator.

### 2.2.5. Tablet Formulation

PROG co-crystal tablets were formulated with the excipients detailed in Table 1 using the PROG-PABA co-crystal produced through milling (method 2.2.2).

**Table 1:** Tablet composition

| **Component** | **Tablet Weight (250 mg)** |
|---|---|
| Progesterone (as co-crystal) | 20 % |
| Disintegrant (PolyPlasdone XL) | 3 % |
| Lubricant (magnesium stearate) | 1 % |
| Filler (α-Lactose monohydrate) | to 100 % |

Milled co-crystal powder was blended with PolyPlasdone XL and α-Lactose monohydrate using a sheer mixer. Then, magnesium stearate was added, and the powder tumble mixed for 2 mins to coat with lubricant.

250 mg tablets were produced using a manual fill, direct compression method using a round 0.9 cm punch and a compression depth of 10 mm.

## 2.3. Physicochemical Analysis

### 2.3.1. Single Crystal X-ray Diffraction (SC-XRD)

Single crystals showing birefringence under polarised light were selected for analysis, isolated in Paratone-N oil and mounted onto a crystal analysis loop. Diffraction data at 100K were collected using a Rigaku Synergy diffractometer equipped with a Cu microsource, a HyPix detector and an Oxford Cryosystems Cryostream device. Crystal structures were solved using ShelXT[11] and refined using ShelXL[12] (using the Olex2[13] program) and crosschecked with the Cambridge Structural Database (CSD) database[14], then rendered using Mercury[15].

### 2.3.2. Powder X-ray Diffraction (PXRD)

Transmission capillary PXRD data were collected using a Brucker D8 Advance diffractometer (Billerica, MA, USA) equipped with a monochromatic CuK$\alpha_1$ source. Samples were packed into a 0.7 mm borosilicate glass capillary then scanned in the range 4° to 45° 2θ using step size 0.0171° with a count time of 1.4 seconds per step. Data for the starting materials were also collected using the same settings to be used as a reference. PXRD data for the tablet surface was collected using a Brucker D8 Advance diffractometer operating in a reflection geometry using the same settings as the transmission data collection.

### 2.3.3. Fourier -Transform Infrared Spectroscopy (FTIR)

FTIR spectra were collected using a Perkin-Elmer 100 FTIR Spectrometer equipped with a diamond attenuated total reflectance (ATR) accessory (Shelton, CT, USA). Transmission was recorded from an average of 16 scans over the range 650 – 4000 $cm^{-1}$ with a resolution of 4 $cm^{-1}$.

### 2.3.4. Differential Scanning Calorimetry (DSC)

Thermal properties of samples were analysed using DSC with samples hermetically sealed into aluminium pans with pierced lids to allow for any pressure release. All samples were heated to 190 °C at 10 °C/min in a $N_2$ atmosphere using a TA Q2000 DSC instrument (New Castle, DE USA). Results were analysed using TA Universal Analysis to identify thermal events.

### 2.3.5. Scanning Electron Microscopy (SEM)

Images of samples were obtained using a Quanta 600F scanning electron microscope (Hillsboro, ORE, USA) under high vacuum. Samples were attached to carbon tabs,

mounted on aluminium pins, then sputter-coated with gold for 3 min at 30 mA (Emitech K550).

## 2.4. Physical property analysis

### 2.4.1. Stability

Milled co-crystal powder was weighed into vials and stored in a sealed container at 37 °C and 75% relative humidity. 75% relative humidity was generated by adding a reservoir containing a saturated NaCl solution to the sealed container separate from the powders. Humidity was verified using a humidity testing meter.

### 2.4.2. UV-HPLC

PROG separation was achieved with ACE 3 C18 column (75 x 4.6mm, 3 µm) and gradient elution with water:acetonitrile mobile phase. The UV detector was set to 245 nm for PROG and 290 nm corresponding to reported lambda max values. A linear calibration curve was generated ($r^2 > 0.99$) from a stock solution of PROG in 50:50 acetonitrile:water over a range of 0.1 $mgml^{-1}$ to 200 $mgml^{-1}$.

### 2.4.3. In-Vitro Solubility Analysis

The solubility of milled co-crystal and PROG were assessed in ultra-pure water over a period of 48 hours at 20 °C (± 1 °C) in triplicate. Excess solid was added to 1 ml of UP-$H_2O$ and mixed on a mechanical mixer with temperature probe to monitor temperature. At 72 hours, samples were centrifuged at 13,000 rpm for 5 mins then the supernatant was collected, diluted, and PROG and PABA concentrations were determined using HPLC.

### 2.4.4. Dissolution Analysis

Dissolution experiments comparing milled co-crystal to PROG starting material and then co-crystal tablet to UTRO formulation were performed using the following method. All experiments were performed using a Copley Scientific DIS 8000 instrument equipped with paddle dissolution apparatus. Experiments were run at 37.5 °C (± 0.5 °C) with stirring at 50 rpm over 2 hours in 900 ml of degassed ultrapure water. Samples were removed at time intervals of 5, 15, 30, 60 and 120 mins, filtered using a 0.22 µm syringe filter (Ministart®) and PROG concentration determined using the HPLC method outlined in section 2.4.2.

For co-crystal and PROG powder dissolution experiment, a size 0 gelatine capsule was filled with powder equivalent to 100 mg PROG placed in a stainless-steel capsule sinker.

For co-crystal tablet and UTRO experiments, tablets equivalent to 100 mg of PROG and a Utrogestan® 100 mg capsule were used. A capsule sinker was used for the UTRO formulation and the experiment was performed in 900 ml of 0.1 % w/v sodium lauryl sulphate (SLS) solution. Residual UTRO capsule and co-crystal tablet were isolated and analysed using FTIR.

### 2.5. Statistical Analysis

Statistical analysis was carried out using SPSS software (IBM SPSS version 27.0, SPSS Inc.). Data were compared with appropriate test following test for normality and variance. In each case, statistical significance was defined as $p < 0.05$ with significance levels: *** = $p < 0.001$, ** $p < 0.01$, * = $p < 0.05$ and NS = $p > 0.05$.

## 3. Results

### 3.1. Co-crystal Screening and Characterisation

#### 3.1.1. Single Crystal X-ray Diffraction

All co-crystal crystallisation screening experiments yielded crystals suitable for SC-XRD analysis. The solid phases were analysed, and their results are detailed in Table 2.

**Table 2:** Results of experimental co-crystal screening

| Coformer | Crystalline Product |
|---|---|
| para-Aminobenzoic Acid | PROG-PABA co-crystal |
| Hippuric Acid | Separate phases |
| Pimelic Acid | Separate phases |
| Caffeine | Separate phases |
| Methylparaben | Separate phases |
| Tartaric Acid | Separate phases |

CSD searching showed that the PROG-PABA co-crystal was a novel crystal structure and was selected for further experimentation. Table 3 summarises the crystal information of the PROG-PABA co-crystal.

PROG-PABA crystallises in space group $P2_12_12_1$ with two PROG and two PABA molecules in the asymmetric unit (Figure 2). The carboxylic acid groups of the PABA molecules pair up in an $R_2^2(8)$ motif. The amino group of one PABA molecule forms a $C_2^1(4)$ motif with two symmetry-related PROG molecules, H1A-N1-H1B···O1···H1A, whilst the amino group of the other PABA molecule links with O2 of the aforementioned PROG

molecule (N2-H2A···O2) and O4 of the other PROG molecule (N2-H2B···O4) which is not H-bonded to any other molecules in the structure.

**Table 3:** SC-XRD data for PROG-PABA co-crystal

| **Summary** | |
|---|---|
| Identification code | PROG-PABA |
| Empirical formula | $C_{28}H_{37}NO_4$ |
| Formula weight | 451.58 |
| Temperature/K | 99.99(10) |
| Crystal system | orthorhombic |
| Space group | $P2_12_12_1$ |
| a/Å | 7.54410(10) |
| b/Å | 12.90940(10) |
| c/Å | 49.8923(5) |
| α/° | 90 |
| β/° | 90 |
| γ/° | 90 |
| Volume/Å3 | 4859.00(9) |
| Z | 8 |
| $\rho_{calc}$g/cm$^3$ | 1.235 |
| μ/mm$^{-1}$ | 0.647 |
| F(000) | 1952.0 |
| Crystal size/mm$^3$ | 0.19 × 0.04 × 0.03 |
| Radiation | Cu Kα (λ = 1.54184) |
| 2Θ range for data collection/° | 7.074 to 153.068 |
| Index ranges | -9 ≤ h ≤ 8, -16 ≤ k ≤ 15, -61 ≤ l ≤ 60 |
| Reflections collected | 45225 |
| Independent reflections | 9768 [$R_{int}$ = 0.0430, $R_{sigma}$ = 0.0312] |
| Data/restraints/parameters | 9768/0/625 |
| Goodness-of-fit on $F^2$ | 1.039 |
| Final R indexes [I>=2σ (I)] | $R_1$ = 0.0331, $wR_2$ = 0.0839 |

| | |
|---|---|
| Final R indexes [all data] | $R_1$ = 0.0377, $wR_2$ = 0.0862 |
| Largest diff. peak/hole / e Å$^{-3}$ | 0.17/-0.18 |
| Flack parameter | -0.04(6) |

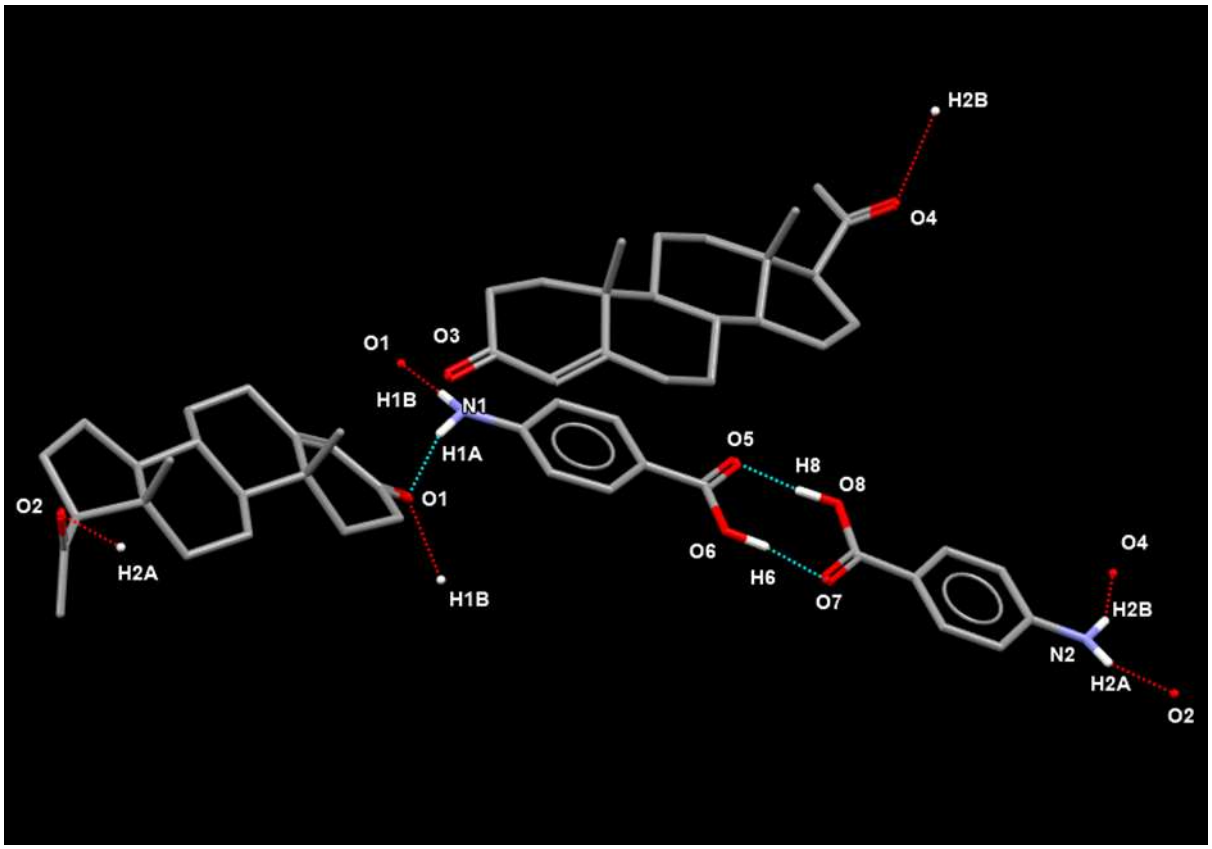


**Figure 2:** A Mercury diagram for the PROG-PABA asymmetric unit, showing hydrogen bonding between key bonding functional groups (dashed lines).

Changes to the nature of intermolecular bonding in the carbonyl and amine regions is also seen when comparing the FTIR data of starting materials and co-crystal (Figure S1 and S2). At the amine region of absorption, corresponding with the N-H stretch (i.e. 3400 – 3250 cm$^{-1}$), there is a "blue-shift" in peak positioning corresponding to a shortening of the hydrogen bond for PABA when bonding with PROG rather than itself.
Similarly, in the carbonyl region of absorption, corresponding to C=O stretching (i.e. 1760 – 1690 cm$^{-1}$), the blue-shift associated with PROG C=O bond from ~1695 cm$^{-1}$ to ~1690 cm$^{-1}$ is observed. This change to a higher energy frequency is expected since this functional group begins to participate in hydrogen bonding, rather than short contact interactions, following formation of a co-crystal, since PROG does not possess any hydrogen bond donor groups.

This blue-shifting in functional groups is in line with previously reported co-crystals of PROG and is indicative of the formation of strong intermolecular hydrogen bonds [5, 7]

DSC was used to analyse the thermal properties of the PROG-PABA co-crystal and showed a single sharp endothermic event with onset temperature of 153.98 °C (Figure 3). This corresponds to the melting point of the co-crystal and is situated between the melting points of PROG and PABA at 129.72 °C and 188.22 °C respectively. The melting point increase compared to the PROG starting material is in line with the formation of intermolecular hydrogen bonds within the co-crystal structure.

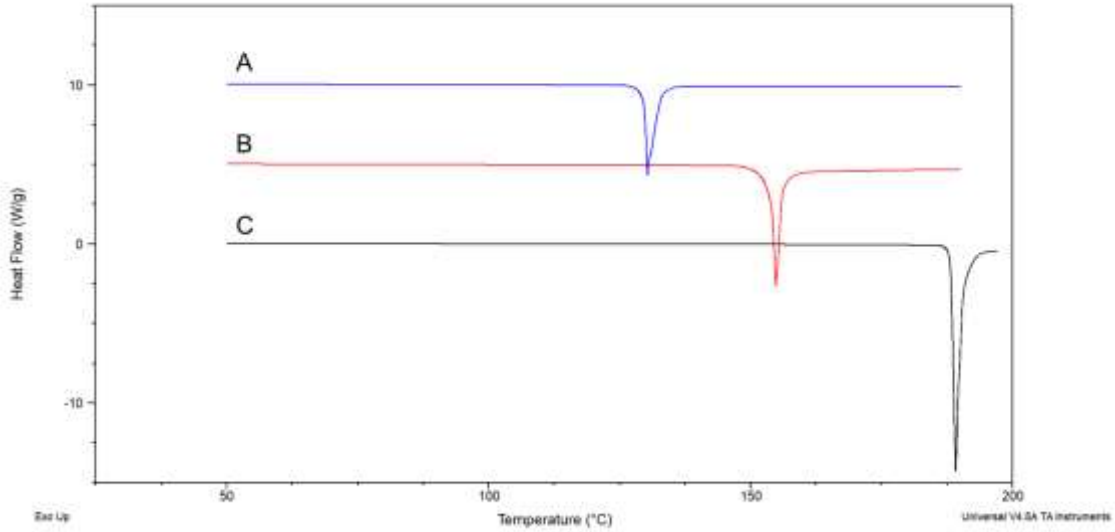


**Figure 3:** DSC Data for A) progesterone reference (blue), B) PROG-PABA co-crystal (red), C) para-aminobenzoic acid reference (black).

### 3.2. Co-crystal Scale Up Characterisation

Spray drying, antisolvent and milling methods were investigated for scale up of the PROG-PABA co-crystal as described in methods 2.2.2, 2.2.3 and 2.2.4. Successful co-crystal preparation was determined through Powder X-ray Diffraction (PXRD) compared to a simulated PXRD pattern from the PROG-PABA crystal structure (Mercury).

PXRD analysis of milled, antisolvent and spray dried product indicated co-crystal formation for all three methods. Comparing the product to starting material references, novel powder patterns are seen which correspond well with the powder pattern generated from the PROG-PABA SC-XRD data (Figure 4, Figure S3). This is most clearly seen with the generation of new diffraction peaks at ~7, ~9.7 and ~12.2 °2θ and the elimination of starting material reference peaks at ~9.5 and 12.8 °2θ for PROG and ~ 9.52 and ~ 14.79 °2θ for PABA. SD and AS methods show larger crystallite size compared to the milled method as seen by larger FWHM values i.e. peak at ~7 °2θ,

milled = 0.067°, AS = 0.084°, SD = 0.117°. There are also additional peaks present in the AS and SD formulations which are not accounted for by the starting materials or co-crystal. These peaks at ~13.7 °2θ and ~14.7 °2θ are likely due to the presence of an additional phase formed alongside the co-crystal. We conclude that this phase can be attributed to the Form II polymorph of PROG which is known to be favoured following rapid precipitation [16].

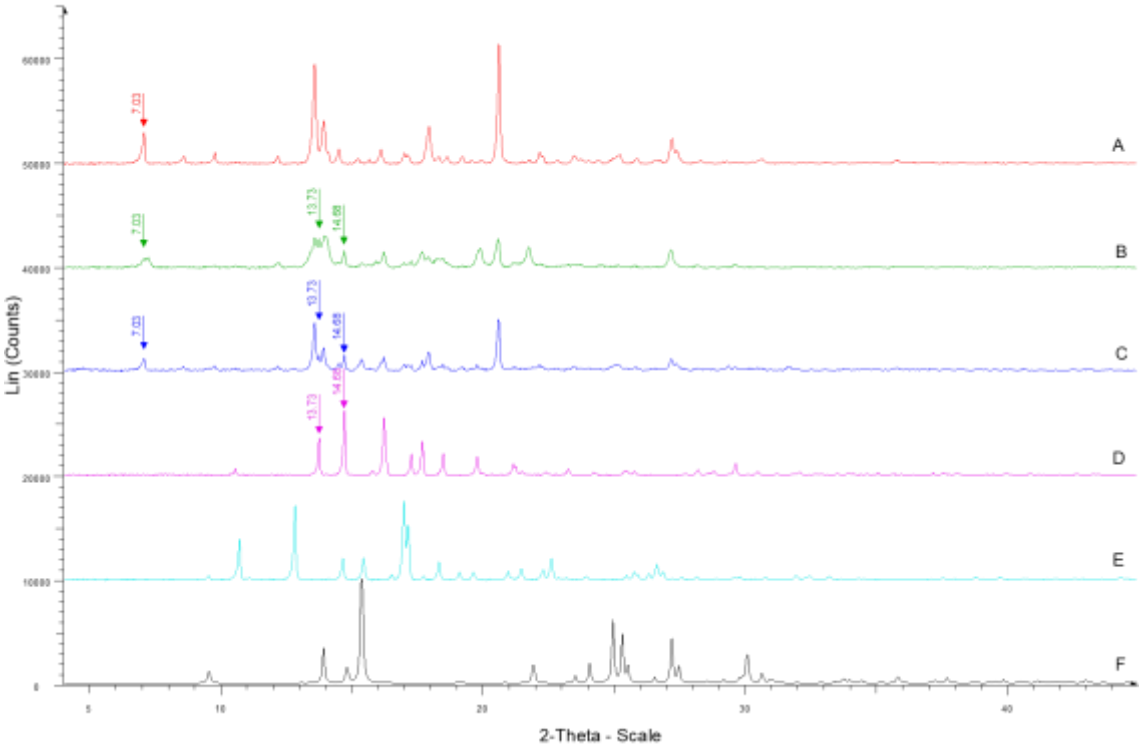


**Figure 4:** PXRD data showing A) PROG-PABA milled (Red), B) PROG-PABA antisolvent (Green), C) PROG-PABA spray dried (Blue), D) PROG Form II polymorph reference (Pink), E) PROG Form I polymorph reference, F) PABA Reference. Note PROG Form II (D) peaks at 13.73 °2θ and 14.66 °2θ in antisolvent product (B) and spray dried (C) products.

Co-crystals prepared through milled, AS and SD methods were also viewed using SEM (Figure 5). All preparation methods show a similar particle size although there are clear differences in the morphology between the milled and solvent based methods. AS and SD methods show clearly defined crystals with needle like morphology as well as agglomerate like particles in the sample. The milled co-crystal appears to be more uniform in morphology with the absence of needle like crystals.

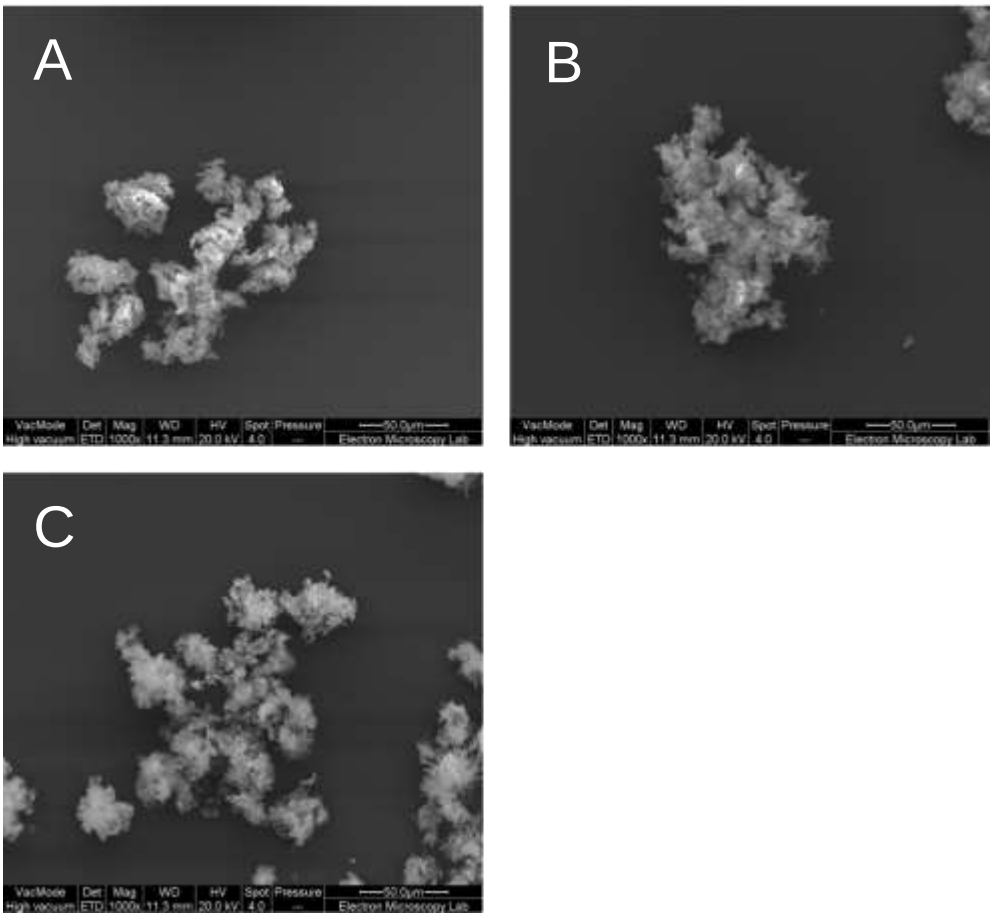


**Figure 5:** SEM images comparing A) PROG-PABA milled, B) PROG-PABA Spray dried, C) PROG-PABA Antisolvent.

In the absence of any starting material phases and relatively uniform particle size and morphology, PROG-PABA formed through milling was selected as a suitable scaleup method for preparing this co-crystal and used for further experiments.

### 3.3. Physical Property Analysis

#### 3.3.1. In Vitro Stability Study

Following preparation through milling, PXRD and FTIR reference spectra for milled PROG-PABA were collected, then the co-crystal was stored in a high relative humidity environment for three months. PXRD data following three months shows no apparent difference in the diffraction pattern for PROG-PABA, seen through identical peak positioning and the absence of any additional diffraction peaks (Figure 6). If the co-crystal form had changed or degraded over the course of the experiment, clear changes to the crystal structure would have been seen by the X-ray diffraction pattern.

FTIR data confirms there was no structural change during the experiment through identical functional group peak positionings which are indicative of the same molecular bonding environment (Figure S4). Also, in the absence of any additional absorption at ~ 3500 $cm^{-1}$, FTIR confirms that there has been no absorption of water into the sample from the high humidity atmosphere. Therefore PROG-PABA was seen as a stable crystalline compound through testing at accelerated storage conditions.

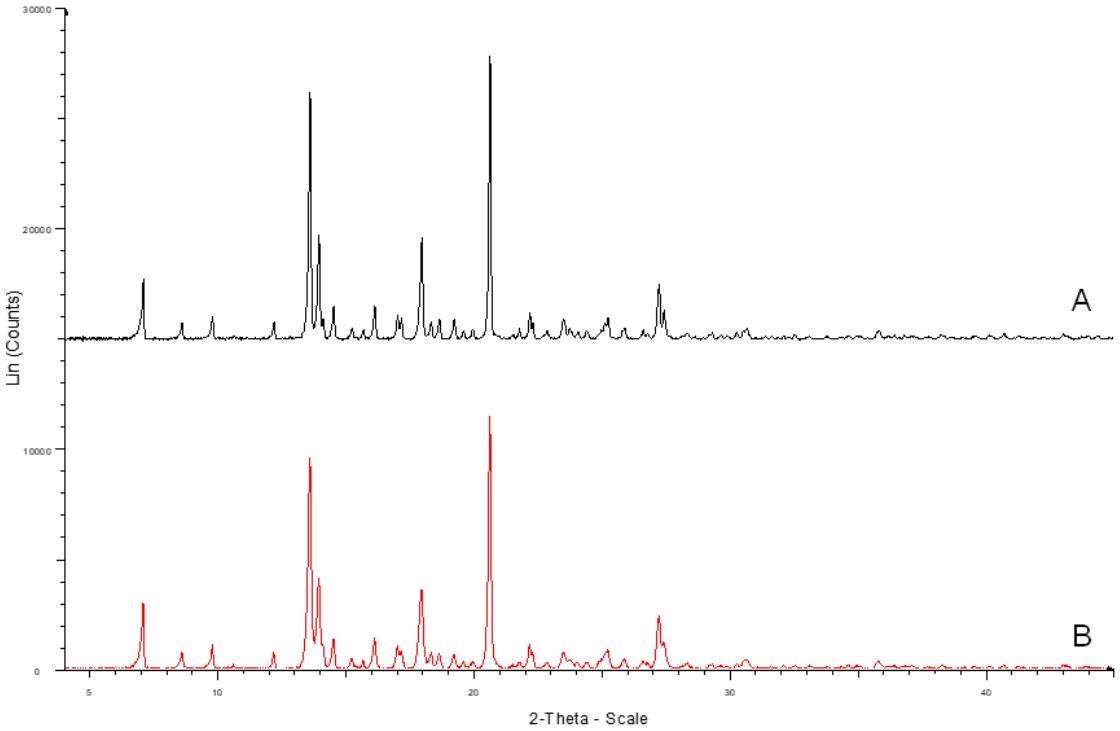


**Figure 6:** PXRD data for milled PROG-PABA **A)** after humidity study for 3 months at 37.5 °C and 75% relative humidity (black), **B)** before humidity study (red).

### 3.3.2. Milled Powder Solubility and Dissolution Studies

There is no significant difference between the concentration of PROG in aqueous solution at 48 hrs when comparing PROG and PROG-PABA co-crystal. PXRD analysis shows the residual solid phases at 48hrs to be PROG Form I and PROG-PABA exclusively (Fig S5). Therefore, these solubility values correspond to PROG Form I and PROG-PABA in equilibrium with water respectively.

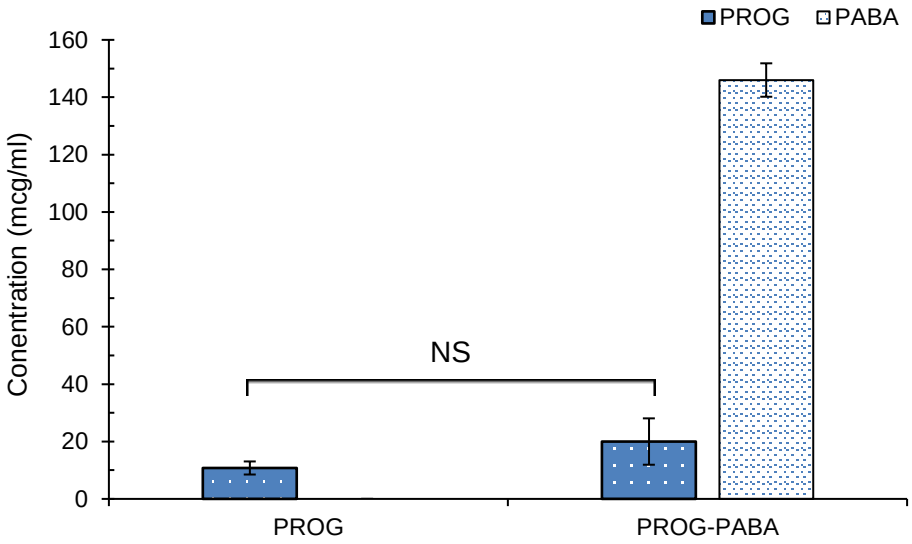


**Figure 7:** Aqueous solubility data for PROG and PROG-PABA co-crystal at 48 hours.

The mean solubility value for PROG-PABA is higher than PROG although there is much more variation around the mean leading to no significant difference. Some co-crystal repeats show double the concentration of PROG in solution which suggests that the co-crystal may be able to initiate a higher solubility which is kinetic in nature and works towards equilibrium at 48 hrs. Further experimentation detailing the extent and duration of a higher kinetic solubility is required through concentration analysis at time points during the experiment.

Comparing dissolution of PROG-PABA powder to PROG Form I starting material shows a clear increase in dissolution for the co-crystal compared to pure PROG, as shown in Fig 8. This is most clearly seen within the first 30 mins of the experiment, where, by the 5 min time point, PROG-PABA shows ~ 10% dissolution compared to ~ 1% dissolution for PROG. This difference increases to 20% by the 15 min time point where PROG-PABA has reached ~ 30% dissolution. However, both experiments appear to have plateaued by the 30 min time point at ~ 15% and ~ 35% dissolution for PROG and PROG-PABA respectively which continues until the end of the experiment.

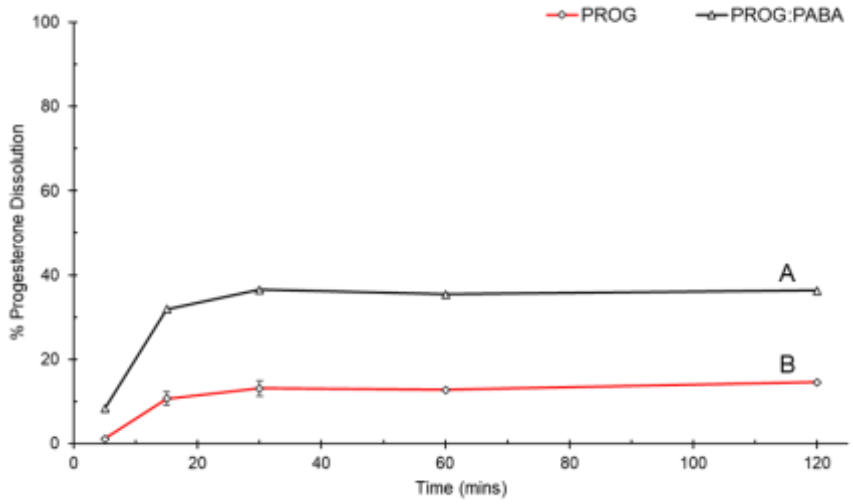


**Figure 8:** Dissolution data for powder dissolution experiment. **A)** PROG-PABA milled powder (black) and PROG starting material (red).

### 3.3.3. PROG-PABA Tablet Formation

Tablets were produced using a direct compression method described in method 2.2.5 which was able to consistently produce tablets of the required mass and of a suitable hardness [17, 18]. Following tablet formation, the tablet surface was analysed via PXRD using a flat plate function in reflectance mode (Figure S6). PROG-PABA can be identified on the surface of the tablet although the peaks are much lower in intensity than those of α-Lactose monohydrate. Identification of co-crystal and excipient peaks on the surface of the tablet highlights the generation of a good physical mix between co-crystal and excipients during the formulation process. Identification of the co-crystal also points to the stability of PROG-PABA through the direct compression tabletting process suggesting that this is a suitable formulation method for oral delivery.

### 3.3.4. PROG-PABA Tablet Dissolution

Dissolution experiments comparing the PROG-PABA tablet with UTRO formulation were performed in 0.1% SLS media as per the precedent for using SLS in literature [19, 20]. There is a clear increase in dissolution of PROG from the tablet formulation compared to the soft capsule formulation as shown in Figure 9. After 5 mins, PROG dissolution of 17.5% was observed from the tablet formulation compared to 0.5% in the soft capsule. This increase in dissolution continues throughout the experiment where at the 3-hour time point, 46% and 1.7% dissolution were observed for the tablet and soft capsule respectively. This is an almost 30x increase in the amount of PROG dissolved compared to a current marketed formulation. To validate these findings, the residual solid phases

from the dissolution experiment were filtered from the dissolution media and their composition analysed. FTIR analysis confirmed the presence of PROG for solid residues from both tablet and soft-gelatine capsule dissolution experiments (Figure S7). This indicates that the low % dissolution seen for UTRO was due to poor solution properties rather than sampling error during the dissolution experiment. With respect to the tablet formulation, presence of PROG rather than PROG-PABA in the dissolution residue suggests that PROG has dissolved then precipitated out of solution during the course of the experiment. This fits with the understood “spring and parachute” model of supersaturation which has been suggested to described co-crystal solution properties [21].

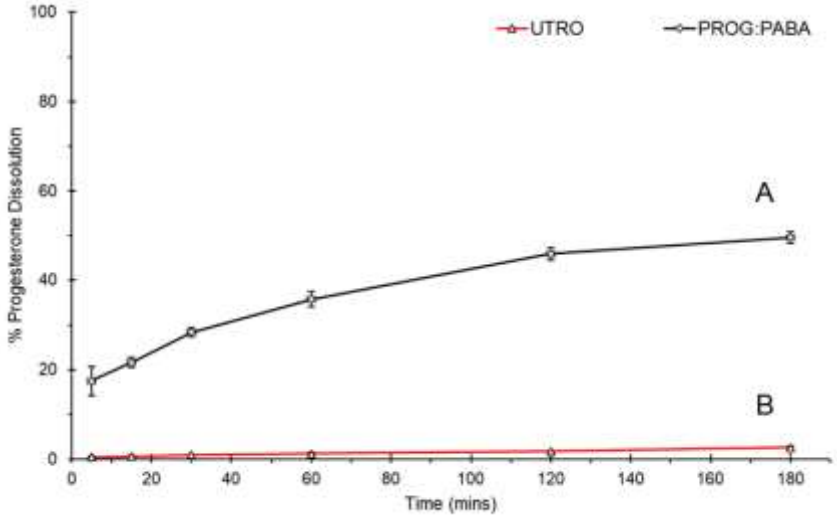


**Figure 9:** PROG-PABA tablet vs Utrogestan® dissolution experiment

The PROG-PABA tablet also shows an increase in dissolution compared to the PROG-PABA powder filled capsule. This is likely to be due to two main factors, firstly, it points to the utility of the tablet formulation for encouraging disintegration and therefore promoting better dissolving at the start of the experiment. This is seen by an increase of ~10% in dissolution between powder and tablet formulations at the 5 min time point. Secondly, the addition of 0.1% surfactant to the dissolution media will facilitate a higher amount of PROG in solution as seen by comparing the % dissolution at the 2-hour mark i.e. ~35% dissolution compared to ~45% dissolution. The tablet formulation also seems to be continuing to trend up wards at the end of the experiment compared to powder dissolution which has plateaued.

In general, these experiments show the benefits of co-crystallisation and tablet formulation on the dissolution of PROG.

## 4. Conclusion

A new co-crystal of PROG and PABA with distinct physical properties is reported and successfully produced through solution crystallisation and milling methods. PROG-PABA crystal structure was solved through SC-XRD and distinct crystalline melting point reported using DSC. Of the three scale up methods trialled, milling was selected as the most suitable for PROG-PABA preparation since spray drying and antisolvent methods were observed to form a mixture of co-crystal and starting material phases. When assessing physical properties, PROG-PABA co-crystal showed distinct solubility and more complete dissolution in aqueous media than PROG starting material. Following formulation into tablets, the PROG-PABA co-crystal showed a significant increase in the % dissolution compared to the Utrogestan® soft-gel capsule formulation. The marked increase in dissolution for the co-crystal tablet formulation may help increase the oral bioavailability for PROG through a cost-efficient alternative to the current formulation. Further studies to optimise the spray drying and antisolvent production methods as a rapid option for co-crystal preparation are required.

## References


1. N. Asi, K. Mohammed, Q. Haydour, M. R. Gionfriddo, O. L. Vargas, L. J. Prokop, S. S. Faubion and M. H. Murad, *Syst Rev*, 2016, **5**, 121.
2. S. Furness, H. Roberts, J. Marjoribanks and A. Lethaby, *Cochrane Database Syst Rev*, 2012, **2012**, CD000402.
3. G. N. Wagh, K. M. Kundavi Shankar and S. Bachani, *Drugs Context*, 2021, **10**.
4. F. Damian, M. Harati, J. Schwartzenhauer, O. Van Cauwenberghe and S. D. Wettig, *Pharmaceutics*, 2021, **13**, 214.
5. M. Samipillai and S. Rohani, *Journal of Crystal Growth*, 2019, **507**, 270-282.
6. C. Guo, Q. Zhang, B. Zhu, Z. Zhang, X. Ma, W. Dai, X. Gong, G. Ren and X. Mei, *Crystal Growth & Design*, 2020, **20**, 3053-3063.
7. H. Zeng, J. Xiong, Z. Zhao, J. Qiao, D. Xu, M. Miao, L. He and X. Wu, *Molecules*, 2019, **24**, 3936.
8. Y. Yunxia, N. Huihui, X. Shiying, G. yingwa and W. Xiangxiang, *Journal of Crystal Growth*, 2022, **585**, 126601.
9. L. Fábián, *Crystal Growth & Design*, 2009, **9**, 1436-1443.
10. P. Ying, J. Yu and W. Su, *Advanced Synthesis & Catalysis*, 2021, **363**, 1246-1271.
11. G. M. Sheldrick, *Acta Crystallographica Section A: Foundations and Advances*, 2015, **71**, 3-8.

12. G. M. Sheldrick, *Acta Crystallographica Section C: Structural Chemistry*, 2015, **71**, 3-8.
13. O. V. Dolomanov, L. J. Bourhis, R. J. Gildea, J. A. Howard and H. Puschmann, *Journal of applied crystallography*, 2009, **42**, 339-341.
14. C. R. Groom, I. J. Bruno, M. P. Lightfoot and S. C. Ward, *Acta Crystallographica Section B: Structural Science, Crystal Engineering and Materials*, 2016, **72**, 171-179.
15. C. F. Macrae, I. Sovago, S. J. Cottrell, P. T. Galek, P. McCabe, E. Pidcock, M. Platings, G. P. Shields, J. S. Stevens and M. Towler, *Journal of applied crystallography*, 2020, **53**, 226-235.
16. A. Sarkar, D. Ragab and S. Rohani, *Crystal Growth & Design*, 2014, **14**, 4574-4582.
17. MHRA, *Journal*, 2023, Appendix XII C. Consistency of Formulated Preparations.
18. B. Mittal, *How to develop Robust solid oral dosage forms: from conception to post-approval*, Academic press, 2016.
19. B. A. Bernick, J. M. Amadio, P. H. Persicaner, J. L. Cacace, T. Thorsteinsson and F. D. Sancilio, *Journal*, 2018.
20. B. Agnus and A. Besins, Progesterone tablet and its manufacturing process, *Patent*, 2000.
21. D. D. Bavishi and C. H. Borkhataria, *Progress in Crystal Growth and Characterization of Materials*, 2016, **62**, 1-8.

Chapter 7

# Evaluation of Spay Drying to Prepare Co-Crystals of Salicylic Acid and Caffeine with Improved Physicochemical Properties for Oral Administration

**Thomas Hibbard**[1], Kenneth Shankland[1], Hisham Al-Obaidi[1]

[1]School of Pharmacy, University of Reading, Reading, RG6 6AD, UK

Chapter Summary:

In this chapter, spray drying for the generation of co-crystals is explored using the salicylic acid:caffeine model system. Solvent composition and spray drying nozzle type were varied and all methods were shown to be successful in generating the co-crystal. However, an additional phase to the co-crystal was present in all samples to differing proportions dependent on the feedstock composition. Co-crystals showed stability during storage at high humidity and during a direct compression tabletting process.

Author Contributions:

TH: conceptualisation, investigation, methodology, writing – original draft, review & editing.

KS: crystallographic investigation, writing – original draft, review & editing; HAO: conceptualisation, investigation, methodology, project administration, writing – original draft, review & editing.

**Abstract**

Formation of co-crystals using spray drying remains a challenging task due to the rapid nature of the process and the possible impact of solvents on the formation of the co-crystals. The purpose of this work was to generate co-crystals via two-fluid and three-fluid nozzle spray drying using the model system of salicylic acid and caffeine (SAL-CAF). The prepared co-crystal showed a strong tendency to form through spray drying, from a variety of feedstock compositions and through both two-fluid and three-fluid drying methods.

PXRD, FT-IR and DSC were used to characterise the spray dried powders through comparison to the reported crystal structure and SAL-CAF formed through milling. All spray dried powders showed good agreement to the reported crystal structure but with an additional phase present, determined as the β polymorph of caffeine. This additional phase was present at different proportions corresponding to the solvent, feedstock concentration and method used. For the three-fluid nozzle method, the feedstock composition was shown to have a large influence on the proportion of co-crystal in the final sample and all three-fluid nozzle samples showed reduced crystallinity compared to the two-fluid nozzle method. The spray dried co-crystals showed stability under stress conditions over a period of 4 months and remained detectable following a tableting process.

Spray drying is a suitable technique for the preparation of the SAL-CAF co-crystal and may be superior to milling with optimised process parameters.

## 1. Introduction

Co-crystals have become a successful crystal engineering strategy to formulate weakly ionisable, poorly soluble molecules for pharmaceutical applications [1]. New co-crystal forms of APIs are discovered and reported regularly, and now co-crystal formulations exist as licensed marketed products to be used clinically [2, 3]. Of these products, Entresto ® and Seglentis ®, are drug-drug co-crystals where both components in the crystal structure have active pharmaceutical properties. The advantage of these new solid forms is that the resultant material will have modified physicochemical properties as well as synergistic pharmacodynamic effects. This may lead to a compound with enhanced absorption, therapeutic effect, and a reduction in the treatment burden for the patient. One drug-drug co-crystal which has been reported but not marketed is composed of salicylic acid (SAL) and caffeine (CAF), where CAF is known to have a synergistic effect for the management of pain [4]. SAL-CAF crystal structure has been reported previously and co-crystal forms of CAF are also known to display much improved stability through prevention of CAF hydration [5, 6]. Since SAL is a poorly soluble API, generation of a co-crystal with a highly soluble coformer, such as CAF, may also be beneficial for enhancing solution properties.

Many production methods exist for the formation of co-crystals including solid state, solution, and hot-melt extrusion [1]. However, there are limitations associated with these approaches, including but not limited to, poor scalability, starting material or product degradation and reliance on large quantities of solvent. One approach which is highly scalable, adaptable, and non-destructive is spray drying. Spray drying is commonplace in industry and has been shown to be able to generate co-crystals [7-12]. These studies indicated that spray drying is even able to generate co-crystals not readily formed through traditional slurry or reaction crystallisation methods [7], to an equivalent quality as milling methods [8] and in the presence of other excipients [9]. However, there is limited research with respect to the influence which process parameters have on the formation of a co-crystal during spray drying, which is essential when considering scale up preparation. Here the model system of SAL-CAF is studied, where co-crystal preparation is assessed following systematic variation of feedstock solvent composition, solute concentration and spray drying nozzle type.

Since SAL and CAF have different aqueous solubilities, a co-solvent feedstock with aqueous and organic phases is advantageous to ensure high solubility of both components. In this study, the solvent used as the organic phase was varied since the composition of the solvent system can have a large impact on which crystalline phases and

what stoichiometric ratios will nucleate from a multicomponent system [13]. SAL-CAF preparation was also assessed using three-fluid nozzle spray drying, where SAL and CAF in separate feedstock solutions met at the point of atomisation which is an advantage considering the different solubilities [14]. It also allows the potential for higher feedstock concentrations which can limit solvent use, another variable which is evaluated in this study. To date, there are no studies reporting the use of three-fluid nozzle spray drying to prepare co-crystals, despite its potential to be an advantageous approach for formulation development. In this study, formulations were generated from systematically varying three organic solvents at three aqueous:organic ratios through two-fluid and three-fluid nozzle methods. Acetone, ethanol and propan-2-ol were chosen based on salicylic acid solubility and their range of boiling points. The influence of feedstock composition and spray drying method on co-crystal generation was investigated through crystallinity and composition analysis.

## 2. Material and methods

### 2.1. Materials

Salicylic acid, caffeine, α-Lactose monohydrate, Polyplasdone XL™ and Magnesium Stearate were obtained from Sigma-Aldrich (Dorset, UK); acetone, ethanol and propan-2-ol were obtained from Fisher-Scientific Limited (Leicestershire, UK). All chemicals were used as received.

### 2.2. Preparation of Salicylic Acid:Caffeine Co-crystal

#### 2.2.1. Spray Drying Methods

Spray drying experiments were performed using a B-290 spray dryer (Büchi, Labortechnik AG Switzerland) operated in closed loop mode with a nitrogen atomising gas and nitrogen drying atmosphere. The aspirator was set to 100% generating a vacuum of -100 mbar and the atomising gas flow set to 660 L/hr. An inlet temperature of 110 °C was used for all experiments which were started when the outlet temperature stabilised at 60 °C. A two-fluid nozzle (2-FN) or a three-fluid nozzle (3-FN) with diameter 0.5 mm was used and feedstock was pumped at 5 $mL \cdot min^{-1}$. For the 3-FN, two feedstocks were pumped through the different nozzle channels simultaneously, using separate, synced pumps. Pumps were synced by measuring the time taken to pump a fixed volume of solvent.

Feedstocks were prepared according to Table 1 and contained SAL and CAF in a 1:1 molar ratio. For the 2-FN experiments, initially CAF and SAL were dissolved separately in aqueous and organic solvent phases respectively. Organic and aqueous phases were

then combined and stirred using a magnetic stirrer to create a clear feedstock with the required final concentration. The organic solvent used, and total feedstock concentration were varied systematically in two-level factorial design.

The experiments in Table 1 were repeated using 3-FN spray drying in which CAF was used as the internal feed and SAL as the external feed.

**Table 1:** Spray-drying methods for SAL-CAF formulations

| Experiment | Organic Solvent | Feedstock Concentration % w/v |
|---|---|---|
| 1 | Acetone | 2 |
| 2 | Acetone | 0.5 |
| 3 | Acetone | 1 |
| 4 | Ethanol | 0.5 |
| 5 | Ethanol | 2 |
| 6 | Ethanol | 1 |
| 7 | Propan-2-ol | 2 |
| 8 | Propan-2-ol | 1 |
| 9 | Propan-2-ol | 0.5 |

#### 2.2.2. Mechanochemical Activation Method (Milling)

A milling method was used as a comparison to spray drying for the preparation of the SAL-CAF co-crystal as is a successful co-crystallisation method for CAF and SAL co-crystals alike [15-17]. An equimolar ratio of SAL and CAF were milled together with a small quantity of ethanol (2 $\mu L mg^{-1}$), using a Retsch MM 500 ball mill. 2.5 mm ball bearings were used in a 1:20 ball to starting material ratio and the sample was milled for 30 mins at a frequency of 25 Hz.

### 2.3. Physicochemical Analysis of Spray Dried Samples

#### 2.3.1. Powder X-ray Diffraction (PXRD)

Transmission capillary PXRD data was collected for all spray dried formulations using a Brucker D8 Advance diffractometer equipped with a monochromatic $CuK\alpha_1$ source. Samples were packed into a 0.7 mm borosilicate glass capillary then scanned in the range 4° to 45° 2θ using step size 0.0171° with a count time of 1.4 seconds per step.

Data for the starting materials were also collected using the same settings to be used as references. Full width half max (FWHM) values were calculated using EVA program (Bruker) for known SAL-CAF diffraction peaks as a comparison between spray drying methods. A two-phase Rietveld refinement, using the structures of CSD refcodes XOBCAT01 and NIFWEE03, was performed using TOPAS[18] for all spray dried samples.

PXRD data for the tablet surface were collected using a Brucker D8 Advance diffractometer operating in a reflection geometry using the same collection settings as the transmission data collection.

### 2.3.2. Fourier -Transform Infrared Spectroscopy (FTIR)

FTIR spectra were collected using a Perkin-Elmer 100 FTIR Spectrometer equipped with a diamond attenuated total reflectance (ATR) accessory (Shelton, Connecticut, USA). Transmission was recorded from an average of 16 scans over the range 650 – 4000 $cm^{-1}$ with a resolution of 4 $cm^{-1}$.

### 2.3.3. Differential Scanning Calorimetry (DSC)

Melting point analysis was performed for all samples using a TA-Q2000 Differential Scanning Calorimetry (DSC) instrument (TA instruments, New Castle, USA). Samples were sealed into aluminium hermetic pans, allowed to equilibrate at 30 °C then heated at 10 °C/min to 160 °C. Pan lids were pierced to allow removal of residual solvents from the system during heating. TA Universal Analysis software was used to describe any thermal events. Melting point was calculated using onset temperature and fusion enthalpy through linear integration.

### 2.3.4. Compression testing

Tablets were produced using a direct compression method following sheer mixing of SAL-CAF, disintegrant and filler then coating with lubricant according to Table 2. Three tablet powders were made using the milled SAL-CAF and SAL-CAF from Exp 4 and 4a (representative 2-FN and 3-FN methods).

SAL-CAF tablets were produced using a KBR press with a force of 5 tons for 1 min. Following compression, tablet surface properties were analysed using PXRD.

**Table 2:** Tablet composition SAL-CAF compression tests

| Component | % w/w (to 250 mg) |
|---|---|
| SAL-CAF (milled, 2-FN or 3-FN) | 20 |
| PolyPlasdone XL | 3 |
| α-lactose monohydrate | to 100 |
| Mg Stearate | 1 |

2.3.5. Stability testing

Spray dried powders from Exp 4, 5 and 6 from both 2-FN and 3-FN methods were stored in a sealed desiccator at 37 °C (± 1 °C) for 4 months. A reservoir containing a saturated solution of NaCl was added to the desiccator to generate an environment with 75% relative humidity. The humidity level was verified using a humidity probe. Samples were monitored for a total duration of 4 months then were analysed using PXRD and FTIR.

## 2.4. Statistical Analysis

Statistical analysis was carried out using SPSS software (IBM SPSS version 27.0, SPSS Inc.). Data were compared with appropriate test following test for normality and variance. In each case, statistical significance was defined as $p < 0.05$ with significance levels: *** = $p < 0.001$, ** $p < 0.01$, * = $p < 0.05$ and NS = $p > 0.05$.

# 3. Results

## 3.1. Preparation of SD formulations

Spray dried samples containing SAL and CAF were prepared according to the method outlined in section 2.2. The collected yield was calculated for each sample as a percentage of the total solid dissolved in the feedstock. No significant differences were seen when comparing % yield between different solvents or concentrations of feedstock (ANOVA, $p > 0.05$). Therefore, a mean yield was calculated for all 2-FN and 3FN samples (Fig 1).

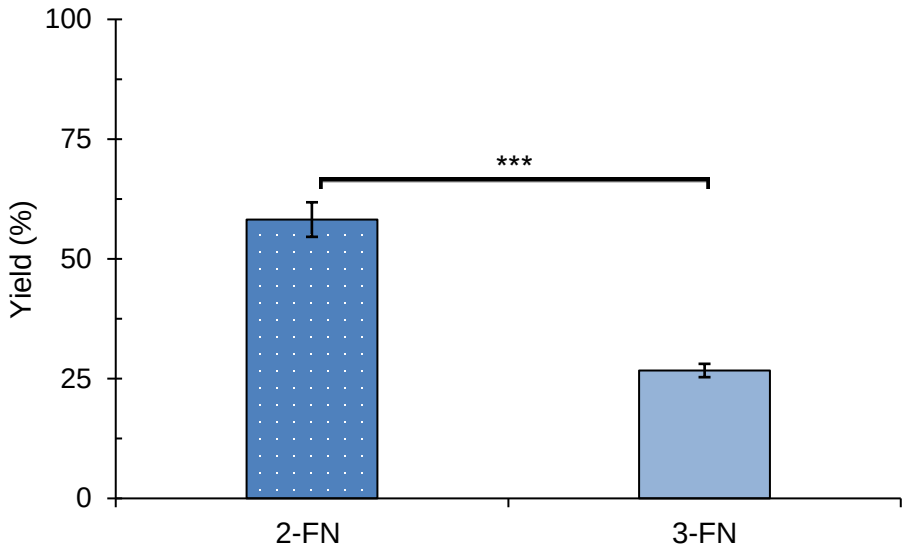


**Figure 1:** Spray drying yields for two-fluid nozzle compared to three-fluid nozzle expressed as a mean of all experiments n = 9, $p < 0.001$.

The 2-FN method shows a significantly higher yield than the 3FN method at 58% compared to 27% respectively. The low yield from the 3-FN could be due to an incomplete drying process leading to deposition within the spray drying apparatus [19]. This is likely since a higher volume of feedstock was being pumped through the nozzle i.e. from two pumps operating at 5 $mL \cdot min^{-1}$ compared to one pump. Optimisation of process parameters for the 3-FN method by increasing inlet temperature or decreasing pump rate could compensate for this difference and potentially increase the yield.

## 3.2. Characterisation of Spray Dried Product

### 3.2.1. Confirmation of Co-crystal formation – PXRD and DSC

PXRD data confirm the formation of a co-crystal through all spray drying methods and from all solvent systems (Fig S1 and S2). The low angle diffraction peak at ~ 6.7° 2θ and the absence of any starting material peaks in the spray dried samples are indicative of co-crystal formation (Fig 2).

In addition to this, DSC thermograms for all spray dried materials showed a single endothermic peak with an onset temperature corresponding to that reported for SAL-CAF (i.e. 138 to 140 °C). This endothermic peak corresponds to the crystalline melting point of a single-phase material, confirming the absence of any residual starting material (Fig 3).

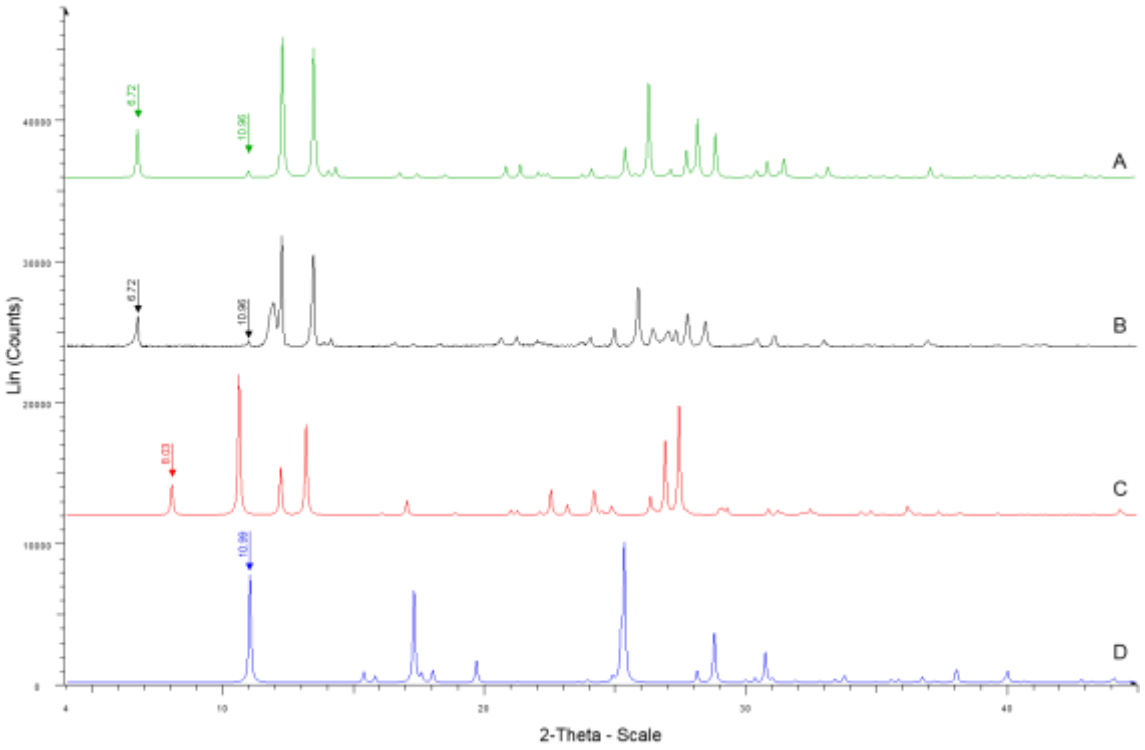


**Figure 2:** PXRD data for A) CSD refcode: XOBCAT01, SAL-CAF simulated powder pattern (green), compared to B) SAL-CAF spray dried (2-FN) co-crystal (black), C) caffeine (red) and D) salicylic acid (blue) references.

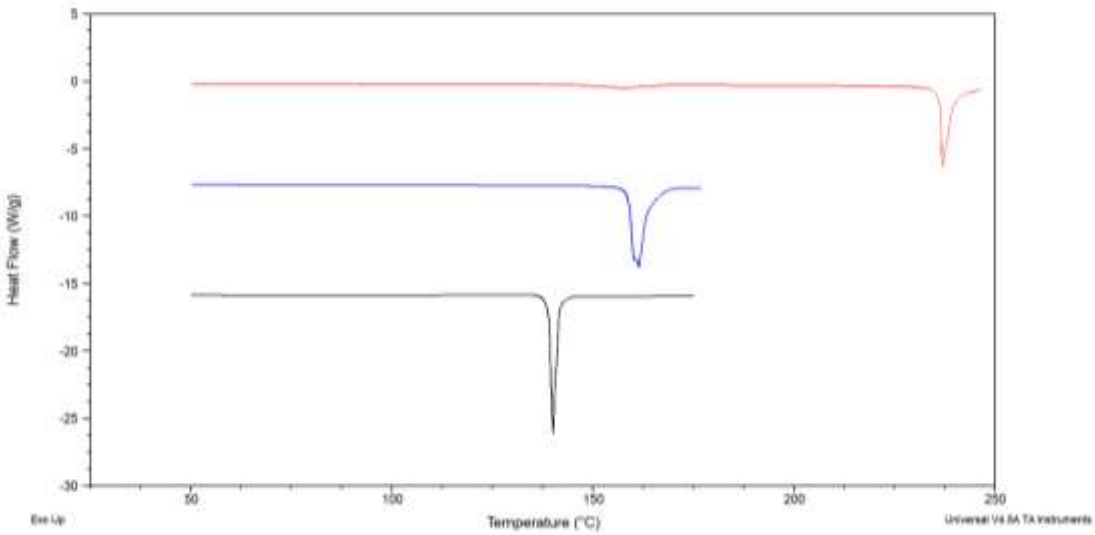


**Figure 3:** DSC data for spray dried SAL-CAF co-crystal (black) compared to caffeine (red) and salicylic acid (blue) references.

There is also evidence of co-crystal formation through the milling method. However, some SAL and CAF reference peaks are still present, seen most clearly at 12.17 ° 2θ

for CAF and 10.99° 2θ and 17.27° 2θ for SAL (Fig S3). This suggests that the milling method used has not completely transformed the starting materials to co-crystal. DSC confirmed that there was a mixture of co-crystal and starting material phases following milling at 25 Hz for 30 mins. This is shown by an additional endothermic peak at ~122 °C corresponding to the eutectic melt between SAL and CAF as reported by Lu et al. and shown experimentally through DSC analysis of a SAL + CAF physical mix (Fig 4 and S4) [6]. Since there is no exothermic peak between the eutectic melt and the main endothermic melt it can be concluded that no recrystallisation has taken place. Therefore, the presence of physical mixture as seen on the PXRD between co-crystal and

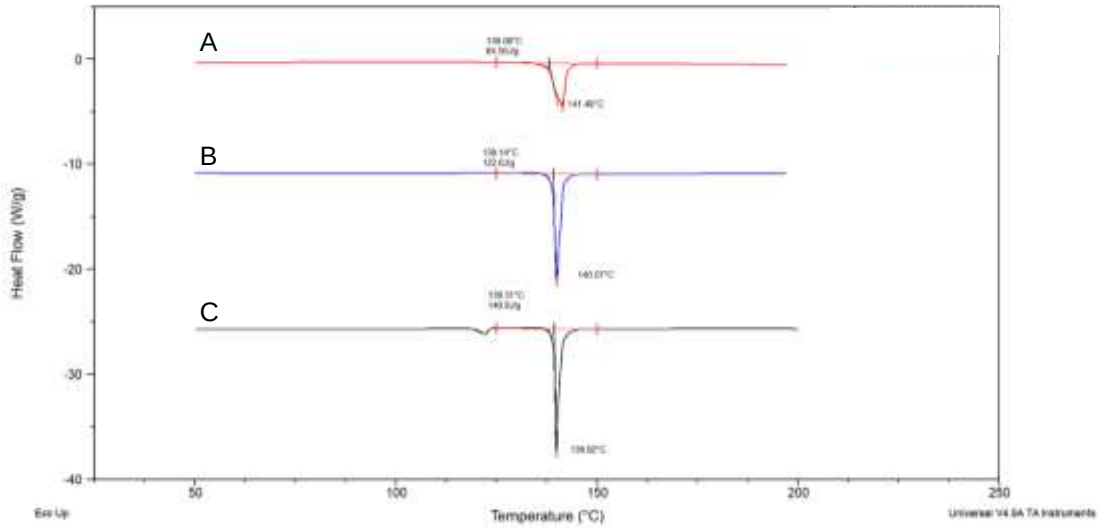


starting material phases is confirmed rather than co-crystal formation following eutectic melting during the DSC experiment.

**Figure 4:** DSC data for SAL-CAF co-crystal prepared through 3-FN (red) and 2-FN (blue) spray drying compared to milled SAL-CAF from milled method (black). The eutectic melt of salicylic acid and caffeine is seen at ~122 °C in the milled sample.

### 3.2.2. Comparison of co-crystal with reported crystal structure

PXRD patterns also show good agreement with the calculated powder pattern[20] for the known crystal structure of SAL-CAF, CSD refcode XOBCAT01[6] (Fig 2). However, for all samples, including milled, there are additional peaks seen at ~11.9° 2θ, 26.5° 2θ and 27° 2θ which are not explained by the SAL or CAF starting materials (Fig 5). Following Rietveld refinement against some reported crystal structures, it was found that these peaks are attributable to the presence of the β polymorph of CAF (CSD refcode NIFWEE03, Fig 5, S5), known to be formed through dehydration of caffeine monohydrate[21] and mechanochemical activation of anhydrous caffeine [22].

These peaks are present in all spray dried samples regardless of the organic solvent or feedstock concentration used, although in different proportions (Fig 6) which can be evaluated from the two-phase (XOBCAT01 and NIFWEE03) Rietveld fit to the data. 2-FN spray drying methods show a much higher proportion of co-crystal in the sample compared to the equivalent 3-FN method when expressed as a mean: 85.1 ±2.06 compared to 62.5 ±9.00. There appears to be a correlation between increasing feedstock concentration and the percentage of co-crystal present, especially for the 3-FN spray drying method with acetone or ethanol organic phase. Increasing the feedstock concentration from 0.5% w/v to 2% w/v showed an ~40% and ~20% increase in co-crystal % for acetone and ethanol formulations respectively. This observation suggests that the generation of the β polymorph of CAF is solvent mediated.

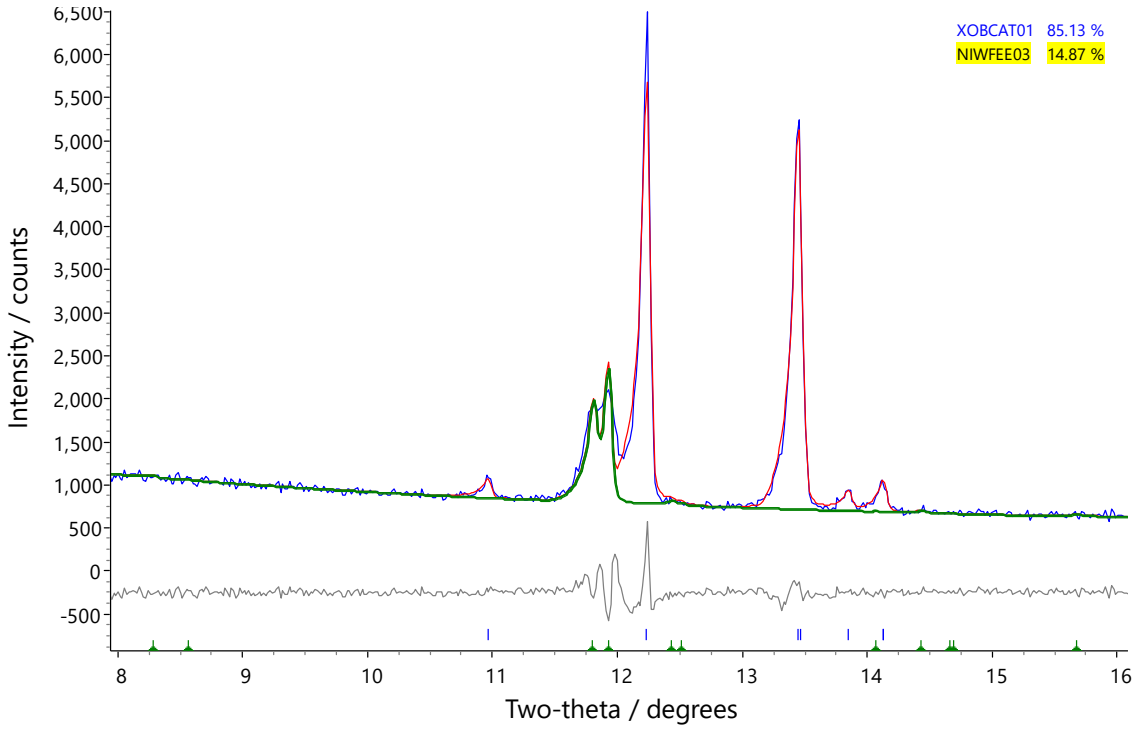


**Figure 5:** Two-phase Rietveld fit of SAL-CAF Exp 4 using the structures corresponding to CSD redcodes XOBCAT01 (SAL-CAF co-crystal) and NIWFEE03 (CAF β polymorph), shown in the range 8-16° 2θ. PXRD data (blue line), the overall fit of co-crystal to the data (red line) and the contribution of the caffeine β polymorph to the fit (green line) is displayed. Blue tick marks indicate the position of reflections associated with co-crystal phase, whilst green tick marks indicate the position of reflection associated with caffeine β polymorph. The two observed reflections below 12° 2θ are explained by the presence of the caffeine β polymorph.

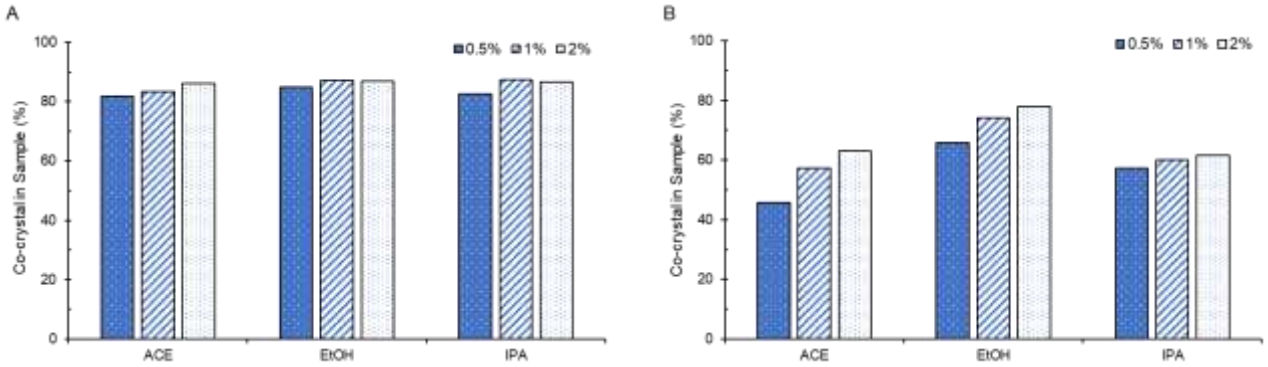


**Figure 6:** Proportion of co-crystal phase present in spray dried samples as a ratio to the additional β caffeine polymorph phase for A) two-fluid nozzle B) three-fluid nozzle.

### 3.2.3. Estimation of Spray Dried Co-Crystal Crystallinity

Diffraction peak full width half max (FWHM) values were calculated for each spray dried sample, which showed there to be no significant difference between the 2-FN and 3-FN methods. Furthermore, there was no significant difference between the solvents, or the concentrations of feedstock used in terms of peak FWHM. However, when calculating net peak area, there is significant difference between the different nozzle types (Fig 7). 3-FN diffraction peaks are significantly smaller than the corresponding 2-FN peaks when measured using the same experimental parameters. However, in comparison to the milled co-crystal, all spray dried co-crystals show a much lower FWHM and net area. For the peak at ~6.7° 2θ: FWHM = ~0.08° 2θ (SD) vs ~0.16° 2θ (milled) and Net Area = ~1.7° 2θ (SD) vs ~4.5° 2θ (milled). These data indicate that in terms of overall crystallinity: milled > 2-FN > 3-FN.

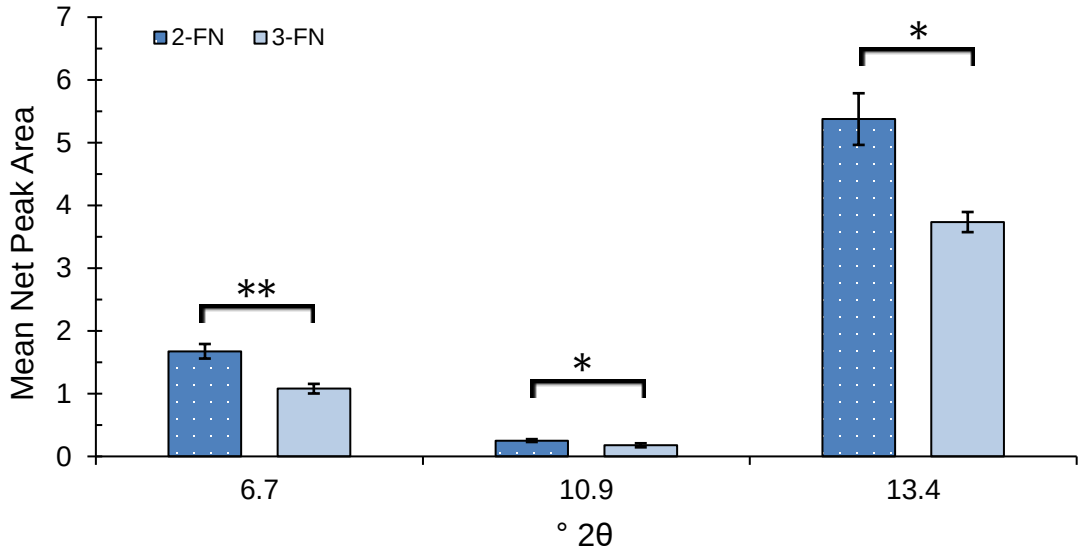


**Figure 7:** Mean net peak area comparing 2-FN to 3-FN SAL-CAF across three co-crystal diffraction peaks.

For the DSC data, there is difference between the enthalpy of fusion between the 2-FN and 3-FN spray dried materials. In general, the powders produced through a 3-FN method have a lower enthalpy of fusion compared to the 2-FN method across all solvent systems. This confirms the PXRD data which indicates that 3-FN spray drying gives a co-crystal with a lower degree of crystallinity to 2-FN spray drying (Table 3). Again, all spray drying products, show a much lower enthalpy of fusion than the milled product.

**Table 3:** DSC data for SAL-CAF samples

| Solvent | Nozzle Type | Feedstock Con-centration (%) | Peak Onset (°C) | $\Delta H_{fus}$ (Jg$^{-1}$) |
|---|---|---|---|---|
| ACE | 2-FN | 0.5 | 139.5 | 103.4 |
| | | 1 | 140.6 | 106.7 |
| | | 2 | 139.6 | 119.0 |
| | 3-FN | 0.5 | 138.3 | 56.4 |
| | | 1 | 138.6 | 70.7 |
| | | 2 | 138.5 | 66.8 |
| EtOH | 2-FN | 0.5 | 139.1 | 124.1 |
| | | 1 | 139.6 | 115.9 |
| | | 2 | 139.2 | 114.0 |
| | 3-FN | 0.5 | 138.1 | 86.6 |
| | | 1 | 139.2 | 93.2 |
| | | 2 | 139.2 | 96.1 |
| IPA | 2-FN | 0.5 | 139.5 | 106.5 |
| | | 1 | 139.3 | 122.7 |
| | | 2 | 139.2 | 116.5 |
| | 3-FN | 0.5 | 138.5 | 73.9 |
| | | 1 | 138.6 | 81.2 |
| | | 2 | 138.8 | 80.0 |
| Milled SAL-CAF | n/a | n/a | 139.3 | 140.9 |

### 3.2.4. Analysis of Intermolecular Interactions (FTIR)

Considering the FTIR data for spray dried samples, there is only slight change in the carbonyl region absorption bands compared to the CAF and SAL references (Fig 8). The absorption bands are a composite of the reference bands at ~1690 $cm^{-1}$, ~1655 $cm^{-1}$, ~1640$cm^{-1}$ and ~1600 $cm^{-1}$ for CAF, SAL, CAF and SAL respectively. The ~1655 $cm^{-1}$ and ~1640$cm^{-1}$ bands overlap and so exist as a single broad absorbance in the product. The formation of a co-crystal, rather than a salt, is supported through these data since during salt formation the carboxylic acid stretching frequency is likely to move to a higher frequency. For example, Cook et al. showed that a series of CAF salts all showed carbonyl absorption bands at a higher frequency ~1720 $cm^{-1}$ and ~1670 $cm^{-1}$ compared to the free base reference which displays absorption at 1698 $cm^{-1}$ and 1656 $cm^{-1}$ [23]. There is a red shift present for the CAF component of the carbonyl region in all spray dried materials from ~1652 $cm^{-1}$ to ~1657 $cm^{-1}$ but this value is smaller than the reported red shift following the formation of CAF salts (to ~1670 $cm^{-1}$[23]). The reduced red shift can be attributed to the formation of hydrogen bonds rather than ionic bonds between SAL and CAF. There is good agreement between the spectra for the 2-FN, 3-FN and milled product confirming the formation of a uniform product through all spray drying methods despite additional phases identified through PXRD analysis.

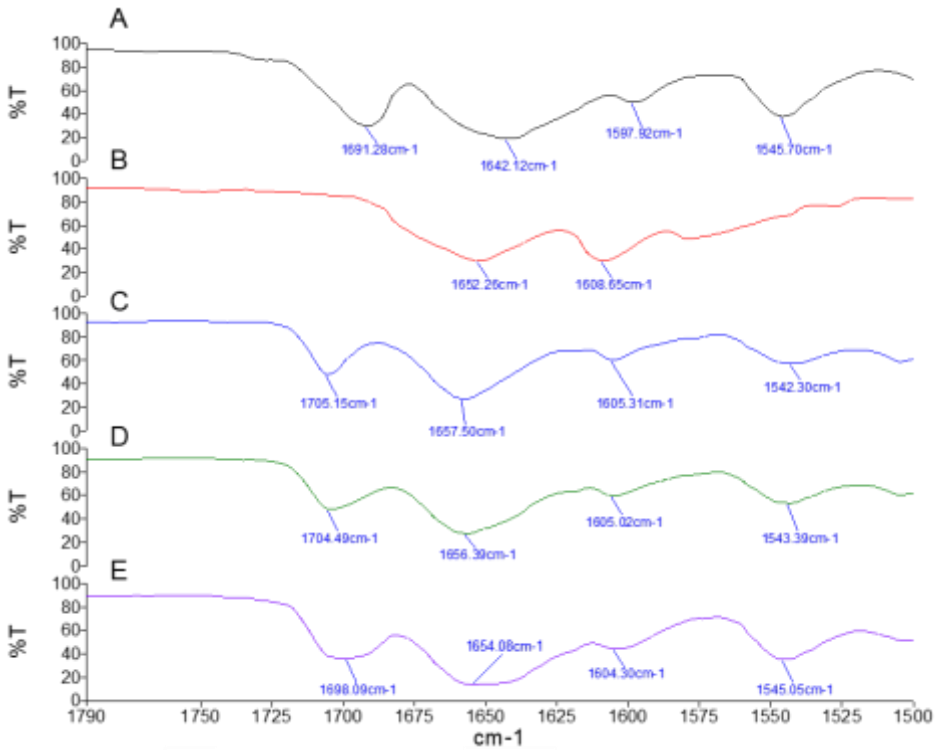


**Figure 8:** FTIR data comparing A) CAF (black), B) SAL (red), C) SAL-CAF milled (blue), D) SAL-CAF 2-FN (green), E) SAL-CAF 3-FN (purple).

## 3.3. Physical Properties of Spray Dried Product

### 3.3.1. Stability Testing

PXRD and FTIR analysis of the samples stored in a high humidity environment for 4 months showed no differences compared to reference spectra taken prior to storage (Fig S6, S7, S8). PXRD shows the same peak positions with no additional peaks corresponding to references seen; if hydration of the co-crystal had occurred, the resultant phase change would been visible through changes to the diffraction pattern. If there had been water sorption into the sample without changes to the crystal structure, FITR would show additional peaks in the 3600 – 2800 $cm^{-1}$ region. However, there is no evidence for this as shown by Fig S6 and S7. In addition to these observations, the additional diffraction peaks associated with the CAF β polymorph are still present in the samples following storage at high humidity.

### 3.3.2. Tablet Compression Testing

PXRD analysis following the tableting process reveals the presence of co-crystal and α-Lactose monohydrate on the surface of the 2-FN, 3-FN and milled co-crystal tablets. This confirms the sheer and tumble mixing processes were able to achieve a good mixture of co-crystal and excipients prior to compression, as seen by the presence of both main crystalline components on the tablet surface (Fig 9, S9). Physical stability of the co-crystal is also confirmed by the clear presence of key co-crystal reference peaks for 2-FN, 3-FN and milled tablets e.g. at 6.86 °2θ.

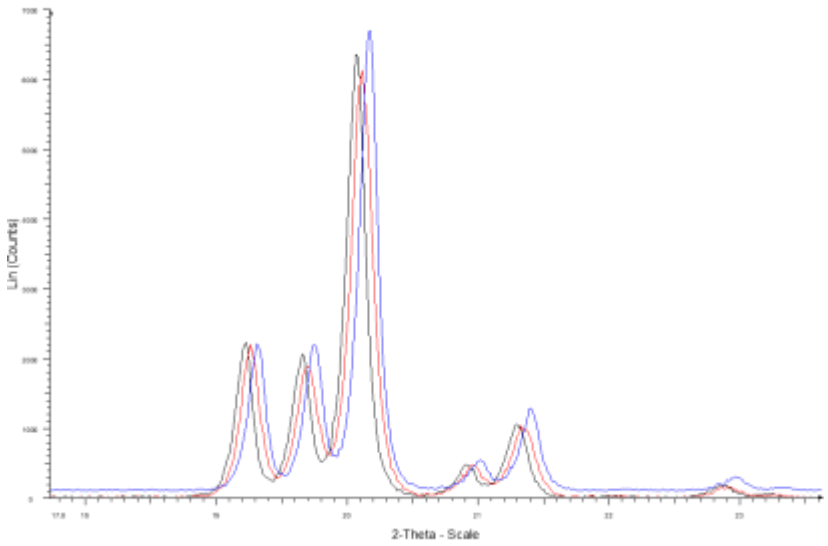


**Figure 9:** A section of PXRD data showing α-lactose monohydrate peaks (~19 °2θ to ~21.5 °2θ) and co-crystal peaks (~23 °2θ) in tablets made from milled product (black),

2-FN product (red) and 3-FN product (blue). Note that the peak position shifts are attributable to small variations in height displacement of the tablets on the diffractometer.

## 4. Conclusions

The co-crystal of salicylic acid and caffeine has been prepared via a series of spray drying methods. SAL-CAF was successfully prepared regardless of the solvent systems, feedstock concentration or nozzle type although all spray drying methods showed the inclusion of phases separate to the co-crystal. Additional phases were also seen in the equivalent milling method. All spray dried powders showed X-ray diffraction patterns associated with SAL-CAF co-crystal and a crystalline melt in agreement with previously reported values. The three-fluid spray drying method, where SAL and CAF combine in the nozzle from separate feedstocks also successfully prepared the co-crystal although to a lower crystallinity and higher proportions of additional phases than the corresponding two-fluid spray drying method. Spray dried co-crystal powders showed stability following storage at elevated temperature and humidity and during a trial tableting direct compression method. Further studies to increase the yield of the three-fluid nozzle formulations and assess the dissolution properties of tablets containing the spray dried co-crystal powders are required.

## References

1. M. Karimi-Jafari, L. Padrela, G. M. Walker and D. M. Croker, *Crystal Growth & Design*, 2018, **18**, 6370-6387.
2. A. Port, C. Almansa, R. Enrech, M. Bordas and C. R. Plata-Salamán, *Crystal Growth & Design*, 2019, **19**, 3172-3182.
3. O. N. Kavanagh, D. M. Croker, G. M. Walker and M. J. Zaworotko, *Drug Discovery Today*, 2019, **24**, 796-804.
4. G. Castañeda-Hernández, M. S. Castillo-Méndez, F. J. López-Muñoz, V. Granados-Soto and F. J. Flores-Murrieta, *Canadian Journal of Physiology and Pharmacology*, 1994, **72**, 1127-1131.
5. A. V. Trask, W. D. S. Motherwell and W. Jones, *Crystal Growth & Design*, 2005, **5**, 1013-1021.
6. E. Lu, N. Rodríguez-Hornedo and R. Suryanarayanan, *CrystEngComm*, 2008, **10**, 665-668.
7. A. Alhalaweh, W. Kaialy, G. Buckton, H. Gill, A. Nokhodchi and S. P. Velaga, *AAPS PharmSciTech*, 2013, **14**, 265-276.
8. S. P. Patil, S. R. Modi and A. K. Bansal, *Eur J Pharm Sci*, 2014, **62**, 251-257.

9. D. Walsh, D. R. Serrano, Z. A. Worku, A. M. Madi, P. O'Connell, B. Twamley and A. M. Healy, *International Journal of Pharmaceutics*, 2018, **551**, 241-256.
10. M. Urano, M. Kitahara, K. Kishi, E. Goto, T. Tagami, T. Fukami and T. Ozeki, *Crystals*, 2020, **10**, 313.
11. L. H. do Amaral, F. A. do Carmo, M. I. Amaro, V. P. de Sousa, L. C. R. P. da Silva, G. S. de Almeida, C. R. Rodrigues, A. M. Healy and L. M. Cabral, *AAPS PharmSciTech*, 2018, **19**, 2687-2699.
12. J. Weng, S. N. Wong, X. Xu, B. Xuan, C. Wang, R. Chen, C. C. Sun, R. Lakerveld, P. C. L. Kwok and S. F. Chow, *Crystal Growth & Design*, 2019, **19**, 2736-2745.
13. T. Leyssens, G. Springuel, R. Montis, N. Candoni and S. Veesler, *Crystal Growth & Design*, 2012, **12**, 1520-1530.
14. S. Focaroli, G. Jiang, P. O'Connell, J. V. Fahy and A. M. Healy, *Pharmaceutics*, 2020, **12**.
15. S. Latif, N. Abbas, A. Hussain, M. S. Arshad, N. I. Bukhari, H. Afzal, S. Riffat and Z. Ahmad, *Drug Development and Industrial Pharmacy*, 2018, **44**, 1099-1108.
16. S. Korde, S. Pagire, H. Pan, C. Seaton, A. Kelly, Y. Chen, Q. Wang, P. Coates and A. Paradkar, *Crystal Growth & Design*, 2018, **18**, 2297-2304.
17. F. Fischer, M. Joester, K. Rademann and F. Emmerling, *Chemistry – A European Journal*, 2015, **21**, 14969-14974.
18. A. Coelho, *Journal of Applied Crystallography*, 2018, **51**, 210-218.
19. M. Maury, K. Murphy, S. Kumar, L. Shi and G. Lee, *European Journal of Pharmaceutics and Biopharmaceutics*, 2005, **59**, 565-573.
20. C. F. Macrae, I. Sovago, S. J. Cottrell, P. T. Galek, P. McCabe, E. Pidcock, M. Platings, G. P. Shields, J. S. Stevens and M. Towler, *Journal of applied crystallography*, 2020, **53**, 226-235.
21. C. W. Lehmann and F. Stowasser, *Chemistry – A European Journal*, 2007, **13**, 2908-2911.
22. J. Pirttimäki, E. Laine, J. Ketolainen and P. Paronen, *International Journal of Pharmaceutics*, 1993, **95**, 93-99.
23. D. Cook and Z. R. Regnier, *Canadian Journal of Chemistry*, 1967, **45**, 2895-2897.

Chapter 8

# General Discussion and Conclusion

Chapter Summary:

In this chapter, the main findings of this work are summarised and discussed. Critical evaluation of the findings and methods used and suggestions for future work in the context of wider research is also included.

## 8.1. Introduction

Crystal engineering of APIs, especially by the formation of solid dispersions in combination with salt and co-crystallisation strategies, is a highly applicable formulation strategy for oral and inhaled drug delivery. The generation of solid dispersions has been shown to enhance API delivery through current routes of administration but can also enable API repurposing for alternative routes; this has the potential to increase the longevity of existing APIs, reduce side effects, and improve treatment outcomes [1, 2].

There are some examples in the literature detailing co-crystal and salt-based solid dispersions generated through scalable methods such as spray drying, but these are rarely in the context of dry powder inhalation [3-6]. In addition, there is often limited discussion regarding the influence that spray drying process parameters have on the nature the solid dispersion produced, especially with respect to the use of 3 fluid nozzle (3-FN) spray drying for the preparation of salt and cocrystal spray dried solid dispersions.

In this thesis, the aim of developing new salt, cocrystal and solid dispersion forms of APIs through a crystal engineering, spray drying approach was addressed. Spray drying was extensively used to generate new formulations and proved to be suitable for their preparation, with products showing significant improvements to API solution properties, inhalation properties and stability.

Here, a brief evaluation of the work is presented, including a summary of previous chapters (§ 8.2), an evaluation of the experimental content, and suggestions for future work (§ 8.3).

## 8.2. Summary of Key Findings

### 8.2.1. Solid Dispersions for Antimicrobial and Anticancer Pulmonary Delivery (Chapter 2)

This chapter provided an overview of the background theory and current advances in the use of solid dispersion formulations for pulmonary delivery. The topic of antimicrobial and anticancer drugs was chosen, since high doses of these APIs are required at the site of action and formulation through the inhaled route is likely to reduce side effects associated with high dose systemic delivery. Solid dispersion formulations without carrier were seen to be a suitable alternative to current dry powder inhalation technology, as shown through studies reporting high percentage of drug deposition and high delivered dose. Formulations which used co-crystal or co-amorphous drug forms or API particles dispersed in a polymer matrix also showed suitable aerosolisation performance. The

preparation method for the inhalable particles and presence of any excipients in the formulation proved to have a large impact on the percentage lung deposition and solution properties following administration. Carrier-free dry powder inhalation was seen as a viable option for the delivery of high doses to the lungs and these findings directed the formulation strategies seen in subsequent chapters.

### 8.2.2. Preparation and Characterisation of Novel Ciprofloxacin Salts (Chapter 3)

This chapter reported the discovery of new salt forms of ciprofloxacin (CFX) with dicarboxylic acid molecules of increasing molecular weight. All salt forms showed modulated aqueous solubility compared to ciprofloxacin base, with similar or greater aqueous solubility than ciprofloxacin hydrochloride. The glutaric acid salt showed the highest aqueous solubility with a 6-fold increase on the ciprofloxacin hydrochloride salt form. The order of aqueous solubility between the salt forms was directly correlated to the reported solubilities of the individual counterions, suggesting that solubility of ciprofloxacin is largely driven by the enthalpy gained through counterion solvation and local pH adjustment following counterion dissolution. Running the solubility experiments in stronger buffer solution decreased the measured aqueous solubility of each of the ciprofloxacin salts which raises questions regarding the utility of the saturation solubility measurement for API salt forms. This is further discussed in section 8.3.2. All salts retained appropriate MIC levels for ciprofloxacin, which suggests that the solubility enhancements may help extend the life span of this antibiotic.

### 8.2.3. Solid Dispersions of Ciprofloxacin Salts Showing Modulated Drug Release (Chapter 4)

The ciprofloxacin salts generated by the work reported in Chapter 3 were formulated into polymer solid dispersions with the aim of preparing particles with controlled CFX release and suitable dry powder inhalation properties through a spray drying, crystal engineering approach. Two distinct formulation types were generated from solution and suspension feedstocks, which analysis suggests were largely amorphous salt solid dispersions. Formulations from solution showed a higher degree of residual crystalline material compared to the suspension formulations. Both solid dispersion types showed improved *in vitro* lung deposition properties compared to spray dried salts without polymer and showed significantly different solution properties to the control and to each other. The solid dispersions spray dried from solution showed controlled ciprofloxacin release from polymer in both sink and non-sink conditions, at a rate attributed to the API diffusing from the hydrated polymer matrix. By contrast, the suspension solid dispersions showed a

biphasic drug release pattern with increasing dissolution rate part way through the experiment. This release pattern was attributed to a change in the predominant dissolution mechanism, from diffusion out of the polymer matrix during hydration to then being API controlled. Since the suspension formulations had a higher amorphous content and potentially smaller residual salt crystallite size, the dissolution rate was greater than that the solution formulations. The suspension formulation showed absorption *in vivo* following oral administration, yet the solution formulation did not show any absorption into systemic circulation. Further pharmacokinetic study quantifying the *in vivo* properties of these solid dispersions, through the oral and inhaled routes is required. This chapter also highlights the utility of the 3-FN spray drying method for the co-spray drying of incompatible feedstocks to generate a uniform solid dispersion.

### 8.2.4. Spray Dried Inhaled Progesterone Formulations (Chapter 5)

The utility of the spray drying method for generating inhalable progesterone powders was shown in chapter 5, with the aim of generating solid dispersions using a neutral, weakly ionisable molecule. Nine spray dried powders of progesterone and L-leucine were generated from a variety of feedstock compositions using different organic solvents and proportions of organic to aqueous phase. These powders showed a variety of inhalation properties, yet it was not clear how the solvent and solvent ratio influences these. Of the nine formulations, two showed an MMAD of less than 5µm which is indicative of good dry powder inhalation performance. It was also confirmed that spray drying progesterone from solution will cause the crystallisation of the Form II polymorph. This polymorph shows higher aqueous solubility than Form I but was shown to transform back to the original Form I polymorph on heating. By adding HPMCAS to the spray drying feedstock, a formulation was developed which prevented Form I recrystallising on heating, instead initiating the formation of a solid dispersion on melting showing drug and polymer to be miscible. The addition of HPMCAS was also shown to increase the low-level lung deposition of the formulation and promote increased kinetic solubility of progesterone. Therefore, the spray drying method was shown as a suitable method for generating a distinct crystalline solid form of progesterone, which could be tailored to prevent polymorphic recrystallisation and modify aqueous solubility.

### 8.2.5. Preparation and Formulation of Novel Progesterone Co-Crystal (Chapter 6)

Building on the understanding of progesterone crystallisation behaviour, this chapter reported the preparation and characterisation of a novel progesterone co-crystal with

para-aminobenzoic acid. The co-crystal was generated following an *in silico* and experimental screening process, to select a suitable coformer molecule. Three scale-up co-crystal generation methods were trialled, of which milling was shown to be the most reliable for co-crystal generation. The spray drying and antisolvent methods trialled for co-crystal scale up, although quicker, showed the presence of Form II progesterone alongside the co-crystal which is generated through rapid crystallisation, as shown in chapter 4. Further work to optimise these processes to produce a single-phase co-crystal product is required. The milled co-crystal powder was shown to be stable at high humidity for 4 months and showed higher dissolution than progesterone alone. The co-crystal showed no significant increase in the saturated aqueous solubility of progesterone, although a larger variation around the mean was detected for the co-crystal. This suggests that the co-crystal may temporarily increase the kinetic solubility of progesterone which equates with progesterone at equilibrium. The extent and duration of this possible saturated state will need to be studied further. Tablets of the co-crystal were then formulated through a direct compression method through which the co-crystal remained stable as shown through PXRD analysis. The resulting tablets showed a significantly increased dissolution profile compared to a current micronized soft gel capsule formulation (Utrogestan®). These findings suggest that formulation of progesterone as a co-crystal tablet could be a viable, cost-effective alternative to the current soft gel capsule formulation.

### 8.2.6. Preparation of Salicylic Acid:Caffeine Co-Crystal Through Spray Drying (Chapter 7)

This chapter aimed to optimise the spray drying method for the generation of co-crystals by using a model system i.e. salicylic acid and caffeine. Co-crystal formation was successful for all spray drying methods regardless of the solvent, feedstock concentration or type of spray drying nozzle used. However, analysis showed there to be an additional phase present unaccounted in addition to the co-crystal, confirmed to be the β-polymorph of caffeine. This additional phase was present regardless of the organic solvent used and the proportion was linked with feedstock concentration. The 3-FN spray drying method was seen to generate co-crystals at a lower yield and lower crystallinity than the corresponding 2-FN methods. It was concluded that optimisation of the 3-FN processing parameters though a reduction in pumping rate or increase in inlet temperature may increase the yield and crystallinity of the products. Despite this, spray dried co-crystal powders showed stability following storage at high humidity, crucially without the absorption of water reported with caffeine [7]. Spray dried co-crystal was also shown to be stable through a direct compression tabletting process as shown through

surface PXRD analysis. The presence of additional phases in the spray dried product is in line with the finding from Chapter 6 and suggests that a thorough understanding of the co-crystal crystallisation kinetics is required for successful preparation through spray drying.

## 8.3. Evaluation of Experimental Content and Suggestions for Future Work

### 8.3.1. Identification of Co-crystal and Salt Forms

Much of the work in this thesis has been focussed on accurately characterising solid forms, with particular interest in distinguishing between salts and co-crystals. For example, with the CFX salt forms reported in chapter 3, the positioning of the hydrogen atom within the intermolecular bond was precisely located through SC-XRD and confirmed through DFT-D calculations. Through this method, these new multicomponent crystals were shown to be salts as opposed to co-crystals. Following solving the crystal structures in this way, PXRD and FTIR reference patterns were able to be generated/ collected which were used to confirm that the milled powder samples were also salts.

Other research on CFX reports the formation of new co-crystals without first solving the crystal structure, which may have led to incorrect categorisation of these multicomponent crystals. New CFX co-crystals with nicotinic and isonicotinic acids ($\Delta pK_a$ = 5.95 and 5.01 respectively) were reported and characterised through PXRD, DSC and FTIR without SC-XRD [8]. Salt formation was excluded by the authors, based on carbonyl stretching seen in FTIR analysis without commenting that multiple phases were present as seen in PXRD and DSC data. It seems likely that a variety of solid phases, including starting materials, are present which causes the misidentification of CFX ionisation state. Some preliminary work to investigate these results suggests that the CFX:isonicotinic acid system has a high propensity to form salts as predicted by the $\Delta pK_a$. Such a hypothesis should only be excluded following collection of accurate crystal structure data. Subsequent research from other research groups which cites these co-crystals has also been published but without thorough analysis to exclude the possibility of salt formation [9].

Similar studies reporting co-crystals of CFX with picolinic acid, pyrazinoic acid and *p*-aminobenzoic acid have also been published ($\Delta pK_a$ = 3.34, 5.84 and 6.36 respectively) [10, 11]. These compounds all exhibit a $\Delta pK_a$ within the accepted range for salt formation, and since there was no attempt to determine the nature of intermolecular interactions outside of FTIR analysis, clarification as to whether co-crystals have formed is required. There is research to suggest that CFX can form co-crystals which has been confirmed with SC-XRD data. These studies show the complex bonding within CFX

multicomponent crystals and highlight the ability of the zwitterionic compound to form salts, cocrystals and solvates of different ionisation states [12-14]. Collecting the crystal structures for the previously mentioned compounds would give a better understanding CFX ionisation within multicomponent crystals and whether preparation conditions can direct co-crystal or salt formation.

The utility of X-ray diffraction for identifying additional phases, in addition to a desired co-crystal/salt form was seen in Chapter 6 and 7. In both cases, comparing the experimental PXRD data to calculated diffraction patterns (from known crystal structures) was able to identify the additional phase as distinct from the starting materials and formed co-crystal. In the case of SAL-CAF (Chapter 7), the proportion of additional crystalline phase in relation to co-crystal was able to be calculated from the diffraction data using quantitative phase analysis.

### 8.3.2. Measurement of Solution Properties

The measurement of thermodynamic aqueous solubility throughout this thesis has raised questions relating to the utility of this method for multicomponent systems. For example, in Chapter 3, where the saturated solubility of salt forms was measured at equilibrium, the system became a balance between API and counterion in solution and API with unknown API salt/solvate forms as the solid phase. It is likely that these salts/solvates had formed with water and salt counterion or phosphate ions from the buffer over the course of the experiment. It would be valuable to analyse how the concentration in solution and the composition of the solid phase changes throughout the experiment so that the kinetic solubility can be understood further. Regular sampling of concentration during solubility experiment was shown to be useful for the work in Chapters 4 and 5 where the extent and duration of kinetic solubility was shown to be different depending on formulation type. Future work to determine the nature of the solid phase from the start of the experiment to equilibrium would be useful with respect to understanding the nature of API release from the polymer matrix.

This would also be possible by measuring the intrinsic dissolution of different formulations containing the same API, to reduce the number of variables influencing solubility and dissolution rate. Variables associated with the preparation methods and physical characteristics of the particles, such as particle size and surface area, influence the rate of dissolution. Intrinsic dissolution measures the dissolution rate independent of the formulation particle size and surface area through the formation of a flat disk with one face exposed to the dissolution media. Future work comparing of the intrinsic dissolution for solution and suspension CFX solid dispersions (Chapter 4) would help to

understanding the differences in dissolution profiles between formulation types and CFX salt forms.

### 8.3.3. Measurement of Formulation Properties *in vitro* and *in vivo*

The solid dispersion formulations presented in Chapter 4 showed why additional *in vivo* work is essential for further development of formulations. When these formulations were tested an animal model there was repeated non-absorption into systemic circulation for one formulation type, despite it having performed adequately during *in vitro* dissolution testing. Further experimentation to understand this observation is required to ascertain this apparent failure to absorb.

Additional work to assess the aerodynamic performance of these solid dispersions in a different lung model would be interesting. Cascade impaction is the gold standard for estimating aerodynamic particle size which can be correlated with inhalation within a healthy lung. However, when developing inhaled antibiotic formulations, it would be beneficial to have an *in vitro* inhalation model which includes the impact of disease state in terms reduced air flow. This would help better understand the powder deposition profile for a patient with an infection. Also, developing lung models which can demonstrate the eradication of bacteria and biofilms following deposition of antibiotic powder onto a mucus surface would be useful. Following this, testing these formulations with *in vivo* inhalation animal models would give a better understanding of infection eradication and pulmonary pharmacokinetics. Different pulmonary administration methods measure different properties of a powder; therefore, careful consideration of study parameters is required when designing *in vivo* lung deposition experiment [15-17].

### 8.3.4. Spray Drying as a Crystal Engineering Method

When attempting to prepare the progesterone co-crystal by spray drying, in Chapters 6, two phases were identified in the final product: the co-crystal and a polymorph of starting material. This observation was repeated in Chapter 7 during generation of SAL-CAF by spray drying and points to the necessity of fully understanding the phase relationships between co-crystal, starting materials and the solvent when developing a solvent-based co-crystallisation method. The generation of a ternary phase diagram detailing these interactions would greatly aid the development of a suitable spray drying method and potentially avoid co-precipitation of multiple phases. This is particularly relevant if spray drying using a feedstock where there is a large difference in solubility between the API and coformer, as this will lead to an asymmetric phase diagram where a uniform co-crystal phase will may not necessarily form [18, 19]. By considering the phase diagram, the API-to-coformer ratio for the solvent system used can be changed to ensure the

generation of pure co-crystal at the desired stoichiometric ratio. Recent studies detailing alternative methods of co-crystal phase diagram generation have been published which can accelerate this traditionally time-consuming method [20, 21]. Using the phase diagram approach, may make the generation of co-crystals through spray drying more successful and controllable.

The 3-FN spray drying method was shown to be successful in the preparation of solid dispersions and co-crystals. However, further optimisation of the spray drying process parameters to increase drying yield and ensure consistent drug loading of solid dispersions is required. It is likely that altering process parameters to reduce the volume of feedstock arriving at the nozzle tip for atomisation, like that seen with the 2-FN nozzle spray drying method, will achieve this goal. This may be achieved through a balance of flow rate, inlet temperature and feedstock concentration which would need to be optimised for each individual system. The “design of experiments” factorial design approach would be beneficial in this area, as these three parameters could be varied to assess differences in yield, drug loading and *in vitro* formulation characteristics. There is also research to suggest that alternating which feedstock travels through the “internal” or “external” channel can alter the composition of the final product. This is an interesting future direction as it may be a method for encouraging different core and shell composition for the particles, leading to distinct physical properties [22].

In Chapter 4, the solid dispersions generated from solution and suspension feedstocks showed different proportions of residual crystallinity and thus displayed different dissolution release kinetics. It would be interesting to investigate whether the proportion of residual crystallinity and drug salt particle size within the polymer matrix could be precisely adjusted through optimising spray drying parameters and feedstock compositions. Investigation in this area may lead to the development of solid dispersions with tailored release kinetics.

## References


1. J. S. Shim and J. O. Liu, *Int J Biol Sci*, 2014, **10**, 654-663.
2. S. D. Anderson, *Advanced Drug Delivery Reviews*, 2018, **133**, 19-33.
3. S. P. Patil, S. R. Modi and A. K. Bansal, *Eur J Pharm Sci*, 2014, **62**, 251-257.
4. D. Walsh, D. R. Serrano, Z. A. Worku, A. M. Madi, P. O'Connell, B. Twamley and A. M. Healy, *International Journal of Pharmaceutics*, 2018, **551**, 241-256.
5. J. Weng, S. N. Wong, X. Xu, B. Xuan, C. Wang, R. Chen, C. C. Sun, R. Lakerveld, P. C. L. Kwok and S. F. Chow, *Crystal Growth & Design*, 2019, **19**, 2736-2745.
6. L. H. do Amaral, F. A. do Carmo, M. I. Amaro, V. P. de Sousa, L. C. R. P. da Silva, G. S. de Almeida, C. R. Rodrigues, A. M. Healy and L. M. Cabral, *AAPS PharmSciTech*, 2018, **19**, 2687-2699.
7. A. V. Trask, W. D. S. Motherwell and W. Jones, *Crystal Growth & Design*, 2005, **5**, 1013-1021.
8. A. C. de Almeida, C. Torquetti, P. O. Ferreira, R. P. Fernandes, E. C. dos Santos, A. C. Kogawa and F. J. Caires, *Thermochimica Acta*, 2020, **685**, 178346.
9. M. Karimi-Jafari, A. Ziaee, E. O'Reilly, D. Croker and G. Walker, *Journal*, 2022, **14**.
10. A. C. de Almeida, P. O. Ferreira, C. Torquetti, B. Ekawa, A. C. S. Carvalho, E. C. dos Santos and F. J. Caires, *Journal of Thermal Analysis and Calorimetry*, 2020, **140**, 2293-2303.
11. C. Torquetti, P. O. Ferreira, A. C. de Almeida, R. P. Fernandes and F. J. Caires, *Journal of Thermal Analysis and Calorimetry*, 2022, **147**, 1299-1306.
12. O. Shemchuk, S. d'Agostino, C. Fiore, V. Sambri, S. Zannoli, F. Grepioni and D. Braga, *Crystal Growth & Design*, 2020, **20**, 6796-6803.
13. Y. P. Nugraha, H. Sugiyama and H. Uekusa, *Acta Crystallographica Section E*, 2022, **78**, 259-263.
14. A. Gunnam, K. Suresh, R. Ganduri and A. Nangia, *Chemical Communications*, 2016, **52**, 12610-12613.
15. D. N. Price, L. R. Stromberg, N. K. Kunda and P. Muttil, *Molecular Pharmaceutics*, 2017, **14**, 4741-4750.
16. M. Karashima, N. Sano, S. Yamamoto, Y. Arai, K. Yamamoto, N. Amano and Y. Ikeda, *European Journal of Pharmaceutics and Biopharmaceutics*, 2017, **115**, 65-72.
17. Y. B. Wang, A. B. Watts, J. I. Peters, S. Liu, A. Batra and R. O. Williams, 3rd, *AAPS PharmSciTech*, 2014, **15**, 981-993.

18. Q. Jia, J. Wang, S. Zhang, J. Zhang, N. Liu and K. Kou, *RSC Advances*, 2021, **11**, 9542-9549.
19. T. Leyssens, G. Springuel, R. Montis, N. Candoni and S. Veesler, *Crystal Growth & Design*, 2012, **12**, 1520-1530.
20. V. Svoboda, R. Venkatramanan, M. Jaap, L. Lue, J. H. ter Horst and J. Sefcik, *Crystal Growth & Design*, 2022, **22**, 3376-3384.
21. C. Loschen and A. Klamt, *Crystal Growth & Design*, 2018, **18**, 5600-5608.
22. A. Mohammed, J. Zurek, S. Madueke, H. Al-Kassimy, M. Yaqoob, C. Houacine, A. Ferraz, R. Kalgudi, M. G. Zariwala, N. Hawkins and H. Al-Obaidi, *Pharmaceutical Research*, 2020, **37**, 150.

## Supplementary Information

# Preparation and Physiochemical Analysis of Novel Ciprofloxacin / Dicarboxylic Acid Salts

Supplementary Information

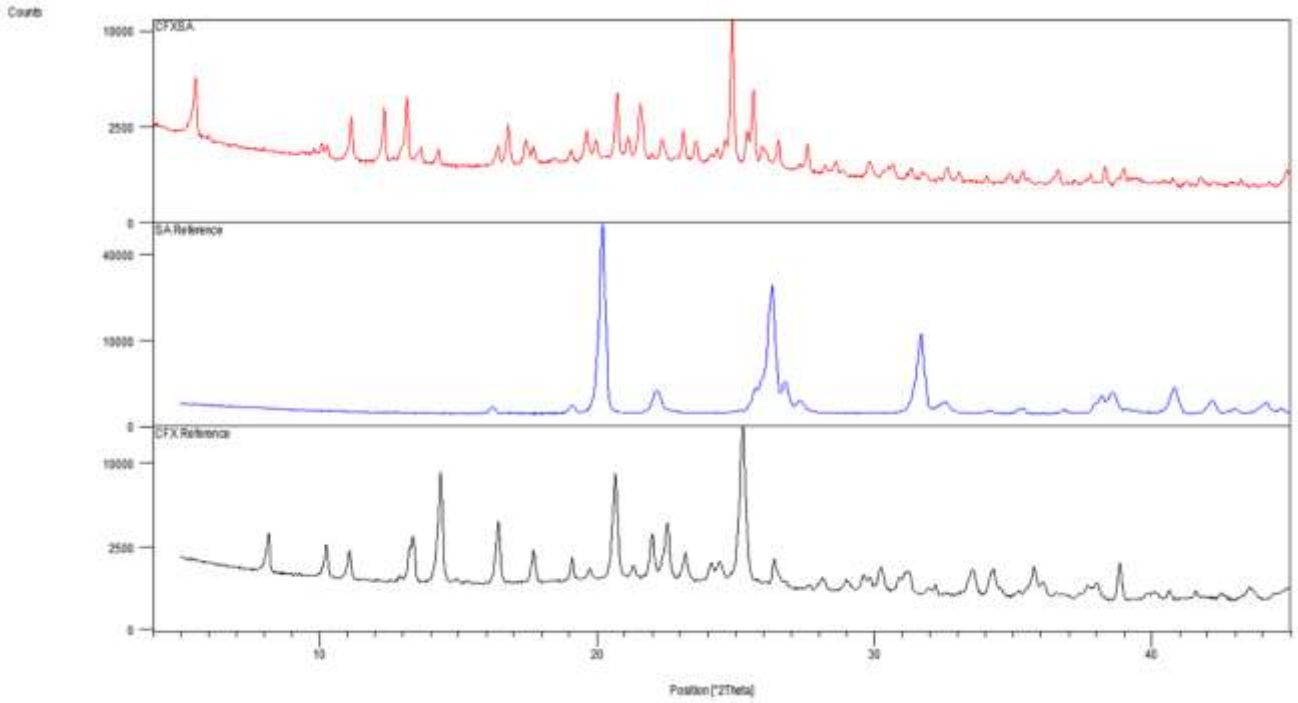


**Figure S1:** XRPD data comparing milled CFXSA with CFX and SA starting materials

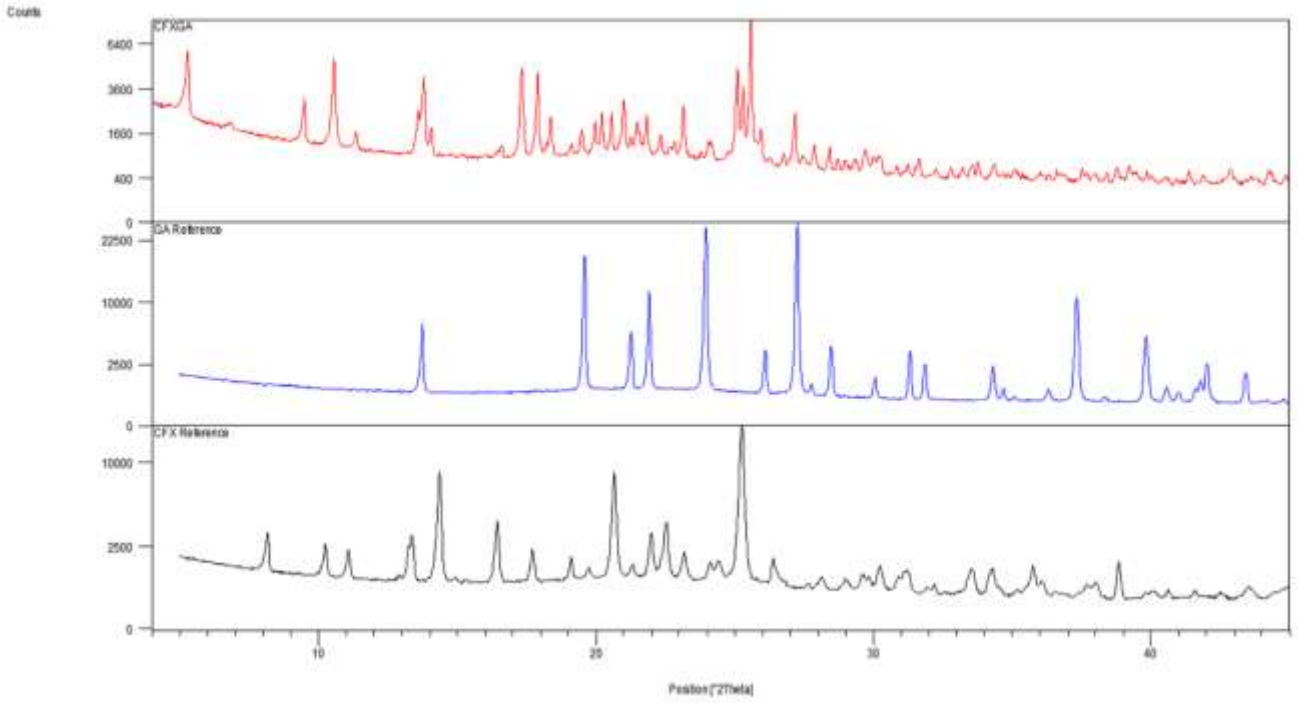


**Figure S2:** XRPD data comparing milled CFXGA with CFX and GA starting materials

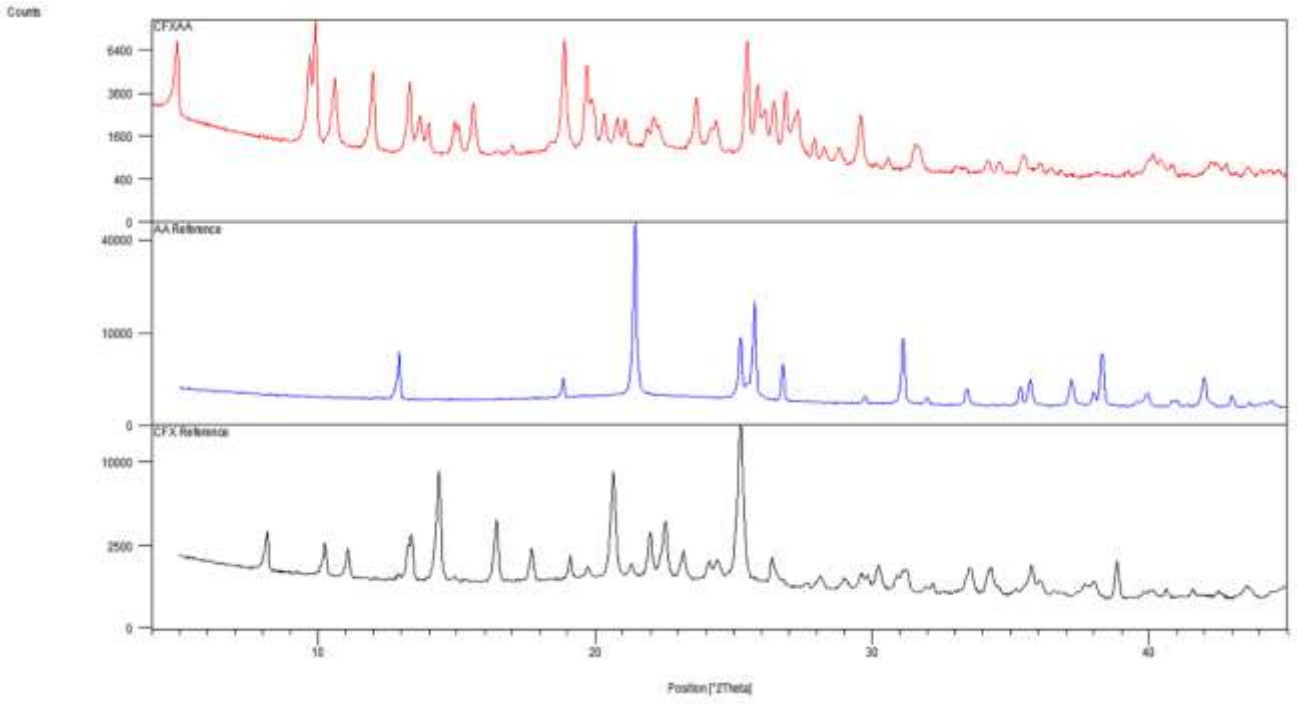


**Figure S3:** XRPD data comparing milled CFXAA with CFX and AA starting materials

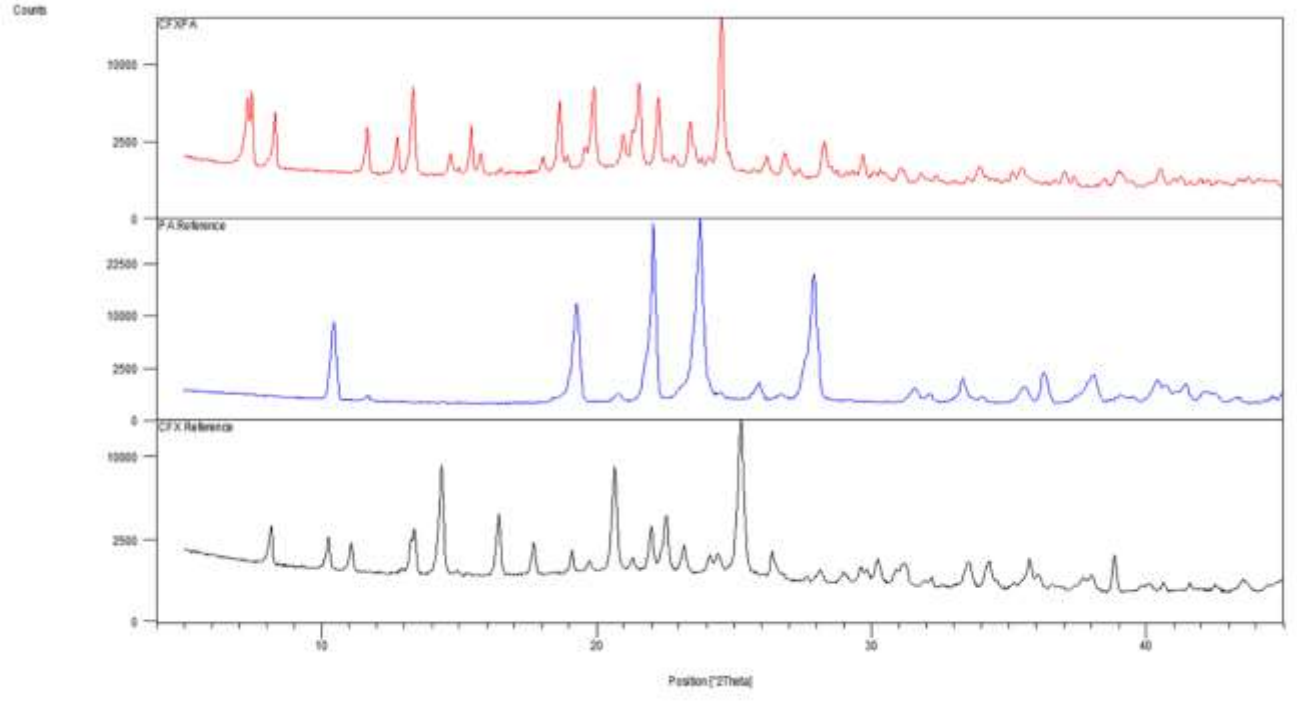


**Figure S4:** XRPD data comparing milled CFXPA with CFX and PA starting materials

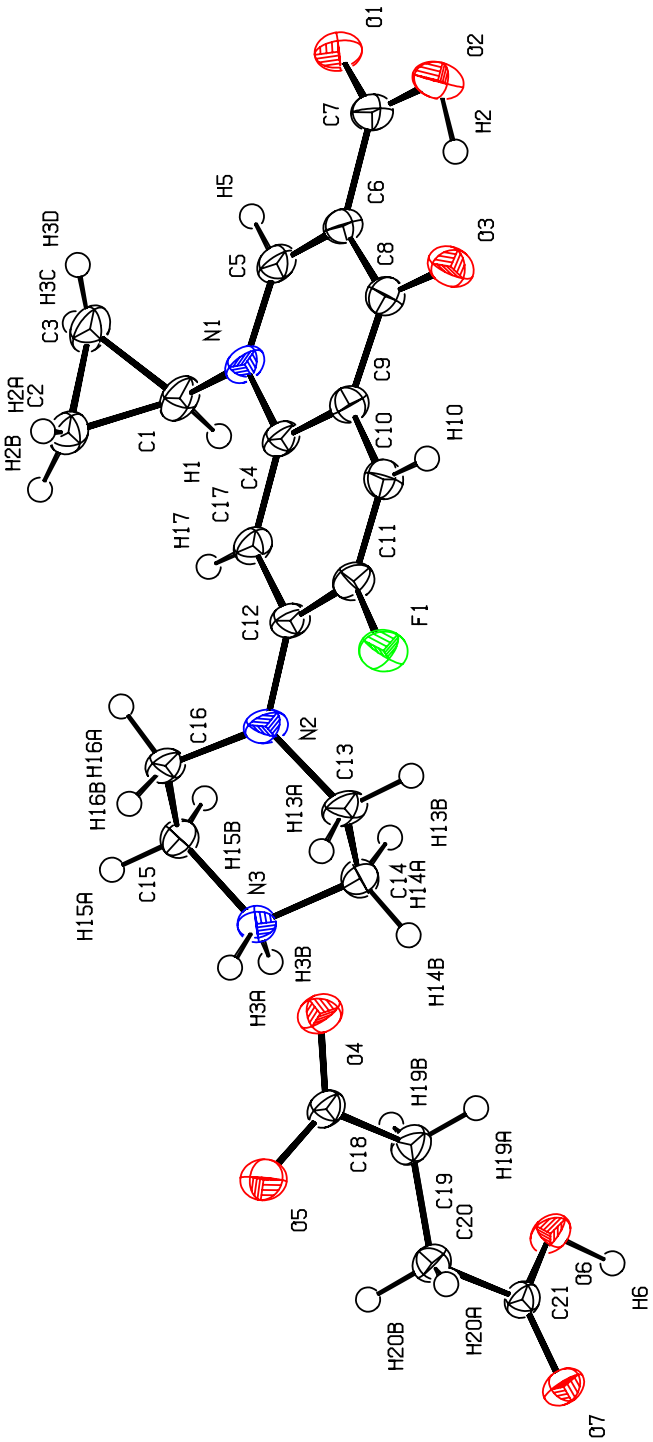


**Figure S5A**: ORTEP view of asymmetric unit of CFX-SA with atom labelling

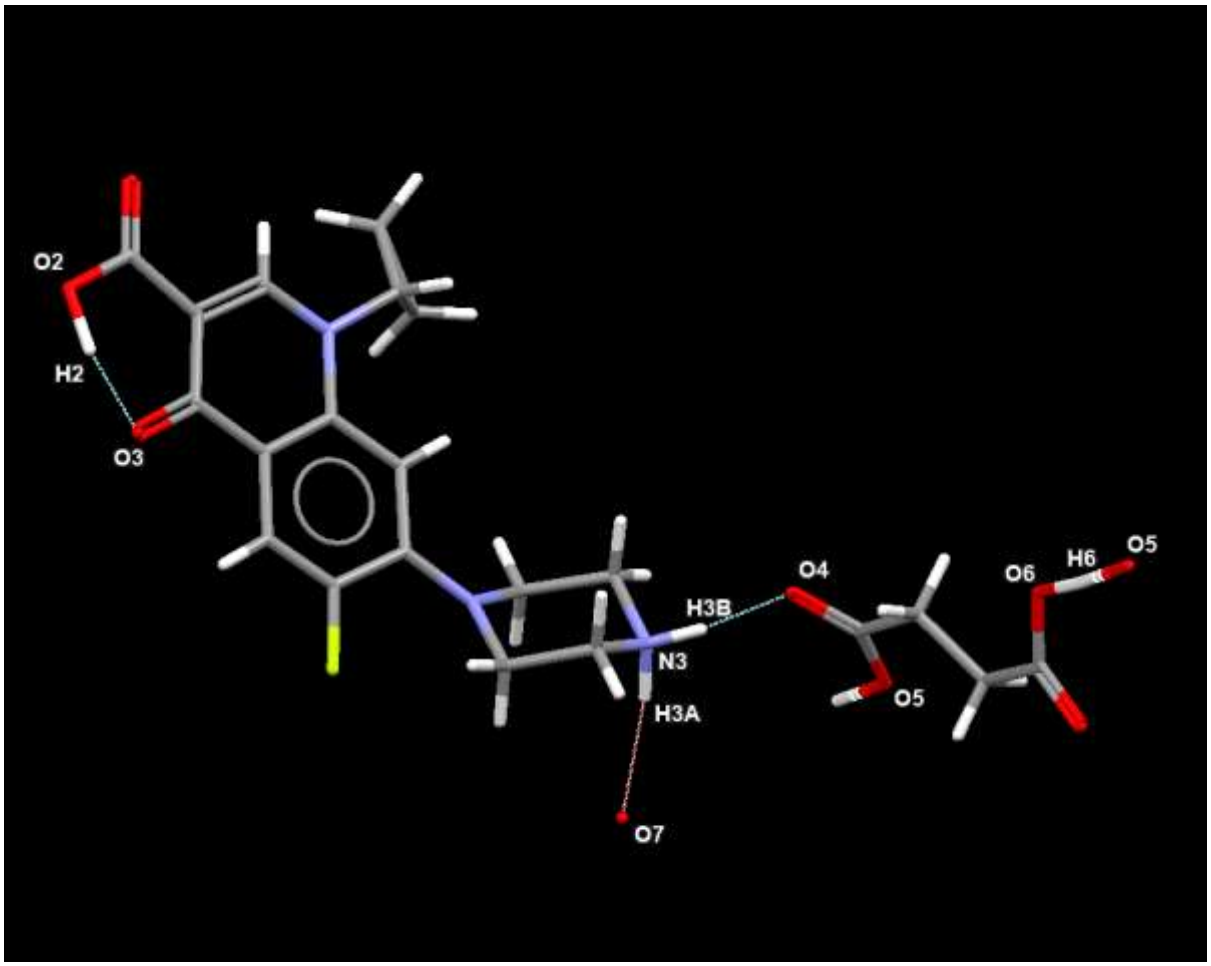


| Donor | H | Accept | D-H / Å | H…A / Å | D…A / Å | D-H…A / ° | Symm |
|---|---|---|---|---|---|---|---|
| O2 | H2 | O3 | 1.04(4) | 1.53(4) | 2.545(2) | 163(3) | x,y,z |
| N3 | H3A | O7 | 0.94(3) | 1.98(3) | 2.8703(19) | 157(2) | -x+1,-y+2,-z |
| N3 | H3B | O4 | 0.92(2) | 1.75(2) | 2.654(2) | 167(2) | x,y,z |
| O6 | H6 | O5 | 1.09(3) | 1.35(3) | 2.4384(17) | 175(2) | x-1,y,z |

**Figure S5B**. A Mercury diagram for the asymmetric unit of CFX-SA, showing the unique set of hydrogen bonds (dashed lines) and the associated bond distances and angles.

**Table S1** Bond distances and angles for CFX-SA

```
loop_
_space_group_symop_id
_space_group_symop_operation_xyz
   1 x,y,z
   2 -x,-y,-z

_geom_special_details
;
 Bond distances, angles etc. have been calculated using the
 rounded fractional coordinates. All su's are estimated
 from the variances of the (full) variance-covariance matrix.
 The cell esds are taken into account in the estimation of
 distances, angles and torsion angles
;

loop_
_geom_bond_atom_site_label_1
_geom_bond_atom_site_label_2
_geom_bond_distance
_geom_bond_site_symmetry_1
_geom_bond_site_symmetry_2
_geom_bond_publ_flag
 F1      C11        1.360(2)                    .      .                 yes
 O1      C7         1.221(2)                    .      .                 yes
 O2      C7         1.329(3)                    .      .                 yes
 O3      C8         1.266(2)                    .      .                 yes
 N1      C1         1.453(3)                    .      .                 yes
 N1      C4         1.403(2)                    .      .                 yes
 N1      C5         1.340(3)                    .      .                 yes
 N2      C12        1.375(2)                    .      .                 yes
 N2      C13        1.467(2)                    .      .                 yes
 N2      C16        1.455(2)                    .      .                 yes
 O2      H2          1.04(4)                    .      .                 no
 N3      C14        1.490(2)                    .      .                 yes
 N3      C15        1.495(2)                    .      .                 yes
 C1      C3         1.494(3)                    .      .                 no
 C1      C2         1.499(3)                    .      .                 no
 C2      C3         1.500(3)                    .      .                 no
 N3      H3B         0.92(2)                    .      .                 no
 N3      H3A         0.94(3)                    .      .                 no
 C4      C17        1.402(3)                    .      .                 no
 C4      C9         1.409(3)                    .      .                 no
 O4      C18        1.242(2)                    .      .                 yes
 O5      C18        1.274(2)                    .      .                 yes
 C5      C6         1.365(3)                    .      .                 no
 C6      C8         1.434(3)                    .      .                 no
 O6      C21        1.297(2)                    .      .                 yes
 C6      C7         1.486(3)                    .      .                 no
 O7      C21        1.235(2)                    .      .                 yes
 C8      C9         1.445(3)                    .      .                 no
 C9      C10        1.407(3)                    .      .                 no
 C10     C11        1.350(3)                    .      .                 no
 C11     C12        1.420(3)                    .      .                 no
 C12     C17        1.396(2)                    .      .                 no
 C13     C14        1.509(3)                    .      .                 no
 C15     C16        1.515(3)                    .      .                 no
 C1      H1          0.97(2)                    .      .                 no
 C2      H2A          0.9700                    .      .                 no
 C2      H2B          0.9700                    .      .                 no
 C3      H3D          0.9700                    .      .                 no
 C3      H3C          0.9700                    .      .                 no
 C5      H5           0.9300                    .      .                 no
 O6      H6          1.09(3)                    .      .                 no
 C10     H10          0.9300                    .      .                 no
 C13     H13A         0.9700                    .      .                 no
 C13     H13B         0.9700                    .      .                 no
```

```
 C14     H14B         0.9700                    .       .                no
 C14     H14A         0.9700                    .       .                no
 C15     H15A         0.9700                    .       .                no
 C15     H15B         0.9700                    .       .                no
 C16     H16A         0.9700                    .       .                no
 C16     H16B         0.9700                    .       .                no
 C17     H17          0.9300                    .       .                no
 C18     C19        1.504(2)                    .       .                no
 C19     C20        1.521(3)                    .       .                no
 C20     C21        1.510(2)                    .       .                no
 C19     H19A         0.9700                    .       .                no
 C19     H19B         0.9700                    .       .                no
 C20     H20A         0.9700                    .       .                no
 C20     H20B         0.9700                    .       .                no

loop_
_geom_angle_atom_site_label_1
_geom_angle_atom_site_label_2
_geom_angle_atom_site_label_3
_geom_angle
_geom_angle_site_symmetry_1
_geom_angle_site_symmetry_2
_geom_angle_site_symmetry_3
_geom_angle_publ_flag
 C1      N1      C4       119.99(15)              .       .       .       yes
 C1      N1      C5       120.08(15)              .       .       .       yes
 C4      N1      C5       119.74(16)              .       .       .       yes
 C12     N2      C13      121.75(15)              .       .       .       yes
 C12     N2      C16      123.29(15)              .       .       .       yes
 C13     N2      C16      114.63(15)              .       .       .       yes
 C7      O2      H2        101.3(18)              .       .       .       no
 C14     N3      C15      110.94(14)              .       .       .       yes
 N1      C1      C2       119.10(14)              .       .       .       yes
 N1      C1      C3       118.05(16)              .       .       .       yes
 C2      C1      C3        60.14(13)              .       .       .       no
 C1      C2      C3        59.79(13)              .       .       .       no
 C15     N3      H3A       110.3(15)              .       .       .       no
 C15     N3      H3B       108.5(17)              .       .       .       no
 H3A     N3      H3B          112(2)              .       .       .       no
 C1      C3      C2        60.07(13)              .       .       .       no
 C14     N3      H3A       109.3(15)              .       .       .       no
 C14     N3      H3B       106.0(15)              .       .       .       no
 C9      C4      C17      120.94(16)              .       .       .       no
 N1      C4      C17      120.53(16)              .       .       .       yes
 N1      C4      C9       118.50(16)              .       .       .       yes
 N1      C5      C6       124.24(17)              .       .       .       yes
 C5      C6      C8       120.23(18)              .       .       .       no
 C5      C6      C7       118.34(17)              .       .       .       no
 C7      C6      C8       121.41(18)              .       .       .       no
 O1      C7      C6         122.6(2)              .       .       .       yes
 O1      C7      O2         121.7(2)              .       .       .       yes
 O2      C7      C6       115.76(17)              .       .       .       yes
 C6      C8      C9       115.29(17)              .       .       .       no
 O3      C8      C6       122.83(17)              .       .       .       yes
 O3      C8      C9       121.88(17)              .       .       .       yes
 C4      C9      C10      117.92(16)              .       .       .       no
 C8      C9      C10      120.12(17)              .       .       .       no
 C4      C9      C8       121.95(16)              .       .       .       no
 C9      C10     C11      119.99(17)              .       .       .       no
 C10     C11     C12      123.93(17)              .       .       .       no
 F1      C11     C12      117.52(15)              .       .       .       yes
 F1      C11     C10      118.53(16)              .       .       .       yes
 N2      C12     C11      120.72(16)              .       .       .       yes
 N2      C12     C17      123.29(16)              .       .       .       yes
 C11     C12     C17      115.97(16)              .       .       .       no
 N2      C13     C14      110.57(15)              .       .       .       yes
 N3      C14     C13      110.29(17)              .       .       .       yes
 N3      C15     C16      110.12(14)              .       .       .       yes
```

```
 N2      C16     C15      112.05(17)          .       .       .          yes
 C4      C17     C12      121.09(16)          .       .       .          no
 N1      C1      H1        113.4(15)          .       .       .          no
 C2      C1      H1        117.5(14)          .       .       .          no
 C3      C1      H1        118.8(16)          .       .       .          no
 C1      C2      H2A          118.00          .       .       .          no
 C1      C2      H2B          118.00          .       .       .          no
 C3      C2      H2A          118.00          .       .       .          no
 C3      C2      H2B          118.00          .       .       .          no
 H2A     C2      H2B          115.00          .       .       .          no
 C1      C3      H3C          118.00          .       .       .          no
 C1      C3      H3D          118.00          .       .       .          no
 C2      C3      H3C          118.00          .       .       .          no
 C2      C3      H3D          118.00          .       .       .          no
 H3C     C3      H3D          115.00          .       .       .          no
 N1      C5      H5           118.00          .       .       .          no
 C6      C5      H5           118.00          .       .       .          no
 C21     O6      H6        114.3(15)          .       .       .          no
 C9      C10     H10          120.00          .       .       .          no
 C11     C10     H10          120.00          .       .       .          no
 N2      C13     H13B         110.00          .       .       .          no
 C14     C13     H13A         110.00          .       .       .          no
 C14     C13     H13B         110.00          .       .       .          no
 H13A    C13     H13B         108.00          .       .       .          no
 N2      C13     H13A         110.00          .       .       .          no
 N3      C14     H14B         110.00          .       .       .          no
 C13     C14     H14A         110.00          .       .       .          no
 N3      C14     H14A         110.00          .       .       .          no
 H14A    C14     H14B         108.00          .       .       .          no
 C13     C14     H14B         110.00          .       .       .          no
 N3      C15     H15A         110.00          .       .       .          no
 N3      C15     H15B         110.00          .       .       .          no
 C16     C15     H15B         110.00          .       .       .          no
 H15A    C15     H15B         108.00          .       .       .          no
 C16     C15     H15A         110.00          .       .       .          no
 N2      C16     H16B         109.00          .       .       .          no
 C15     C16     H16A         109.00          .       .       .          no
 C15     C16     H16B         109.00          .       .       .          no
 H16A    C16     H16B         108.00          .       .       .          no
 N2      C16     H16A         109.00          .       .       .          no
 C12     C17     H17          119.00          .       .       .          no
 C4      C17     H17          119.00          .       .       .          no
 O4      C18     O5        124.25(15)         .       .       .          yes
 O5      C18     C19       116.89(16)         .       .       .          yes
 O4      C18     C19       118.85(16)         .       .       .          yes
 C18     C19     C20       114.13(14)         .       .       .          no
 C19     C20     C21       114.87(14)         .       .       .          no
 O6      C21     C20       115.18(14)         .       .       .          yes
 O7      C21     C20       120.72(15)         .       .       .          yes
 O6      C21     O7        124.09(14)         .       .       .          yes
 C18     C19     H19A         109.00          .       .       .          no
 C18     C19     H19B         109.00          .       .       .          no
 C20     C19     H19A         109.00          .       .       .          no
 C20     C19     H19B         109.00          .       .       .          no
 H19A    C19     H19B         108.00          .       .       .          no
 C19     C20     H20A         109.00          .       .       .          no
 C19     C20     H20B         109.00          .       .       .          no
 C21     C20     H20A         109.00          .       .       .          no
 C21     C20     H20B         109.00          .       .       .          no
 H20A    C20     H20B         108.00          .       .       .          no

loop_
_geom_torsion_atom_site_label_1
_geom_torsion_atom_site_label_2
_geom_torsion_atom_site_label_3
_geom_torsion_atom_site_label_4
_geom_torsion
_geom_torsion_site_symmetry_1
```

```
_geom_torsion_site_symmetry_2
_geom_torsion_site_symmetry_3
_geom_torsion_site_symmetry_4
_geom_torsion_publ_flag
 C4      N1      C1      C2          71.3(2)     .       .       .       .   no
 C4      N1      C1      C3        140.86(17)    .       .       .       .   no
 C5      N1      C1      C2       -113.71(18)    .       .       .       .   no
 C5      N1      C1      C3         -44.1(2)     .       .       .       .   no
 C1      N1      C4      C9        176.11(14)    .       .       .       .   no
 C1      N1      C4      C17        -1.7(2)     .       .       .       .   no
 C5      N1      C4      C9          1.1(2)     .       .       .       .   no
 C5      N1      C4      C17      -176.74(14)    .       .       .       .   no
 C1      N1      C5      C6       -175.71(15)    .       .       .       .   no
 C4      N1      C5      C6         -0.7(2)     .       .       .       .   no
 C13     N2      C12     C11        -41.7(2)    .       .       .       .   no
 C13     N2      C12     C17       140.15(17)    .       .       .       .   no
 C16     N2      C12     C11       145.33(17)    .       .       .       .   no
 C16     N2      C12     C17        -32.8(2)    .       .       .       .   no
 C12     N2      C13     C14      -120.44(18)    .       .       .       .   no
 C16     N2      C13     C14         53.1(2)    .       .       .       .   no
 C12     N2      C16     C15       121.44(17)    .       .       .       .   no
 C13     N2      C16     C15        -52.0(2)    .       .       .       .   no
 C15     N3      C14     C13        58.65(18)    .       .       .       .   no
 C14     N3      C15     C16       -56.65(19)    .       .       .       .   no
 N1      C1      C2      C3        107.52(19)    .       .       .       .   no
 N1      C1      C3      C2       -109.24(17)    .       .       .       .   no
 N1      C4      C9      C8         -2.2(2)     .       .       .       .   no
 N1      C4      C9      C10       178.89(14)    .       .       .       .   no
 C17     C4      C9      C8        175.65(14)    .       .       .       .   no
 C17     C4      C9      C10        -3.3(2)     .       .       .       .   no
 N1      C4      C17     C12       178.77(14)    .       .       .       .   no
 C9      C4      C17     C12         1.0(2)     .       .       .       .   no
 N1      C5      C6      C7        179.72(16)    .       .       .       .   no
 N1      C5      C6      C8          1.3(2)     .       .       .       .   no
 C5      C6      C7      O1          0.5(3)     .       .       .       .   no
 C5      C6      C7      O2       -179.14(16)    .       .       .       .   no
 C8      C6      C7      O1         178.9(2)    .       .       .       .   no
 C8      C6      C7      O2         -0.8(3)     .       .       .       .   no
 C5      C6      C8      O3        176.79(15)    .       .       .       .   no
 C5      C6      C8      C9         -2.2(2)     .       .       .       .   no
 C7      C6      C8      O3         -1.6(2)     .       .       .       .   no
 C7      C6      C8      C9        179.46(15)    .       .       .       .   no
 O3      C8      C9      C4       -176.32(15)    .       .       .       .   no
 O3      C8      C9      C10         2.6(2)     .       .       .       .   no
 C6      C8      C9      C4          2.7(2)     .       .       .       .   no
 C6      C8      C9      C10      -178.43(14)    .       .       .       .   no
 C4      C9      C10     C11         1.9(2)     .       .       .       .   no
 C8      C9      C10     C11      -177.08(14)    .       .       .       .   no
 C9      C10     C11     F1       -176.36(14)    .       .       .       .   no
 C9      C10     C11     C12         1.9(2)     .       .       .       .   no
 F1      C11     C12     N2         -4.1(2)     .       .       .       .   no
 F1      C11     C12     C17       174.16(13)    .       .       .       .   no
 C10     C11     C12     N2        177.60(15)    .       .       .       .   no
 C10     C11     C12     C17        -4.1(2)     .       .       .       .   no
 N2      C12     C17     C4       -179.18(15)    .       .       .       .   no
 C11     C12     C17     C4          2.6(2)     .       .       .       .   no
 N2      C13     C14     N3         -55.5(2)    .       .       .       .   no
 N3      C15     C16     N2         52.54(19)    .       .       .       .   no
 O4      C18     C19     C20       163.18(17)    .       .       .       .   no
 O5      C18     C19     C20        -17.7(2)    .       .       .       .   no
 C18     C19     C20     C21      -175.77(15)    .       .       .       .   no
 C19     C20     C21     O6         -18.9(2)    .       .       .       .   no
 C19     C20     C21     O7        161.98(16)    .       .       .       .   no

loop_
_geom_hbond_atom_site_label_D
_geom_hbond_atom_site_label_H
_geom_hbond_atom_site_label_A
```

```
_geom_hbond_distance_DH
_geom_hbond_distance_HA
_geom_hbond_distance_DA
_geom_hbond_angle_DHA
_geom_hbond_site_symmetry_A
_geom_hbond_publ_flag
#
#D   H   A   D - H  H...A   D...A    D - H...A  symm(A)
#
O2      H2      O3         1.04(4)    1.53(4)   2.545(2)     163(3)     .   yes
N3      H3A     O7         0.94(3)    1.98(3) 2.8703(19)     157(2)   2_675 yes
N3      H3B     O4         0.92(2)    1.75(2)   2.654(2)     167(2)     .   yes
O6      H6      O5         1.09(3)    1.35(3) 2.4384(17)     175(2)   1_455 yes
```

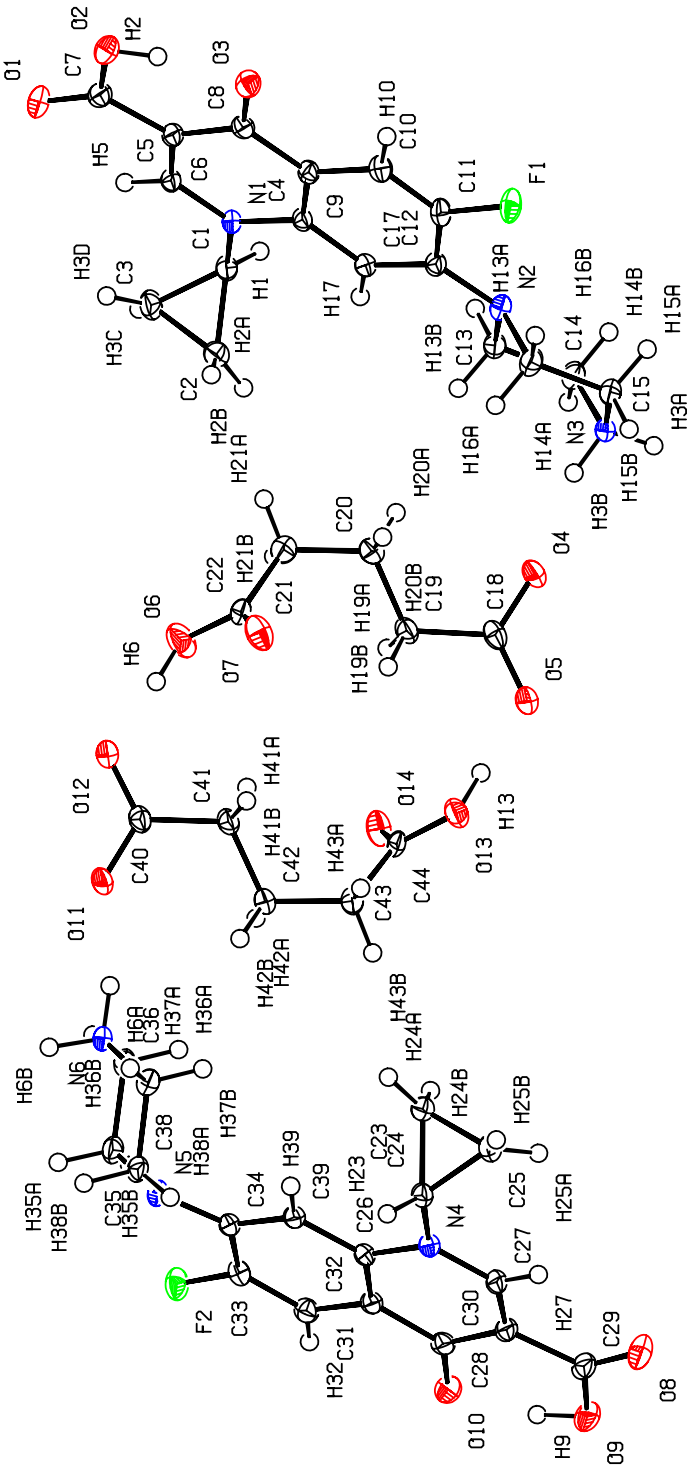


**Figure S6A**: ORTEP view of asymmetric unit of CFX-GA with atom labelling

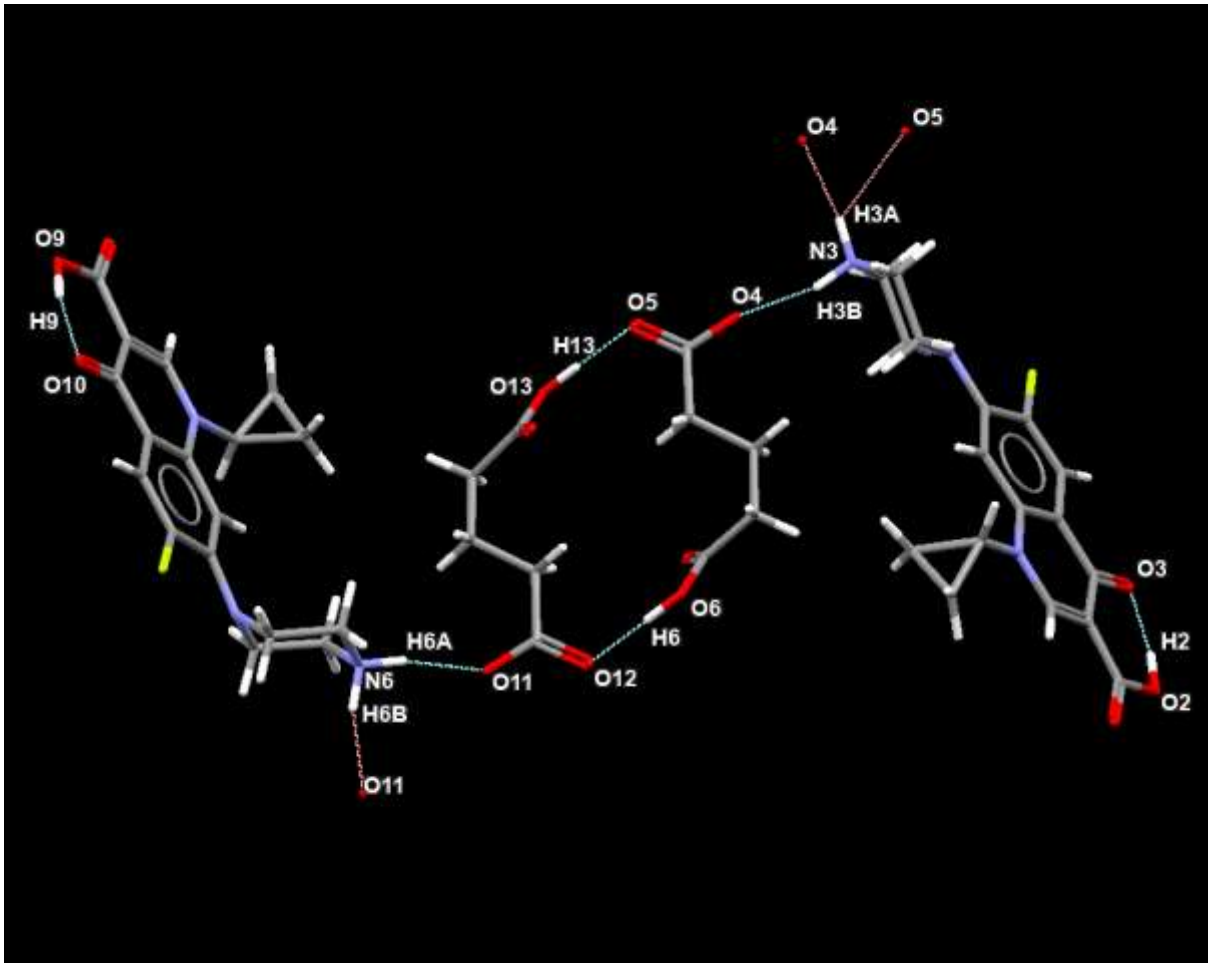


| Donor | H | Accept | D-H / Å | H…A / Å | D…A / Å | D-H…A / ° | Symm |
|---|---|---|---|---|---|---|---|
| O2 | H2 | O3 | 0.93(2) | 1.63(2) | 2.5188(13) | 161(2) | x,y,z |
| N3 | H3A | O4 | 0.912(18) | 1.904(18) | 2.8081(14) | 170.9(14) | -x-1,-y+1,-z+1 |
| N3 | H3A | O5 | 0.912(18) | 2.358(16) | 2.9996(14) | 127.3(13) | -x-1,-y+1,-z+1 |
| N3 | H3B | O4 | 0.913(16) | 1.864(16) | 2.7553(13) | 164.9(16) | x,y,z |
| O6 | H6 | O12 | 0.95(2) | 1.58(2) | 2.5148(14) | 169(2) | x,y,z |
| N6 | H6A | O11 | 0.929(16) | 1.818(16) | 2.7328(13) | 167.8(15) | x,y,z |
| N6 | H6B | O11 | 0.938(16) | 1.845(16) | 2.7575(13) | 163.5(14) | -x+2,-y+1,-z+2 |
| O9 | H9 | O10 | 0.95(2) | 1.61(2) | 2.5308(13) | 159.9(19) | x,y,z |
| O13 | H13 | O5 | 0.94(2) | 1.57(2) | 2.5017(12) | 169(2) | x,y,z |

**Figure S6B**. A Mercury diagram for the asymmetric unit of CFX-GA, showing the unique set of hydrogen bonds (dashed lines) and the associated bond distances and angles.

**Table S2** Bond distances and angles for CFX-GA

```
loop_
_space_group_symop_id
_space_group_symop_operation_xyz
   1 x,y,z
   2 -x,-y,-z


_geom_special_details
;
 Bond distances, angles etc. have been calculated using the
 rounded fractional coordinates. All su's are estimated
 from the variances of the (full) variance-covariance matrix.
 The cell esds are taken into account in the estimation of
 distances, angles and torsion angles
;


loop_
_geom_bond_atom_site_label_1
_geom_bond_atom_site_label_2
_geom_bond_distance
_geom_bond_site_symmetry_1
_geom_bond_site_symmetry_2
_geom_bond_publ_flag
 F1      C11      1.3556(13)                    .      .                 yes
 O1      C7       1.2121(16)                    .      .                 yes
 O2      C7       1.3366(15)                    .      .                 yes
 O3      C8       1.2698(14)                    .      .                 yes
 N1      C1       1.4567(15)                    .      .                 yes
 N1      C4       1.4030(14)                    .      .                 yes
 N1      C5       1.3384(15)                    .      .                 yes
 N2      C12      1.3986(15)                    .      .                 yes
 N2      C13      1.4608(15)                    .      .                 yes
 N2      C16      1.4777(15)                    .      .                 yes
 O2      H2          0.93(2)                    .      .                 no
 F2      C33      1.3561(13)                    .      .                 yes
 N3      C14      1.4884(16)                    .      .                 yes
 N3      C15      1.4894(15)                    .      .                 yes
 C1      C3       1.4962(16)                    .      .                 no
 C1      C2       1.4986(17)                    .      .                 no
 C2      C3       1.5044(17)                    .      .                 no
 N3      H3B       0.913(16)                    .      .                 no
 N3      H3A       0.912(18)                    .      .                 no
 C4      C17      1.4030(16)                    .      .                 no
 C4      C9       1.4064(16)                    .      .                 no
 C5      C6       1.3734(16)                    .      .                 no
 C6      C8       1.4296(16)                    .      .                 no
 C6      C7       1.4836(16)                    .      .                 no
 O8      C29      1.2107(16)                    .      .                 yes
 C8      C9       1.4471(16)                    .      .                 no
 O9      C29      1.3362(14)                    .      .                 yes
 C9      C10      1.4121(16)                    .      .                 no
 C10     C11      1.3541(16)                    .      .                 no
 O10     C30      1.2700(14)                    .      .                 yes
 C11     C12      1.4189(16)                    .      .                 no
 C12     C17      1.3922(16)                    .      .                 no
 C13     C14      1.5136(17)                    .      .                 no
 C15     C16      1.5147(16)                    .      .                 no
 C1      H1           0.9800                    .      .                 no
 C2      H2A          0.9700                    .      .                 no
 C2      H2B          0.9700                    .      .                 no
 C3      H3D          0.9700                    .      .                 no
 C3      H3C          0.9700                    .      .                 no
 N4      C26      1.4000(14)                    .      .                 yes
 N4      C27      1.3424(15)                    .      .                 yes
 N4      C23      1.4573(15)                    .      .                 yes
```

| | | | | | |
|---|---|---|---|---|---|
| N5 | C34 | 1.3816(15) | . | . | yes |
| C5 | H5 | 0.9300 | . | . | no |
| N5 | C38 | 1.4621(15) | . | . | yes |
| N5 | C35 | 1.4690(15) | . | . | yes |
| N6 | C36 | 1.4918(15) | . | . | yes |
| N6 | C37 | 1.4930(15) | . | . | yes |
| O9 | H9 | 0.95(2) | . | . | no |
| C10 | H10 | 0.9300 | . | . | no |
| C13 | H13A | 0.9700 | . | . | no |
| C13 | H13B | 0.9700 | . | . | no |
| C14 | H14A | 0.9700 | . | . | no |
| C14 | H14B | 0.9700 | . | . | no |
| C15 | H15B | 0.9700 | . | . | no |
| C15 | H15A | 0.9700 | . | . | no |
| C16 | H16A | 0.9700 | . | . | no |
| C16 | H16B | 0.9700 | . | . | no |
| C17 | H17 | 0.9300 | . | . | no |
| O4 | C18 | 1.2598(14) | . | . | yes |
| O5 | C18 | 1.2560(14) | . | . | yes |
| N6 | H6B | 0.938(16) | . | . | no |
| N6 | H6A | 0.929(16) | . | . | no |
| O6 | C22 | 1.3140(15) | . | . | yes |
| O7 | C22 | 1.2100(15) | . | . | yes |
| C23 | C24 | 1.5010(16) | . | . | no |
| C23 | C25 | 1.4934(16) | . | . | no |
| C24 | C25 | 1.5076(16) | . | . | no |
| C26 | C39 | 1.4031(16) | . | . | no |
| C26 | C31 | 1.4100(16) | . | . | no |
| C27 | C28 | 1.3753(16) | . | . | no |
| C28 | C30 | 1.4350(16) | . | . | no |
| C28 | C29 | 1.4866(17) | . | . | no |
| C30 | C31 | 1.4454(16) | . | . | no |
| C31 | C32 | 1.4091(16) | . | . | no |
| C32 | C33 | 1.3576(16) | . | . | no |
| C33 | C34 | 1.4208(16) | . | . | no |
| C34 | C39 | 1.3969(16) | . | . | no |
| C35 | C36 | 1.5213(16) | . | . | no |
| C37 | C38 | 1.5212(16) | . | . | no |
| O6 | H6 | 0.95(2) | . | . | no |
| C23 | H23 | 0.9800 | . | . | no |
| C24 | H24B | 0.9700 | . | . | no |
| C24 | H24A | 0.9700 | . | . | no |
| C25 | H25B | 0.9700 | . | . | no |
| C25 | H25A | 0.9700 | . | . | no |
| C27 | H27 | 0.9300 | . | . | no |
| C32 | H32 | 0.9300 | . | . | no |
| C35 | H35B | 0.9700 | . | . | no |
| C35 | H35A | 0.9700 | . | . | no |
| C36 | H36B | 0.9700 | . | . | no |
| C36 | H36A | 0.9700 | . | . | no |
| C37 | H37B | 0.9700 | . | . | no |
| C37 | H37A | 0.9700 | . | . | no |
| C38 | H38B | 0.9700 | . | . | no |
| C38 | H38A | 0.9700 | . | . | no |
| C39 | H39 | 0.9300 | . | . | no |
| O11 | C40 | 1.2607(14) | . | . | yes |
| O12 | C40 | 1.2569(15) | . | . | yes |
| O13 | C44 | 1.3217(15) | . | . | yes |
| O14 | C44 | 1.2111(15) | . | . | yes |
| C18 | C19 | 1.5212(16) | . | . | no |
| C19 | C20 | 1.5209(16) | . | . | no |
| C20 | C21 | 1.5283(18) | . | . | no |
| C21 | C22 | 1.5123(17) | . | . | no |
| O13 | H13 | 0.94(2) | . | . | no |
| C19 | H19B | 0.9700 | . | . | no |
| C19 | H19A | 0.9700 | . | . | no |
| C20 | H20B | 0.9700 | . | . | no |
| C20 | H20A | 0.9700 | . | . | no |

```
 C21     H21A         0.9700                   .       .                no
 C21     H21B         0.9700                   .       .                no
 C40     C41       1.5190(16)                  .       .                no
 C41     C42       1.5217(16)                  .       .                no
 C42     C43       1.5255(16)                  .       .                no
 C43     C44       1.5106(16)                  .       .                no
 C41     H41A         0.9700                   .       .                no
 C41     H41B         0.9700                   .       .                no
 C42     H42A         0.9700                   .       .                no
 C42     H42B         0.9700                   .       .                no
 C43     H43A         0.9700                   .       .                no
 C43     H43B         0.9700                   .       .                no

loop_
_geom_angle_atom_site_label_1
_geom_angle_atom_site_label_2
_geom_angle_atom_site_label_3
_geom_angle
_geom_angle_site_symmetry_1
_geom_angle_site_symmetry_2
_geom_angle_site_symmetry_3
_geom_angle_publ_flag
 C1      N1      C4        118.98(9)              .       .       .          yes
 C1      N1      C5        121.03(9)              .       .       .          yes
 C4      N1      C5       119.98(10)              .       .       .          yes
 C12     N2      C13       115.24(9)              .       .       .          yes
 C12     N2      C16       115.70(9)              .       .       .          yes
 C13     N2      C16       110.91(9)              .       .       .          yes
 C7      O2      H2        104.4(13)              .       .       .          no
 C14     N3      C15       110.81(9)              .       .       .          yes
 N1      C1      C2       117.40(10)              .       .       .          yes
 N1      C1      C3       119.75(10)              .       .       .          yes
 C2      C1      C3         60.31(8)              .       .       .          no
 C1      C2      C3         59.77(8)              .       .       .          no
 C15     N3      H3A       108.9(12)              .       .       .          no
 C15     N3      H3B       109.9(10)              .       .       .          no
 H3A     N3      H3B       108.5(15)              .       .       .          no
 C1      C3      C2         59.92(8)              .       .       .          no
 C14     N3      H3A       109.4(10)              .       .       .          no
 C14     N3      H3B       109.3(10)              .       .       .          no
 C9      C4      C17      120.77(10)              .       .       .          no
 N1      C4      C17      120.18(10)              .       .       .          yes
 N1      C4      C9       119.05(10)              .       .       .          yes
 N1      C5      C6       123.54(10)              .       .       .          yes
 C5      C6      C8       120.35(10)              .       .       .          no
 C5      C6      C7       117.93(10)              .       .       .          no
 C7      C6      C8       121.72(10)              .       .       .          no
 O1      C7      C6       123.87(11)              .       .       .          yes
 O1      C7      O2       121.52(11)              .       .       .          yes
 O2      C7      C6       114.61(11)              .       .       .          yes
 C6      C8      C9       115.77(10)              .       .       .          no
 O3      C8      C6       122.64(10)              .       .       .          yes
 O3      C8      C9       121.59(10)              .       .       .          yes
 C4      C9      C10      118.42(10)              .       .       .          no
 C8      C9      C10      120.34(10)              .       .       .          no
 C4      C9      C8       121.24(10)              .       .       .          no
 C9      C10     C11      119.58(10)              .       .       .          no
 C10     C11     C12      123.54(10)              .       .       .          no
 F1      C11     C12      117.55(10)              .       .       .          yes
 F1      C11     C10      118.89(10)              .       .       .          yes
 N2      C12     C11      119.81(10)              .       .       .          yes
 N2      C12     C17      123.36(10)              .       .       .          yes
 C11     C12     C17      116.75(10)              .       .       .          no
 N2      C13     C14       110.45(9)              .       .       .          yes
 N3      C14     C13      110.22(10)              .       .       .          yes
 N3      C15     C16       109.87(9)              .       .       .          yes
 N2      C16     C15       110.35(9)              .       .       .          yes
 C4      C17     C12      120.82(10)              .       .       .          no
```

| | | | | | | | |
|---|---|---|---|---|---|---|---|
| N1 | C1 | H1 | 116.00 | . | . | . | no |
| C2 | C1 | H1 | 116.00 | . | . | . | no |
| C3 | C1 | H1 | 116.00 | . | . | . | no |
| C1 | C2 | H2A | 118.00 | . | . | . | no |
| C1 | C2 | H2B | 118.00 | . | . | . | no |
| C3 | C2 | H2A | 118.00 | . | . | . | no |
| C3 | C2 | H2B | 118.00 | . | . | . | no |
| H2A | C2 | H2B | 115.00 | . | . | . | no |
| C1 | C3 | H3C | 118.00 | . | . | . | no |
| C1 | C3 | H3D | 118.00 | . | . | . | no |
| C2 | C3 | H3C | 118.00 | . | . | . | no |
| C2 | C3 | H3D | 118.00 | . | . | . | no |
| H3C | C3 | H3D | 115.00 | . | . | . | no |
| C26 | N4 | C27 | 120.46(10) | . | . | . | yes |
| C23 | N4 | C26 | 118.57(9) | . | . | . | yes |
| C23 | N4 | C27 | 120.97(9) | . | . | . | yes |
| N1 | C5 | H5 | 118.00 | . | . | . | no |
| C6 | C5 | H5 | 118.00 | . | . | . | no |
| C35 | N5 | C38 | 111.71(9) | . | . | . | yes |
| C34 | N5 | C35 | 121.58(9) | . | . | . | yes |
| C34 | N5 | C38 | 121.14(9) | . | . | . | yes |
| C36 | N6 | C37 | 111.41(9) | . | . | . | yes |
| C29 | O9 | H9 | 105.1(12) | . | . | . | no |
| C9 | C10 | H10 | 120.00 | . | . | . | no |
| C11 | C10 | H10 | 120.00 | . | . | . | no |
| N2 | C13 | H13B | 110.00 | . | . | . | no |
| C14 | C13 | H13A | 110.00 | . | . | . | no |
| C14 | C13 | H13B | 110.00 | . | . | . | no |
| H13A | C13 | H13B | 108.00 | . | . | . | no |
| N2 | C13 | H13A | 110.00 | . | . | . | no |
| N3 | C14 | H14A | 110.00 | . | . | . | no |
| H14A | C14 | H14B | 108.00 | . | . | . | no |
| C13 | C14 | H14A | 110.00 | . | . | . | no |
| N3 | C14 | H14B | 110.00 | . | . | . | no |
| C13 | C14 | H14B | 110.00 | . | . | . | no |
| N3 | C15 | H15A | 110.00 | . | . | . | no |
| N3 | C15 | H15B | 110.00 | . | . | . | no |
| H15A | C15 | H15B | 108.00 | . | . | . | no |
| C16 | C15 | H15B | 110.00 | . | . | . | no |
| C16 | C15 | H15A | 110.00 | . | . | . | no |
| N2 | C16 | H16A | 110.00 | . | . | . | no |
| C15 | C16 | H16A | 110.00 | . | . | . | no |
| C15 | C16 | H16B | 110.00 | . | . | . | no |
| H16A | C16 | H16B | 108.00 | . | . | . | no |
| N2 | C16 | H16B | 110.00 | . | . | . | no |
| C4 | C17 | H17 | 120.00 | . | . | . | no |
| C12 | C17 | H17 | 120.00 | . | . | . | no |
| H6A | N6 | H6B | 105.6(14) | . | . | . | no |
| C36 | N6 | H6B | 110.1(10) | . | . | . | no |
| C36 | N6 | H6A | 111.1(9) | . | . | . | no |
| C37 | N6 | H6A | 109.1(10) | . | . | . | no |
| C37 | N6 | H6B | 109.3(9) | . | . | . | no |
| N4 | C23 | C25 | 119.89(9) | . | . | . | yes |
| N4 | C23 | C24 | 117.40(9) | . | . | . | yes |
| C24 | C23 | C25 | 60.46(8) | . | . | . | no |
| C23 | C24 | C25 | 59.52(8) | . | . | . | no |
| C23 | C25 | C24 | 60.02(7) | . | . | . | no |
| C31 | C26 | C39 | 120.66(10) | . | . | . | no |
| N4 | C26 | C39 | 120.57(10) | . | . | . | yes |
| N4 | C26 | C31 | 118.77(10) | . | . | . | yes |
| N4 | C27 | C28 | 123.28(10) | . | . | . | yes |
| C27 | C28 | C30 | 120.21(10) | . | . | . | no |
| C27 | C28 | C29 | 118.05(10) | . | . | . | no |
| C29 | C28 | C30 | 121.75(10) | . | . | . | no |
| O8 | C29 | C28 | 123.89(11) | . | . | . | yes |
| O8 | C29 | O9 | 121.57(11) | . | . | . | yes |
| O9 | C29 | C28 | 114.54(11) | . | . | . | yes |
| C28 | C30 | C31 | 115.88(10) | . | . | . | no |

| | | | | | | | |
|---|---|---|---|---|---|---|---|
| O10 | C30 | C28 | 122.79(10) | . | . | . | yes |
| O10 | C30 | C31 | 121.33(10) | . | . | . | yes |
| C26 | C31 | C32 | 118.17(10) | . | . | . | no |
| C30 | C31 | C32 | 120.47(10) | . | . | . | no |
| C26 | C31 | C30 | 121.35(10) | . | . | . | no |
| C31 | C32 | C33 | 120.09(11) | . | . | . | no |
| C32 | C33 | C34 | 123.48(10) | . | . | . | no |
| F2 | C33 | C34 | 118.06(10) | . | . | . | yes |
| F2 | C33 | C32 | 118.38(10) | . | . | . | yes |
| N5 | C34 | C33 | 120.11(10) | . | . | . | yes |
| N5 | C34 | C39 | 123.44(10) | . | . | . | yes |
| C33 | C34 | C39 | 116.29(10) | . | . | . | no |
| N5 | C35 | C36 | 110.71(9) | . | . | . | yes |
| N6 | C36 | C35 | 110.15(9) | . | . | . | yes |
| N6 | C37 | C38 | 109.45(9) | . | . | . | yes |
| N5 | C38 | C37 | 112.48(9) | . | . | . | yes |
| C26 | C39 | C34 | 121.31(10) | . | . | . | no |
| C22 | O6 | H6 | 113.1(12) | . | . | . | no |
| N4 | C23 | H23 | 116.00 | . | . | . | no |
| C24 | C23 | H23 | 116.00 | . | . | . | no |
| C25 | C23 | H23 | 116.00 | . | . | . | no |
| C23 | C24 | H24B | 118.00 | . | . | . | no |
| C25 | C24 | H24A | 118.00 | . | . | . | no |
| C25 | C24 | H24B | 118.00 | . | . | . | no |
| H24A | C24 | H24B | 115.00 | . | . | . | no |
| C23 | C24 | H24A | 118.00 | . | . | . | no |
| C23 | C25 | H25A | 118.00 | . | . | . | no |
| C23 | C25 | H25B | 118.00 | . | . | . | no |
| C24 | C25 | H25B | 118.00 | . | . | . | no |
| H25A | C25 | H25B | 115.00 | . | . | . | no |
| C24 | C25 | H25A | 118.00 | . | . | . | no |
| N4 | C27 | H27 | 118.00 | . | . | . | no |
| C28 | C27 | H27 | 118.00 | . | . | . | no |
| C31 | C32 | H32 | 120.00 | . | . | . | no |
| C33 | C32 | H32 | 120.00 | . | . | . | no |
| N5 | C35 | H35B | 110.00 | . | . | . | no |
| C36 | C35 | H35A | 110.00 | . | . | . | no |
| C36 | C35 | H35B | 110.00 | . | . | . | no |
| H35A | C35 | H35B | 108.00 | . | . | . | no |
| N5 | C35 | H35A | 110.00 | . | . | . | no |
| N6 | C36 | H36A | 110.00 | . | . | . | no |
| C35 | C36 | H36A | 110.00 | . | . | . | no |
| C35 | C36 | H36B | 110.00 | . | . | . | no |
| N6 | C36 | H36B | 110.00 | . | . | . | no |
| H36A | C36 | H36B | 108.00 | . | . | . | no |
| N6 | C37 | H37B | 110.00 | . | . | . | no |
| C38 | C37 | H37A | 110.00 | . | . | . | no |
| N6 | C37 | H37A | 110.00 | . | . | . | no |
| H37A | C37 | H37B | 108.00 | . | . | . | no |
| C38 | C37 | H37B | 110.00 | . | . | . | no |
| N5 | C38 | H38A | 109.00 | . | . | . | no |
| C37 | C38 | H38A | 109.00 | . | . | . | no |
| C37 | C38 | H38B | 109.00 | . | . | . | no |
| H38A | C38 | H38B | 108.00 | . | . | . | no |
| N5 | C38 | H38B | 109.00 | . | . | . | no |
| C26 | C39 | H39 | 119.00 | . | . | . | no |
| C34 | C39 | H39 | 119.00 | . | . | . | no |
| O4 | C18 | O5 | 121.76(11) | . | . | . | yes |
| O4 | C18 | C19 | 119.65(10) | . | . | . | yes |
| O5 | C18 | C19 | 118.52(10) | . | . | . | yes |
| C18 | C19 | C20 | 116.33(10) | . | . | . | no |
| C19 | C20 | C21 | 112.16(10) | . | . | . | no |
| C20 | C21 | C22 | 113.42(10) | . | . | . | no |
| O6 | C22 | C21 | 112.95(10) | . | . | . | yes |
| O7 | C22 | C21 | 123.45(11) | . | . | . | yes |
| O6 | C22 | O7 | 123.60(11) | . | . | . | yes |
| C44 | O13 | H13 | 113.1(14) | . | . | . | no |
| C18 | C19 | H19A | 108.00 | . | . | . | no |

```
 C18     C19     H19B         108.00             .      .      .          no
 C20     C19     H19B         108.00             .      .      .          no
 H19A    C19     H19B         107.00             .      .      .          no
 C20     C19     H19A         108.00             .      .      .          no
 C19     C20     H20A         109.00             .      .      .          no
 C21     C20     H20A         109.00             .      .      .          no
 C21     C20     H20B         109.00             .      .      .          no
 C19     C20     H20B         109.00             .      .      .          no
 H20A    C20     H20B         108.00             .      .      .          no
 C20     C21     H21B         109.00             .      .      .          no
 C22     C21     H21A         109.00             .      .      .          no
 C22     C21     H21B         109.00             .      .      .          no
 H21A    C21     H21B         108.00             .      .      .          no
 C20     C21     H21A         109.00             .      .      .          no
 O11     C40     O12       122.42(11)            .      .      .          yes
 O11     C40     C41       119.40(10)            .      .      .          yes
 O12     C40     C41       118.10(10)            .      .      .          yes
 C40     C41     C42        116.10(9)            .      .      .          no
 C41     C42     C43       112.31(10)            .      .      .          no
 C42     C43     C44        113.38(9)            .      .      .          no
 O13     C44     C43       112.58(10)            .      .      .          yes
 O14     C44     C43       123.33(10)            .      .      .          yes
 O13     C44     O14       124.09(11)            .      .      .          yes
 C40     C41     H41A         108.00             .      .      .          no
 C40     C41     H41B         108.00             .      .      .          no
 C42     C41     H41A         108.00             .      .      .          no
 C42     C41     H41B         108.00             .      .      .          no
 H41A    C41     H41B         107.00             .      .      .          no
 C41     C42     H42A         109.00             .      .      .          no
 C41     C42     H42B         109.00             .      .      .          no
 C43     C42     H42A         109.00             .      .      .          no
 C43     C42     H42B         109.00             .      .      .          no
 H42A    C42     H42B         108.00             .      .      .          no
 C42     C43     H43A         109.00             .      .      .          no
 C42     C43     H43B         109.00             .      .      .          no
 C44     C43     H43A         109.00             .      .      .          no
 C44     C43     H43B         109.00             .      .      .          no
 H43A    C43     H43B         108.00             .      .      .          no

loop_
_geom_torsion_atom_site_label_1
_geom_torsion_atom_site_label_2
_geom_torsion_atom_site_label_3
_geom_torsion_atom_site_label_4
_geom_torsion
_geom_torsion_site_symmetry_1
_geom_torsion_site_symmetry_2
_geom_torsion_site_symmetry_3
_geom_torsion_site_symmetry_4
_geom_torsion_publ_flag
 C4      N1      C1      C2        79.04(13)     .      .      .      .   no
 C4      N1      C1      C3       148.78(10)     .      .      .      .   no
 C5      N1      C1      C2      -102.27(12)     .      .      .      .   no
 C5      N1      C1      C3       -32.53(15)     .      .      .      .   no
 C1      N1      C4      C9        177.07(9)     .      .      .      .   no
 C1      N1      C4      C17       -3.68(14)     .      .      .      .   no
 C5      N1      C4      C9        -1.64(14)     .      .      .      .   no
 C5      N1      C4      C17      177.61(10)     .      .      .      .   no
 C1      N1      C5      C6      -179.16(10)     .      .      .      .   no
 C4      N1      C5      C6        -0.48(16)     .      .      .      .   no
 C13     N2      C12     C11     -167.21(10)     .      .      .      .   no
 C13     N2      C12     C17        9.38(15)     .      .      .      .   no
 C16     N2      C12     C11       61.13(13)     .      .      .      .   no
 C16     N2      C12     C17     -122.27(11)     .      .      .      .   no
 C12     N2      C13     C14       167.58(9)     .      .      .      .   no
 C16     N2      C13     C14      -58.53(12)     .      .      .      .   no
 C12     N2      C16     C15      -167.67(9)     .      .      .      .   no
 C13     N2      C16     C15       58.67(11)     .      .      .      .   no
```

| | | | | | | | | | |
|---|---|---|---|---|---|---|---|---|---|
| C15 | N3 | C14 | C13 | -56.76(12) | . | . | . | . | no |
| C14 | N3 | C15 | C16 | 56.76(12) | . | . | . | . | no |
| N1 | C1 | C2 | C3 | 110.36(11) | . | . | . | . | no |
| N1 | C1 | C3 | C2 | -106.51(12) | . | . | . | . | no |
| N1 | C4 | C9 | C8 | 1.58(15) | . | . | . | . | no |
| N1 | C4 | C9 | C10 | -177.92(9) | . | . | . | . | no |
| C17 | C4 | C9 | C8 | -177.67(10) | . | . | . | . | no |
| C17 | C4 | C9 | C10 | 2.83(15) | . | . | . | . | no |
| N1 | C4 | C17 | C12 | -179.69(10) | . | . | . | . | no |
| C9 | C4 | C17 | C12 | -0.45(16) | . | . | . | . | no |
| N1 | C5 | C6 | C7 | -177.23(10) | . | . | . | . | no |
| N1 | C5 | C6 | C8 | 2.66(16) | . | . | . | . | no |
| C5 | C6 | C7 | O1 | 2.24(16) | . | . | . | . | no |
| C5 | C6 | C7 | O2 | -177.95(10) | . | . | . | . | no |
| C8 | C6 | C7 | O1 | -177.64(10) | . | . | . | . | no |
| C8 | C6 | C7 | O2 | 2.17(15) | . | . | . | . | no |
| C5 | C6 | C8 | O3 | 177.54(10) | . | . | . | . | no |
| C5 | C6 | C8 | C9 | -2.54(15) | . | . | . | . | no |
| C7 | C6 | C8 | O3 | -2.58(16) | . | . | . | . | no |
| C7 | C6 | C8 | C9 | 177.35(9) | . | . | . | . | no |
| O3 | C8 | C9 | C4 | -179.60(10) | . | . | . | . | no |
| O3 | C8 | C9 | C10 | -0.11(15) | . | . | . | . | no |
| C6 | C8 | C9 | C4 | 0.48(14) | . | . | . | . | no |
| C6 | C8 | C9 | C10 | 179.97(9) | . | . | . | . | no |
| C4 | C9 | C10 | C11 | -1.95(15) | . | . | . | . | no |
| C8 | C9 | C10 | C11 | 178.54(10) | . | . | . | . | no |
| C9 | C10 | C11 | F1 | 176.84(9) | . | . | . | . | no |
| C9 | C10 | C11 | C12 | -1.32(17) | . | . | . | . | no |
| F1 | C11 | C12 | N2 | 2.26(15) | . | . | . | . | no |
| F1 | C11 | C12 | C17 | -174.55(9) | . | . | . | . | no |
| C10 | C11 | C12 | N2 | -179.55(10) | . | . | . | . | no |
| C10 | C11 | C12 | C17 | 3.64(16) | . | . | . | . | no |
| N2 | C12 | C17 | C4 | -179.36(10) | . | . | . | . | no |
| C11 | C12 | C17 | C4 | -2.67(15) | . | . | . | . | no |
| N2 | C13 | C14 | N3 | 57.37(12) | . | . | . | . | no |
| N3 | C15 | C16 | N2 | -57.24(12) | . | . | . | . | no |
| C26 | N4 | C23 | C24 | -75.76(12) | . | . | . | . | no |
| C26 | N4 | C23 | C25 | -145.72(10) | . | . | . | . | no |
| C27 | N4 | C23 | C24 | 104.36(12) | . | . | . | . | no |
| C27 | N4 | C23 | C25 | 34.39(15) | . | . | . | . | no |
| C23 | N4 | C26 | C31 | 179.44(9) | . | . | . | . | no |
| C23 | N4 | C26 | C39 | -0.36(14) | . | . | . | . | no |
| C27 | N4 | C26 | C31 | -0.67(15) | . | . | . | . | no |
| C27 | N4 | C26 | C39 | 179.53(10) | . | . | . | . | no |
| C23 | N4 | C27 | C28 | -179.97(11) | . | . | . | . | no |
| C26 | N4 | C27 | C28 | 0.14(16) | . | . | . | . | no |
| C35 | N5 | C34 | C33 | -51.47(15) | . | . | . | . | no |
| C35 | N5 | C34 | C39 | 133.36(11) | . | . | . | . | no |
| C38 | N5 | C34 | C33 | 157.05(10) | . | . | . | . | no |
| C38 | N5 | C34 | C39 | -18.12(16) | . | . | . | . | no |
| C34 | N5 | C35 | C36 | -97.73(12) | . | . | . | . | no |
| C38 | N5 | C35 | C36 | 56.18(12) | . | . | . | . | no |
| C34 | N5 | C38 | C37 | 98.12(12) | . | . | . | . | no |
| C35 | N5 | C38 | C37 | -55.92(12) | . | . | . | . | no |
| C37 | N6 | C36 | C35 | 57.26(11) | . | . | . | . | no |
| C36 | N6 | C37 | C38 | -55.63(11) | . | . | . | . | no |
| N4 | C23 | C24 | C25 | -110.58(11) | . | . | . | . | no |
| N4 | C23 | C25 | C24 | 106.52(11) | . | . | . | . | no |
| N4 | C26 | C31 | C30 | 2.00(15) | . | . | . | . | no |
| N4 | C26 | C31 | C32 | -178.88(9) | . | . | . | . | no |
| C39 | C26 | C31 | C30 | -178.21(10) | . | . | . | . | no |
| C39 | C26 | C31 | C32 | 0.92(15) | . | . | . | . | no |
| N4 | C26 | C39 | C34 | 178.93(10) | . | . | . | . | no |
| C31 | C26 | C39 | C34 | -0.87(16) | . | . | . | . | no |
| N4 | C27 | C28 | C29 | 179.41(10) | . | . | . | . | no |
| N4 | C27 | C28 | C30 | -0.92(17) | . | . | . | . | no |
| C27 | C28 | C29 | O8 | -5.52(17) | . | . | . | . | no |
| C27 | C28 | C29 | O9 | 175.07(10) | . | . | . | . | no |

```
C30     C28     C29     O8       174.81(11)     .       .       .       .   no
C30     C28     C29     O9        -4.60(15)     .       .       .       .   no
C27     C28     C30     O10     -177.53(10)     .       .       .       .   no
C27     C28     C30     C31       2.10(15)     .       .       .       .   no
C29     C28     C30     O10       2.14(16)     .       .       .       .   no
C29     C28     C30     C31     -178.24(10)     .       .       .       .   no
O10     C30     C31     C26      176.97(10)     .       .       .       .   no
O10     C30     C31     C32       -2.14(16)     .       .       .       .   no
C28     C30     C31     C26       -2.66(15)     .       .       .       .   no
C28     C30     C31     C32      178.23(10)     .       .       .       .   no
C26     C31     C32     C33       -0.15(16)     .       .       .       .   no
C30     C31     C32     C33      178.99(10)     .       .       .       .   no
C31     C32     C33     F2      -177.46(10)     .       .       .       .   no
C31     C32     C33     C34       -0.71(17)     .       .       .       .   no
F2      C33     C34     N5         2.02(16)     .       .       .       .   no
F2      C33     C34     C39       177.53(9)     .       .       .       .   no
C32     C33     C34     N5      -174.75(11)     .       .       .       .   no
C32     C33     C34     C39        0.76(17)     .       .       .       .   no
N5      C34     C39     C26      175.38(10)     .       .       .       .   no
C33     C34     C39     C26        0.03(15)     .       .       .       .   no
N5      C35     C36     N6       -56.67(12)     .       .       .       .   no
N6      C37     C38     N5        54.85(12)     .       .       .       .   no
O4      C18     C19     C20      -19.90(15)     .       .       .       .   no
O5      C18     C19     C20      163.09(10)     .       .       .       .   no
C18     C19     C20     C21      169.99(10)     .       .       .       .   no
C19     C20     C21     C22       54.63(13)     .       .       .       .   no
C20     C21     C22     O6      -143.97(11)     .       .       .       .   no
C20     C21     C22     O7        36.00(17)     .       .       .       .   no
O11     C40     C41     C42       17.78(15)     .       .       .       .   no
O12     C40     C41     C42     -165.31(10)     .       .       .       .   no
C40     C41     C42     C43     -169.12(10)     .       .       .       .   no
C41     C42     C43     C44      -58.02(13)     .       .       .       .   no
C42     C43     C44     O13      146.22(10)     .       .       .       .   no
C42     C43     C44     O14      -33.78(17)     .       .       .       .   no

loop_
_geom_hbond_atom_site_label_D
_geom_hbond_atom_site_label_H
_geom_hbond_atom_site_label_A
_geom_hbond_distance_DH
_geom_hbond_distance_HA
_geom_hbond_distance_DA
_geom_hbond_angle_DHA
_geom_hbond_site_symmetry_A
_geom_hbond_publ_flag
#
#D   H   A   D - H  H...A   D...A    D - H...A  symm(A)
#
O2      H2      O3        0.93(2)    1.63(2) 2.5188(13)     161(2)      .   yes
N3      H3A     O4      0.912(18)  1.904(18) 2.8081(14)  170.9(14)   2_466 yes
N3      H3A     O5      0.912(18)  2.358(16) 2.9996(14)  127.3(13)   2_466 yes
N3      H3B     O4      0.913(16)  1.864(16) 2.7553(13)  164.9(16)     .   yes
O6      H6      O12       0.95(2)    1.58(2) 2.5148(14)     169(2)      .   yes
N6      H6A     O11     0.929(16)  1.818(16) 2.7328(13)  167.8(15)     .   yes
N6      H6B     O11     0.938(16)  1.845(16) 2.7575(13)  163.5(14)   2_767 yes
O9      H9      O10       0.95(2)    1.61(2) 2.5308(13)  159.9(19)     .   yes
O13     H13     O5        0.94(2)    1.57(2) 2.5017(12)     169(2)      .   yes
```

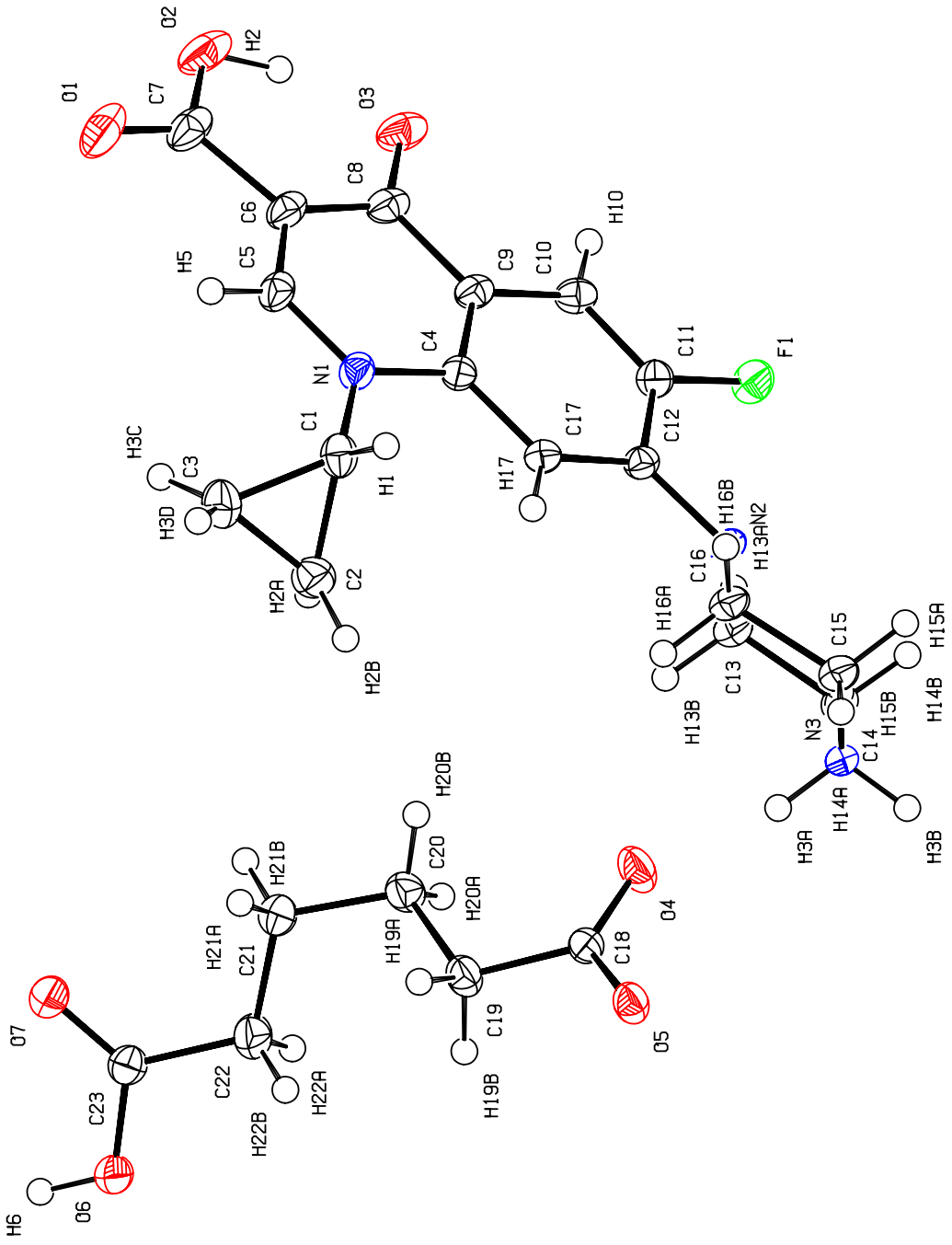


**Figure S7A**: ORTEP view of asymmetric unit of CFX-AA with atom labelling

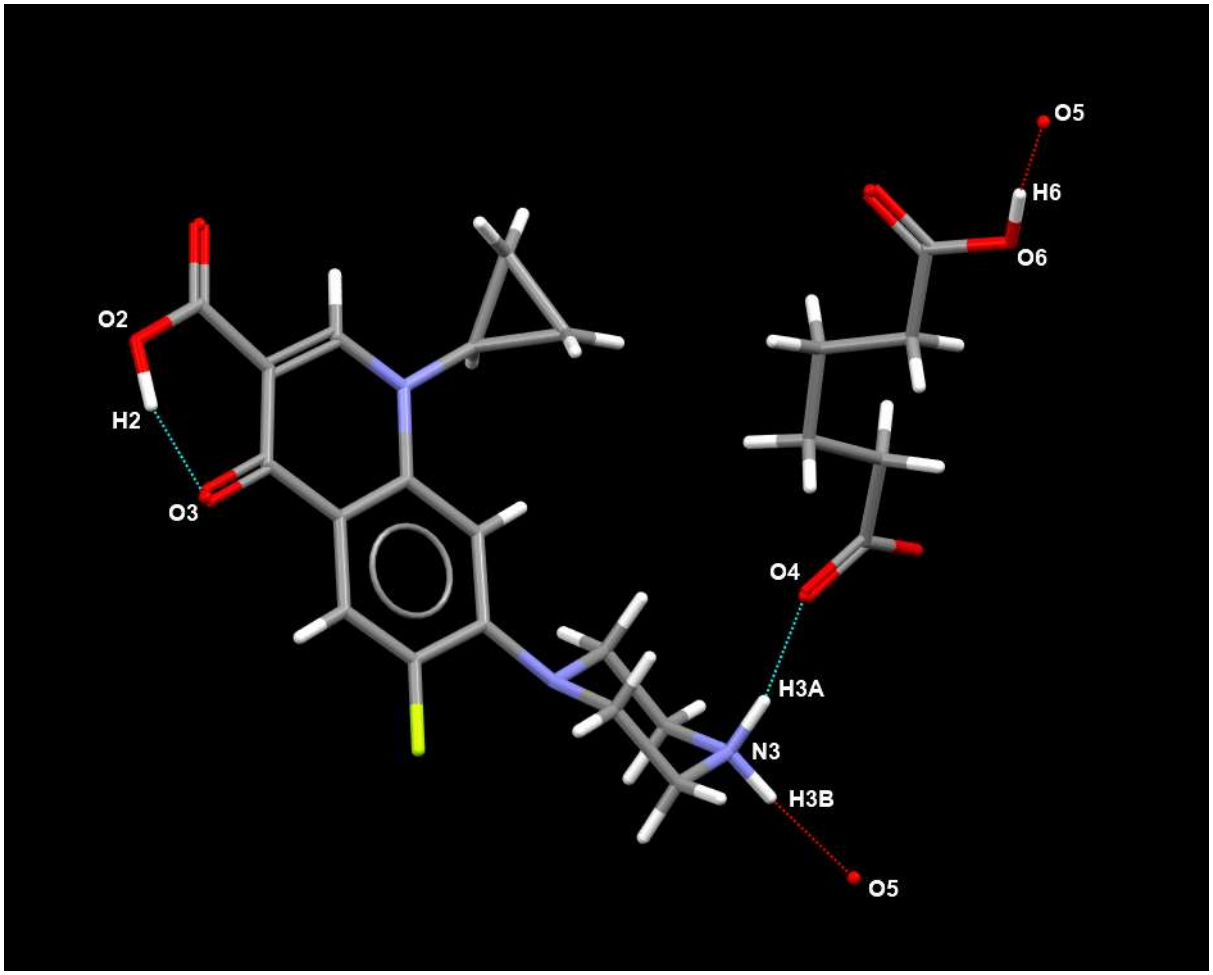


| Donor | H | Accept | D-H / Å | H…A / Å | D…A / Å | D-H…A / ° | Symm |
|---|---|---|---|---|---|---|---|
| O2 | H2 | O3 | 0.98(3) | 1.61(3) | 2.5360(17) | 156(3) | x,y,z |
| N3 | H3A | O4 | 0.932(19) | 1.79(2) | 2.7054(16) | 165.8(17) | x,y,z |
| N3 | H3B | O5 | 0.94(2) | 1.77(2) | 2.7155(15) | 175(2) | x,1/2-y,-1/2+z |
| O6 | H6 | O5 | 0.93(3) | 1.58(3) | 2.5079(15) | 173(3) | -1+x,1/2-y,1/2+z |

**Figure S7B**. A Mercury diagram for the asymmetric unit of CFX-AA, showing the unique set of hydrogen bonds (dashed lines) and the associated bond distances and angles.

**Table S3**: Bond distances and angles for CFX-AA

```
loop_
_space_group_symop_id
_space_group_symop_operation_xyz
   1 x,y,z
   2 -x,1/2+y,1/2-z
   3 -x,-y,-z
   4 x,1/2-y,1/2+z

_geom_special_details
;
 Bond distances, angles etc. have been calculated using the
 rounded fractional coordinates. All su's are estimated
 from the variances of the (full) variance-covariance matrix.
 The cell esds are taken into account in the estimation of
 distances, angles and torsion angles
;

loop_
_geom_bond_atom_site_label_1
_geom_bond_atom_site_label_2
_geom_bond_distance
_geom_bond_site_symmetry_1
_geom_bond_site_symmetry_2
_geom_bond_publ_flag
 F1      C11      1.3532(14)                    .      .                 yes
 O1      C7         1.209(2)                    .      .                 yes
 O2      C7         1.338(2)                    .      .                 yes
 O3      C8       1.2661(18)                    .      .                 yes
 N1      C1       1.4576(17)                    .      .                 yes
 N1      C4       1.4028(16)                    .      .                 yes
 N1      C5       1.3409(17)                    .      .                 yes
 N2      C12      1.4044(17)                    .      .                 yes
 N2      C13      1.4837(18)                    .      .                 yes
 N2      C16      1.4617(18)                    .      .                 yes
 O2      H2          0.98(3)                    .      .                 no
 N3      C14      1.4893(18)                    .      .                 yes
 N3      C15      1.4905(19)                    .      .                 yes
 C1      C3       1.4940(19)                    .      .                 no
 C1      C2         1.502(2)                    .      .                 no
 C2      C3         1.500(2)                    .      .                 no
 N3      H3B         0.94(2)                    .      .                 no
 N3      H3A        0.932(19)                   .      .                 no
 C4      C17      1.4029(19)                    .      .                 no
 C4      C9       1.4052(19)                    .      .                 no
 O4      C18      1.2396(17)                    .      .                 yes
 O5      C18      1.2790(17)                    .      .                 yes
 C5      C6         1.370(2)                    .      .                 no
 C6      C8         1.435(2)                    .      .                 no
 O6      C23      1.3148(18)                    .      .                 yes
 C6      C7         1.490(2)                    .      .                 no
 O7      C23      1.2147(17)                    .      .                 yes
 C8      C9         1.452(2)                    .      .                 no
 C9      C10      1.4097(18)                    .      .                 no
 C10     C11      1.3583(19)                    .      .                 no
 C11     C12      1.4139(19)                    .      .                 no
 C12     C17      1.3888(17)                    .      .                 no
 C13     C14      1.5149(19)                    .      .                 no
 C15     C16      1.5177(19)                    .      .                 no
 C1      H1          0.9800                     .      .                 no
 C2      H2A         0.9700                     .      .                 no
 C2      H2B         0.9700                     .      .                 no
 C3      H3D         0.9700                     .      .                 no
 C3      H3C         0.9700                     .      .                 no
 C5      H5          0.9300                     .      .                 no
 O6      H6         0.93(3)                     .      .                 no
 C10     H10         0.9300                     .      .                 no
```

```
 C13     H13A         0.9700                    .       .                 no
 C13     H13B         0.9700                    .       .                 no
 C14     H14A         0.9700                    .       .                 no
 C14     H14B         0.9700                    .       .                 no
 C15     H15B         0.9700                    .       .                 no
 C15     H15A         0.9700                    .       .                 no
 C16     H16B         0.9700                    .       .                 no
 C16     H16A         0.9700                    .       .                 no
 C17     H17          0.9300                    .       .                 no
 C18     C19       1.5111(19)                   .       .                 no
 C19     C20         1.516(2)                   .       .                 no
 C20     C21         1.521(2)                   .       .                 no
 C21     C22         1.515(2)                   .       .                 no
 C22     C23         1.510(2)                   .       .                 no
 C19     H19A          0.9700                   .       .                 no
 C19     H19B          0.9700                   .       .                 no
 C20     H20A          0.9700                   .       .                 no
 C20     H20B          0.9700                   .       .                 no
 C21     H21A          0.9700                   .       .                 no
 C21     H21B          0.9700                   .       .                 no
 C22     H22A          0.9700                   .       .                 no
 C22     H22B          0.9700                   .       .                 no

loop_
_geom_angle_atom_site_label_1
_geom_angle_atom_site_label_2
_geom_angle_atom_site_label_3
_geom_angle
_geom_angle_site_symmetry_1
_geom_angle_site_symmetry_2
_geom_angle_site_symmetry_3
_geom_angle_publ_flag
 C1      N1      C4       119.73(11)              .       .       .          yes
 C1      N1      C5       120.40(10)              .       .       .          yes
 C4      N1      C5       119.87(11)              .       .       .          yes
 C12     N2      C13      112.81(11)              .       .       .          yes
 C12     N2      C16      115.77(10)              .       .       .          yes
 C13     N2      C16      111.53(10)              .       .       .          yes
 C7      O2      H2        107.1(19)              .       .       .          no
 C14     N3      C15      110.53(10)              .       .       .          yes
 N1      C1      C2       118.13(12)              .       .       .          yes
 N1      C1      C3       119.00(12)              .       .       .          yes
 C2      C1      C3        60.11(10)              .       .       .          no
 C1      C2      C3         59.68(9)              .       .       .          no
 C15     N3      H3A       108.5(12)              .       .       .          no
 C15     N3      H3B       111.1(13)              .       .       .          no
 H3A     N3      H3B       106.5(17)              .       .       .          no
 C1      C3      C2         60.21(9)              .       .       .          no
 C14     N3      H3A       109.6(12)              .       .       .          no
 C14     N3      H3B       110.4(12)              .       .       .          no
 C9      C4      C17      120.57(11)              .       .       .          no
 N1      C4      C17      120.32(12)              .       .       .          yes
 N1      C4      C9       119.10(12)              .       .       .          yes
 N1      C5      C6       123.80(12)              .       .       .          yes
 C5      C6      C8       120.35(13)              .       .       .          no
 C5      C6      C7       118.11(13)              .       .       .          no
 C7      C6      C8       121.54(13)              .       .       .          no
 O1      C7      C6       123.41(16)              .       .       .          yes
 O1      C7      O2       121.74(16)              .       .       .          yes
 O2      C7      C6       114.85(13)              .       .       .          yes
 C6      C8      C9       115.50(12)              .       .       .          no
 O3      C8      C6       123.04(13)              .       .       .          yes
 O3      C8      C9       121.46(13)              .       .       .          yes
 C4      C9      C10      118.70(12)              .       .       .          no
 C8      C9      C10      119.93(12)              .       .       .          no
 C4      C9      C8       121.37(12)              .       .       .          no
 C9      C10     C11      119.51(13)              .       .       .          no
 C10     C11     C12      123.20(12)              .       .       .          no
```

| | | | | | | | |
|---|---|---|---|---|---|---|---|
| F1 | C11 | C12 | 117.45(11) | . | . | . | yes |
| F1 | C11 | C10 | 119.33(12) | . | . | . | yes |
| N2 | C12 | C11 | 118.76(11) | . | . | . | yes |
| N2 | C12 | C17 | 123.98(12) | . | . | . | yes |
| C11 | C12 | C17 | 117.26(12) | . | . | . | no |
| N2 | C13 | C14 | 110.16(11) | . | . | . | yes |
| N3 | C14 | C13 | 109.80(10) | . | . | . | yes |
| N3 | C15 | C16 | 108.81(11) | . | . | . | yes |
| N2 | C16 | C15 | 109.45(10) | . | . | . | yes |
| C4 | C17 | C12 | 120.72(12) | . | . | . | no |
| N1 | C1 | H1 | 116.00 | . | . | . | no |
| C2 | C1 | H1 | 116.00 | . | . | . | no |
| C3 | C1 | H1 | 116.00 | . | . | . | no |
| C1 | C2 | H2A | 118.00 | . | . | . | no |
| C1 | C2 | H2B | 118.00 | . | . | . | no |
| C3 | C2 | H2A | 118.00 | . | . | . | no |
| C3 | C2 | H2B | 118.00 | . | . | . | no |
| H2A | C2 | H2B | 115.00 | . | . | . | no |
| C1 | C3 | H3C | 118.00 | . | . | . | no |
| C1 | C3 | H3D | 118.00 | . | . | . | no |
| C2 | C3 | H3C | 118.00 | . | . | . | no |
| C2 | C3 | H3D | 118.00 | . | . | . | no |
| H3C | C3 | H3D | 115.00 | . | . | . | no |
| N1 | C5 | H5 | 118.00 | . | . | . | no |
| C6 | C5 | H5 | 118.00 | . | . | . | no |
| C23 | O6 | H6 | 113.1(16) | . | . | . | no |
| C11 | C10 | H10 | 120.00 | . | . | . | no |
| C9 | C10 | H10 | 120.00 | . | . | . | no |
| N2 | C13 | H13A | 110.00 | . | . | . | no |
| C14 | C13 | H13A | 110.00 | . | . | . | no |
| C14 | C13 | H13B | 110.00 | . | . | . | no |
| H13A | C13 | H13B | 108.00 | . | . | . | no |
| N2 | C13 | H13B | 110.00 | . | . | . | no |
| N3 | C14 | H14A | 110.00 | . | . | . | no |
| N3 | C14 | H14B | 110.00 | . | . | . | no |
| C13 | C14 | H14B | 110.00 | . | . | . | no |
| H14A | C14 | H14B | 108.00 | . | . | . | no |
| C13 | C14 | H14A | 110.00 | . | . | . | no |
| N3 | C15 | H15B | 110.00 | . | . | . | no |
| C16 | C15 | H15A | 110.00 | . | . | . | no |
| C16 | C15 | H15B | 110.00 | . | . | . | no |
| H15A | C15 | H15B | 108.00 | . | . | . | no |
| N3 | C15 | H15A | 110.00 | . | . | . | no |
| N2 | C16 | H16A | 110.00 | . | . | . | no |
| N2 | C16 | H16B | 110.00 | . | . | . | no |
| C15 | C16 | H16B | 110.00 | . | . | . | no |
| H16A | C16 | H16B | 108.00 | . | . | . | no |
| C15 | C16 | H16A | 110.00 | . | . | . | no |
| C4 | C17 | H17 | 120.00 | . | . | . | no |
| C12 | C17 | H17 | 120.00 | . | . | . | no |
| O4 | C18 | C19 | 119.50(13) | . | . | . | yes |
| O5 | C18 | C19 | 116.54(12) | . | . | . | yes |
| O4 | C18 | O5 | 123.95(13) | . | . | . | yes |
| C18 | C19 | C20 | 115.21(12) | . | . | . | no |
| C19 | C20 | C21 | 112.87(12) | . | . | . | no |
| C20 | C21 | C22 | 112.38(12) | . | . | . | no |
| C21 | C22 | C23 | 115.34(13) | . | . | . | no |
| O6 | C23 | C22 | 111.04(12) | . | . | . | yes |
| O7 | C23 | C22 | 125.03(14) | . | . | . | yes |
| O6 | C23 | O7 | 123.93(13) | . | . | . | yes |
| C18 | C19 | H19A | 108.00 | . | . | . | no |
| C18 | C19 | H19B | 108.00 | . | . | . | no |
| C20 | C19 | H19A | 108.00 | . | . | . | no |
| C20 | C19 | H19B | 108.00 | . | . | . | no |
| H19A | C19 | H19B | 108.00 | . | . | . | no |
| C19 | C20 | H20A | 109.00 | . | . | . | no |
| C19 | C20 | H20B | 109.00 | . | . | . | no |
| C21 | C20 | H20A | 109.00 | . | . | . | no |

```
 C21     C20     H20B         109.00             .       .       .          no
 H20A    C20     H20B         108.00             .       .       .          no
 C20     C21     H21A         109.00             .       .       .          no
 C20     C21     H21B         109.00             .       .       .          no
 C22     C21     H21A         109.00             .       .       .          no
 C22     C21     H21B         109.00             .       .       .          no
 H21A    C21     H21B         108.00             .       .       .          no
 C21     C22     H22A         108.00             .       .       .          no
 C21     C22     H22B         108.00             .       .       .          no
 C23     C22     H22A         108.00             .       .       .          no
 C23     C22     H22B         108.00             .       .       .          no
 H22A    C22     H22B         107.00             .       .       .          no

loop_
_geom_torsion_atom_site_label_1
_geom_torsion_atom_site_label_2
_geom_torsion_atom_site_label_3
_geom_torsion_atom_site_label_4
_geom_torsion
_geom_torsion_site_symmetry_1
_geom_torsion_site_symmetry_2
_geom_torsion_site_symmetry_3
_geom_torsion_site_symmetry_4
_geom_torsion_publ_flag
 C4      N1      C1      C2       -73.15(16)     .       .       .       .   no
 C4      N1      C1      C3      -142.67(13)     .       .       .       .   no
 C5      N1      C1      C2       107.36(14)     .       .       .       .   no
 C5      N1      C1      C3        37.84(18)     .       .       .       .   no
 C1      N1      C4      C9       179.25(12)     .       .       .       .   no
 C1      N1      C4      C17        0.74(19)     .       .       .       .   no
 C5      N1      C4      C9        -1.25(19)     .       .       .       .   no
 C5      N1      C4      C17     -179.76(13)     .       .       .       .   no
 C1      N1      C5      C6      -179.03(13)     .       .       .       .   no
 C4      N1      C5      C6           1.5(2)     .       .       .       .   no
 C13     N2      C12     C11       -69.77(15)     .       .       .       .   no
 C13     N2      C12     C17       110.99(14)     .       .       .       .   no
 C16     N2      C12     C11       160.06(12)     .       .       .       .   no
 C16     N2      C12     C17       -19.18(19)     .       .       .       .   no
 C12     N2      C13     C14       170.10(10)     .       .       .       .   no
 C16     N2      C13     C14       -57.61(13)     .       .       .       .   no
 C12     N2      C16     C15      -169.67(11)     .       .       .       .   no
 C13     N2      C16     C15        59.55(14)     .       .       .       .   no
 C15     N3      C14     C13       -58.20(14)     .       .       .       .   no
 C14     N3      C15     C16        59.95(13)     .       .       .       .   no
 N1      C1      C2      C3       -109.08(14)     .       .       .       .   no
 N1      C1      C3      C2        107.64(14)     .       .       .       .   no
 N1      C4      C9      C8           0.9(2)     .       .       .       .   no
 N1      C4      C9      C10      -178.66(12)     .       .       .       .   no
 C17     C4      C9      C8        179.43(13)     .       .       .       .   no
 C17     C4      C9      C10         -0.2(2)     .       .       .       .   no
 N1      C4      C17     C12       176.62(12)     .       .       .       .   no
 C9      C4      C17     C12         -1.9(2)     .       .       .       .   no
 N1      C5      C6      C7        178.20(13)     .       .       .       .   no
 N1      C5      C6      C8         -1.3(2)     .       .       .       .   no
 C5      C6      C7      O1           0.0(2)     .       .       .       .   no
 C5      C6      C7      O2       -179.50(13)     .       .       .       .   no
 C8      C6      C7      O1        179.53(15)     .       .       .       .   no
 C8      C6      C7      O2           0.0(2)     .       .       .       .   no
 C5      C6      C8      O3       -179.51(14)     .       .       .       .   no
 C5      C6      C8      C9           0.9(2)     .       .       .       .   no
 C7      C6      C8      O3           1.0(2)     .       .       .       .   no
 C7      C6      C8      C9       -178.61(13)     .       .       .       .   no
 O3      C8      C9      C4        179.65(13)     .       .       .       .   no
 O3      C8      C9      C10         -0.8(2)     .       .       .       .   no
 C6      C8      C9      C4         -0.72(19)     .       .       .       .   no
 C6      C8      C9      C10       178.85(13)     .       .       .       .   no
 C4      C9      C10     C11          1.4(2)     .       .       .       .   no
 C8      C9      C10     C11      -178.24(13)     .       .       .       .   no
```

```
 C9      C10     C11     F1      -179.35(12)     .       .       .       .   no
 C9      C10     C11     C12         -0.6(2)     .       .       .       .   no
 F1      C11     C12     N2         -1.89(19)    .       .       .       .   no
 F1      C11     C12     C17        177.40(12)   .       .       .       .   no
 C10     C11     C12     N2         179.32(13)   .       .       .       .   no
 C10     C11     C12     C17           -1.4(2)   .       .       .       .   no
 N2      C12     C17     C4      -178.17(12)     .       .       .       .   no
 C11     C12     C17     C4          2.58(19)    .       .       .       .   no
 N2      C13     C14     N3         55.91(14)    .       .       .       .   no
 N3      C15     C16     N2        -59.99(14)    .       .       .       .   no
 O4      C18     C19     C20       -12.74(18)    .       .       .       .   no
 O5      C18     C19     C20       168.23(12)    .       .       .       .   no
 C18     C19     C20     C21     -169.99(11)     .       .       .       .   no
 C19     C20     C21     C22       -56.44(16)    .       .       .       .   no
 C20     C21     C22     C23     -179.28(12)     .       .       .       .   no
 C21     C22     C23     O6      -174.05(12)     .       .       .       .   no
 C21     C22     C23     O7           6.2(2)     .       .       .       .   no

loop_
_geom_hbond_atom_site_label_D
_geom_hbond_atom_site_label_H
_geom_hbond_atom_site_label_A
_geom_hbond_distance_DH
_geom_hbond_distance_HA
_geom_hbond_distance_DA
_geom_hbond_angle_DHA
_geom_hbond_site_symmetry_A
_geom_hbond_publ_flag
#
#D   H   A   D - H  H...A   D...A    D - H...A  symm(A)
#
O2      H2      O3         0.98(3)    1.61(3) 2.5360(17)     156(3)      .   yes
N3      H3A     O4       0.932(19)    1.79(2) 2.7054(16)  165.8(17)      .   yes
N3      H3B     O5         0.94(2)    1.77(2) 2.7155(15)     175(2)   4_554 yes
O6      H6      O5         0.93(3)    1.58(3) 2.5079(15)     173(3)   4_455 yes
```

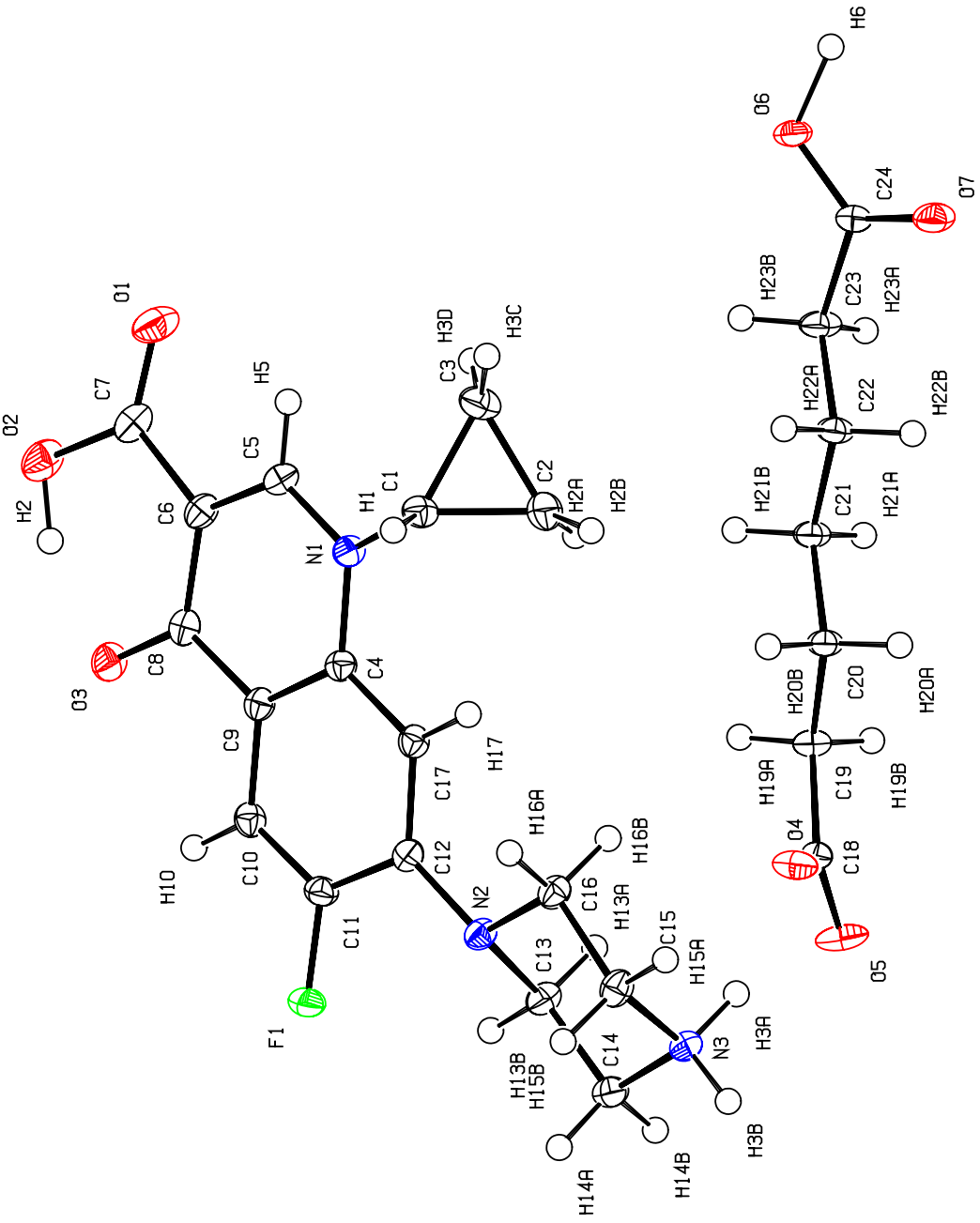


**Figure S8A**: ORTEP view of asymmetric unit of CFX-PA with atom labelling

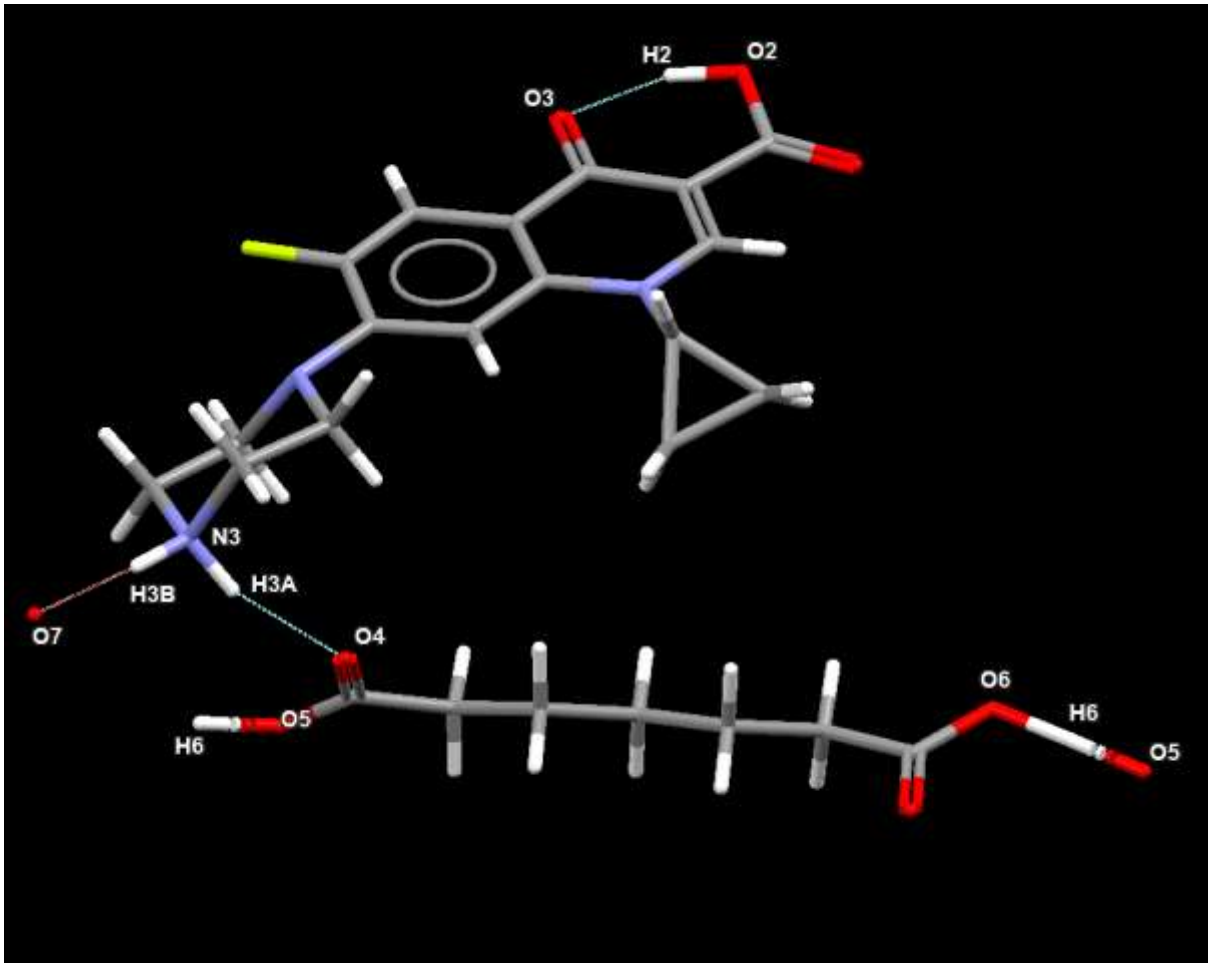


| Donor | H | Accept | D-H / Å | H…A / Å | D…A / Å | D-H…A / ° | Symm |
|---|---|---|---|---|---|---|---|
| O2 | H2 | O3 | 0.97(2) | 1.63(2) | 2.5525(12) | 157.5(17) | x,y,z |
| N3 | H3A | O4 | 0.956(15) | 1.863(16) | 2.7891(12) | 162.4(14) | x,y,z |
| N3 | H3B | O7 | 0.929(16) | 1.891(16) | 2.8183(12) | 175.4(12) | 1/2-x,-y+2,z-1/2 |
| O6 | H6 | O5 | 1.20(2) | 1.23(2) | 2.4280(10) | 177(2) | x,3/2-y,1/2+z |

**Figure S8B**. A Mercury diagram for the asymmetric unit of CFX-PA, showing the unique set of hydrogen bonds (dashed lines) and the associated bond distances and angles.

**Table S4** Bond distances and angles for CFX-PA

```
loop_
_space_group_symop_id
_space_group_symop_operation_xyz
   1 x,y,z
   2 1/2-x,-y,1/2+z
   3 1/2+x,1/2-y,-z
   4 -x,1/2+y,1/2-z
   5 -x,-y,-z
   6 1/2+x,y,1/2-z
   7 1/2-x,1/2+y,z
   8 x,1/2-y,1/2+z

_geom_special_details
;
 Bond distances, angles etc. have been calculated using the
 rounded fractional coordinates. All su's are estimated
 from the variances of the (full) variance-covariance matrix.
 The cell esds are taken into account in the estimation of
 distances, angles and torsion angles
;

loop_
_geom_bond_atom_site_label_1
_geom_bond_atom_site_label_2
_geom_bond_distance
_geom_bond_site_symmetry_1
_geom_bond_site_symmetry_2
_geom_bond_publ_flag
 O4      C18      1.2354(12)                    .       .                 yes
 O5      C18      1.2836(12)                    .       .                 yes
 O6      C24      1.2894(14)                    .       .                 yes
 O7      C24      1.2351(14)                    .       .                 yes
 F1      C11      1.3546(14)                    .       .                 yes
 O5      H6          1.23(2)                    .     8_564               no
 O6      H6          1.20(2)                    .       .                 no
 O1      C7       1.2088(15)                    .       .                 yes
 O2      C7       1.3374(14)                    .       .                 yes
 O3      C8       1.2660(13)                    .       .                 yes
 C18     C19      1.5082(14)                    .       .                 no
 C19     C20      1.5178(14)                    .       .                 no
 C20     C21      1.5223(14)                    .       .                 no
 C21     C22      1.5212(14)                    .       .                 no
 C22     C23      1.5208(15)                    .       .                 no
 C23     C24      1.5115(16)                    .       .                 no
 N1      C5       1.3421(14)                    .       .                 yes
 N1      C4       1.4011(13)                    .       .                 yes
 N1      C1       1.4591(13)                    .       .                 yes
 N2      C12      1.4025(14)                    .       .                 yes
 N2      C16      1.4677(14)                    .       .                 yes
 N2      C13      1.4840(15)                    .       .                 yes
 O2      H2          0.97(2)                    .       .                 no
 N3      C14      1.4937(14)                    .       .                 yes
 N3      C15      1.4913(15)                    .       .                 yes
 C19     H19B        0.9900                     .       .                 no
 C19     H19A        0.9900                     .       .                 no
 C20     H20B        0.9900                     .       .                 no
 C20     H20A        0.9900                     .       .                 no
 C21     H21A        0.9900                     .       .                 no
 C21     H21B        0.9900                     .       .                 no
 C22     H22A        0.9900                     .       .                 no
 C22     H22B        0.9900                     .       .                 no
 C23     H23B        0.9900                     .       .                 no
 C23     H23A        0.9900                     .       .                 no
 C1      C3       1.4931(17)                    .       .                 no
 C1      C2       1.5019(16)                    .       .                 no
 C2      C3       1.5124(17)                    .       .                 no
```

```
 N3      H3B       0.929(16)                    .      .                 no
 N3      H3A       0.956(15)                    .      .                 no
 C4      C17      1.4047(15)                    .      .                 no
 C4      C9       1.4063(15)                    .      .                 no
 C5      C6       1.3750(16)                    .      .                 no
 C6      C7       1.4876(16)                    .      .                 no
 C6      C8       1.4345(17)                    .      .                 no
 C8      C9       1.4511(16)                    .      .                 no
 C9      C10      1.4086(17)                    .      .                 no
 C10     C11      1.3579(16)                    .      .                 no
 C11     C12      1.4193(15)                    .      .                 no
 C12     C17      1.3922(17)                    .      .                 no
 C13     C14      1.5160(16)                    .      .                 no
 C15     C16      1.5148(16)                    .      .                 no
 C1      H1           1.0000                    .      .                 no
 C2      H2A          0.9900                    .      .                 no
 C2      H2B          0.9900                    .      .                 no
 C3      H3C          0.9900                    .      .                 no
 C3      H3D          0.9900                    .      .                 no
 C5      H5           0.9500                    .      .                 no
 C10     H10          0.9500                    .      .                 no
 C13     H13A         0.9900                    .      .                 no
 C13     H13B         0.9900                    .      .                 no
 C14     H14A         0.9900                    .      .                 no
 C14     H14B         0.9900                    .      .                 no
 C15     H15A         0.9900                    .      .                 no
 C15     H15B         0.9900                    .      .                 no
 C16     H16A         0.9900                    .      .                 no
 C16     H16B         0.9900                    .      .                 no
 C17     H17          0.9500                    .      .                 no

loop_
_geom_angle_atom_site_label_1
_geom_angle_atom_site_label_2
_geom_angle_atom_site_label_3
_geom_angle
_geom_angle_site_symmetry_1
_geom_angle_site_symmetry_2
_geom_angle_site_symmetry_3
_geom_angle_publ_flag
 C18     O5      H6        115.5(11)           .      .     8_564        no
 C24     O6      H6        113.3(11)           .      .       .          no
 O4      C18     O5        123.95(9)           .      .       .          yes
 O4      C18     C19       121.12(9)           .      .       .          yes
 O5      C18     C19       114.91(9)           .      .       .          yes
 C18     C19     C20       115.31(9)           .      .       .          no
 C19     C20     C21       111.20(9)           .      .       .          no
 C20     C21     C22       114.04(9)           .      .       .          no
 C21     C22     C23       111.86(9)           .      .       .          no
 C22     C23     C24       114.25(9)           .      .       .          no
 O7      C24     C23      121.12(10)           .      .       .          yes
 O6      C24     O7       124.76(10)           .      .       .          yes
 O6      C24     C23       114.12(9)           .      .       .          yes
 C1      N1      C4        119.50(9)           .      .       .          yes
 C1      N1      C5        119.62(9)           .      .       .          yes
 C4      N1      C5        120.26(9)           .      .       .          yes
 C13     N2      C16       111.43(9)           .      .       .          yes
 C12     N2      C16       115.78(9)           .      .       .          yes
 C7      O2      H2        105.4(11)           .      .       .          no
 C12     N2      C13       112.91(9)           .      .       .          yes
 C14     N3      C15       108.73(9)           .      .       .          yes
 C18     C19     H19B         108.00           .      .       .          no
 C18     C19     H19A         108.00           .      .       .          no
 C20     C19     H19B         108.00           .      .       .          no
 H19A    C19     H19B         107.00           .      .       .          no
 C20     C19     H19A         108.00           .      .       .          no
 C19     C20     H20B         109.00           .      .       .          no
 C21     C20     H20A         109.00           .      .       .          no
```

| | | | | | | | |
|---|---|---|---|---|---|---|---|
| C21 | C20 | H20B | 109.00 | . | . | . | no |
| H20A | C20 | H20B | 108.00 | . | . | . | no |
| C19 | C20 | H20A | 109.00 | . | . | . | no |
| C22 | C21 | H21A | 109.00 | . | . | . | no |
| C20 | C21 | H21A | 109.00 | . | . | . | no |
| C20 | C21 | H21B | 109.00 | . | . | . | no |
| C22 | C21 | H21B | 109.00 | . | . | . | no |
| H21A | C21 | H21B | 108.00 | . | . | . | no |
| C23 | C22 | H22A | 109.00 | . | . | . | no |
| C21 | C22 | H22B | 109.00 | . | . | . | no |
| C23 | C22 | H22B | 109.00 | . | . | . | no |
| C21 | C22 | H22A | 109.00 | . | . | . | no |
| H22A | C22 | H22B | 108.00 | . | . | . | no |
| C22 | C23 | H23B | 109.00 | . | . | . | no |
| C24 | C23 | H23A | 109.00 | . | . | . | no |
| C24 | C23 | H23B | 109.00 | . | . | . | no |
| H23A | C23 | H23B | 108.00 | . | . | . | no |
| C22 | C23 | H23A | 109.00 | . | . | . | no |
| N1 | C1 | C2 | 119.98(10) | . | . | . | yes |
| N1 | C1 | C3 | 120.02(9) | . | . | . | yes |
| C2 | C1 | C3 | 60.66(8) | . | . | . | no |
| C1 | C2 | C3 | 59.39(8) | . | . | . | no |
| C15 | N3 | H3A | 109.3(9) | . | . | . | no |
| C15 | N3 | H3B | 109.1(9) | . | . | . | no |
| H3A | N3 | H3B | 107.8(13) | . | . | . | no |
| C1 | C3 | C2 | 59.96(8) | . | . | . | no |
| C14 | N3 | H3A | 109.4(9) | . | . | . | no |
| C14 | N3 | H3B | 112.5(10) | . | . | . | no |
| C9 | C4 | C17 | 120.28(9) | . | . | . | no |
| N1 | C4 | C17 | 120.65(10) | . | . | . | yes |
| N1 | C4 | C9 | 119.06(9) | . | . | . | yes |
| N1 | C5 | C6 | 123.37(11) | . | . | . | yes |
| C5 | C6 | C8 | 120.28(10) | . | . | . | no |
| C5 | C6 | C7 | 118.10(10) | . | . | . | no |
| C7 | C6 | C8 | 121.61(10) | . | . | . | no |
| O1 | C7 | C6 | 124.14(10) | . | . | . | yes |
| O1 | C7 | O2 | 121.25(11) | . | . | . | yes |
| O2 | C7 | C6 | 114.61(10) | . | . | . | yes |
| C6 | C8 | C9 | 115.74(10) | . | . | . | no |
| O3 | C8 | C6 | 122.85(10) | . | . | . | yes |
| O3 | C8 | C9 | 121.42(10) | . | . | . | yes |
| C4 | C9 | C10 | 118.65(10) | . | . | . | no |
| C8 | C9 | C10 | 120.10(10) | . | . | . | no |
| C4 | C9 | C8 | 121.24(10) | . | . | . | no |
| C9 | C10 | C11 | 119.84(10) | . | . | . | no |
| C10 | C11 | C12 | 123.18(11) | . | . | . | no |
| F1 | C11 | C12 | 118.32(10) | . | . | . | yes |
| F1 | C11 | C10 | 118.45(10) | . | . | . | yes |
| N2 | C12 | C11 | 119.77(10) | . | . | . | yes |
| N2 | C12 | C17 | 123.54(9) | . | . | . | yes |
| C11 | C12 | C17 | 116.68(10) | . | . | . | no |
| N2 | C13 | C14 | 111.59(9) | . | . | . | yes |
| N3 | C14 | C13 | 110.09(9) | . | . | . | yes |
| N3 | C15 | C16 | 109.70(9) | . | . | . | yes |
| N2 | C16 | C15 | 110.05(9) | . | . | . | yes |
| C4 | C17 | C12 | 121.24(9) | . | . | . | no |
| N1 | C1 | H1 | 115.00 | . | . | . | no |
| C2 | C1 | H1 | 115.00 | . | . | . | no |
| C3 | C1 | H1 | 115.00 | . | . | . | no |
| C1 | C2 | H2A | 118.00 | . | . | . | no |
| C1 | C2 | H2B | 118.00 | . | . | . | no |
| C3 | C2 | H2A | 118.00 | . | . | . | no |
| C3 | C2 | H2B | 118.00 | . | . | . | no |
| H2A | C2 | H2B | 115.00 | . | . | . | no |
| C1 | C3 | H3C | 118.00 | . | . | . | no |
| C1 | C3 | H3D | 118.00 | . | . | . | no |
| C2 | C3 | H3C | 118.00 | . | . | . | no |
| C2 | C3 | H3D | 118.00 | . | . | . | no |

```
 H3C     C3      H3D          115.00             .      .      .          no
 N1      C5      H5           118.00             .      .      .          no
 C6      C5      H5           118.00             .      .      .          no
 C9      C10     H10          120.00             .      .      .          no
 C11     C10     H10          120.00             .      .      .          no
 N2      C13     H13A         109.00             .      .      .          no
 N2      C13     H13B         109.00             .      .      .          no
 C14     C13     H13A         109.00             .      .      .          no
 C14     C13     H13B         109.00             .      .      .          no
 H13A    C13     H13B         108.00             .      .      .          no
 N3      C14     H14A         110.00             .      .      .          no
 N3      C14     H14B         110.00             .      .      .          no
 C13     C14     H14A         110.00             .      .      .          no
 C13     C14     H14B         110.00             .      .      .          no
 H14A    C14     H14B         108.00             .      .      .          no
 N3      C15     H15A         110.00             .      .      .          no
 N3      C15     H15B         110.00             .      .      .          no
 C16     C15     H15A         110.00             .      .      .          no
 C16     C15     H15B         110.00             .      .      .          no
 H15A    C15     H15B         108.00             .      .      .          no
 N2      C16     H16A         110.00             .      .      .          no
 N2      C16     H16B         110.00             .      .      .          no
 C15     C16     H16A         110.00             .      .      .          no
 C15     C16     H16B         110.00             .      .      .          no
 H16A    C16     H16B         108.00             .      .      .          no
 C4      C17     H17          119.00             .      .      .          no
 C12     C17     H17          119.00             .      .      .          no

loop_
_geom_torsion_atom_site_label_1
_geom_torsion_atom_site_label_2
_geom_torsion_atom_site_label_3
_geom_torsion_atom_site_label_4
_geom_torsion
_geom_torsion_site_symmetry_1
_geom_torsion_site_symmetry_2
_geom_torsion_site_symmetry_3
_geom_torsion_site_symmetry_4
_geom_torsion_publ_flag
 O4      C18     C19     C20       23.15(15)     .      .      .      .   no
 O5      C18     C19     C20     -158.55(10)     .      .      .      .   no
 C18     C19     C20     C21      -176.53(9)     .      .      .      .   no
 C19     C20     C21     C22     -174.36(10)     .      .      .      .   no
 C20     C21     C22     C23     -179.65(10)     .      .      .      .   no
 C21     C22     C23     C24     -173.96(10)     .      .      .      .   no
 C22     C23     C24     O6      -144.82(10)     .      .      .      .   no
 C22     C23     C24     O7        36.02(16)     .      .      .      .   no
 C4      N1      C1      C2        75.25(13)     .      .      .      .   no
 C4      N1      C1      C3       146.58(10)     .      .      .      .   no
 C5      N1      C1      C2      -113.73(12)     .      .      .      .   no
 C5      N1      C1      C3       -42.40(15)     .      .      .      .   no
 C1      N1      C4      C9        170.19(9)     .      .      .      .   no
 C1      N1      C4      C17      -10.82(14)     .      .      .      .   no
 C5      N1      C4      C9        -0.77(14)     .      .      .      .   no
 C5      N1      C4      C17       178.22(9)     .      .      .      .   no
 C1      N1      C5      C6      -171.52(10)     .      .      .      .   no
 C4      N1      C5      C6        -0.57(15)     .      .      .      .   no
 C13     N2      C12     C11       60.22(13)     .      .      .      .   no
 C13     N2      C12     C17     -121.39(11)     .      .      .      .   no
 C16     N2      C12     C11     -169.63(10)     .      .      .      .   no
 C16     N2      C12     C17        8.76(14)     .      .      .      .   no
 C12     N2      C13     C14      -173.17(9)     .      .      .      .   no
 C16     N2      C13     C14       54.52(12)     .      .      .      .   no
 C12     N2      C16     C15       172.70(9)     .      .      .      .   no
 C13     N2      C16     C15      -56.45(12)     .      .      .      .   no
 C15     N3      C14     C13       58.85(11)     .      .      .      .   no
 C14     N3      C15     C16      -61.46(11)     .      .      .      .   no
 N1      C1      C2      C3       109.77(11)     .      .      .      .   no
```

```
 N1      C1      C3      C2      -109.71(12)     .       .       .       .   no
 N1      C4      C9      C8        0.08(15)      .       .       .       .   no
 N1      C4      C9      C10     -178.47(9)      .       .       .       .   no
 C17     C4      C9      C8      -178.92(9)      .       .       .       .   no
 C17     C4      C9      C10       2.53(14)      .       .       .       .   no
 N1      C4      C17     C12     -178.67(9)      .       .       .       .   no
 C9      C4      C17     C12       0.31(14)      .       .       .       .   no
 N1      C5      C6      C7      -178.33(10)     .       .       .       .   no
 N1      C5      C6      C8        2.60(16)      .       .       .       .   no
 C5      C6      C7      O1       13.71(18)      .       .       .       .   no
 C5      C6      C7      O2      -165.90(10)     .       .       .       .   no
 C8      C6      C7      O1      -167.24(11)     .       .       .       .   no
 C8      C6      C7      O2       13.16(16)      .       .       .       .   no
 C5      C6      C8      O3      176.82(10)      .       .       .       .   no
 C5      C6      C8      C9       -3.07(15)      .       .       .       .   no
 C7      C6      C8      O3       -2.22(16)      .       .       .       .   no
 C7      C6      C8      C9      177.89(10)      .       .       .       .   no
 O3      C8      C9      C4      -178.10(9)      .       .       .       .   no
 O3      C8      C9      C10       0.43(14)      .       .       .       .   no
 C6      C8      C9      C4        1.79(14)      .       .       .       .   no
 C6      C8      C9      C10     -179.68(9)      .       .       .       .   no
 C4      C9      C10     C11      -2.32(14)      .       .       .       .   no
 C8      C9      C10     C11     179.12(10)      .       .       .       .   no
 C9      C10     C11     F1       176.88(9)      .       .       .       .   no
 C9      C10     C11     C12      -0.74(16)      .       .       .       .   no
 F1      C11     C12     N2        4.36(15)      .       .       .       .   no
 F1      C11     C12     C17     -174.13(9)      .       .       .       .   no
 C10     C11     C12     N2      -178.01(10)     .       .       .       .   no
 C10     C11     C12     C17       3.49(16)      .       .       .       .   no
 N2      C12     C17     C4       178.36(9)      .       .       .       .   no
 C11     C12     C17     C4       -3.21(14)      .       .       .       .   no
 N2      C13     C14     N3       -55.59(12)     .       .       .       .   no
 N3      C15     C16     N2        60.43(12)     .       .       .       .   no

loop_
_geom_hbond_atom_site_label_D
_geom_hbond_atom_site_label_H
_geom_hbond_atom_site_label_A
_geom_hbond_distance_DH
_geom_hbond_distance_HA
_geom_hbond_distance_DA
_geom_hbond_angle_DHA
_geom_hbond_site_symmetry_A
_geom_hbond_publ_flag
#
#D   H   A   D - H  H...A   D...A    D - H...A  symm(A)
#
O2      H2      O3        0.97(2)    1.63(2) 2.5525(12)  157.5(17)     .   yes
N3      H3A     O4       0.956(15)  1.863(16) 2.7891(12)  162.4(14)     .   yes
N3      H3B     O7       0.929(16)  1.891(16) 2.8183(12)  175.4(12)   2_574 yes
O6      H6      O5        1.20(2)    1.23(2) 2.4280(10)     177(2)   8_565 yes
```

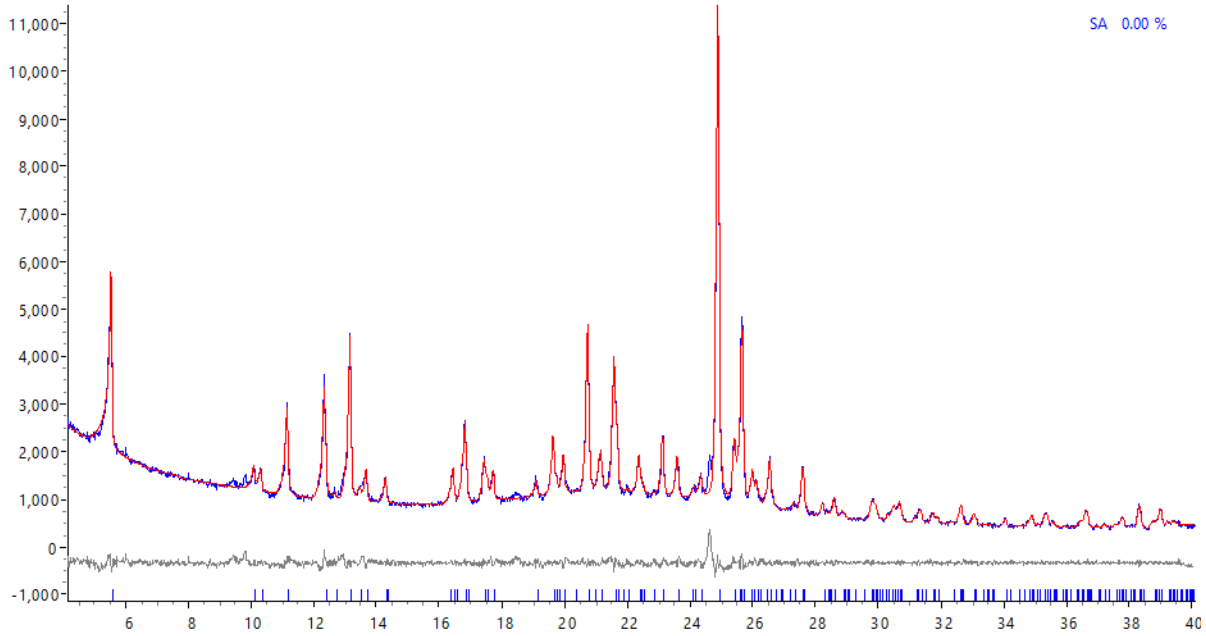


**Figure S9:** Pawley-Fit of milled CFX-SA

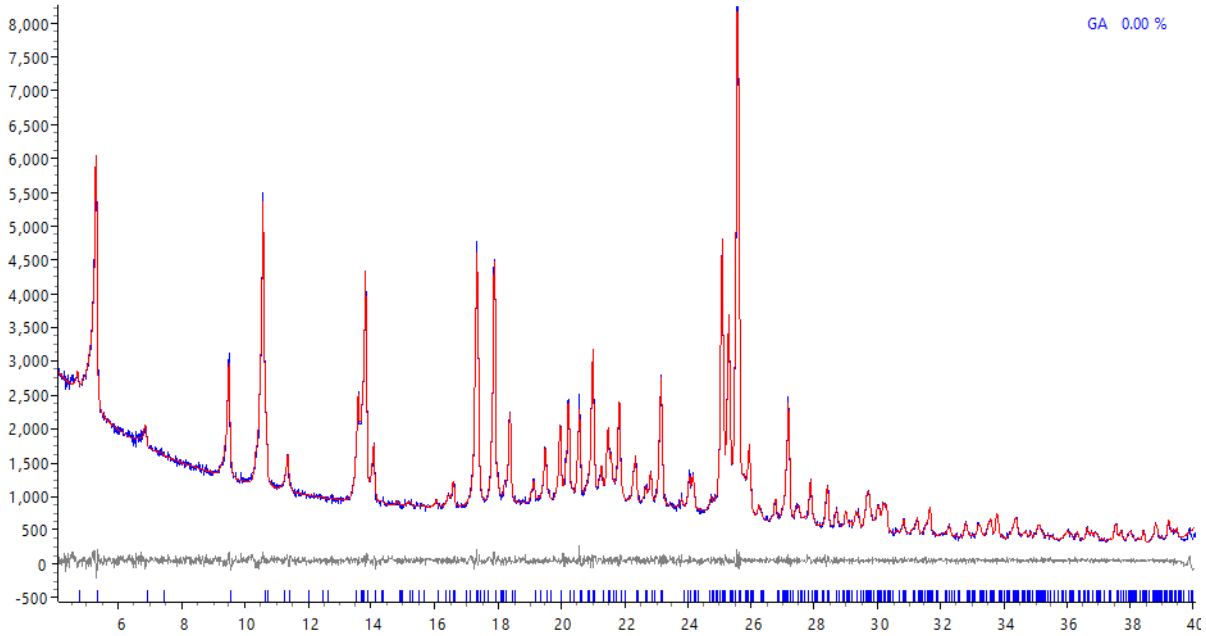


**Figure S10:** Pawley-Fit of milled CFX-GA

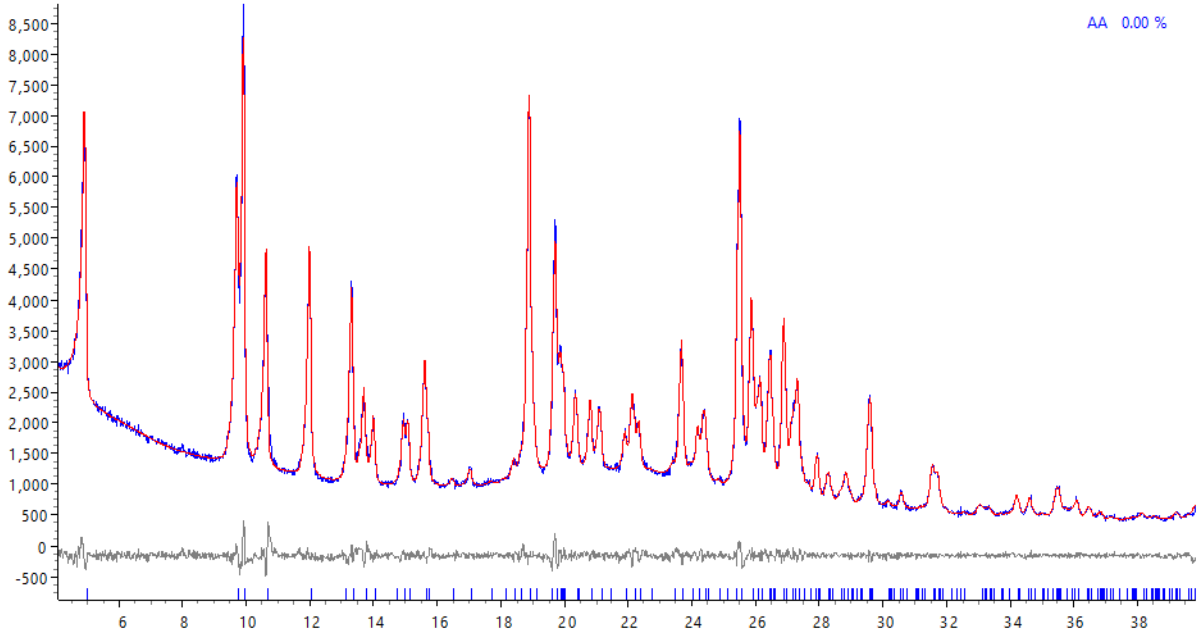


**Figure S11:** Pawley-Fit of milled CFX-AA

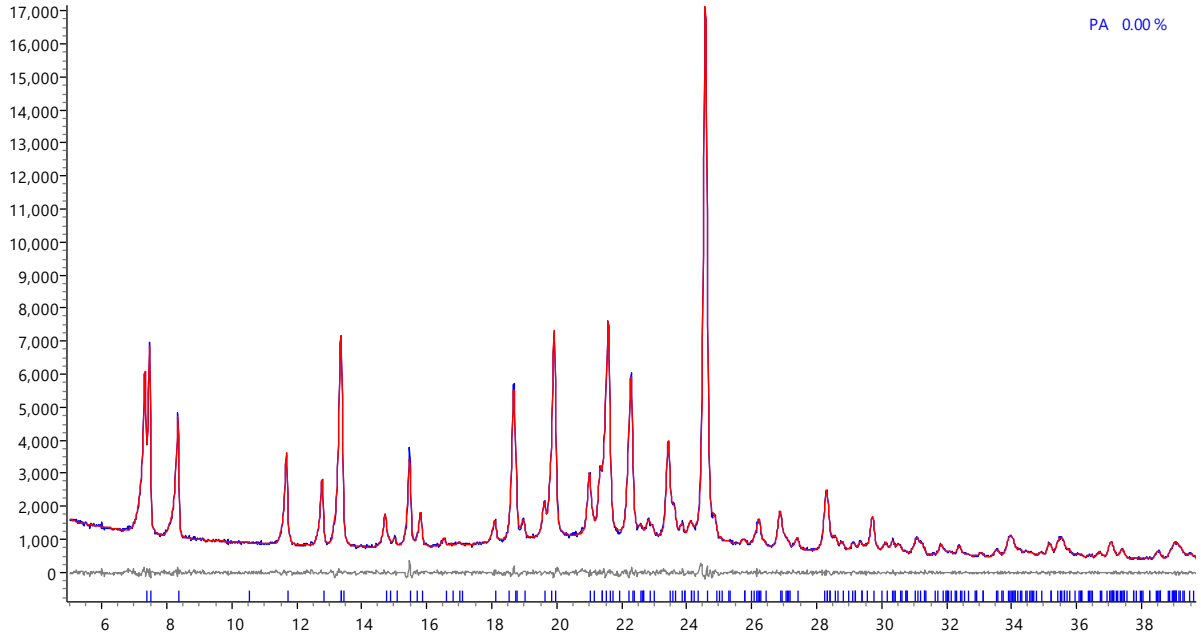


**Figure S12:** Pawley-Fit of milled CFX-PA

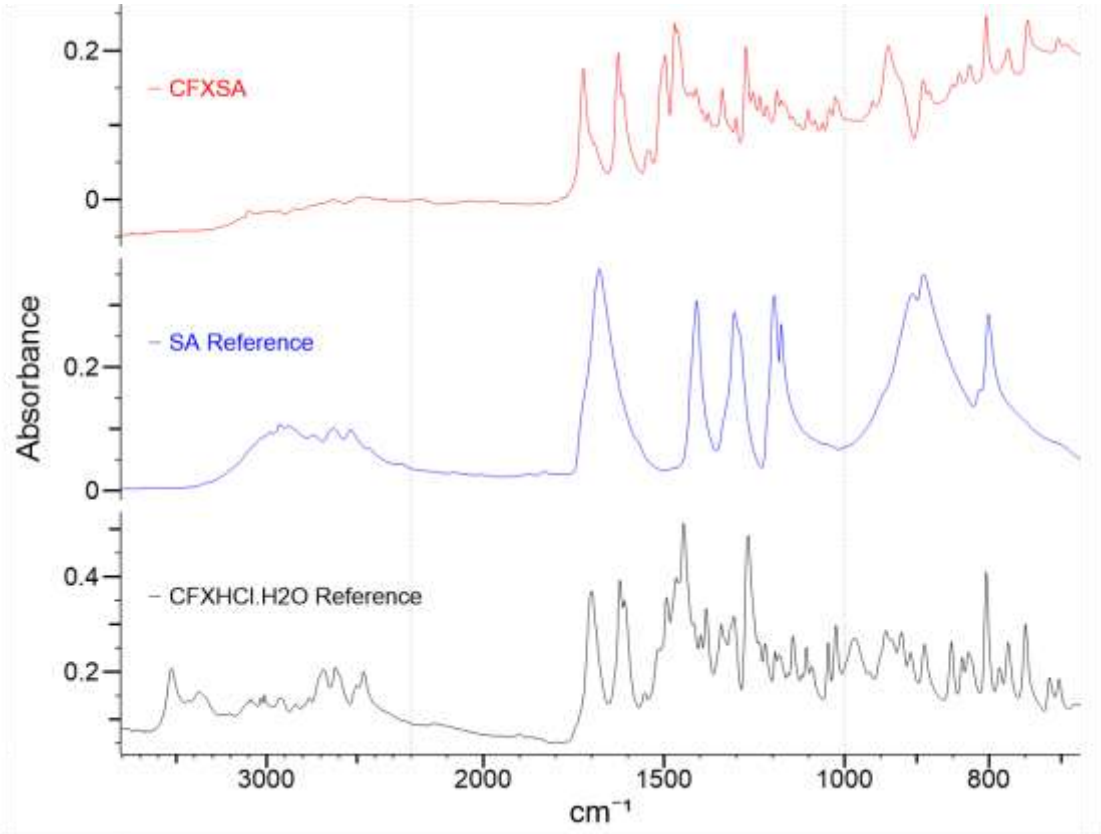


**Figure S13:** FTIR data comparing milled CFX-SA with CFX and SA starting materials

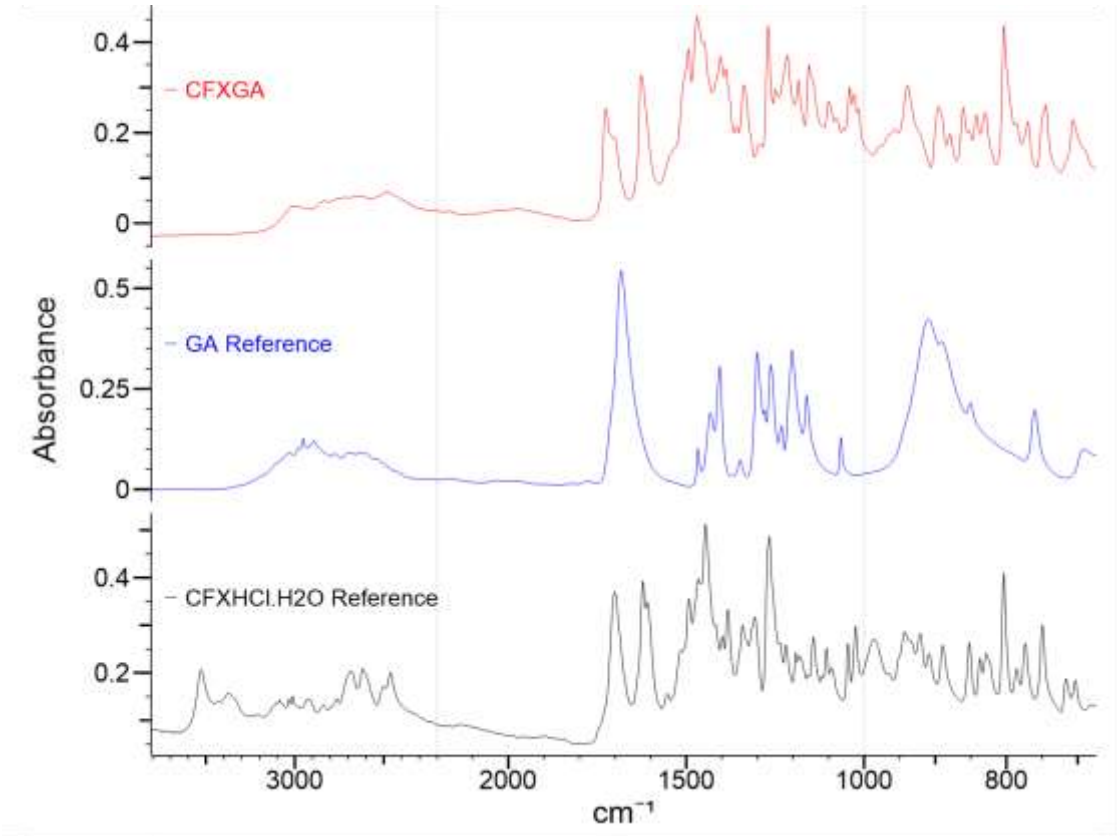


**Figure S14:** FTIR data comparing milled CFX-GA with CFX and GA starting materials

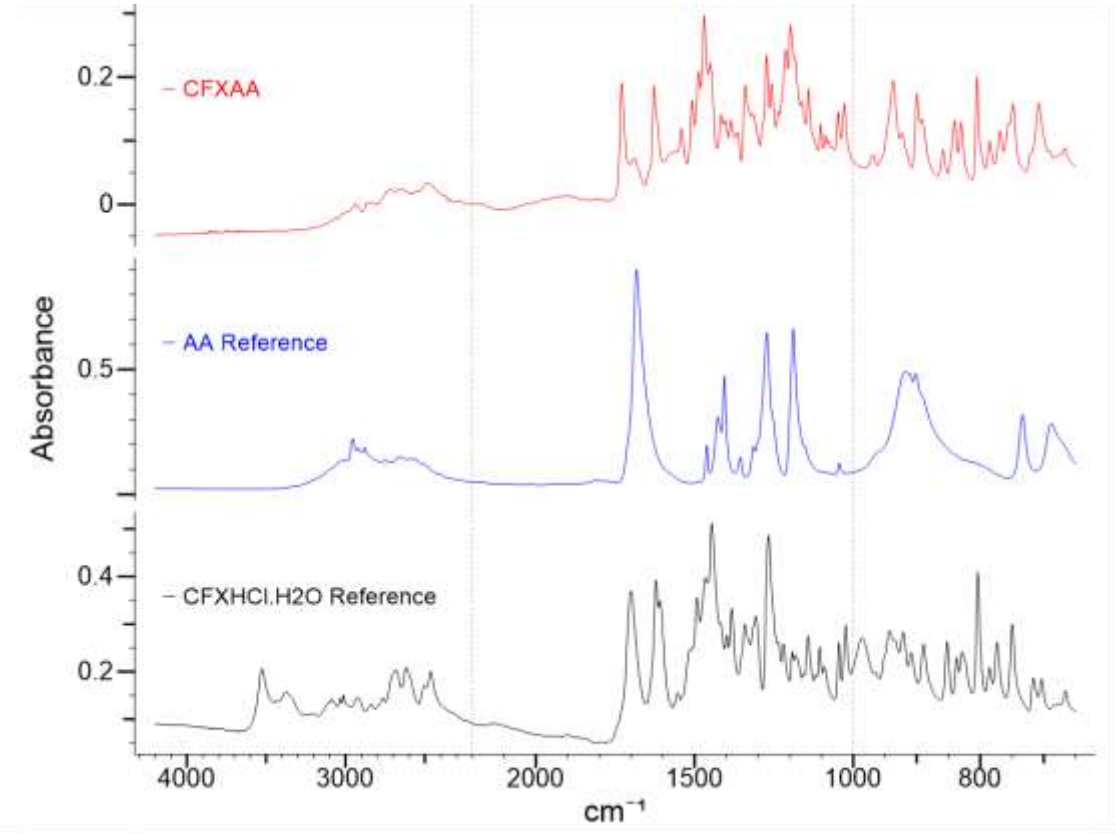


**Figure S15:** FTIR data comparing milled CFX-AA with CFX and AA starting materials

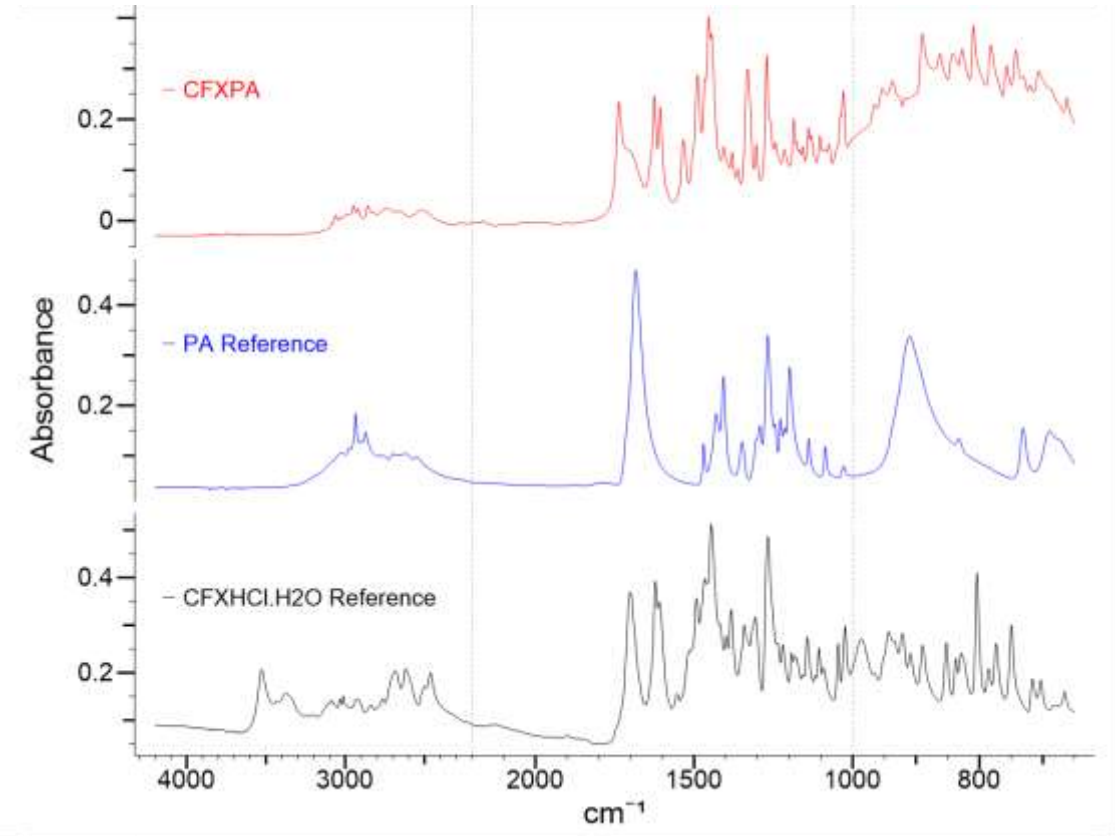


**Figure S16:** FTIR data comparing milled CFX-PA with CFX and PA starting materials

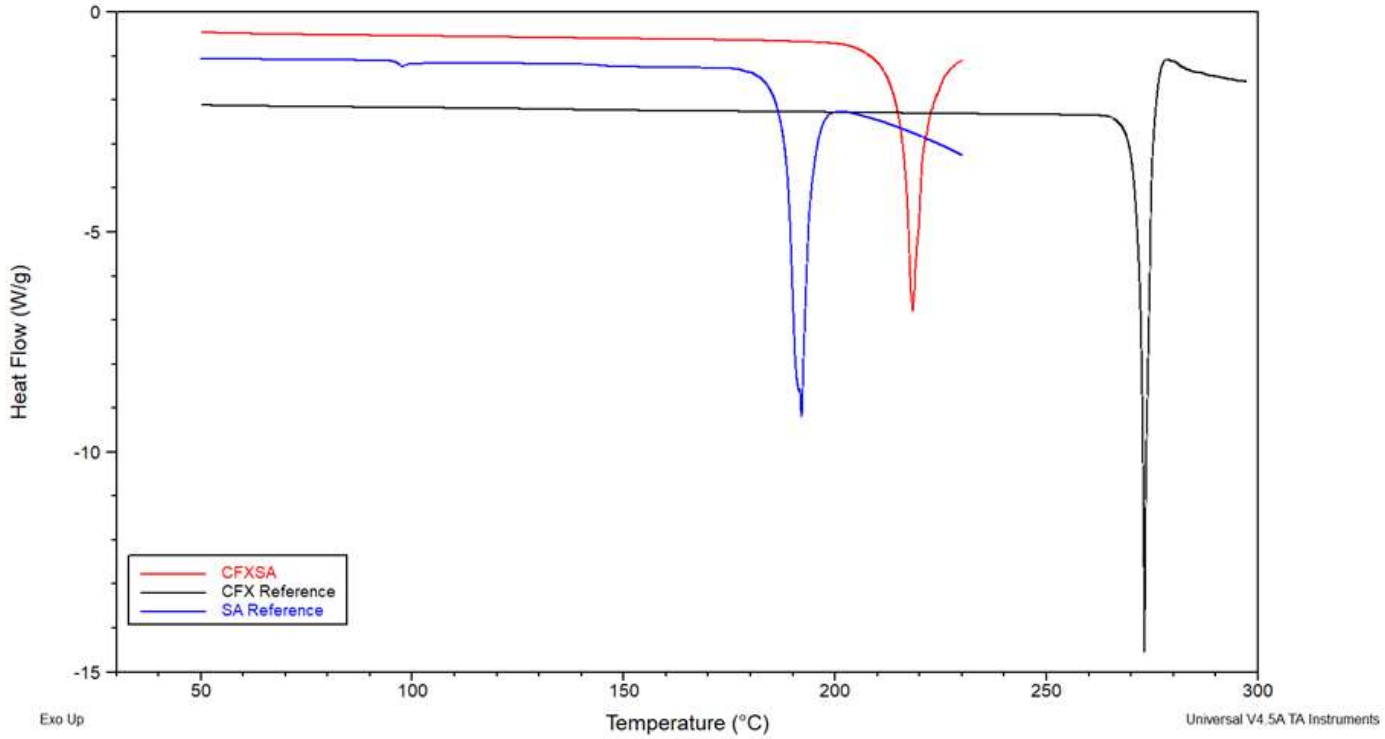


**Figure S17:** DSC data comparing milled CFX-SA with CFX and SA starting materials

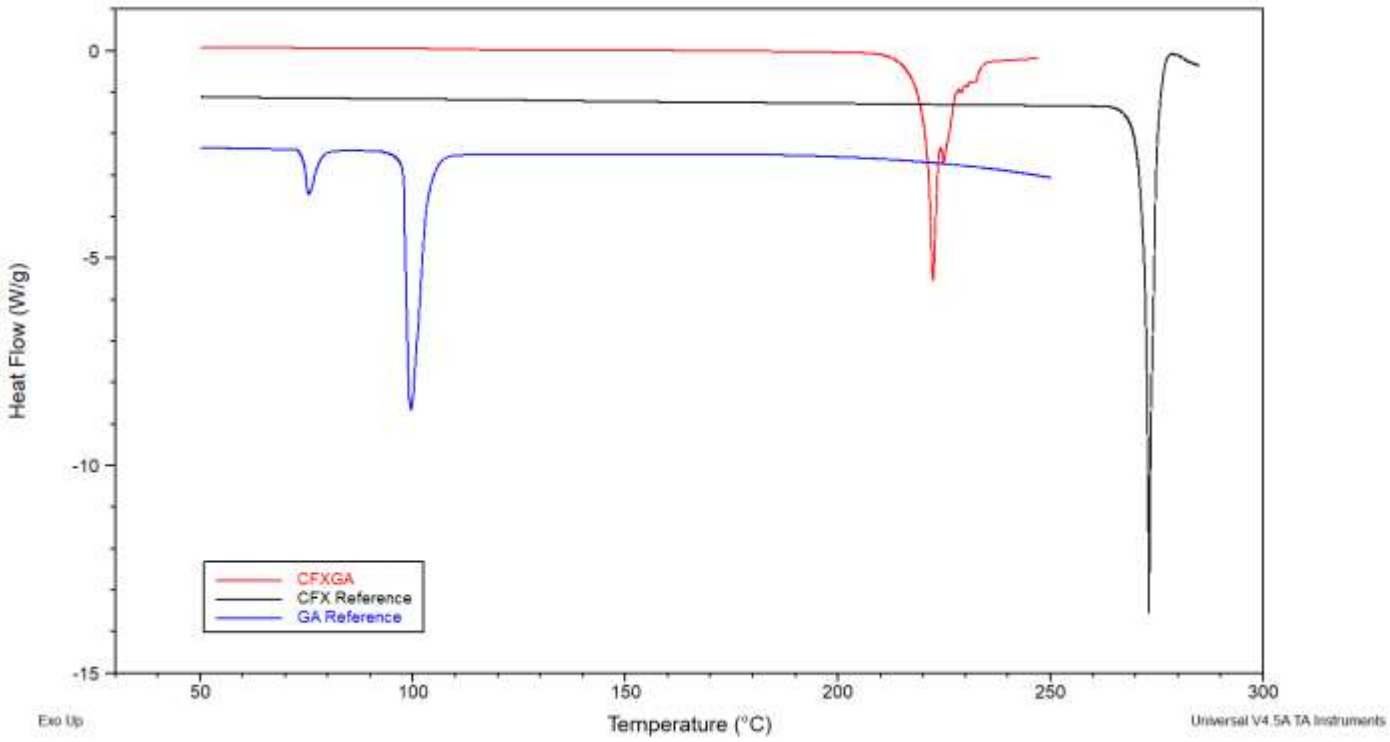


**Figure S18:** DSC data comparing milled CFX-GA with CFX and GA starting materials

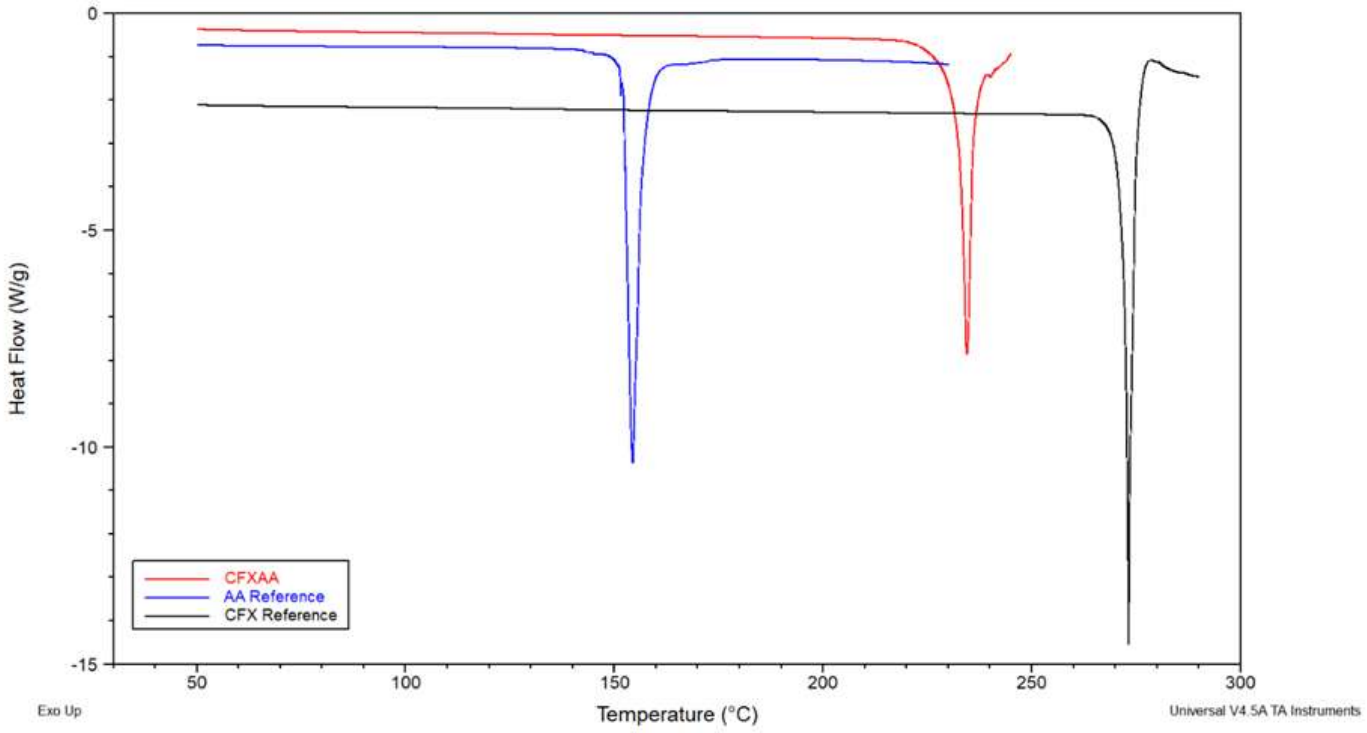


**Figure S19:** DSC data comparing milled CFX-AA with CFX and AA starting materials

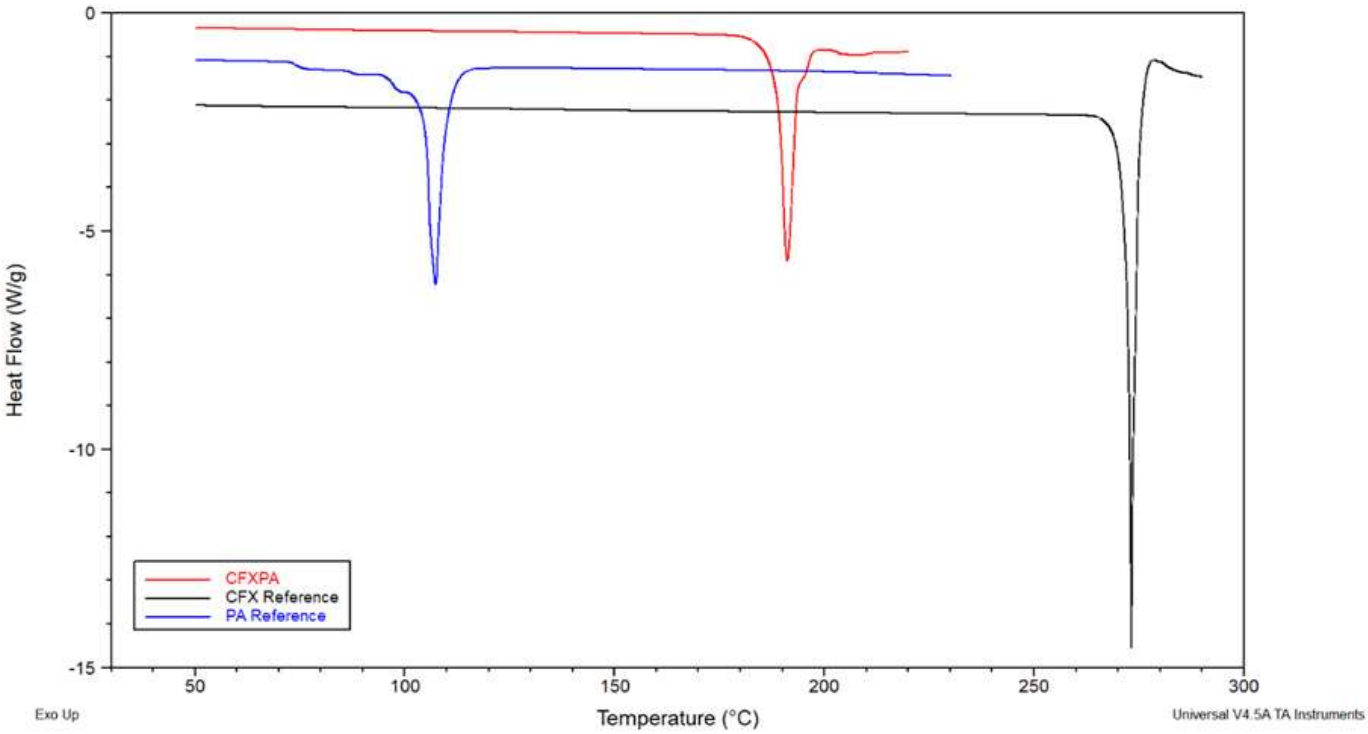


**Figure S20:** DSC data comparing milled CFX-PA with CFX and PA starting materials

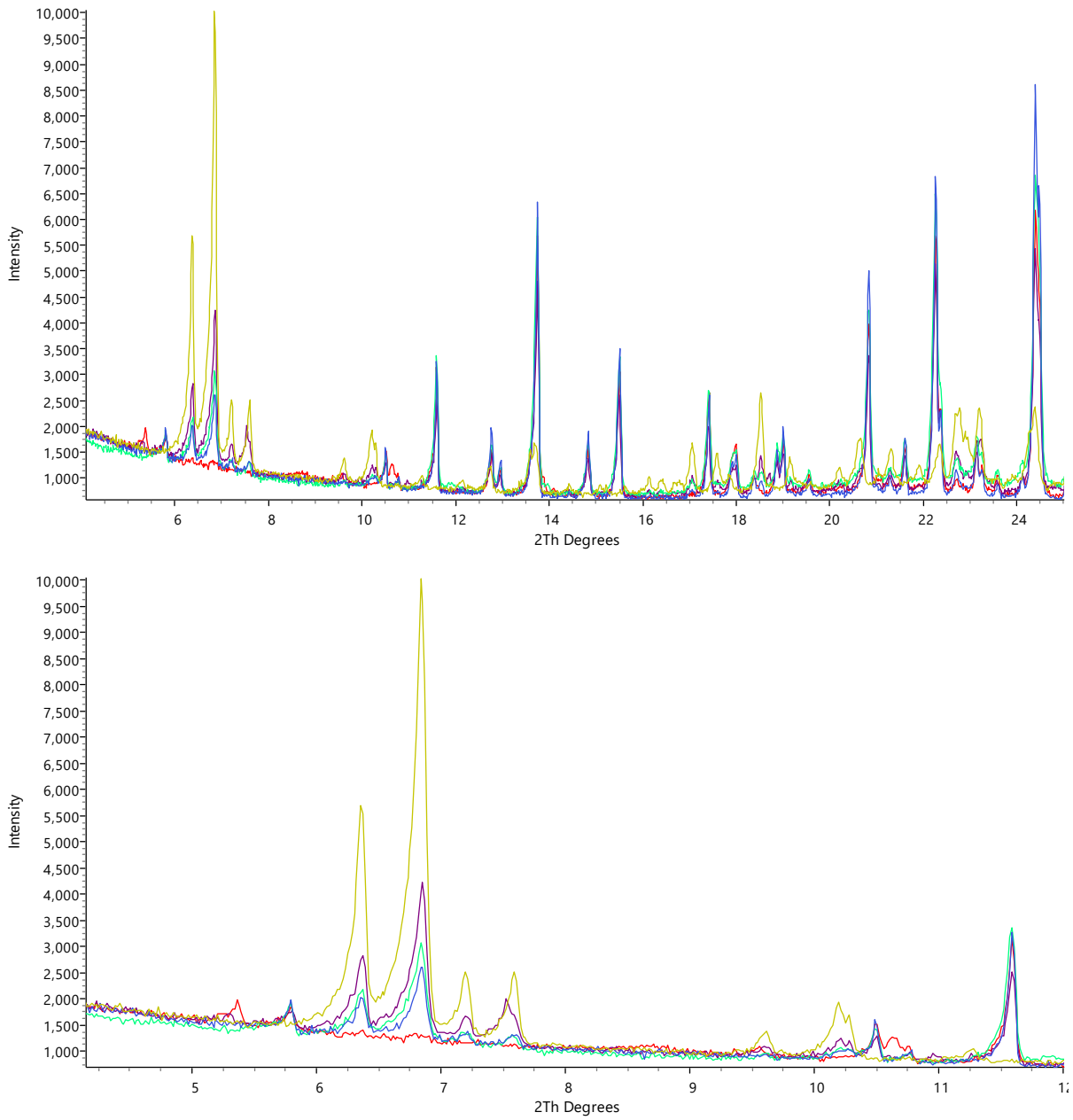


**Figure S21**: PXRD patterns for the excess solids recovered at the end of the dissolution experiments. Two ranges are shown to highlight the similarities and differences between the excesses from starting materials CFX-GA (red), CFX-SA (green), CFX-PA (purple), CFX base (mustard) and CFX-HCl·H2O (blue). Note that CFX-GA pattern between 5° and 8° two-theta is markedly different from that of the other patterns. Note also that the peak at ca. 11.5° two-theta is absent in the CFX base pattern.

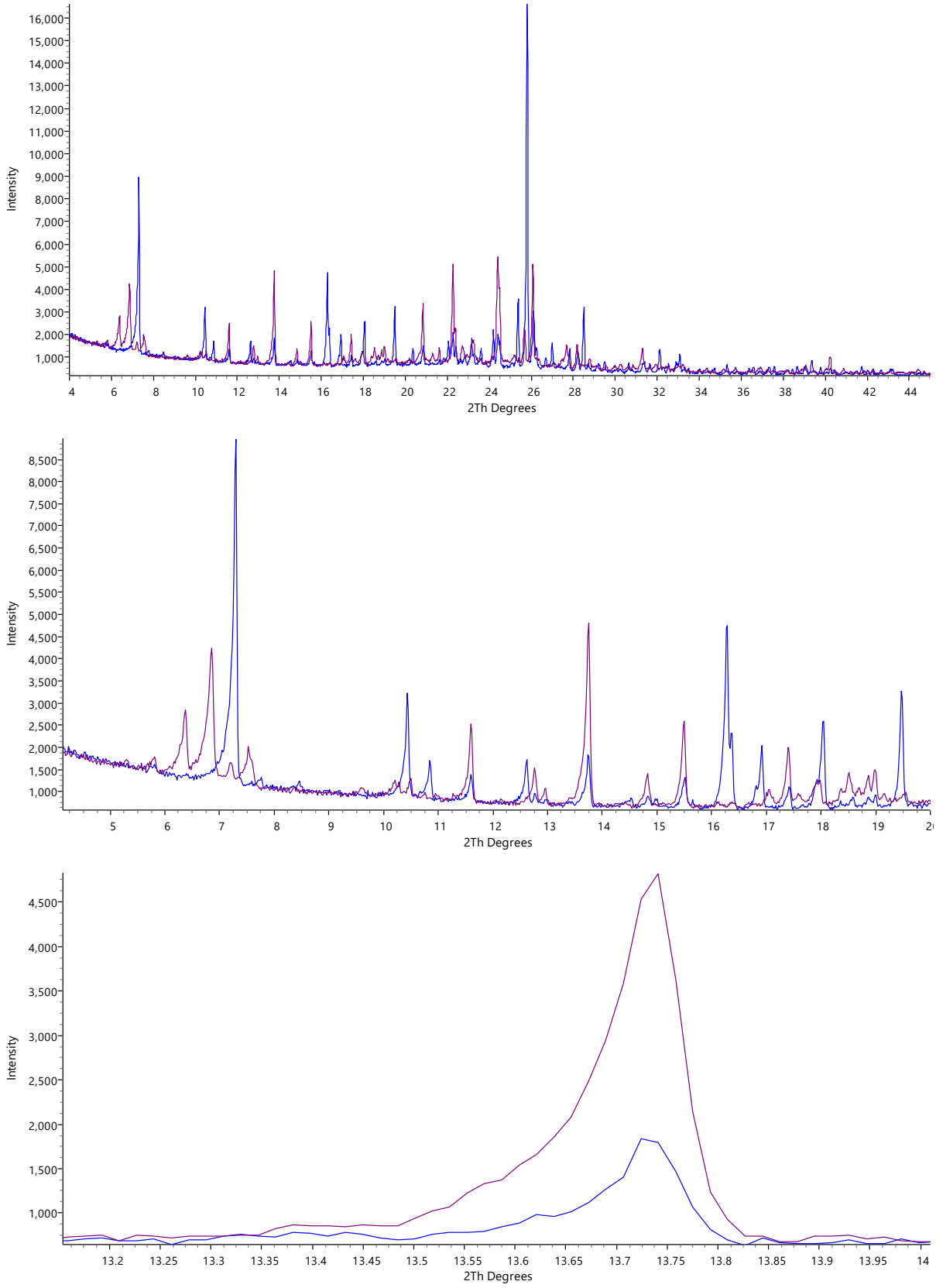


**Figure S22**: PXRD patterns for excess solids recovered at the end of the dissolution experiments. Three ranges are shown to highlight the marked differences between the excesses from starting materials CFX-AA (blue) and CFX-PA (purple) used as a representative of the patterns exhibited by CFX-SA, CFX-PA, CFX base and CFX-HCl·H2O in Figure S21.

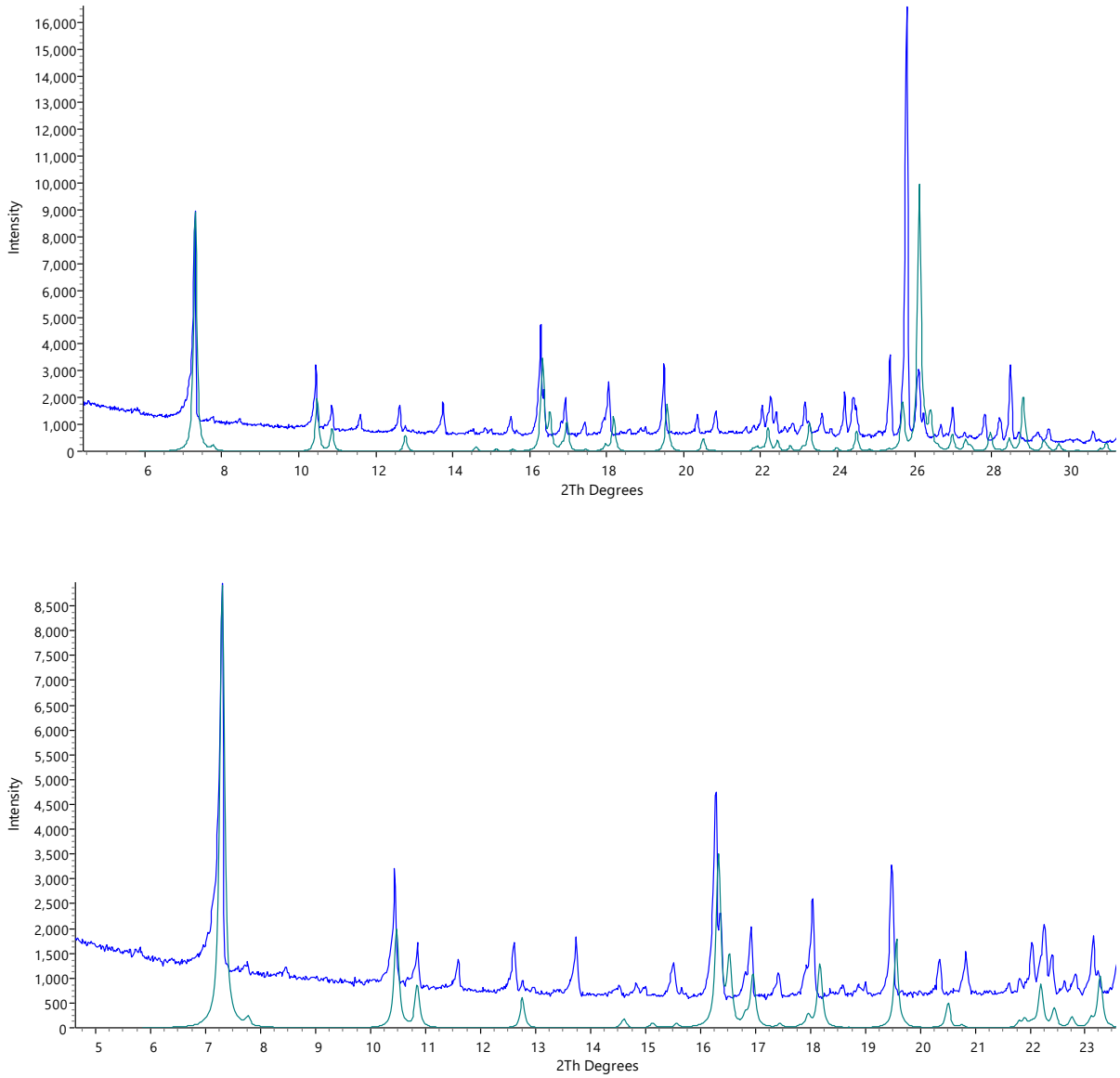


**Figure S23**: Experimental PXRD pattern for the excess solid recovered at the end of the CFX-AA dissolution experiment (blue) and a simulated PXRD pattern (green) for ciprofloxacin hemikis(adipate) dihydrate [CSD refcode QUKHOV]. Two ranges are shown to highlight the strong level of agreement (taking into account the fact that the experimental data were collected at 298 K whilst the single-crystal structure of QUKHOV was collected at 100 K) between the two patterns, that suggests that ciprofloxacin hemikis(adipate) dihydrate is a major component of the excess material. This conclusion was further strengthened by isolation of a small crystal from the excess solid, whose cell dimensions as ascertained by single-crystal diffraction were flagged as matching those of QUKHOV

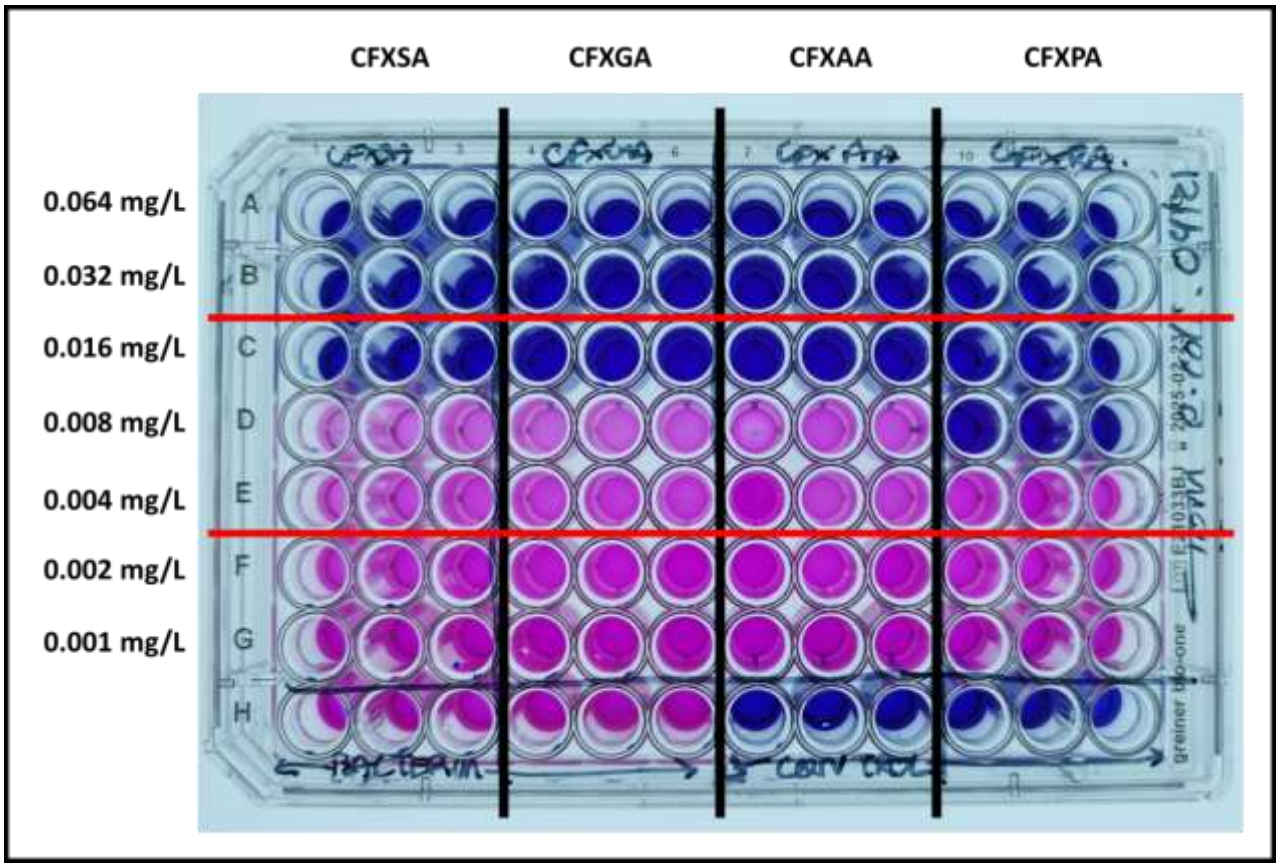


**Figure S24:** 96 well plate showing results to MIC test. Area between red lines shows acceptable EUCAST guidelines for ciprofloxacin with *Escherichia coli* ATCC 25922. Resazurin dye changes to pink in the presence of live bacteria.

# Modulated Drug Release of Ciprofloxacin Salts from Three-Fluid Nozzle Spray Dried Solid Dispersions

Supplementary Information

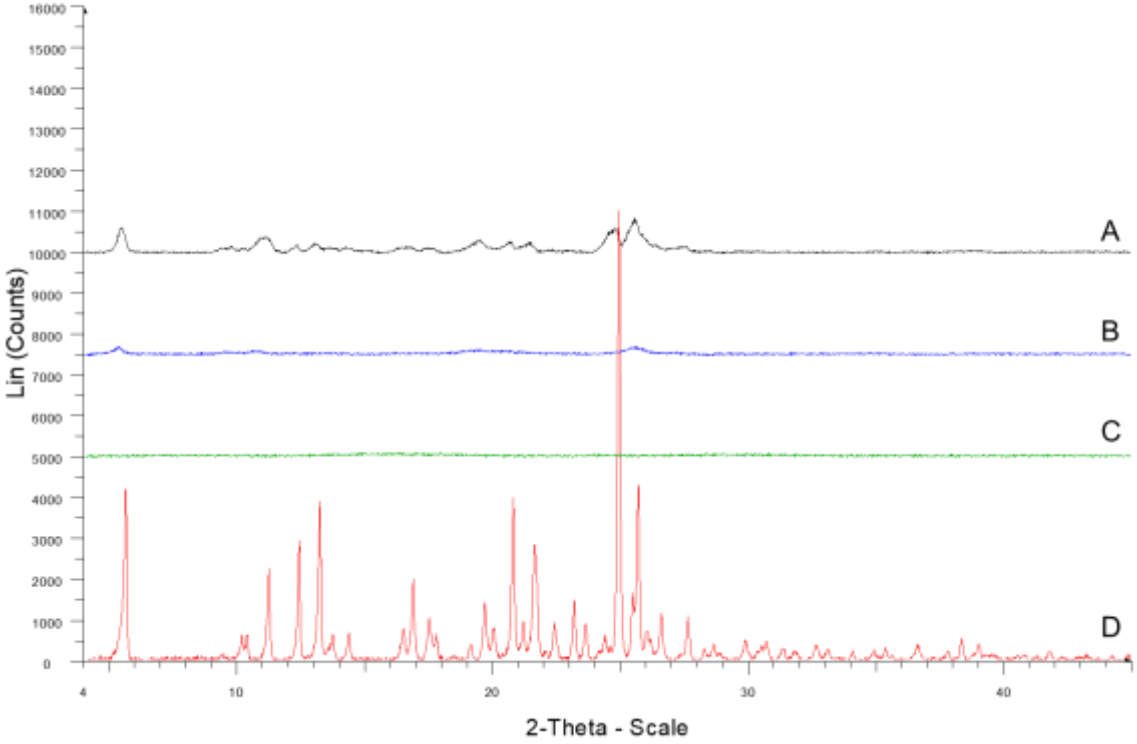


**Figure S1:** PXRD patterns with background scattering removed showing SD formulations of **A)** Salt (black), **B)** Solution (blue) and **C)** Suspension (green) compared to **D)** CFX salt reference (red) for ciprofloxacin succinic acid formulations.

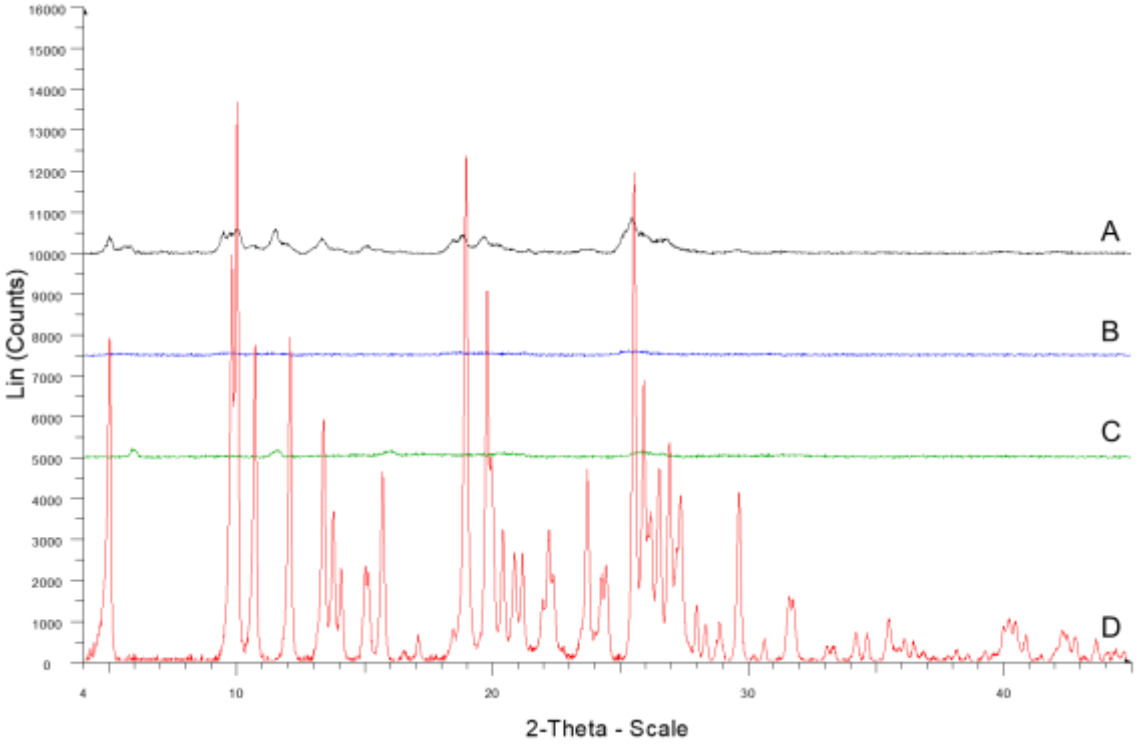


**Figure S2:** PXRD patterns with background scattering removed showing SD formulations of **A)** Salt (black), **B)** Solution (blue) and **C)** Suspension (green) compared to **D)** CFX salt reference (red) for ciprofloxacin adipic acid formulations.

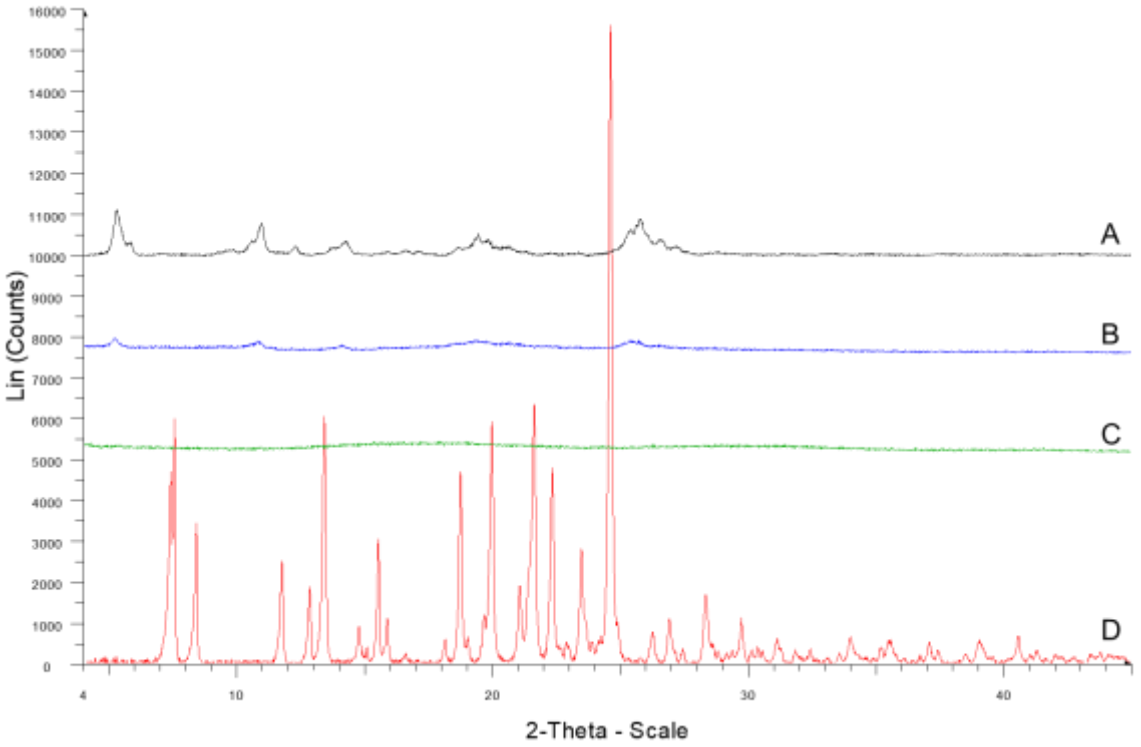


**Figure S3:** PXRD patterns with background scattering removed showing SD formulations of **A)** Salt (black), **B)** Solution (blue) and **C)** Suspension (green) compared to **D)** CFX salt reference (red) for ciprofloxacin pimelic acid formulations.

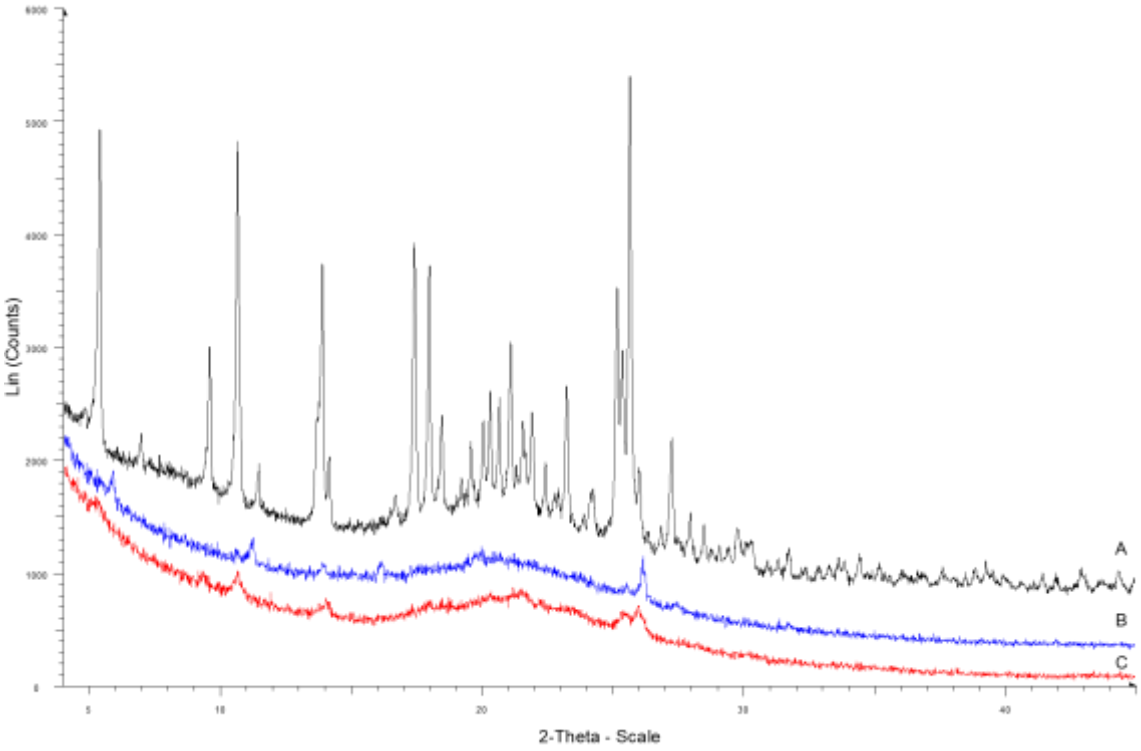


**Figure S4:** PXRD patterns including background scattering for A) CFX-GA + HPMC physical mix (1:1 mass ratio) (black), B) CGAH-sus (blue), C) CGAH-sol (red).

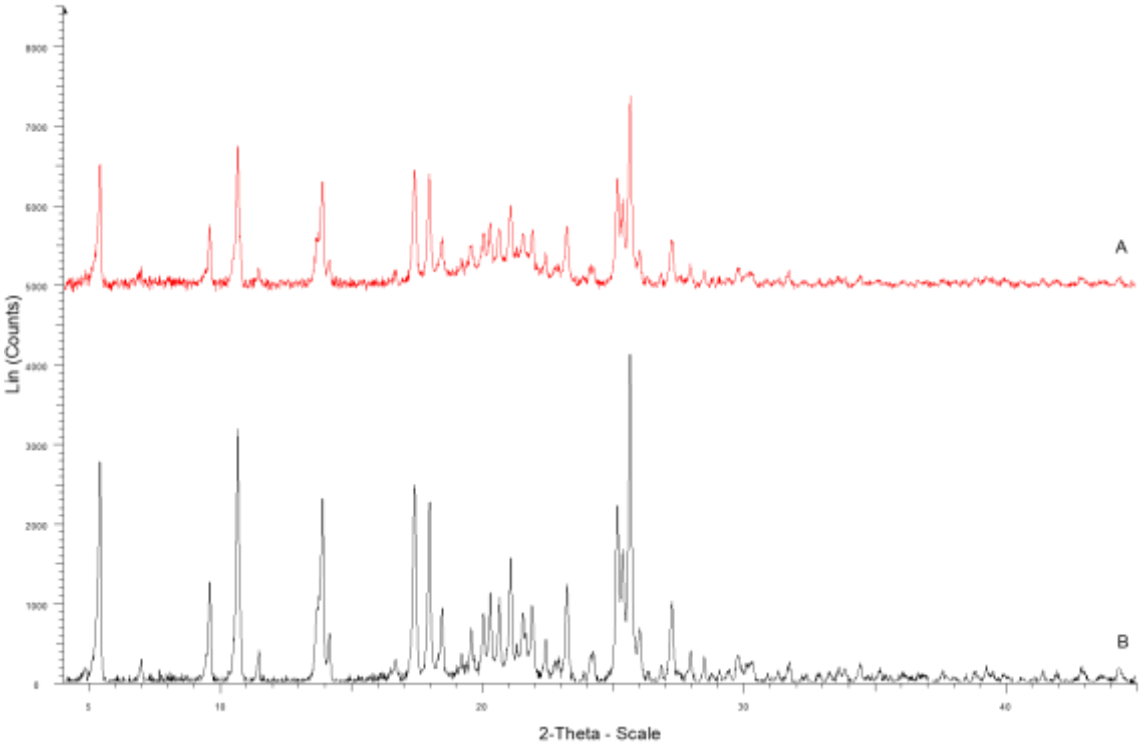


**Figure S5:** PXRD patterns with background scattering removed for A) CFX-GA separated from suspension following sheer mixing and sonication (red), B) CFX-GA prior to sheer mixing and sonication (black).

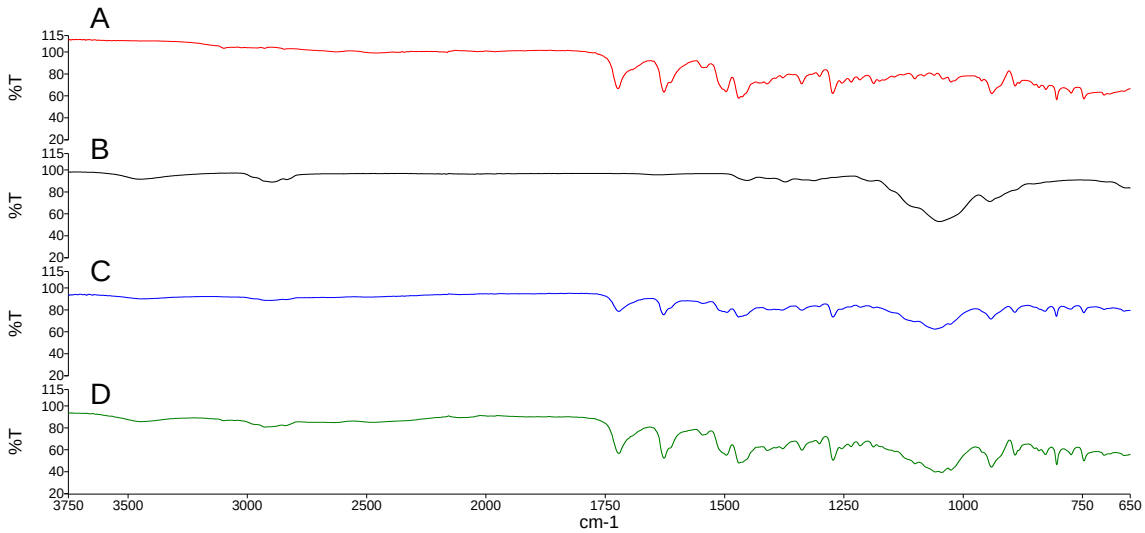


**Figure S6:** FTIR data comparing physical mixtures of **A)** CFX-SA milled reference (red), **B)** HPMC reference (black) and SD formulations of **C)** CSAH-sol (blue) and **D)** CSAH-sus (green).

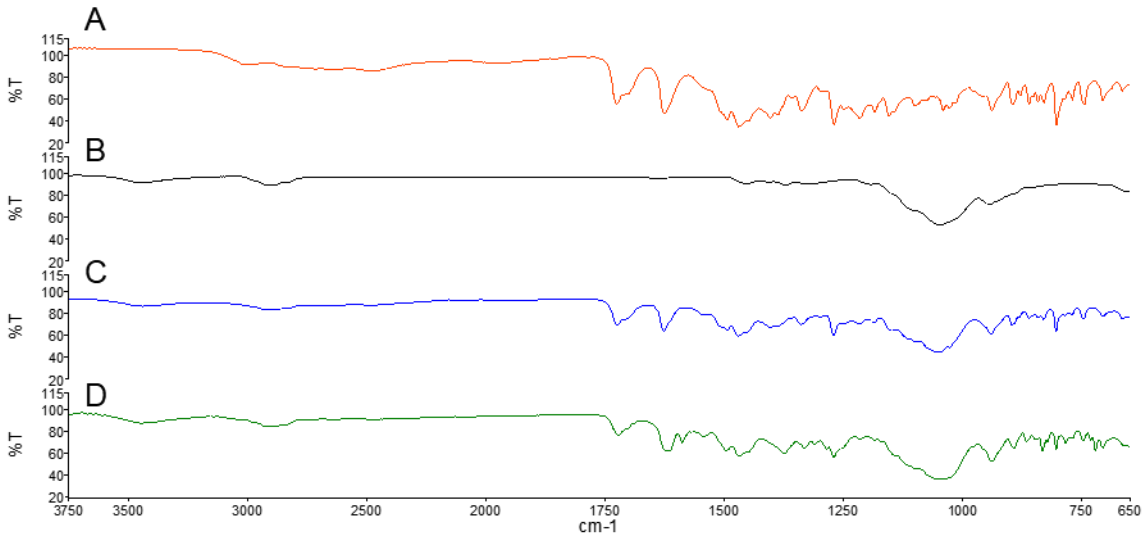


**Figure S7:** FTIR data comparing physical mixtures of **A)** CFX-GA milled reference (red), **B)** HPMC reference (black) and SD formulations of **C)** CGAH-sol (blue) and **D)** CGAH-sus (green).

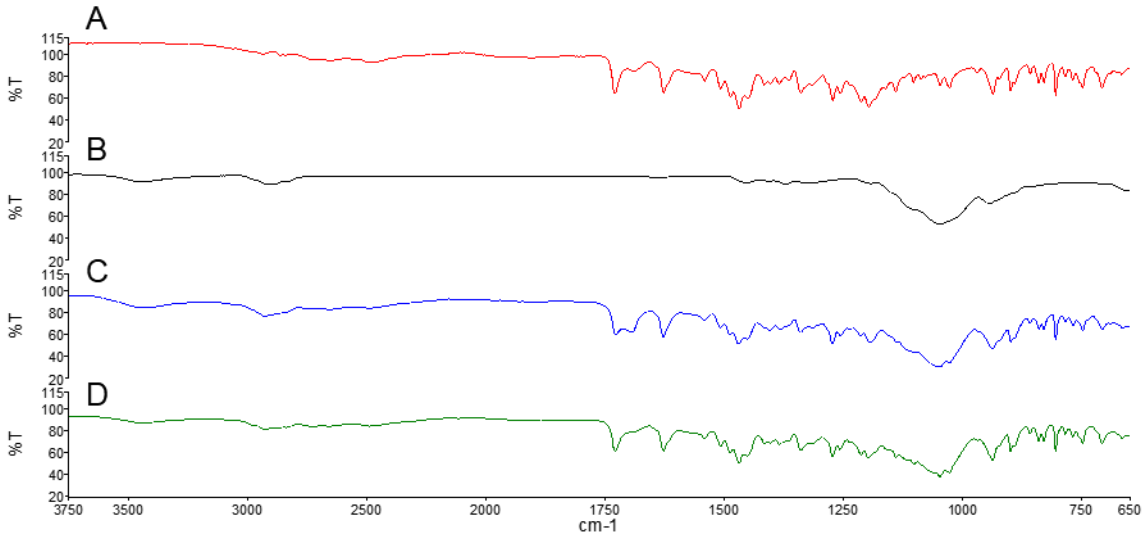


**Figure S8:** FTIR data comparing physical mixtures of **A)** CFX-AA milled reference (red), **B)** HPMC reference (black) and SD formulations of **C)** CAAH-sol (blue) and **D)** CAAH-sus (green).

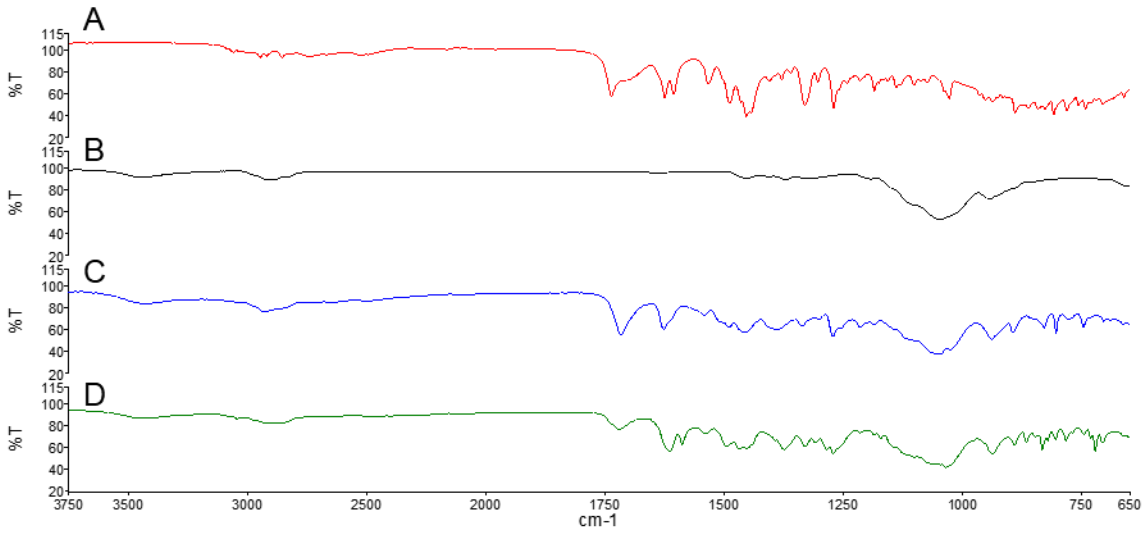


**Figure S9:** FTIR data comparing physical mixtures of **A)** CFX-PA milled reference (red), **B)** HPMC reference (black) and SD formulations of **C)** CPAH-sol (blue) and **D)** CPAH-sus (green).

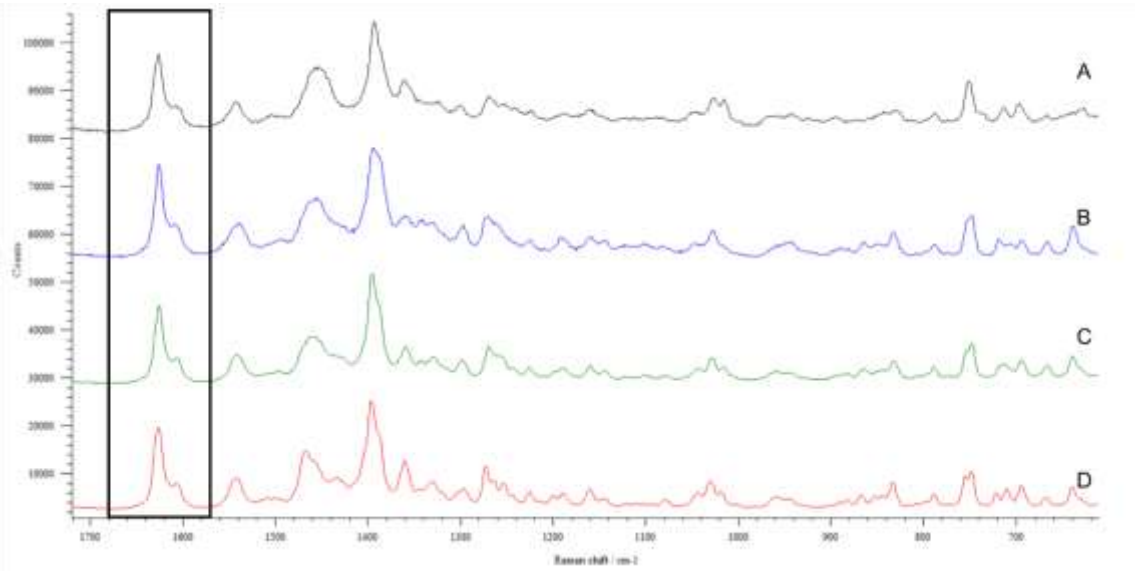


**Figure S10:** Raman data comparing A) CGA (black), B) CGAH-sol (blue), C) CGAH-sus (green) and D) CFX-GA reference (red).

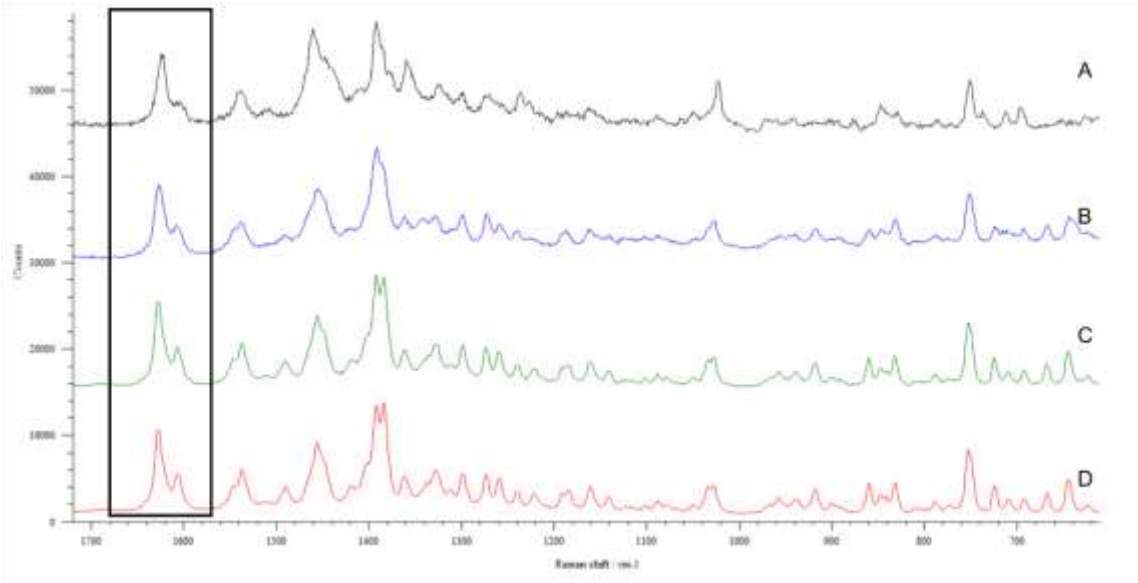


**Figure S11:** Raman data comparing A) CAA (black), B) CAAH-sol (blue), C) CAAH-sus (green) and D) CFX-AA reference (red).

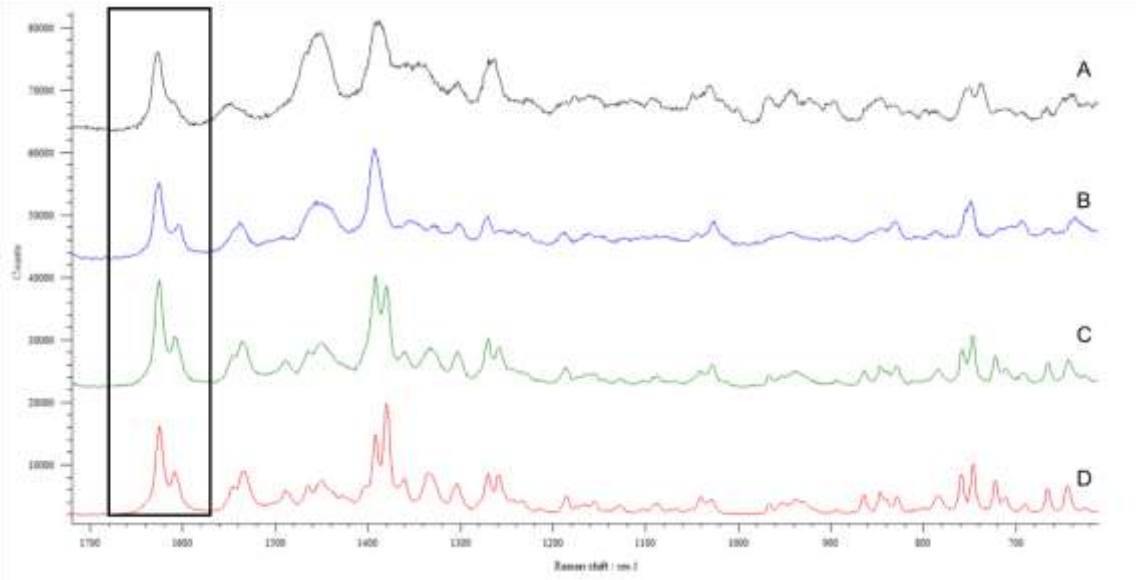


**Figure S12:** Raman data comparing A) CPA (black), B) CPAH-sol (blue), C) CPAH-sus (green) and D) CFX-PA reference (red).

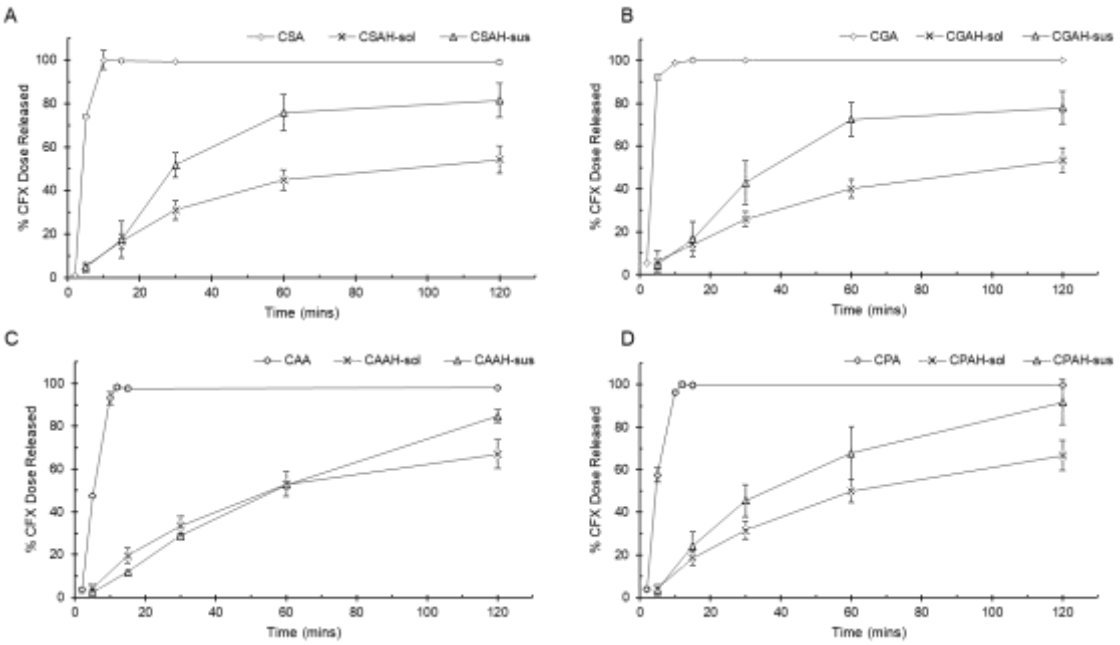


**Figure S13:** In-vitro dissolution data comparing Salt, Solution and Suspension formulations over 2 hours per salt form. A) SA formulations, B) GA formulations, C) AA formulations, D) PA formulations.

# Spray Dried Progesterone Formulations for Carrier Free Dry Powder Inhalation

Supplementary Information

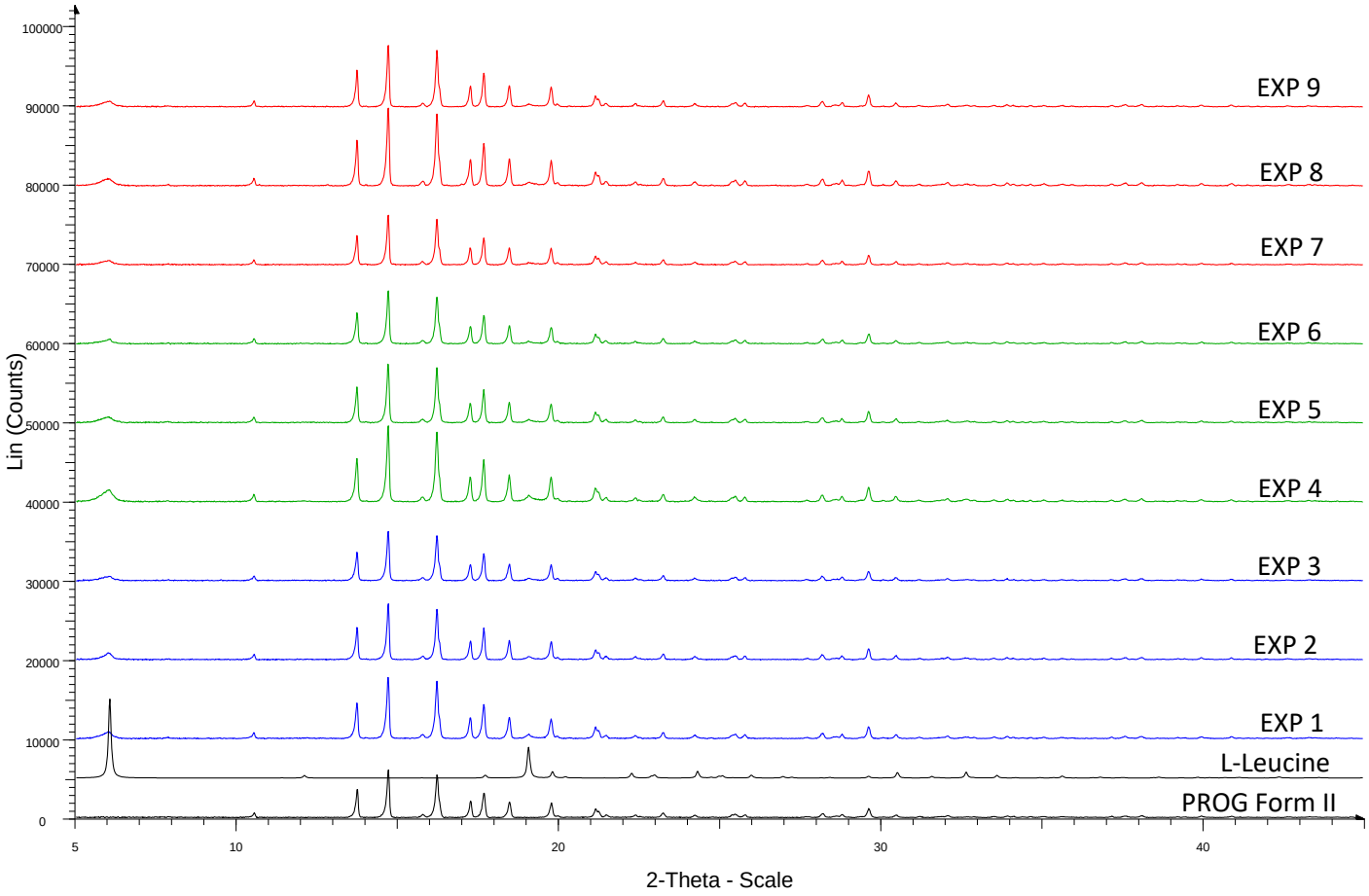


**Figure S1:** PXRD data comparing milled PROG-LEU formulations (as listed in Table 1) with PROG Form II reference and L-Leucine reference

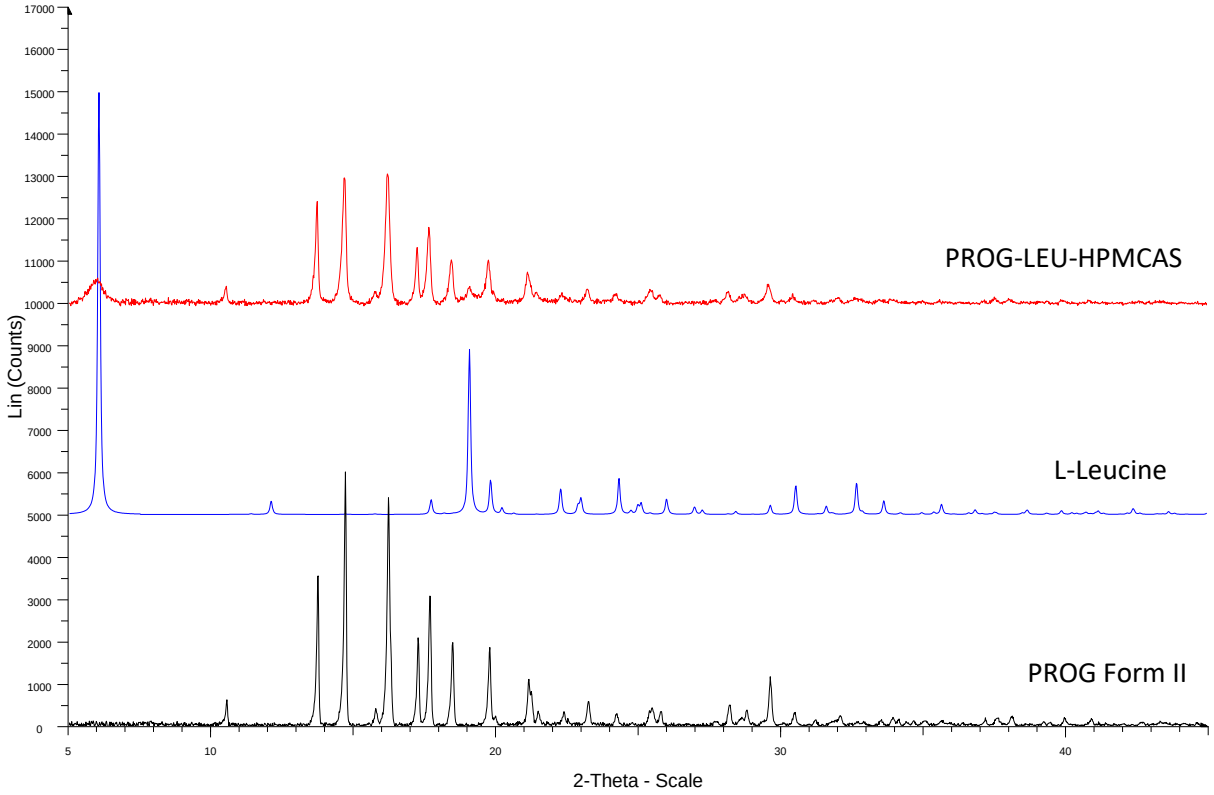


**Figure S2:** PXRD data for PROG-LEU-HPMCAS compared to Prog Form II and L-Leucine.

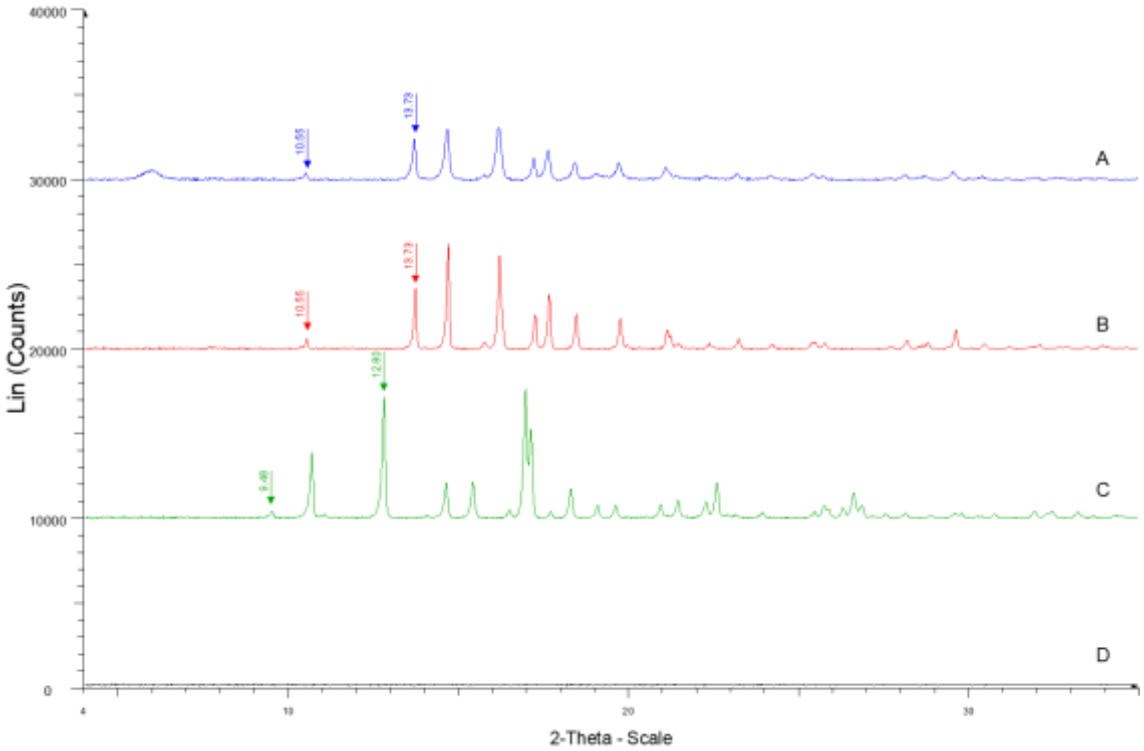


**Figure S3:** PXRD data for (A) PROG-LEU-HPMCAS compared to (B) Prog Form II, (C) Prog Form I, (D) HPMCAS

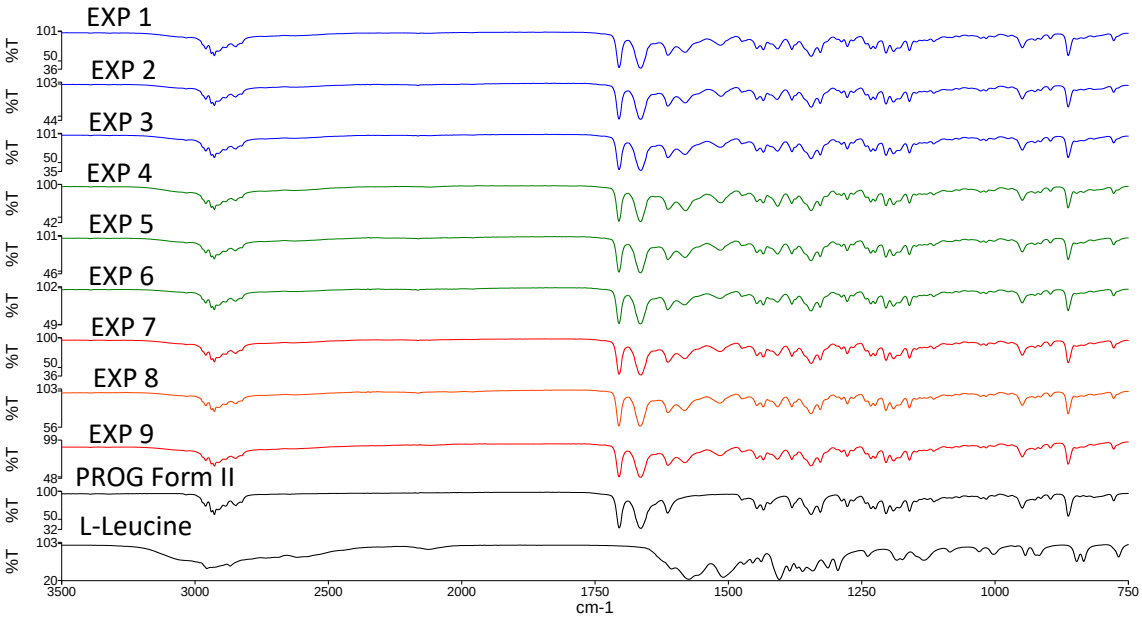


**Figure S4:** FTIR data for all PROG-LEU formulations (as listed in Table 1) compared to PROG Form II and L-Leucine.

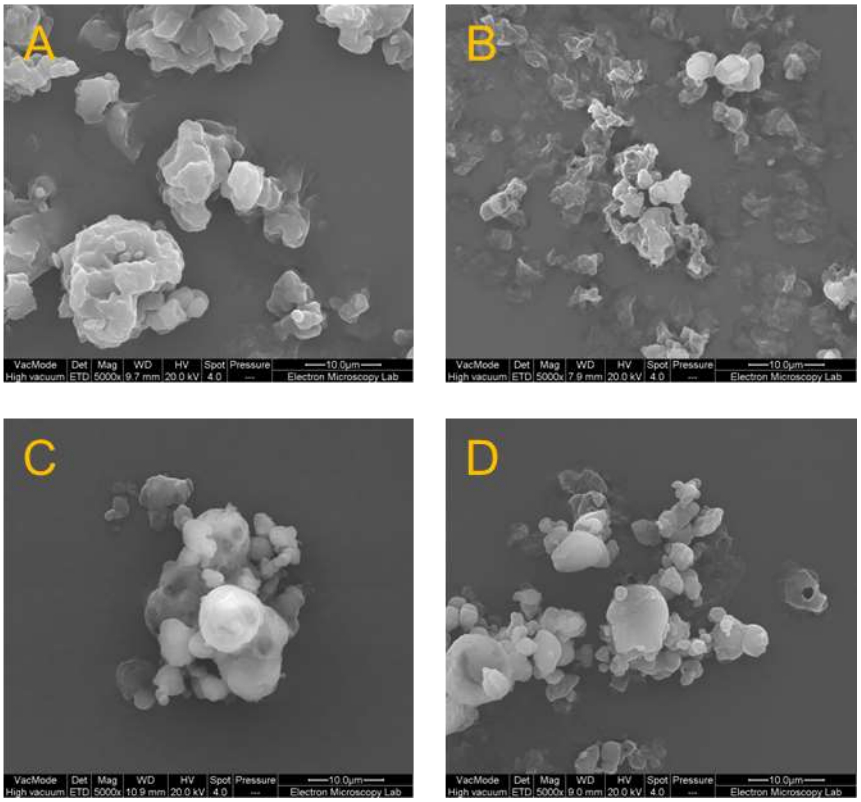


**Figure S5:** SEM images showing A) PROG-LEU-HPMCAS, B) PROG-LEU from IPA, C) PROG-LEU from ACE, D) PROG-LEU from EtOH.

Table S1: PROG solubility values reported in literature

| **Progesterone Polymorph** | **Solubility ($\mu g ml^{-1}$)** | **Media** | **Temperature (°C)** | **Ref.** |
|---|---|---|---|---|
| Form I | 0.569 | Water | 21 | 1 |
| Form I | 0.805 | PBS | 21 | 1 |
| Form I | 88.99 | Water | 30.2 | 1 |
| Form I | 125.78 | PBS | 30.2 | 1 |
| Form I | 11.49 | PBS | 22 | 2 |
| Form I | 0.5 | 0.9% NaCl | “room temp” | 3 |
| Form I | 6 | 0.9% NaCl | 37 | 3 |
| Form I | 11 (calculated) | Water | 37 | 4 |
| Form I | 8.16 | Water | 25 | 5 |
| Form II | 3270.38 | Water | 21 | 1 |
| Form II | 11477.79 | PBS | 21 | 1 |
| Form II | 4654.01 | Water | 30.2 | 1 |
| Form II | 13207.32 | PBS | 30.2 | 1 |
| Form II | 11.70 | Water | 24 | 5 |

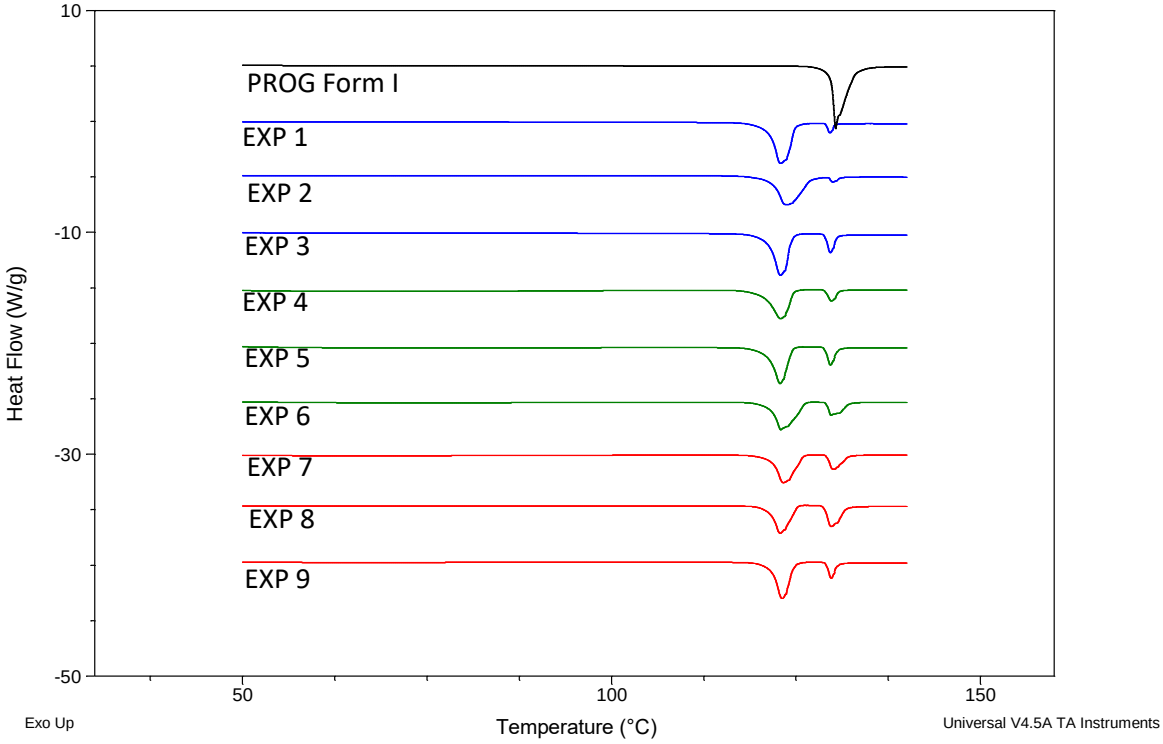


**Figure S6:** DSC data for all PROG-LEU formulations (as listed in Table 1) compared to PROG Form I

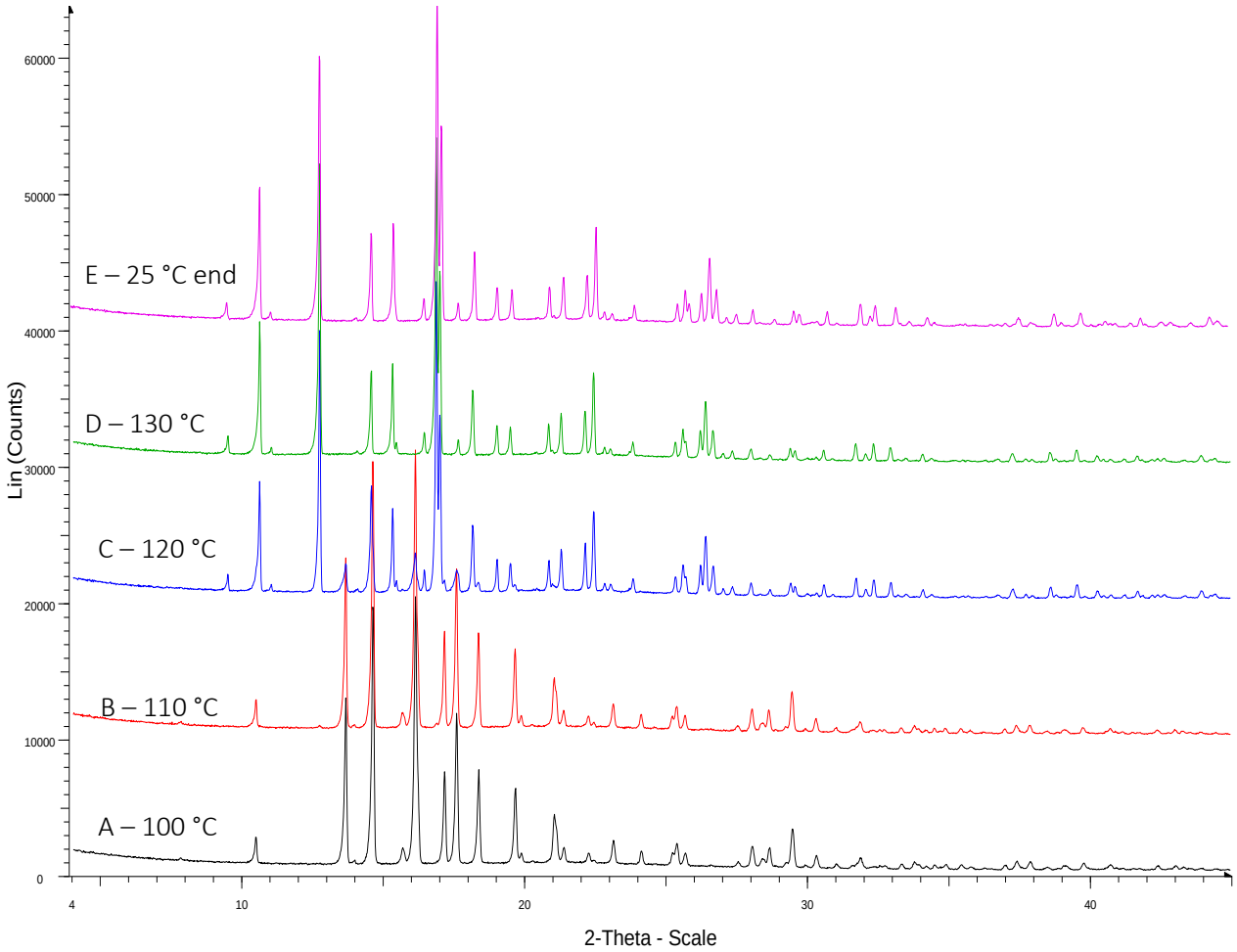


**Figure S7:** VT-PXRD data for PROG-SD showing temperature-induced polymorphic transformation from Form II to Form I during a heating ramp experiment from A (100 °C) to D (130 °C) then following cooling to E (25 °C). Changes associated with the presence of Form I by the addition of peaks at 9.48 °2θ, 10.68 °2θ and 12.80 °2θ, first seen clearly at 120 °C. The peaks associated with Form I appear alongside Form II peaks confirming the presence of both phases in the sample at this temperature. Form I then remains exclusively in the sample following cooling to 25 °C.

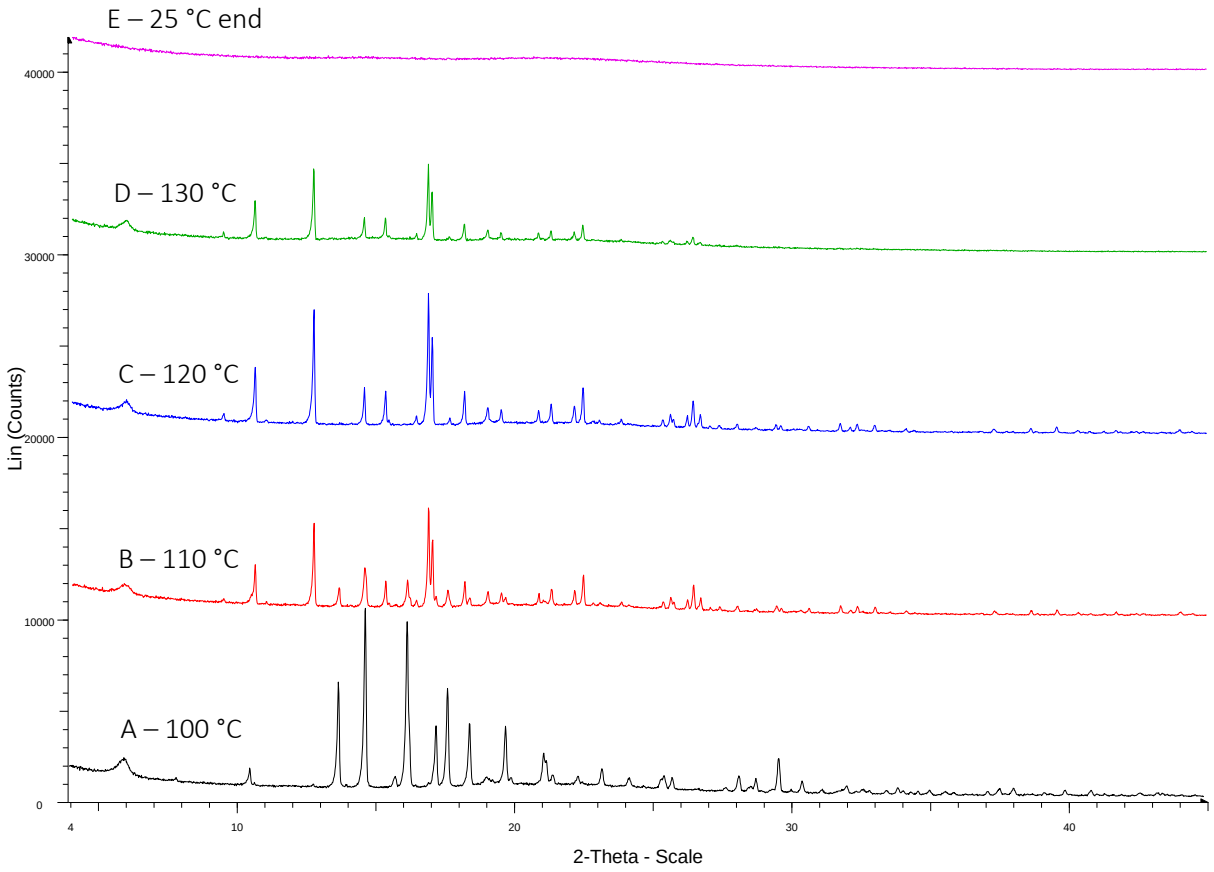


**Figure S8:** VT-PXRD data for PROG-LEU formulation showing temperature induced polymorphic transformation from Form II to Form I then melting.

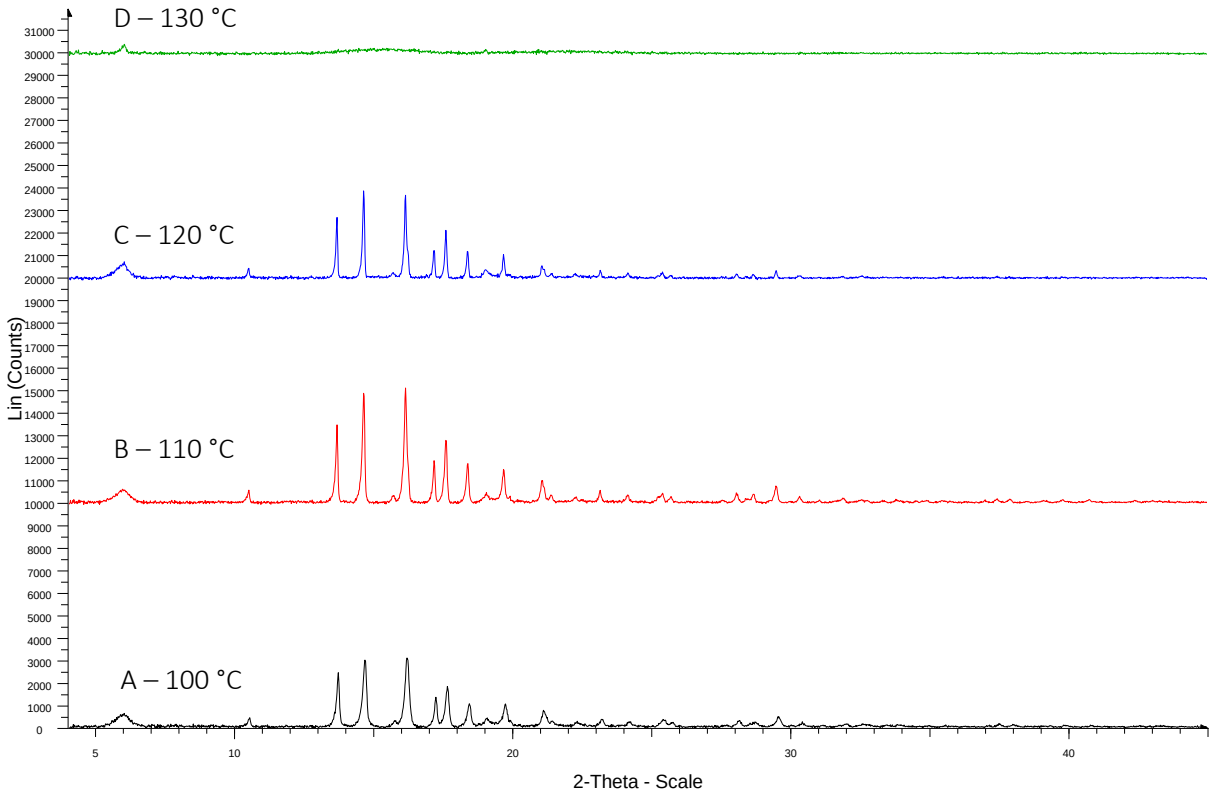


**Figure S9:** VT-PXRD data for PROGL-HPMCAS formulation showing with no transformation to Form II then melting.

## References

1. A. Sarkar, D. Ragab and S. Rohani, *Crystal Growth & Design*, 2014, **14**, 4574-4582.
2. X. Chen, I. Partheniadis, I. Nikolakakis and H. Al-Obaidi, *Journal*, 2020, **12**.
3. A. L. Haskins, *Proceedings of the Society for Experimental Biology and Medicine*, 1949, **70**, 228-229.
4. M. Lahiani-Skiba, C. Barbot, F. Bounoure, S. Joudieh and M. Skiba, *Drug Dev Ind Pharm*, 2006, **32**, 1043-1058.
5. M. Muramatsu, M. Iwahashi and U. Takeuchi, *Journal of Pharmaceutical Sciences*, 1979, **68**, 175-177.

# Preparation and Formulation of Progesterone para-Aminobenzoic Acid Co-crystal

Supplementary Information

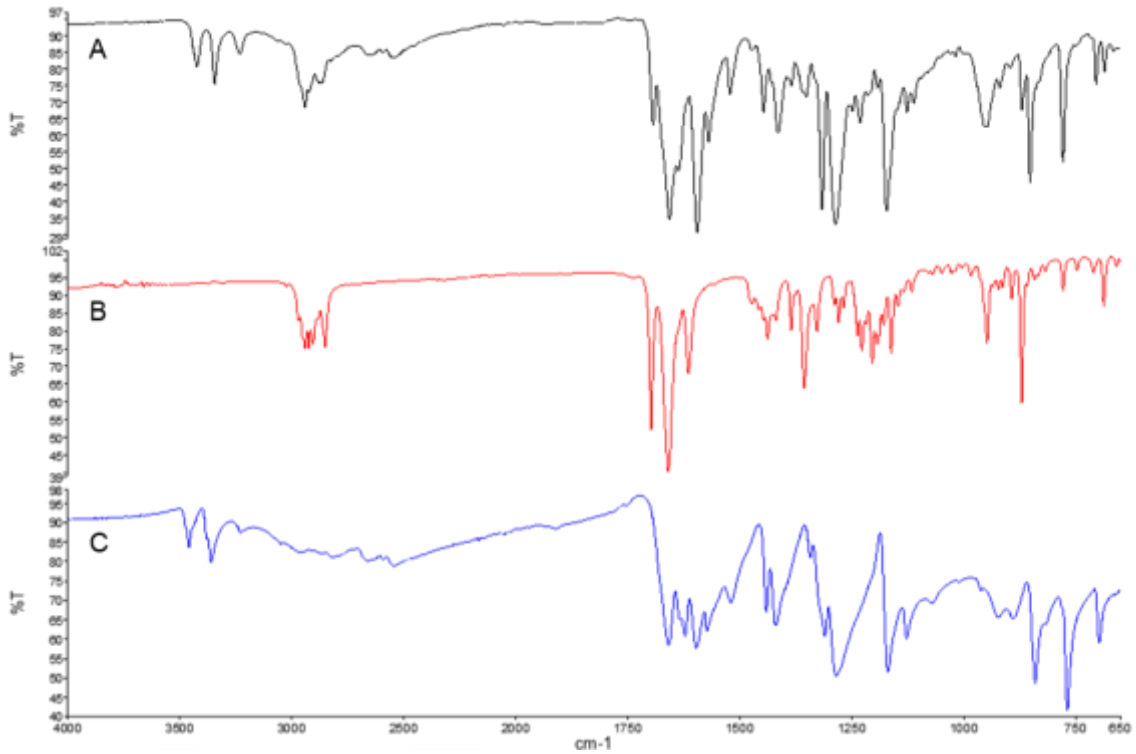


**Figure S1:** FTIR data comparing (A) PROG:PABA (black) to (B) PROG (red) and (C) PABA (blue) references.

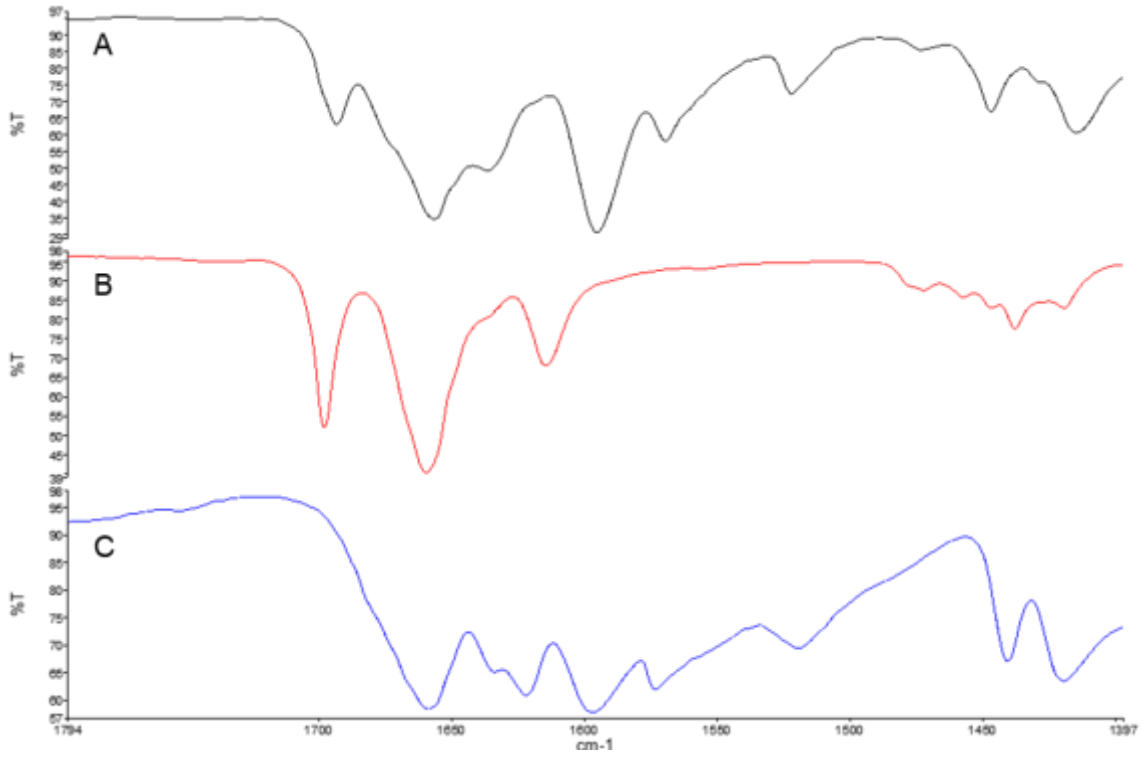


**Figure S2:** FTIR data comparing (A) PROG:PABA (black) to (B) PROG (red) and (C) PABA (blue) references. Focussed on the carbonyl region.

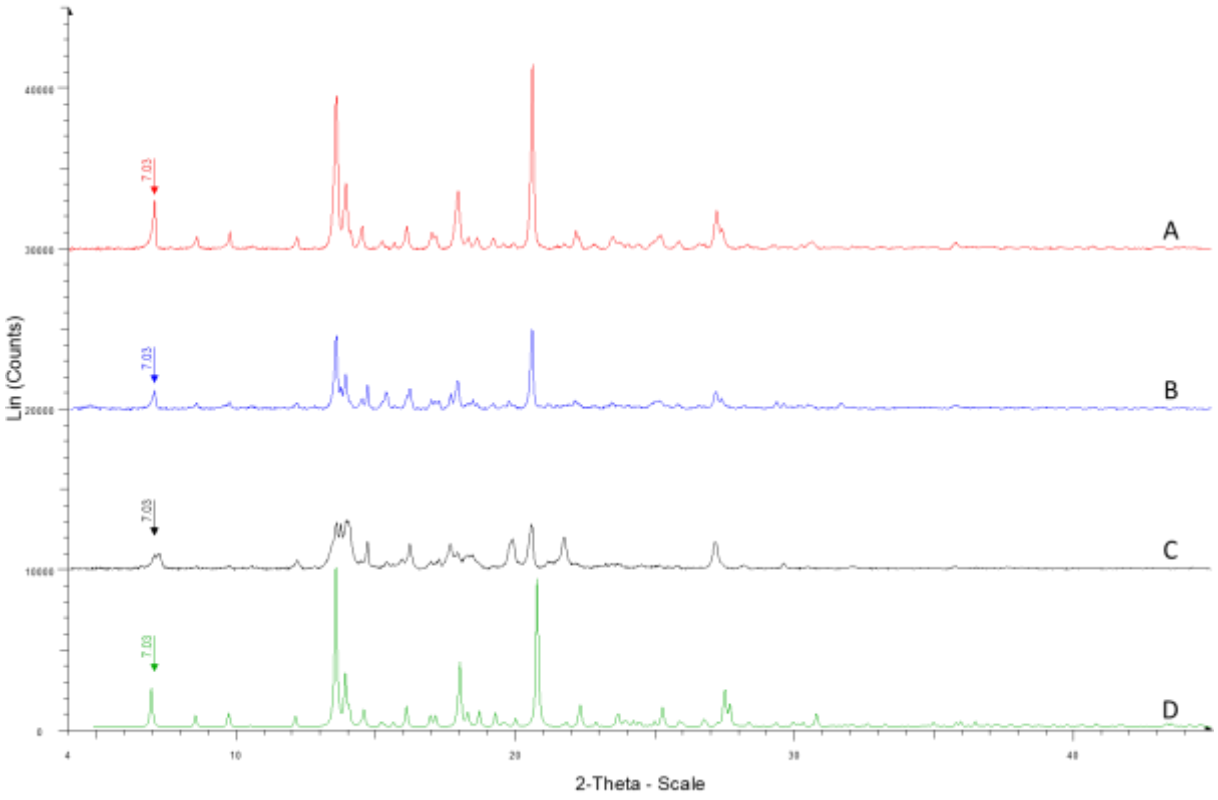


**Figure S3:** PXRD data for A) Milled PROG:PABA, B) Antisolvent PROG:PABA, C) Spray Dried PROG:PABA compared to D) simulated X-ray diffraction pattern from SC-XRD data (Black) compared to B) PXRD data from milled sample (Red). Note slight differences in peak positioning for the SC-XRD data since this data was collected at 100K rather than 293K for PXRD data.

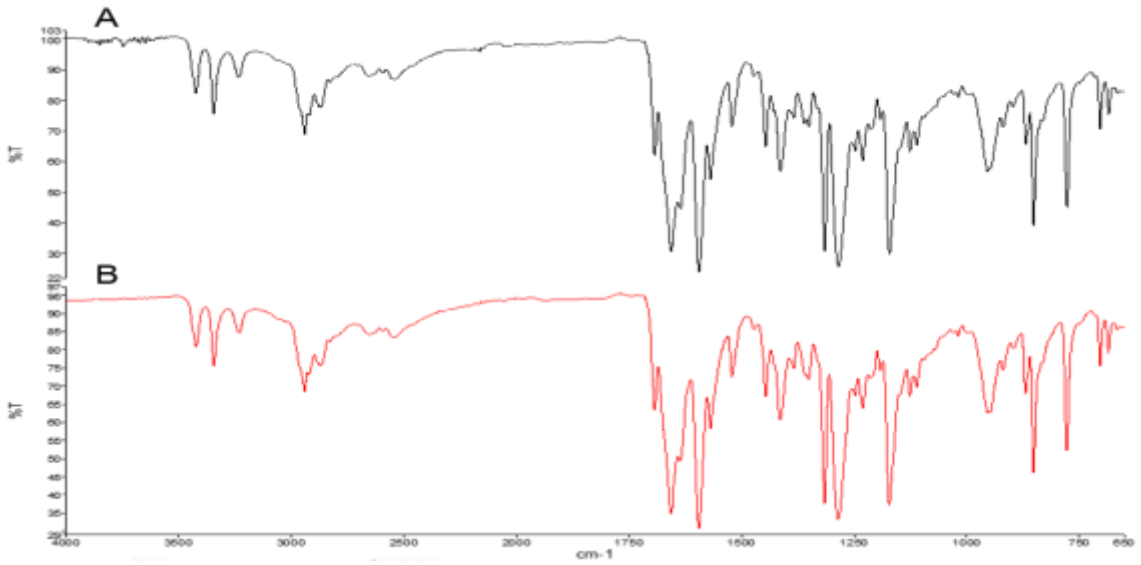


**Figure S4:** FTIR data for PROG:PABA milled cocrystal A) after humidity study and B) before humidity study.

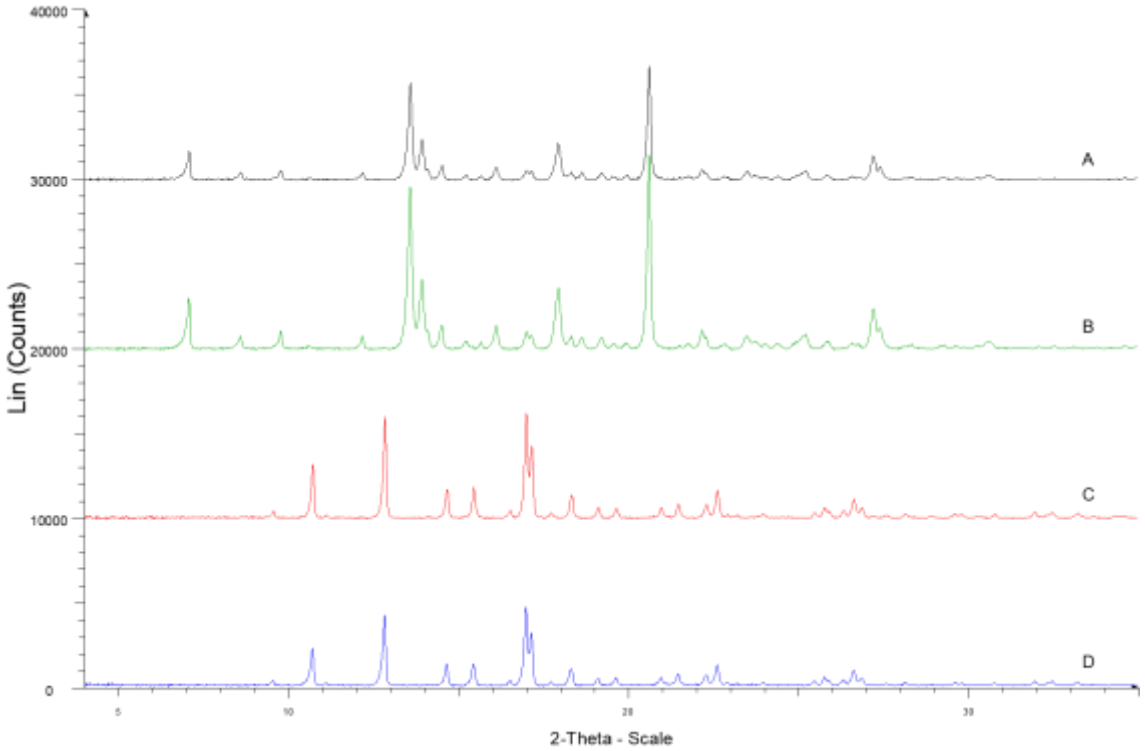


**Figure S5:** PXRD data for solubility solid residue following 48 hours for A) PROG-PABA post experiment (black), B) PROG-PABA pre experiment (green), C) PROG post experiment (red), D) PROG pre experiment (blue). Solid phases are identical.

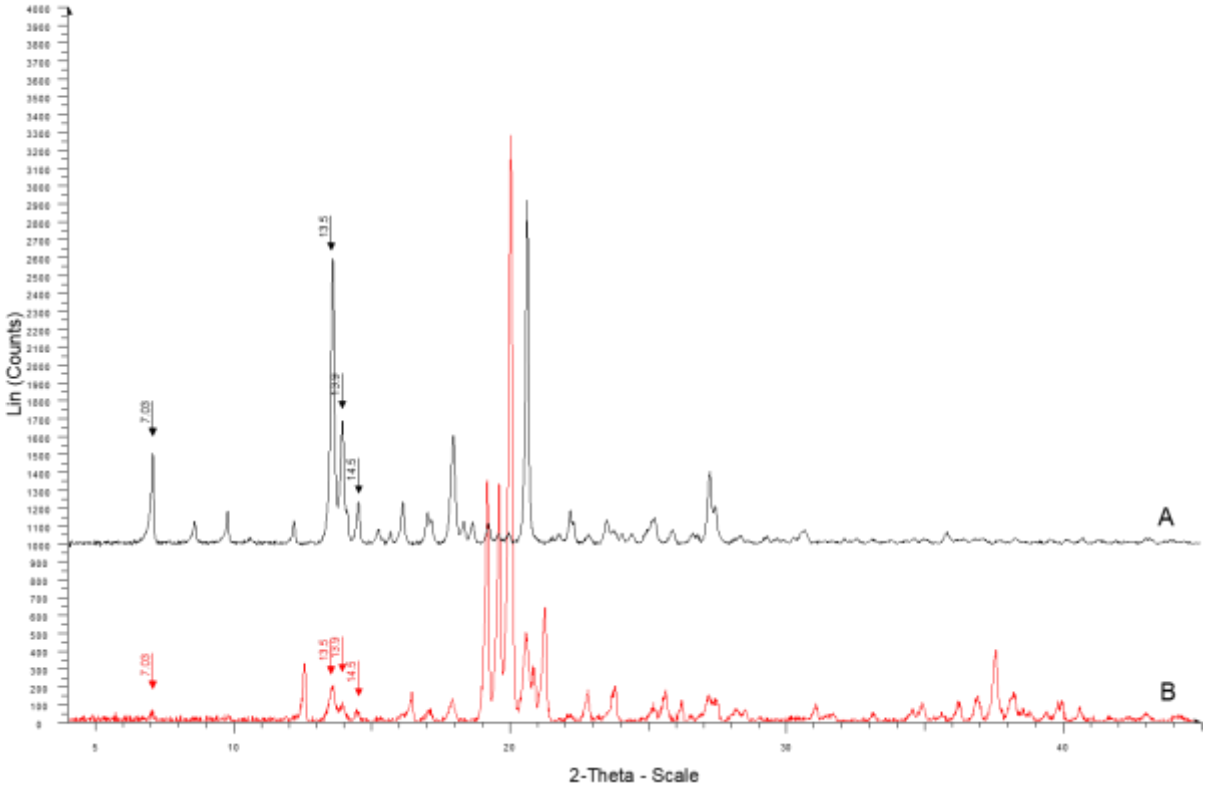


**Figure S6:** PXRD data of (A) tablet surface (red) compared to (B) PROG:PABA milled reference (black). Key co-crystal peaks marked, note the intense peaks at ~ 20° 2θ corresponding to α-lactose monohydrate.

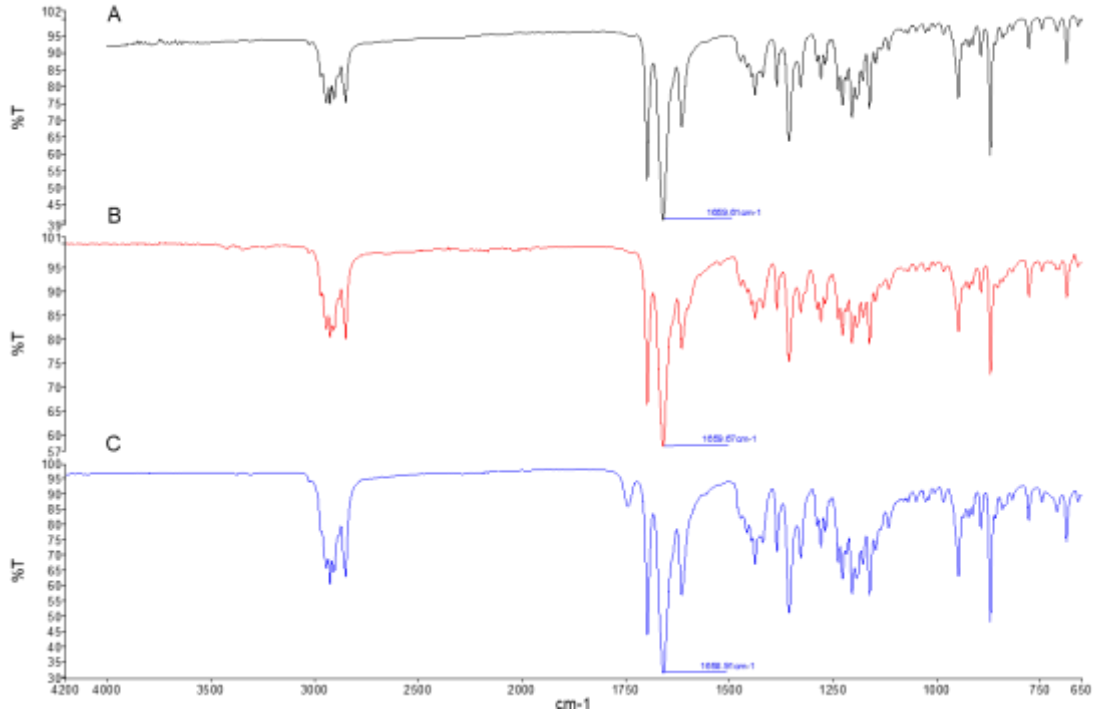


**Figure S7:** FTIR data comparing B) PROG:PABA dissolution residue (red) and C) Utrogestran™ dissolution reside (blue) compared to A) PROG reference (black), following the 3 hour dissolution experiment.

# Evaluation of Spay Drying to Prepare Co-Crystals of Salicylic Acid and Caffeine with Improved Physicochemical Properties for Oral Administration

Supplementary Information

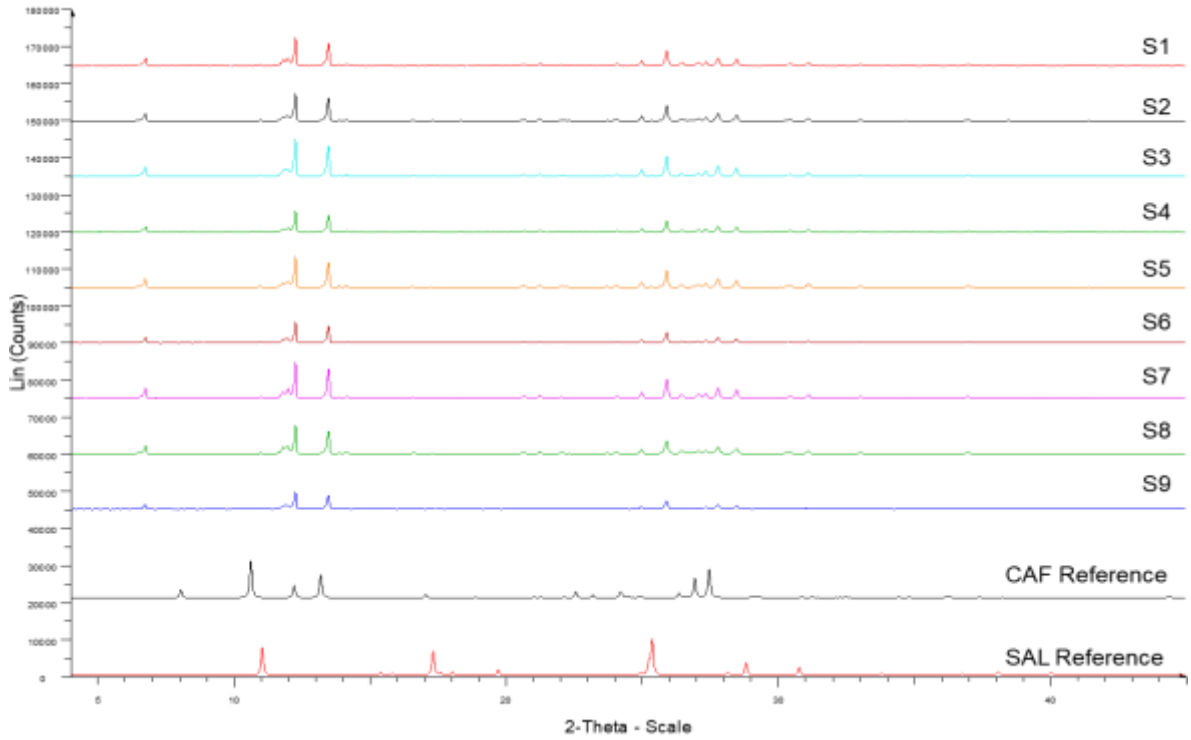


**Figure S1:** PXRD data comparing SAL-CAF two-fluid nozzle experiments with reference diffraction patterns.

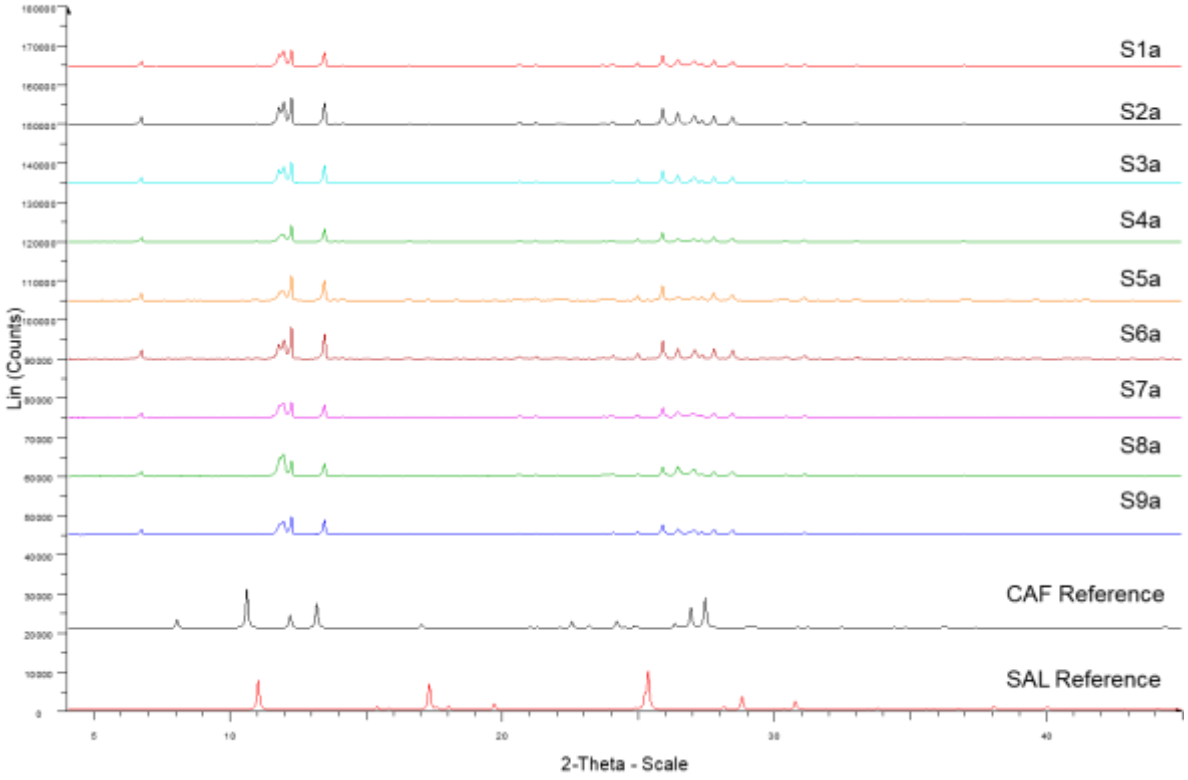


**Figure S2:** PXRD data comparing SAL-CAF three-fluid nozzle experiments with reference diffraction patterns.

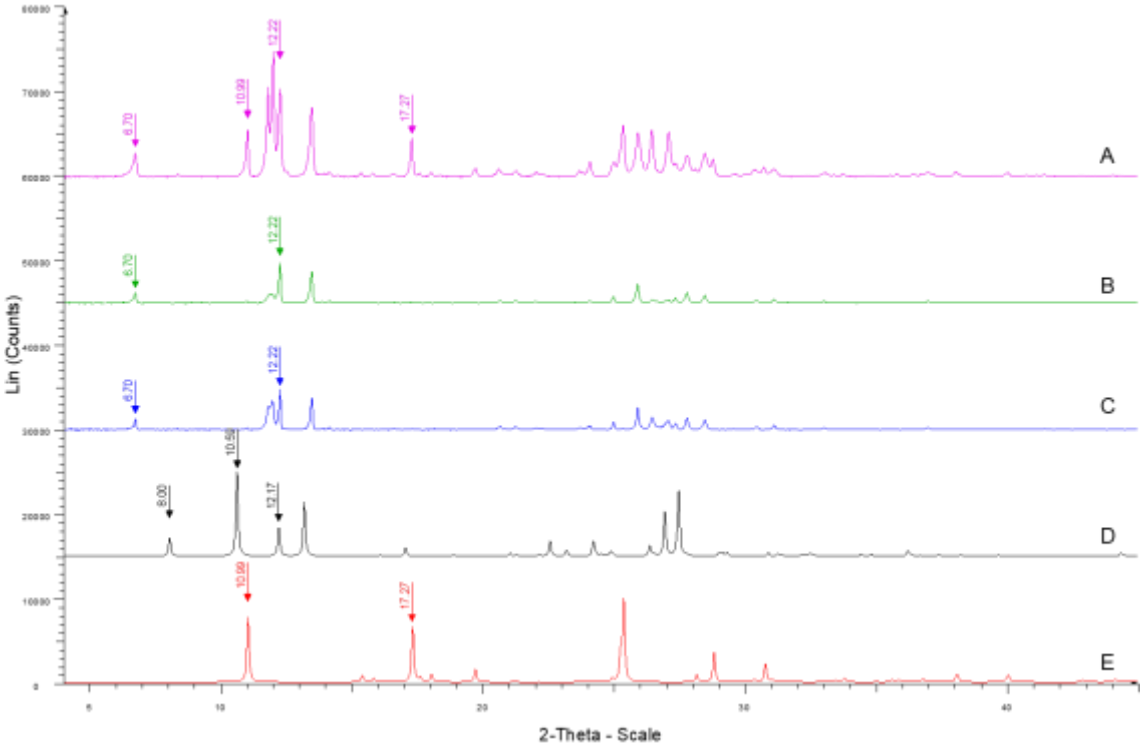


**Figure S3:** PXRD data comparing A) milled SAL-CAF (pink), B) 3-FN spray dried SAL-CAF, C) 2-FN spray dried SAL-CAF, D) CAF reference (black), E) SAL reference (red).

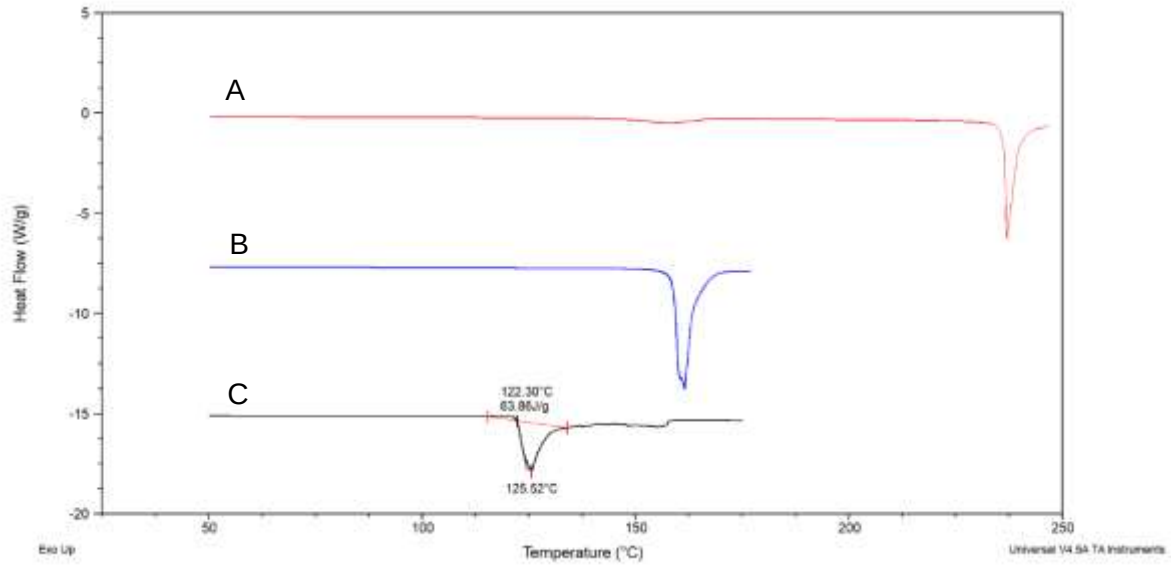


**Figure S4:** DSC data comparing C) physical mixture of salicylic acid and caffeine (black) to B) salicylic acid (blue) and (A) caffeine (red) references. These data show the eutectic melt of salicylic acid and caffeine at ~ 122 °C.

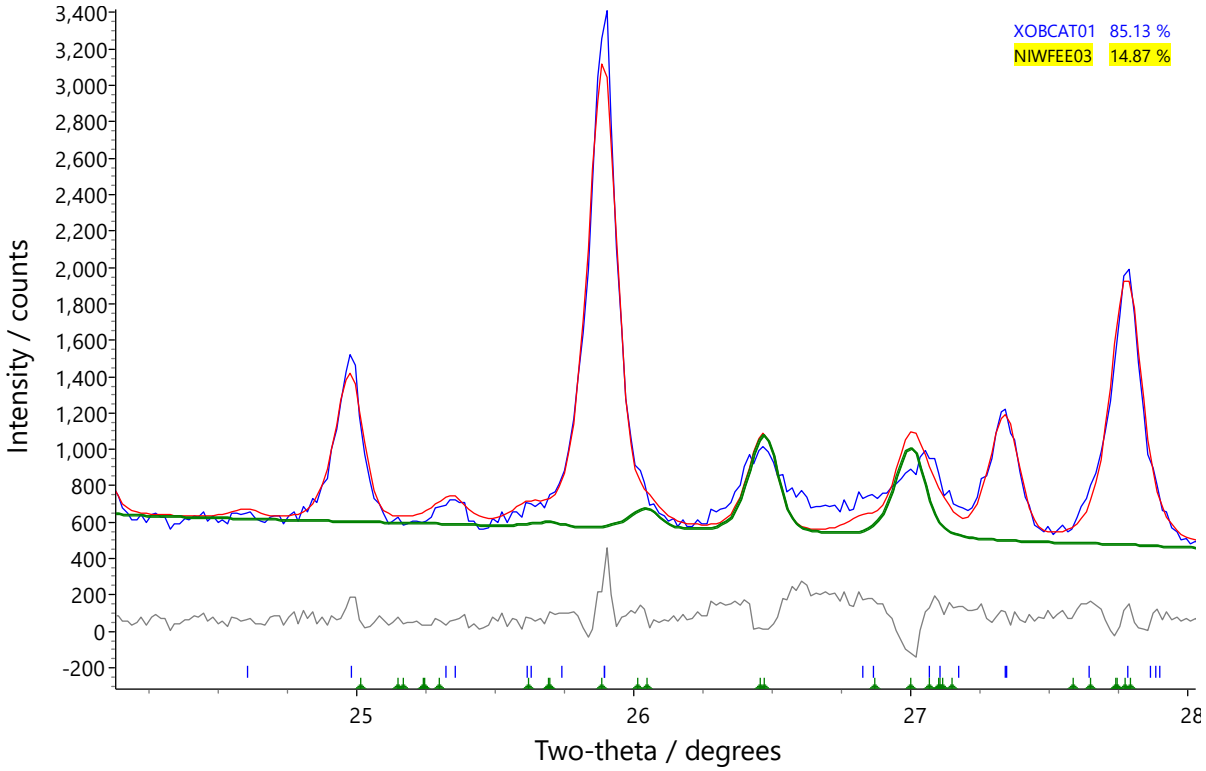


**Figure S5:** The two phase Rietveld fit described in Fig 5, shown in the range 24-28° 2θ. PXRD data (blue line), the overall fit of co-crystal to the data (red line) and the contribution of the caffeine β polymorph to the fit (green line) is displayed. Blue tick marks indicate the position of reflections associated with co-crystal phase, whilst green tick marks indicate the position of re-flection associated with caffeine beta polymorph. The two observed reflections below 12° 2θ are explained by the presence of the caffeine β polymorph.

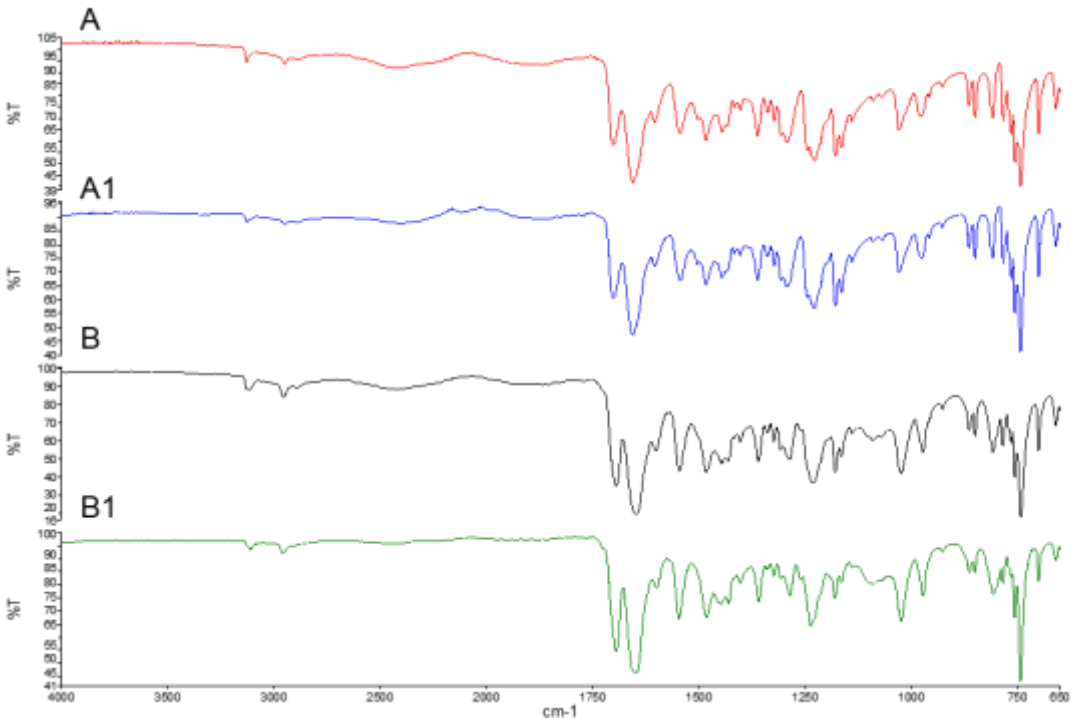


**Figure S6:** FTIR Data before and after storage at 75% relative humidity and 37 deg C for 4 months. A) S4 before, A1) S4 after, B) S4a before, B1) S4a after.

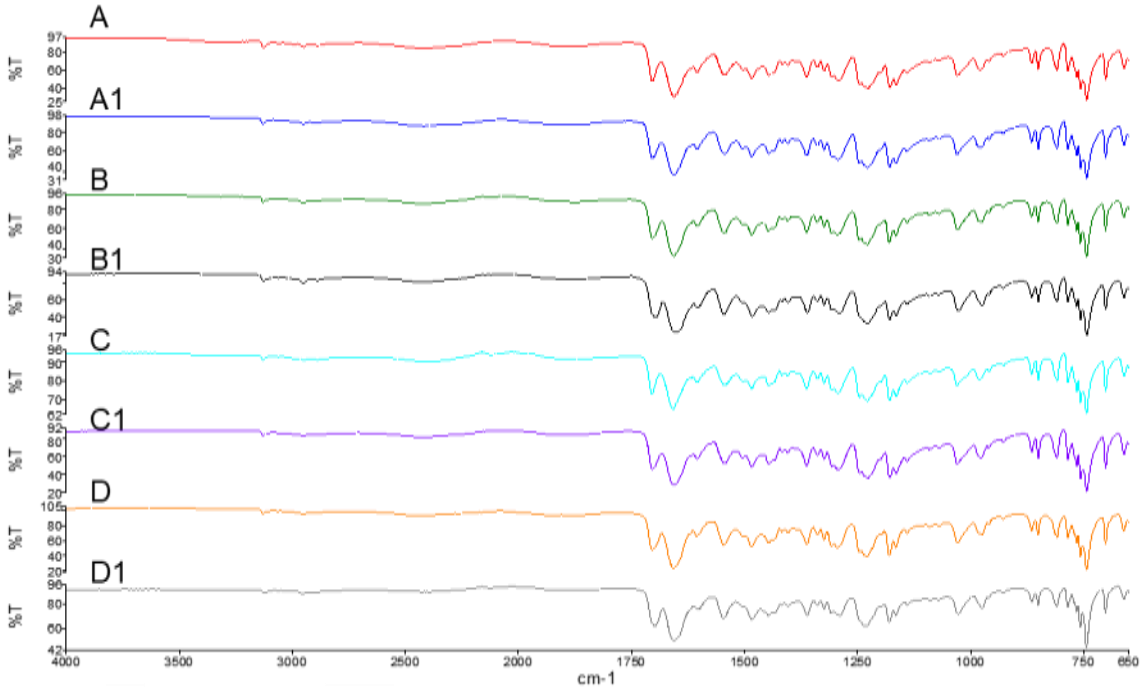


**Figure S7:** FTIR Data before and after storage at 75% relative humidity and 37 deg C for 4 months. A) S5 before, A1) S5 after, B) S5a before, B1) S5a after, C) S6 before, C1) S6 after, D) S6a before, D1) S6a after.

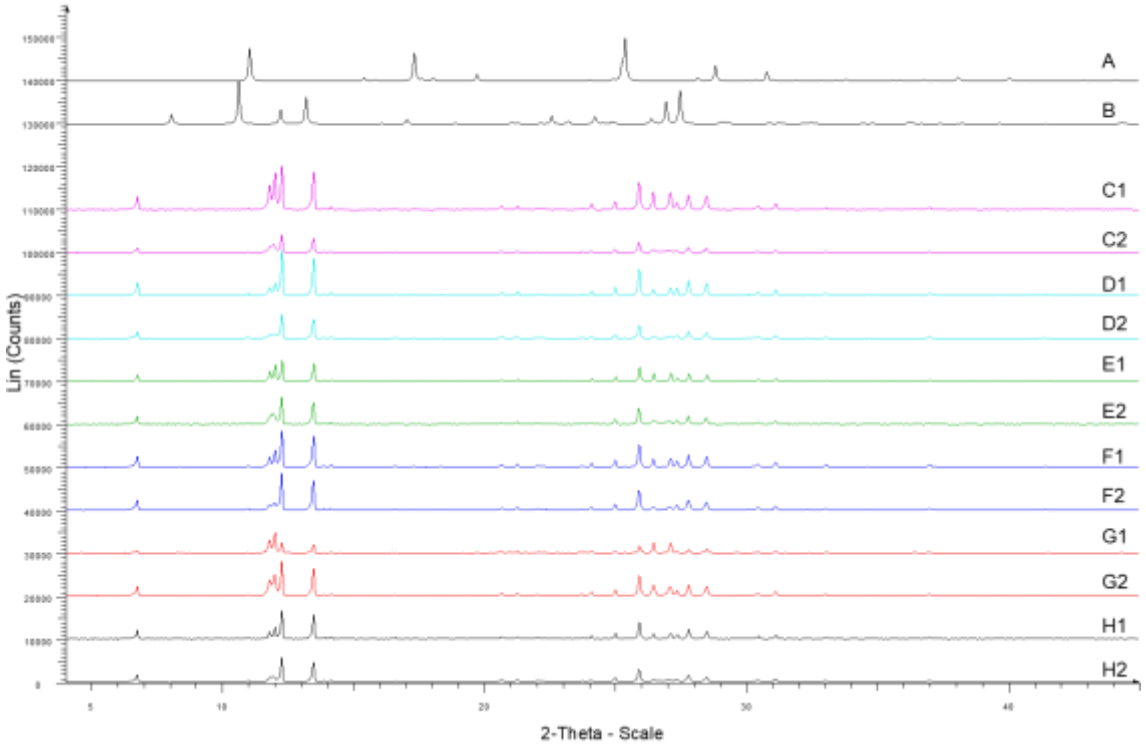


**Figure S8:** PXRD data before and after storage at 75% relative humidity and 37 deg C for 4 months. A) Salicylic Acid Reference, B) Caffeine reference, C1) S4 before, C2) S4 after, D1) S4a after, D2) S4a before, E1) S5 after, E2) S5 before, F1) S5a after, F2) S5a before, G1) S6 after, G2) S6 before, H1) S6a after, H2) S6a before.

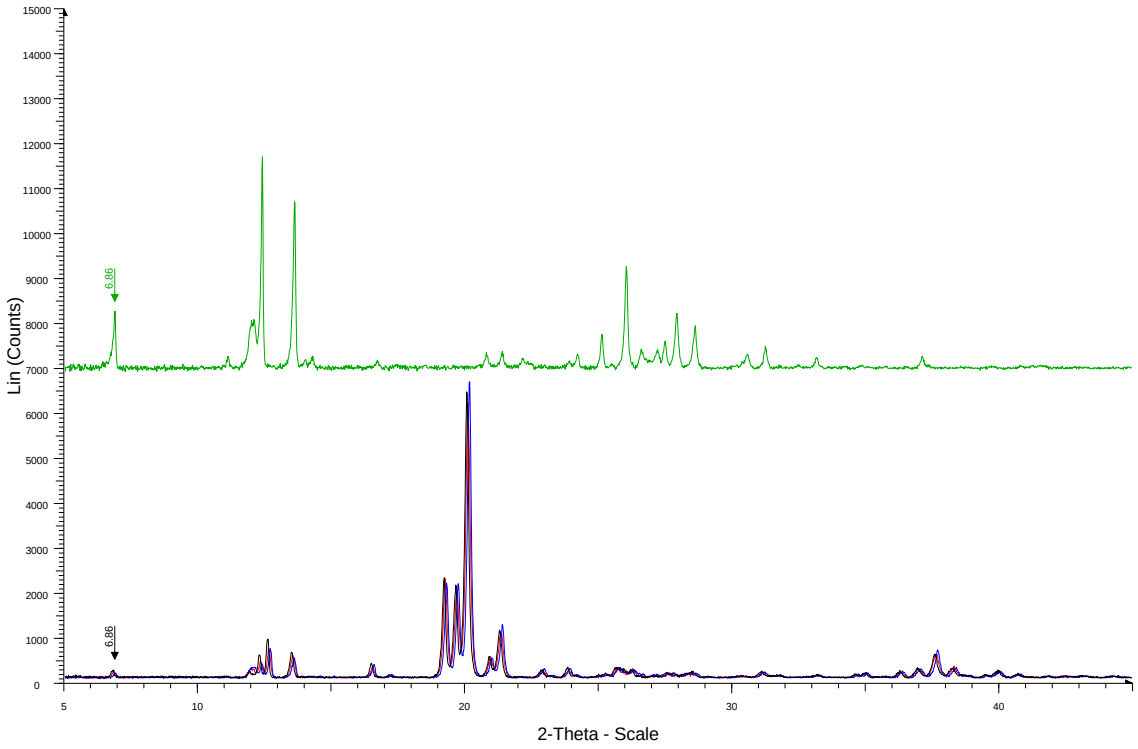


**Figure S9:** PXRD data comparing SAL-CAF tablet surfaces (Blue, Black, Red) with SAL-CAF co-crystal reference (green).